VOLUME 29 NOVEMBER, 1951 NUMBER 6

Canadian Journal of Physics

Editor: G. M. VOLKOFF

Published by THE NATIONAL RESEARCH COUNCIL
OTTAWA CANADA

CANADIAN JOURNAL OF PHYSICS

This was formerly *Section A, Canadian Journal of Research.* The change to the new name took place January 1, 1951. The CANADIAN JOURNAL OF PHYSICS is published six times annually.

The CANADIAN JOURNAL OF PHYSICS is published by the National Research Council of Canada under the authority of the Chairman of the Committee of the Privy Council on Scientific and Industrial Research. Matters of general policy are the responsibility of a joint Editorial Board consisting of members of the National Research Council of Canada and the Royal Society of Canada.

The National Research Council of Canada publishes also the following Journals: *Canadian Journal of Botany, Canadian Journal of Chemistry, Canadian Journal of Medical Sciences, Canadian Journal of Technology, Canadian Journal of Zoology.*

Subscription rate: $2.00 a year. All enquiries concerning subscriptions should be addressed to the CANADIAN JOURNAL OF PHYSICS, National Research Council, Ottawa, Canada. Special rates can be obtained for subscriptions to more than one of the Journals published by the National Research Council.

Canadian Journal of Physics

Issued by THE NATIONAL RESEARCH COUNCIL OF CANADA

VOLUME 29 NOVEMBER, 1951 NUMBER 6

CONSERVATION LAWS IN FEYNMAN'S MODIFIED ELECTRODYNAMICS[1]

BY P. N. DAYKIN[2]

Abstract

In Feynman's treatment of the self-energy problem, the divergence is eliminated by introducing a convergence factor into the integral over the virtual photon momentum space. Feynman has remarked that his choice of convergence factor is inconsistent with the conservation of energy for the radiation field of an atom. This problem is examined in a more general way. The modification of the Maxwell equations caused by the convergence factor is deduced. The modified field equations belong to the generalized electrodynamics described by Podolsky. The modified energy-momentum tensor is shown to satisfy the conservation law for the field with source.

In Feynman's (1, 2) treatment of the self-energy problem, the divergence which occurs for high momentum exchanges between electron and virtual photon is eliminated by introducing a relativistic cutoff. This cutoff is equivalent to expressing the self-energy as the difference between the effects of photons of zero rest mass and those of rest mass λ. The divergencies then cancel and the self-energy of the free electron can be expressed as a change in mass independent of the momentum.

In the expression for the self-energy of a bound electron, the largest term, which depends logarithmically on λ, can be eliminated by recalculating the term energies with the renormalized mass. Of the remaining terms, the real part gives the term shift and the imaginary part gives the radiation resistance.

Feynman has remarked, however, that this modification of quantum electrodynamics is incomplete because the radiation resistance depends slightly on the cutoff whereas the radiation field at great distances is independent of the cutoff. Thus the energy lost by an atom would not check with the energy absorbed by distant absorbers.

This remark consists of two separate points. Firstly, the source strength of the radiating atom depends on the cutoff. Secondly, the radiation field of a given source cannot be conserved because it depends on the cutoff near the source, but at great distances is independent of the cutoff. It is only the second point that is discussed in this paper.

[1] *Manuscript received June 21, 1951.*
Contribution from the Department of Physics, University of British Columbia, Vancouver, B.C.
[2] *Holder of a Fellowship under the National Research Council of Canada.*

For this point we need to investigate the conservation law for the field of a given arbitrary source. Feynman's notation will be used throughout. We consider a particular vector potential solution of the Maxwell equations,

$$\Box^2 A_\mu = -4\pi J_\mu \tag{1a}$$

$$\frac{\partial A_\mu}{\partial x_\mu} = 0, \tag{1b}$$

which may be written

$$A_\mu(2) = \int \delta_+(s_{21}^2)\, J_\mu(1)\, d^3x_1\, dt_1 \tag{1c}$$

where J_μ is the four-vector current of a source which is conserved and δ_+ is the singular solution of (1*a*) used by Feynman to express the Möller interaction between two charges, which consists of incoming waves from the past and outgoing waves to the future. Thus $A_\mu(2)$ is the sum of the field emitted by $J_\mu(1)$ in the past and the field to be absorbed by $J_\mu(1)$ in the future.

The modification of the classical electrodynamics results from the replacement of the singular δ_+ by some nonsingular function, f_+. To find the corresponding effect on the field equations, it is simplest to work in momentum space. The Fourier transform of A_μ, defined by

$$A_\mu(x) = \int a_\mu(k) \exp(-ik \cdot x) d^4k,$$

can be written $a_\mu(k) = -4\pi k^{-2} j_\mu(k)$. This is because $(-1/\pi k^2)$ is the transform of the δ_+ function and $j_\mu(k)$ is the transform of $J_\mu(x)$; the additional $4\pi^2$ comes from the integration over $d^3x_1\, dt_1$.

Feynman chooses for the transform of f_+ for the self-energy problem the function $(-\lambda^2/(k^2 - \lambda^2)k^2)$. The field transform a_μ is then altered to $a'_\mu(k)$,

$$a'_\mu(k) = 4\pi\lambda^2(k^2 - \lambda^2)^{-1} k^{-2} j_\mu(k).$$

Multiplication on the left by $(1 - k^2\lambda^{-2})k^2$ and k_μ shows that a'_μ satisfies the equations

$$(1 - k^2\lambda^{-2})k^2 a'_\mu(k) = -4\pi j_\mu(k),$$
$$k_\mu a'_\mu(k) = 0.$$

The second equation follows from the current conservation,

$$k_\mu j_\mu(k) = 0.$$

These are the transforms of the field equations

$$(1 - \lambda^{-2}\Box^2)\Box^2 A'_\mu(x) = -4\pi J_\mu(x), \tag{2a}$$

$$\frac{\partial A'_\mu}{\partial x_\mu} = 0, \tag{2b}$$

which are satisfied by A'_μ given by (1*c*), but with f_+ for δ_+.

If we take for the energy-momentum tensor of the field the Maxwell tension tensor, with the modified field strengths substituted for the Maxwell field strengths, (the primes are dropped for the rest of the paper),

$$4\pi T_{\mu\nu} = F_{\mu\alpha} F_{\alpha\nu} + \tfrac{1}{4} F_{\alpha\beta} F_{\alpha\beta} \delta_{\mu\nu}, \tag{3}$$

where $$F_{\mu\nu} = \frac{\partial A_\nu}{\partial x_\mu} - \frac{\partial A_\mu}{\partial x_\nu} = A_{\nu,\mu} - A_{\mu,\nu};$$

then the four-divergence of this tensor is

$$T_{\mu\nu,\nu} = - F_{\mu\alpha} J_\alpha + (4\pi\lambda^2)^{-1} F_{\mu\nu} \Box^2 F_{\mu\alpha,\alpha}, \tag{4}$$

as shown in the appendix.

The four-divergence of the energy-momentum in a charge free space does not vanish. Thus, for a source surrounded by distant absorbers, energy-momentum would be lost in the space between. The term which spoils the conservation law vanishes as λ^{-2} if λ is allowed to become infinite after mass renormalization. This result verifies the second point of Feynman's remark.

However Equations (2), the field equations, belong to the generalized electrodynamics described by Podolsky and others (3). The appropriate energy-momentum tensor for this field has been derived by Podolsky from the Lagrangian which gives the field equations (Equations (2)). Translated into Feynman's notation, and with a for λ^{-1}, this is

$$4\pi T_{\mu\nu} = F_{\mu\alpha} F_{\alpha\nu} + \tfrac{1}{4} F_{\alpha\beta} F_{\alpha\beta} \delta_{\mu\nu} - \frac{a^2}{2} [F_{\alpha\beta} \Box^2 F_{\alpha\beta} - F_{\alpha\beta,\beta} F_{\alpha\gamma,\gamma}] \delta_{\mu\nu}$$

$$+ a^2 [F_{\mu\alpha} \Box^2 F_{\nu\alpha} + F_{\nu\alpha} \Box^2 F_{\mu\alpha} - F_{\mu\alpha,\alpha} F_{\alpha\beta,\beta}]$$

where $$F_{\alpha\beta,\gamma} = \partial F_{\alpha\beta} / \partial x_\gamma, \text{ etc.}$$

The field then satisfies the energy-momentum conservation law

$$T_{\mu\nu,\nu} = - F_{\mu\alpha} J_\alpha,$$

as shown in the appendix.

The energy-momentum of the field may therefore be redefined in a way consistent with the modified electrodynamics so that the conservation law is satisfied. The expression for the force density, $F_{\mu\alpha} J_\alpha$, is formally the same as for the Maxwell field, but the field strengths are defined by the non-Maxwell Equations (2).

Acknowledgments

The author is indebted to the National Research Council for the grant of a Fellowship under which this research was carried out. The author wishes to thank Prof. F. A. Kaempffer for suggesting the problem and for his helpful advice and discussions during the investigation.

References

1. FEYNMAN, R. P. Phys. Rev. 74: 1430. 1948.
2. FEYNMAN, R. P. Phys. Rev. 76: 778. 1949.
3. PODOLSKY, B. Phys. Rev. 62: 68. 1942.

Appendix

Proof of Conservation Law

With the field strengths defined by

$$F_{\mu\nu} = A_{\nu,\mu} - A_{\mu,\nu} = -F_{\nu\mu} \tag{1}$$

where

$$A_{\nu,\mu} = \frac{\partial A_\nu}{\partial x_\mu},$$

we have the field equations

$$(1 - a^2\,\Box^2)\,F_{\mu\nu,\nu} = -4\pi J_\mu, \tag{2}$$

$$F_{\alpha\beta,\gamma} + F_{\gamma\alpha,\beta} + F_{\beta\gamma,\alpha} = 0. \tag{3}$$

From (1) and (3) follow the useful relations

$$F_{\alpha\beta,\beta\alpha} = F_{\alpha\beta,\alpha\beta} = 0,$$

$$(\tfrac{1}{2}\,F_{\alpha\beta,\mu} + F_{\mu\alpha,\beta})\,F_{\alpha\beta} = 0. \tag{4}$$

Differentiating the tensor expression gives

$$\begin{aligned}4\pi T_{\mu\nu,\nu} &= F_{\mu\alpha,\nu}\,F_{\alpha\nu} + F_{\mu\alpha}F_{\alpha\nu,\nu} + \tfrac{1}{2}\,F_{\alpha\beta,\mu}\,F_{\alpha\beta} \\ &\quad - \frac{a^2}{2}[F_{\alpha\beta,\mu}\,\Box^2 F_{\alpha\beta} + F_{\alpha\beta}\,\Box^2 F_{\alpha\beta,\mu} - 2\,F_{\alpha\beta,\beta\mu}F_{\alpha\gamma,\gamma}] \\ &\quad + a^2[F_{\mu\alpha,\nu}\,\Box^2 F_{\nu\alpha} + F_{\mu\alpha}\,\Box^2 F_{\nu\alpha,\nu} + F_{\nu\alpha,\nu}\,\Box^2 F_{\mu\alpha} + F_{\nu\alpha}\,\Box^2 F_{\mu\alpha,\nu} - F_{\mu\alpha,\alpha\nu}F_{\mu\beta,\beta}] \\ &= F_{\mu\alpha}(1 - a^2\,\Box^2)\,F_{\alpha\nu,\nu}.\end{aligned}$$

The remaining terms in a^2 can be rewritten, with the help of (1), as

$$\begin{aligned}&-(\tfrac{1}{2}\,F_{\alpha\beta,\mu} + F_{\mu\alpha,\beta})\,\Box^2 F_{\alpha\beta} - F_{\alpha\beta}\,\Box^2(\tfrac{1}{2}\,F_{\alpha\beta,\mu} + F_{\mu\alpha,\beta}) \\ &+ F_{\alpha\gamma,\gamma}(F_{\alpha\beta,\beta\mu} - \Box^2 F_{\mu\alpha} - F_{\mu\beta,\beta\alpha}).\end{aligned}$$

The first two brackets vanish by (4) and the third by (2) and (3). The conservation law then follows from (2).

For the Maxwell tension tensor the terms in a^2 are absent so the four-divergence is simply $4\pi T_{\mu\nu,\nu} = F_{\mu\alpha}\,F_{\alpha\nu,\nu}$. Equation (4) of the text then follows from (2) of the appendix.

NUCLEAR MAGNETIC MOMENT OF SCANDIUM OF MASS 45[1]

By D. M. Hunten[2]

Abstract

By the method of nuclear magnetic resonance, the magnetic moment of Sc^{45} (without diamagnetic correction) is found to be 4.74916 ± 0.00012. The correction is $+0.00717$ with unknown and possibly large error. The equipment designed to search for magnetic resonance by varying the field of the magnet is described, with special emphasis on the magnet current regulator.

Introduction

Nuclear magnetic resonance absorption (3,4) has been widely used in recent years to determine nuclear moments. The principles and general practice are well described in the literature and will not be repeated here. One of the greatest difficulties arises from the fact that the point of resonance is not usually very well known in advance, and therefore a search must be conducted. Most earlier experimenters (10,11,19) have chosen to fix the magnetic field and vary the frequency. This inevitably results in loss of flexibility in the radio-frequency apparatus. In the present work a magnet current regulator was so designed and constructed as to permit a slow, regular variation of magnetic field over a range of 2 to 1. This allowed the use of a radio-frequency bridge which would have been almost impossible to tune automatically. In practice this regulator maintained the field within one part in 140,000; such a system might well find use in other fields and is therefore described in detail below.

Apparatus

1. Magnet

An available magnet with $3\frac{3}{4}$ in. poles and adjustable gap had previously been used in work of this type (1). With a 1 in. gap, it required 5 amp. at 85 v. for 8000 gauss. This power was supplied by a motor-generator set and was regulated by controlling the generator field current. At its best, this system never regulated to better than one part in 10,000, and it was usually worse. This regulation was not considered good enough for automatic searching, though it was entirely adequate for observing resonances on the oscilloscope.

In order that the magnet current might be carried by a vacuum tube, the coils were rewound with number 22 Formex wire; 500 ma. at 900 v. then gave 8300 gauss. In practice, fields above 7000 gauss were not used, since in this region saturation of the iron in the poles made the field much less uniform.

[1] *Manuscript received April 4, 1951.*
Contribution from the Radiation Laboratory, McGill University, Montreal, Que.
[2] *Holder of a Fellowship under the National Research Council of Canada, 1948–49. Present address: Department of Physics, University of Saskatchewan, Saskatoon, Sask.*

Exact parallelism of the pole faces was found to be very important for uniformity. They were carefully ground flat and held parallel by a three-legged spacer. Ring shims were used to extend the region of the uniform field. By trial and error, the best thickness was found to be 1.5 times greater than those calculated from the article by Rose (13).

A very convenient device was used to check the uniformity of the field. This was a double probe consisting of two coils in series—placed ½ in. apart—and each containing a water (plus cupric chloride) sample about 2 mm. in diameter. This probe could be rotated about an axis passing through one of the water samples. A regenerative detector (1, 6) was connected to it, and this gave a separate peak on the oscilloscope for each sample, provided they were located in different fields. Differences of 0.2 gauss could be detected in this way.

2. Magnet Current Regulator

A block diagram of the regulator is shown in Fig. 1. Part of the voltage across the shunt is compared with the voltage of a Weston standard cell; the difference is chopped into 60 cycle a-c. by a Brown converter vibrator. This a-c. is amplified and converted back to d-c. by a phase sensitive detector which preserves the original polarity. After further amplification, this voltage controls the magnet current.

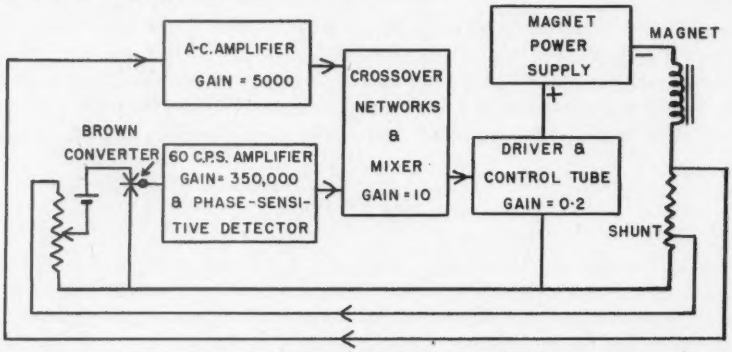

FIG. 1. *Block diagram of the magnet current regulator.*

This system appears to be the only one sufficiently stable for this application (5). It has, however, two defects: first, the d-c. output of the phase sensitive detector contains a large 120 cycle ripple component; and second, the high-frequency (i.e. transient) response is poor. The more the ripple is filtered out, the worse becomes the high-frequency response. Both defects are remedied by an a-c. channel in parallel with the above. By its regulating action, it suppresses the ripple by a factor of 5000, and at the same time it supplies the high-frequency response.

The loop gain is 100,000 for d-c. and 10,000 for a-c. Thus, output fluctuations will be reduced by these factors. For 10% line voltage change, the magnet current should change by one part in a million; rapid changes of 1% should

have the same effect. The ripple from the phase-sensitive detector is held to the same amount. If the voltage at A (on the shunt, Fig. 2) is considered the output, the feedback factor for a-c. is 1 and d-c. is 0.02 (when the potentiometer is at center-scale). This leads to the gains shown on the diagram for the various amplifiers, since the Brown converter–phase sensitive detector combination has a gain of 7. In actual practice, the gains were adjusted to give best operation and were not measured; hence the values shown are the design values only.

The schematic circuit is given in Fig. 2, with the blocks of Fig. 1 identified. Because of the wide range of currents to be handled by a single control (i.e. without change of supply voltage), the control tube must have a large plate dissipation rating; hence tubes such as 6AS7's are not suitable. A 304TH is very satisfactory, but at the higher currents the grid must be driven about 35 v. positive and then draws about 55 ma. This is supplied by the 6L6 cathode follower. The 180 ohm cathode resistor allows the grid to go negative while staying positive with respect to ground. The potentiometer in the grid circuit is used to cut off the magnet current slowly, in order to avoid dangerous switching transients. When it is turned all the way up, a cam on the shaft closes a microswitch, so that the sliding contact need not carry the grid current.

The shunt is wound with insulated manganin wire on a water cooled brass tube. A tap at 4 ohms feeds the d-c. comparing circuit, while the full 100 ohms feeds the a-c. channel. The network in parallel with the magnet makes the load a constant resistance of 1790 ohms at all frequencies, and produces a smooth and nearly flat response up to 20,000 cycles, the limit of the measurements. Without the network, the gain varies with frequency in an extremely complicated way, evidently as a result of self-resonances in the magnet. Since rapid changes in current are not expected to arise in the magnet itself, the regulation of the magnet current should not be affected.

The potentiometer in the comparing circuit is a 10 turn Helipot, driven by a clock motor through a gear train and a friction clutch which allows manual adjustments. The scanning rate may be changed by changing gears and by switching additional resistance in series. These wire-wound precision resistors also reduce the effect of the steps in the Helipot, which are quite perceptible when it is used alone.

The 60 cycle amplifier has a passband from 2 to 700 cycles; high frequencies are cut off to keep stray voltages from affecting the detector. This is simply a grid-controlled full-wave rectifier; the plate voltage is supplied by a small receiver power transformer. The small phase shift that was required is produced by the network in the primary circuit. The variable resistor in the cathode circuit serves as a manual current control; for best operation it should be set (with the regulator not operating) to give a current near that to be used.

The a-c. amplifier has a pass band from 0.1 to 200 cycles; the high-frequency cutoff goes at an average of 9 db. per octave to about one megacycle. This has an important bearing on the stability of the regulator and will be discussed below.

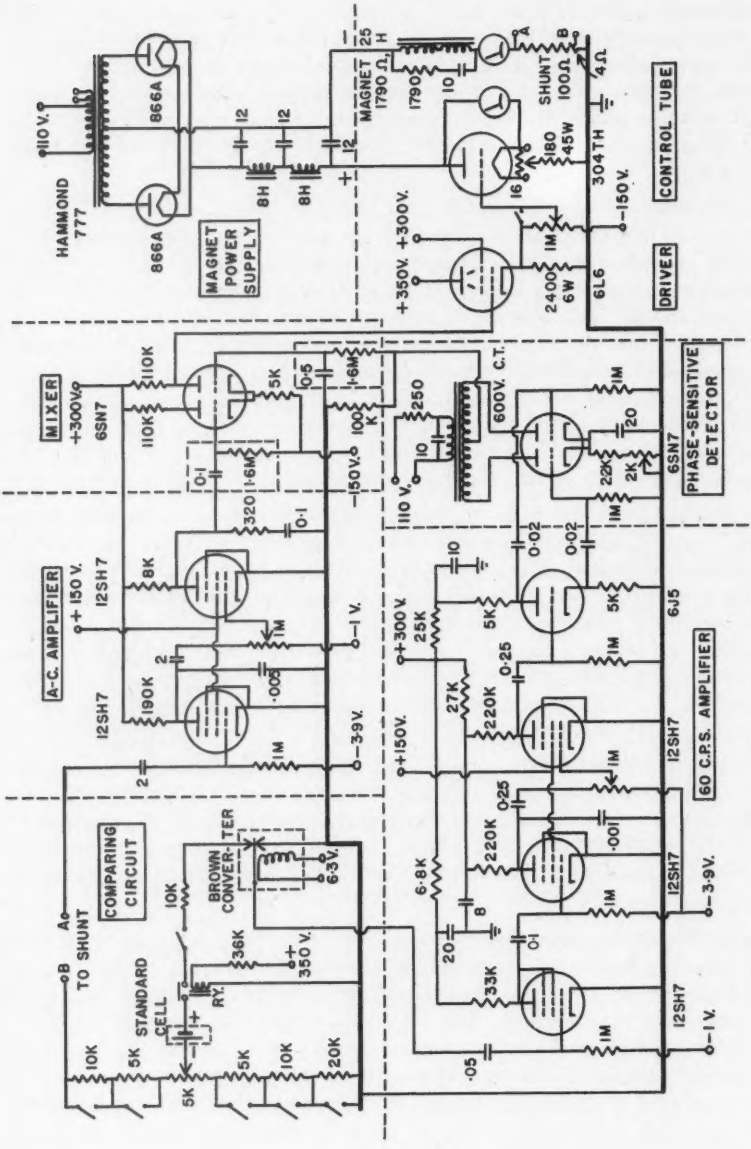

FIG. 2. *Circuit of the magnet current regulator.*

In order to avoid trouble with hum, which would be particularly bad in the 60 cycle amplifier, the five 12SH7's are heated with d-c. from the high-voltage supply. 12SH7's were used because they happened to be plentiful; but, in any case, the high-frequency cutoff of the a-c. channel requires tubes of high transconductance if it is to be shaped correctly.

Because of the unbypassed cathode resistor, the mixer stage adds the voltages applied to the grids. The crossover networks, shown enclosed in dotted lines, shape the cutoffs of the two channels to give a smooth transition in over-all gain from 100,000 to 10,000. This is important since improper choice of filter constants could easily produce enough phase shift, of opposite sign in the two channels, to give mutual cancellation of gain and a drop in the over-all characteristic below the gain of either channel alone. The crossover frequency is about 0.5 cycle per sec.; thus the low frequency filter removes a good deal of the 120 cycle ripple from the phase sensitive detector, and the a-c. channel removes the rest.

In order that the regulator should not oscillate, the loop gain should be less than 1 at any frequency where the phase shift is 180°. A high-frequency cutoff of 12 db. per octave will produce such a phase shift; any smaller slope is safe. As already noted, the actual slope is 9 db. per octave to one megacycle; the loop gain is down to 1 at 100 kc.

The d-c. power requirements are as follows: for the magnet, 1500 v., 500 ma.; for the regulator, 350 v., 250 ma. (6L6 and 12 v. heaters), 300 v. (regulated) at 35 ma., + 150 v. (VR tube) at 16 ma., and − 150 v. (VR tube) at 4 ma. The bias voltages of − 1 and − 3.9 are derived from the last; the 3.9 v. tap had to be decoupled by a 200 μf. condenser to ground.

Observation of the proton resonance on the oscilloscope showed that the magnetic field variations were about 1/20 gauss peak-to-peak, out of 7000 gauss total. Long-term stability was probably not quite so good; but in any case, it was not measured since it was of no importance for this application. Scanning was smooth and even, and readings could be reproduced as accurately as the dial could be read.

This system would be well adapted to control by the proton resonance. It was felt, however, that scanning would then be a good deal more difficult. It is likely that the radio-frequency spectrograph of Pound (10) would work equally well.

3. Other Apparatus

A twin-T bridge (2) was used; it was found to be very much easier to adjust than the type described by Bloembergen, Purcell, and Pound (4). The radio-frequency source was a General Radio 1001-A signal generator. This was fairly satisfactory, but did not have as good frequency stability as could be desired. A low-noise preamplifier (18) was followed by a Hallicrafters SX-42 receiver, lock-in amplifier, and recording meter in the usual arrangement. The magnetic field was modulated at 30 cycles by small coils around the magnet poles.

The regenerative detector already mentioned was used, with a different probe, to give the proton resonance for measurement of magnetic moments. Since the field was slightly different at the unknown sample, the proton resonance was observed simultaneously with the bridge. The regenerative detector could be made to lock in with the signal generator, and the difference in magnetic field measured on the oscilloscope. It never exceeded 0.5 gauss.

Method of Search

Since magnetic moments are known in advance only to $\pm 10\%$, and since one must not sweep over a resonance in less than several times the time constant of the indicating circuit, long searches are necessary. Experiments on the proton resonance showed that it could be considerably broadened, with no visible loss of amplitude on the recorder, by using modulation amplitudes larger than the line width; 1 gauss was about the best value. A scanning rate of 1 gauss per four time constants then gave a trace which was distorted but still easily recognized. This is an improvement of at least 10 times over the conditions that give an undistorted record.

The big advantage of a bridge over the circuits that scan in frequency (10, 11) is that it can observe the dispersion component of a resonance. Thus the radio-frequency voltage applied need only be chosen large to get the largest possible signal. For absorption, the sensitivity is best only for a certain voltage which is not known in advance. On the other hand, the bridge balance is not stable enough to allow it to be left unattended.

Experiments on Sc^{45}

Scandium has one isotope of mass 45. Spectroscopic measurements (7, 8, 14) give a spin of 7/2 and a magnetic moment of 4.8 nuclear magnetons. Theory (4) thus indicates that the signal should be strong. A solution of scandium nitrate was prepared by dissolving scandium oxide (spectroscopically pure) in nitric acid. The resonance was easily found near the expected place. Comparison with the proton resonance as described below gave the frequency ratios shown

TABLE I

OBSERVATIONS ON THE SCANDIUM RESONANCE

Run No.	Scandium frequency, Mc.	Proton frequency, Mc.	Ratio Sc/P
1	6.90100	28.40740	0.242930
2	6.90000	28.40356	0.242927
3	6.89930	28.40128	0.242922
4	6.89930	28.40141	0.242943
5	6.89929	28.40124	0.242945
6	6.89930	28.40127	0.242944
7	6.89932	28.40156	0.242951
8	6.89933	28.40090	0.242948
Mean ratio			0.242939 ± 0.000003

in Table I. Measurements were taken in rapid succession, each one consuming about 10 min. There was no evidence of drift in the magnetic field.

The Helipot dial setting for the center of the scandium resonance was noted as the field was slowly scanned past; this was done three times to make sure that everything was stable. The dial was set to this point and the proton resonance centered on a 1 gauss oscilloscope sweep, and the two frequencies measured.

If the g-factor of the proton is taken (16) as 5.58536 ± 0.00012, the magnetic moment of Sc^{45} is 4.74916 ± 0.00012 nuclear magnetons. The diamagnetic correction (9, 17) is $+ 0.00717$, with a probable error difficult to assign. If it is taken as 10%, the final result is 4.756 ± 0.0007 nuclear magnetons. The spectroscopic value, + 4.8, is thus only 1% low.

Discussion

In view of the recently observed dependence of resonance frequency on chemical compound, this result is not as accurate as is indicated by the probable error of observation. It is not possible at present to say how large such an error might be.

Other workers have independently found this resonance and measured the magnetic moment. Proctor and Yu (12) find a frequency ratio of 0.24289 ± 0.00004, with scandium nitrate, and Sheriff and Williams (15) 0.24296 ± 0.00005 with the chloride. Both agree within their errors with the more accurate measurements reported here.

The author is indebted to many members of the Radiation Laboratory for stimulating discussions, to the machine shop staff for their careful work, and to Dr. A. L. Thompson for help with the sample. He wishes to thank especially Dr. D. A. Anderson, who built the original apparatus, Mr. M. Bloom, who helped with the rebuilding, and Dr. J. S. Foster, who supervised the work and contributed valuable suggestions and encouragement.

References

1. ANDERSON, D. A. Thesis, McGill University. April, 1949. Phys. Rev. 76: 434. 1949.
2. ANDERSON, H. L. Phys. Rev. 76: 1460. 1949.
3. BLOCH, F., HANSEN, W. W., and PACKARD, M. Phys. Rev. 69: 127. 1946.
4. BLOEMBERGEN, N., PURCELL, E. M., and POUND, R. V. Phys. Rev. 73: 679. 1948.
5. GREENWOOD, I. A. JR., HOLDAM, J. V. JR., and MACRAE, D. JR. Electronic instruments. McGraw-Hill Book Co. Inc., New York. 1948. p. 513.
6. HOPKINS, N. J. Rev. Sci. Instruments, 20: 401. 1949.
7. KOPFERMANN, H. and RASMUSSEN, E. Z. Physik, 92: 82. 1934.
8. KOPFERMANN, H. and WITTKE, H. Z. Physik, 105: 16. 1937.
9. LAMB, W. E. JR. Phys. Rev. 60: 817. 1941.
10. POUND, R. V. and KNIGHT, W. D. Rev. Sci. Instruments, 21: 219. 1950.
11. PROCTOR, W. G. Phys. Rev. 79: 35. 1950.
12. PROCTOR, W. G. and YU, F. C. Phys. Rev. 78: 471. 1950.
13. ROSE, M. E. Phys. Rev. 53: 715. 1938.
14. SCHULER, H. and SCHMIDT, TH. Naturwissenschaften, 22:758. 1934.
15. SHERIFF, R. E. and WILLIAMS, D. Phys. Rev. 79: 175. 1950.
16. SOMMER, H., THOMAS, H. A., and HIPPLE, J. A. Phys. Rev. 80: 487. 1950.
17. TAUB, H. and KUSCH, P. Phys. Rev. 75: 1481. 1949.
18. VALLEY, G. E. JR. and WALLMAN, H. Vacuum tube amplifiers. Chapt. 10. McGraw-Hill Book Co. Inc., New York. 1948.
19. ZIMMERMAN, J. R. and WILLIAMS, D. Phys. Rev. 76: 350. 1949.

A FUNDAMENTAL THEORY OF THE MAGNETISM OF MASSIVE ROTATING BODIES[1]

By George Luchak[2]

Abstract

A phenomenological theory, based on a relativistically covariant generalization of Maxwell's equations to include gravitational fields, is developed to account for the magnetic fields of massive rotating bodies. The equations yield the Wilson–Blackett expression for the magnetic moment of the earth and stars but give no magnetic field for mass-bodies moving without rotation in their own gravitational fields. They indicate that the magnetic field due to the motion of the earth in its orbit is negligibly small compared to the field due to its rotational motion, and they provide a possible explanation for the variable magnetic fields of light-variable stars.

Blackett (2) has recently drawn attention to the approximate validity for the earth, sun, and five stars, of the empirical formula

$$\mathbf{P} = -\beta G^{\frac{1}{2}}\mathbf{U}/2c \tag{1}$$

between the magnetic moment $\mathbf{P}$ and the angular momentum $\mathbf{U}$, where G is the gravitational constant, c is the velocity of light, and β is a constant of the order of unity characteristic of the body. $\mathbf{P}$ and $\mathbf{U}$ range in relative value from 10^{10} to 1, and the magnetic fields, on which the values of $\mathbf{P}$ are based, range in relative value from 1800 to 1. From a detailed discussion, Blackett concluded that Equation (1) was the manifestation of a new property of matter not yet included in present day physical theory, and, since it contained the gravitational constant, might well be the result of interaction between gravitational and electromagnetic fields.

A simple hypothesis, from which Equation (1) can be derived, was given by Wilson (14) who postulated that a mass element Δm moving with velocity $\mathbf{V}$ produced a magnetic field at distance r given by

$$\mathbf{H} = -\beta(G^{\frac{1}{2}}/c)\Delta m(\mathbf{V} \times \mathbf{r})/r^3, \tag{2}$$

in analogy with the magnetic field of a moving charge. Wilson's equation can also be written in the equivalent form

$$\mathbf{J} = -\beta(G^{\frac{1}{2}}/c)\rho\mathbf{V}, \tag{3}$$

where ρ is the mass density, $\mathbf{V}$ is the velocity, and $\mathbf{J}$ is a fictitious current due to the motion of the mass. Equation (3) and, through it, Equation (2), are not satisfactory physical laws because they are not relativistically covariant, and predict a magnetic field due to translational motion. Swann (10) tried to remedy the objections to Wilson's theory but his subsequent equations proved to be physically untenable (11). The most recent attempt to improve

[1] *Manuscript received April 30, 1951.*

[2] *Defence Research Board Experimental Station, Ralston, Alta. This research was initiated while the author was a graduate student at the Department of Physics, University of Toronto, Toronto, Ont.*

on the Wilson expression was made by Papapetrou (7) who postulates that to every mass element there corresponds a unique point which he calls its gravitational center. Then, if u^i is the four dimensional velocity vector of the mass element, U^i is the corresponding vector for the gravitational center and ω is a quantity satisfying the equation

$$\Box\, \omega = \frac{\partial p^i}{\partial x^i}, \tag{4}$$

where

$$p^i = \rho G^{\frac{1}{2}}(u^i - U^i), \tag{5}$$

then he writes

$$s_i = \frac{\partial \omega}{\partial x^i} - p_i, \; (p_i = \eta_{ik} p^k) \tag{6}$$

where η_{ik} is the metric tensor of flat space and s_i is the four dimensional current vector to replace the three dimensional current vector **J** in Equation (3). It can be shown (6) that Equations (4) to (6) are not relativistically covariant and, furthermore, do not determine s_i uniquely for any given physical situation.

Since there appears to be no evidence in the quantum mechanics of materials at ordinary temperatures and pressures for an interaction which might lead to Equation (1), it is probable that such an effect manifests itself only under the extreme physical conditions existing in the earth's core and in the sun and stars. Ramsey (8) has recently shown that, at the boundary of the core, the effect of high pressure is sufficient to change radically the properties of matter from a molecular to a metallic state. The presence of such a transition might well lead to quantum effects analogous to those that occur at low temperatures. Since, however, a suitable quantum mechanical theory of superconductivity is not yet available, it seems unlikely that a quantum theory explanation for Equation (1) is to be found easily. It is possible, on the other hand, to proceed from the other end and to produce a phenomenological theory, as was done by London and London (5) to describe superconductivity, by a suitable generalization of Maxwell's equations. Into these equations it will be necessary to incorporate a gravitational field in a relativistically covariant fashion and, in addition, an interaction of the proper sort between the electromagnetic and gravitational vectors. One consequence of such an interaction, according to Tzu (12), is the necessity of introducing at least one new parameter in addition to G and c. Referring again to the London theory, it is interesting to note that the extension of Maxwell's equations to superconducting media is accompanied by the introduction of a parameter Λ whose value depends on the substance and its physical state. It is here suggested that the new parameter which is to appear in the interaction term of a theory which might lead to Equation (1) is not a universal constant for all matter in all states, but varies with physical conditions and is only appreciably different from zero under conditions similar to those that obtain in the sun, stars, and in the core of the earth. This is contrary to the theories of Wilson, Swann, and Papapetrou. Recent work by Runcorn (9)

demonstrating that the outer crust of the earth does not contribute to the main geomagnetic field is corroborating evidence.

I. Formulation of the Equations

Maxwell's equations for macroscopic media, expressed in tensor form, are

$$F_{ab,c} + F_{bc,a} + F_{ca,b} = 0, \tag{7}$$

$$G^{ab}{}_{,b} = 4\pi J^a; \tag{8}$$

to these are added

$$K_a = F_{ab}J^b, \tag{9}$$

where

$$F_{ab} = \begin{bmatrix} 0 & B_z & -B_y & -iE_x \\ -B_z & 0 & B_x & -iE_y \\ B_y & -B_x & 0 & -iE_z \\ iE_x & iE_y & iE_z & 0 \end{bmatrix}, \tag{10}$$

$$G^{ab} = \begin{bmatrix} 0 & H_z & -H_y & -iD_x \\ -H_z & 0 & H_x & -iD_y \\ H_y & -H_x & 0 & -iD_z \\ iD_x & iD_y & iD_z & 0 \end{bmatrix}, \tag{11}$$

$$J^a = [\, J_x/c,\ J_y/c,\ J_z/c,\ i\rho \,], \tag{12}$$

$$K_a = [\, \mathbf{g},\ iW/c \,], \tag{13}$$

and

$$J^b = \eta^{ab}J_a, \tag{14}$$

where imaginary time $x^4 = ict$ is used, where $\eta^{ab} = \begin{pmatrix} 1 & & & \\ & 1 & & \\ & & 1 & \\ & & & 0 \end{pmatrix}$ is the metric tensor of flat space and $\mathbf{g}$ is the force density, ρ the charge density, J_x the x component of the current density, E_x the x component of the electric field, H_x the x component of the magnetic field, B_x the x component of the magnetic induction, and D_x the x component of the electric displacement vector when Equations (7), (8), and (9) are written out in Cartesian coordinates, and gaussian units are used. A formal distinction between covariant and contravariant tensors is unnecessary for flat space but is retained in order that a possible extension of the equations to general covariance will be obvious.

Following Corben (3), Equations (7), (8), and (9) are generalized to include gravitational fields as follows. They are extended to five dimensions while their form and the interpretations of F_{ab}, G^{ab}, J^a, and K^a ($a, b, = 1, 2, 3, 4$) are retained. In the extension, F_{ab} and G^{ab} are kept skew symmetric. Thus, nine new quantities (F_{15}, F_{25}, F_{35}, F_{45}), (G^{15}, G^{25}, G^{35}, G^{45}), and J^5 are introduced. It is obvious that F_{a5} and G^{a5} are four-vectors and J^5 is an invariant when the fifth dimension transforms into itself and the four physical dimensions transform in Lorentz space. Maxwell's equations in five-space are

$$F_{\alpha\beta,\gamma} + F_{\beta\gamma,\alpha} + F_{\gamma\alpha,\beta} = 0, \tag{15}$$

and

$$G^{\alpha\beta}{}_{,\beta} = 4\pi J^\alpha, \ (\alpha, \beta, \gamma = 1, 2, 3, 4, 5). \tag{16}$$

When these equations are rewritten so that five-dependence in the tensors or coordinates is shown explicitly, we get

$$F_{ab,c} + F_{bc,a} + F_{ca,b} = 0, \tag{17}$$

$$F_{5b,c} + F_{bc,5} + F_{c5,b} = 0, \tag{18}$$

$$G^{ab}{}_{,b} + G^{a5}{}_{,5} = 4\pi J^a, \tag{19}$$

and

$$G^{5b}{}_{,b} = 4\pi J^5, \ (a, b, c = 1, 2, 3, 4). \tag{20}$$

If Equation (9) is written out in five dimensions in the familiar vector form,

$$\mathbf{g} = \rho\mathbf{E} + (\mathbf{J} \times \mathbf{B})/c + J^5\mathbf{F}, \tag{21}$$

and

$$W = \mathbf{J} \cdot \mathbf{E} + J^5 cF_{45}/i, \tag{22}$$

where $\mathbf{F}$ is a three-vector whose components are F_{15}, F_{25}, and F_{35}. Thus $J^5\mathbf{F}$ would appear to be the gravitational force per unit volume and $J^5cF_{45}/i \equiv cq$ the rate at which gravitational forces do work on unit volume. This would suggest that a four-vector

$$\mathfrak{F}_a = (J^5/\nu)F_{a5} \tag{23}$$

be introduced, where ν is the rest-mass density in e.s.u., and thus an invariant, and $\mathfrak{F}_a$ is the four dimensional gravitational field vector. Equation (20) reduces to a four dimensional version of the Poisson equation if

$$G^{b5} = (J^5/\nu)\mathfrak{F}^b. \tag{24}$$

Writing $(J^5/\nu) = -\xi$, Equations (23) and (24) become

$$F_{a5} = -\xi^{-1}\mathfrak{F}_a, \tag{25}$$

and

$$G^{b5} = -\xi\mathfrak{F}^b, \tag{26}$$

where ξ is an invariant. It is worth noting that the relation

$$G^{b5} = \xi^2 F^{b5} \tag{27}$$

is analogous to the 'pair' properties $\mathbf{D} = \epsilon\mathbf{E}$ and $\mathbf{B} = \mu\mathbf{H}$ for isotropic media where ϵ and μ are scalar functions of position which characterize the electromagnetic properties of matter in the large. The inference to be drawn is that ξ is still another scalar in the same category. For simplicity we will consider, in all that follows, only homogeneous media for which ξ is constant. The appropriate generalization for nonisotropic, nonhomogeneous media will be obvious. Thus Equations (17) to (20) become

$$F_{ab,c} + F_{bc,a} + F_{ca,b} = 0, \tag{28}$$

$$\mathfrak{F}_{c,b} - \mathfrak{F}_{b,c} - \xi F_{bc,5} = 0, \tag{29}$$

$$G^{ab}{}_{,b} - \xi\mathfrak{F}^a{}_{,5} = 4\pi J^a, \tag{30}$$

and

$$\mathfrak{F}^b{}_{,b} = -4\pi\nu, \ (a, b, c = 1, 2, 3, 4). \tag{31}$$

Now it remains to interpret $F_{bc,5}$ and $\mathfrak{F}^a{}_{,5}$. If $\mathfrak{F}^a{}_{,5} \equiv F_{bc,5} \equiv 0$, we have a generalization of Maxwell's equations with gravitational forces but with no interaction between the electromagnetic and gravitational fields. Such an interpretation is inadequate for the purpose at hand. The simplest remaining interpretation is to take either $F_{bc,5}$ or $\mathfrak{F}^a{}_{,5}$ identically zero and to choose the other in a suitable manner. Suppose $\mathfrak{F}^a{}_{,5} \equiv 0$. Then Equations (28) and (30) become

$$F_{ab,c} + F_{bc,a} + F_{ca,b} = 0,$$

and

$$G^{ab}{}_{,b} = 4\pi J^a.$$

These are the ordinary Maxwell equations. Thus, if there are no impressed charges or currents, the electromagnetic field will go to zero. Such a theory could not account for the Wilson–Blackett expression (1). The other alternative is to take $F_{bc,5} \equiv 0$ and $\mathfrak{F}^a{}_{,5} \not\equiv 0$. Here $\mathfrak{F}^a{}_{,5}$ is a four-vector and, if there is to be interaction, it must depend on $\mathfrak{F}^a$. The dimensions must be $[\mathfrak{F}^a]\,[L]^{-1}$ and, according to the Wilson–Blackett expression, it must vanish identically for a nonrotating sphere in the time-independent state. Thus, the interaction term must depend on the kinematic conditions. The simplest possible kinematic vector is the four-velocity u^c, and we assume that it appears in the interaction term in the simplest possible way. To arrive at an interaction which is also a four-vector, u^c must be multiplied by either a scalar which involves $\mathfrak{F}^a$ or a tensor of rank two formed from $\mathfrak{F}^a$. The simplest scalar that can be constructed is $\mathfrak{F}^a{}_{,a} = -4\pi\nu$. This leads to a four dimensional Wilson–Blackett expression which is rejected as unsatisfactory (7). The simplest tensor of rank two that can be formed from $\mathfrak{F}^a$ is $\mathfrak{F}^a{}_{,c}$. The expression $\mathfrak{F}^a{}_{,c}\, u^c$ fulfills all the required conditions and Equations (28) to (31) can now be written in their final form

$$F_{ab,c} + F_{bc,a} + F_{ca,b} = 0, \tag{32}$$

$$\mathfrak{F}_{c,b} - \mathfrak{F}_{b,c} = 0, \tag{33}$$

$$G^{ab}{}_{,b} - \xi\mathfrak{F}^a{}_{,c}\, u^c = 4\pi J^a, \tag{34}$$

and

$$\mathfrak{F}^b{}_{,b} = -4\pi\nu, \tag{35}$$

where all indices run from 1 to 4.

Equations (32) to (35) are obviously internally consistent, since (33) and (35) can be solved uniquely, as is shown by Corben (3), and (32) and (34) are merely Maxwell's equations for moving media with an additional four dimensional current $\xi\mathfrak{F}^a{}_{,c}\, u^c$. The four dimensional divergence of the latter is not necessarily zero. A consequence is that, in the above description, charges may be induced by the motion of matter through gravitational fields. Maxwell's equations for moving media, without gravitational interaction, exhibit the same phenomenon.

Equations (32) to (35), written in the familiar vector form, become

$$\text{div } \mathbf{B} = 0, \tag{36}$$

$$\text{curl } \mathbf{E} + \frac{1}{c}\frac{\partial \mathbf{B}}{\partial t} = 0, \tag{37}$$

$$\text{curl } \mathbf{H} - \frac{1}{c}\frac{\partial \mathbf{D}}{\partial t} - \frac{\xi}{c}\left[\frac{\partial \mathbf{F}}{\partial t} + V_x\frac{\partial \mathbf{F}}{\partial x} + V_y\frac{\partial \mathbf{F}}{\partial y} + V_z\frac{\partial \mathbf{F}}{\partial z}\right] = \frac{4\pi}{c}\mathbf{J} \tag{38}$$

$$\text{div } \mathbf{D} - \frac{\xi}{c}\left[\frac{\partial q}{\partial t} + \mathbf{V}\cdot\text{grad } q\right] = 4\pi\rho, \tag{39}$$

$$\text{grad } q + \frac{1}{c}\frac{\partial \mathbf{F}}{\partial t} = 0, \tag{40}$$

$$\text{div } \mathbf{F} + \frac{1}{c}\frac{\partial q}{\partial t} = -4\pi\nu, \tag{41}$$

and $$\text{curl } \mathbf{F} = 0, \tag{42}$$

where $\mathbf{V} = (V_x, V_y, V_z)$ is the three dimensional velocity vector, terms of the order of $|\mathbf{V}/c|^2$ or greater have been neglected, and

$$\mathbf{J} = \sigma\left(\mathbf{E} + \frac{\mathbf{V}\times\mathbf{B}}{c}\right) \tag{43}$$

is the well known three dimensional current density for moving media, where σ is the electrical conductivity.

Since Equations (36) to (42) are covariant for special relativity, it is important to designate which are to be inertial systems. These are chosen, in our case, from among those that have no inherent angular velocity. Since it is allowable to speak of velocities of rotation in an absolute manner, without the necessity of specifying any framework with respect to which the angular displacement takes place, the distinction is valid (13).

II. Magnetic Field of a Sphere Rotating in its own Gravitational Field

Consider a sphere for which $\xi \neq 0$, whose angular velocity ω is constant, and for which the rest-mass density ν is constant within the sphere and zero outside. Assume that conditions are independent of time. Equations (36) to (42), for an observer stationary at the center of the sphere, then become

$$\text{div } \mathbf{B} = 0, \tag{44}$$

$$\text{curl } \mathbf{E} = 0, \tag{45}$$

$$\text{curl } \mathbf{H} - \frac{\xi}{c}\left[V_x\frac{\partial \mathbf{F}}{\partial x} + V_y\frac{\partial \mathbf{F}}{\partial y} + V_z\frac{\partial \mathbf{F}}{\partial z}\right] = \frac{4\pi}{c}\mathbf{J}, \tag{46}$$

$$\text{div } \mathbf{D} - \frac{\xi}{c}\mathbf{V}\cdot\text{grad } q = 4\pi\rho, \tag{47}$$

$$\text{grad } q = 0, \tag{48}$$

$$\text{div } \mathbf{F} = -4\pi\eta G^{\frac{1}{2}}, \tag{49}$$

and

$$\text{curl } \mathbf{F} = 0, \tag{50}$$

where $\mathbf{V} = (-\omega y, +\omega x, 0)$, $\eta = G^{-\frac{1}{2}}\nu$ is the rest-mass density in c.g.s units and $\mathbf{B} = \mu\mathbf{H}$, $\mathbf{D} = \epsilon\mathbf{E}$.

Equations (49) and (50) can be solved to give $\mathbf{F} = -\frac{4\pi}{3}\eta G^{\frac{1}{2}}\mathbf{r}$ which, when substituted in Equation (46), leads to

$$\text{div } \mathbf{B} = 0, \tag{51}$$

$$\text{curl } \mathbf{E} = 0, \tag{52}$$

$$\text{curl } \mathbf{H} = \frac{4\pi\sigma}{c}\left[\mathbf{E} + \frac{\mathbf{V}\times\mathbf{B}}{c}\right] - \frac{4\pi}{c}\left(\eta\frac{G^{\frac{1}{2}}\xi}{3}\right)\mathbf{V}, \tag{53}$$

and

$$\text{div } \mathbf{D} = 4\pi\rho. \tag{54}$$

From Equation (53) it can be seen, by taking the divergence of both sides, that

$$\text{div}\left(\mathbf{E} + \frac{\mathbf{V}\times\mathbf{B}}{c}\right) = 0. \tag{55}$$

It is also evident that

$$\text{curl}\left(\mathbf{E} + \frac{\mathbf{V}\times\mathbf{B}}{c}\right) = 0, \tag{56}$$

since curl $\mathbf{E} = 0$, and curl $(\mathbf{V}\times\mathbf{B}) = -\omega\left[\frac{\partial B_r}{\partial\phi}, \frac{\partial B_\theta}{\partial\phi}, \frac{\partial B_\phi}{\partial\phi}\right] = 0$,

where $[B_r, B_\theta, B_\phi]$ is the vector $\mathbf{B}$ in spherical coordinates and there is symmetry in ϕ.

Equations (55) and (56) have the solution

$$\mathbf{E} + \frac{\mathbf{V}\times\mathbf{B}}{c} = 0. \tag{57}$$

Thus Equations (51) to (54) reduce to

$$\text{div } \mathbf{B} = 0, \tag{58}$$

$$\text{curl } \mathbf{E} = 0, \tag{59}$$

$$\text{curl } \mathbf{H} = -\frac{4\pi}{3}\left(\frac{\eta\xi G^{\frac{1}{2}}}{c}\right)\mathbf{V}, \tag{60}$$

and

$$\text{div } \mathbf{D} = 4\pi\rho, \tag{61}$$

where

$$\rho = -\frac{\epsilon}{4\pi c}\,\text{div}\,(\mathbf{V}\times\mathbf{B}), \tag{62}$$

since $$\mathbf{D} = -\frac{\epsilon}{c}(\mathbf{V} \times \mathbf{B}) \text{ from Equation (57).}$$

Equations (58) to (61) lead to the Wilson–Blackett expression (1).

Assuming that $\xi \neq 0$ in the core of the earth and $\xi = 0$ in the crust and in the atmosphere, it turns out that $\xi = 10$ in the core. For the sun, assuming a polar magnetic field of 30 gauss, $\xi \simeq 1.6$, and for the average for five stars $\xi \simeq 1.7$ (*cf.* Blackett (2)). Thus, for the earth and sun, ξ seems to be approximately numerically equal to the density for material at high temperatures and pressures.

III. The Magnetic Field Due to the Motion of the Earth in the Sun's Gravitational Field

The earth, in its motion about the sun, will generate gravitational waves (3). To a first approximation, however, neglecting terms in (V/c) where V is the velocity of a mass element of the earth and c is the velocity of light, the gravitational field is obtained by taking the static field of the earth and transporting it along with the earth in its motion. The gravitational field acting on any mass element is now composed of two parts; the gravitational field due to the sun, and the gravitational field due to the remainder of the earth. If the mass of the sun is M, its average density is ρ_s and its radius is A, then the gravitational field at a distance R is

$$\mathbf{F}_s = -\frac{MG\mathbf{R}}{R^3} \qquad \text{c.g.s. units,}$$

or $$\mathbf{F}_s = -\frac{4\pi}{3}\rho_s G^{\frac{1}{2}}(A/R)^3\,\mathbf{R} \qquad \text{e.s.u.} \tag{63}$$

The gravitational field at a mass element in the core due to the earth itself is

$$\mathbf{F}_e = -\frac{4\pi}{3}\rho_e G^{\frac{1}{2}}\,\mathbf{r} \qquad \text{e.s.u.,} \tag{64}$$

where $\mathbf{r}$ is the distance from the center of the earth to the mass element and ρ_e is the density of the core (assumed to be uniform). It is now necessary to calculate

$$\frac{\partial \mathbf{F}}{\partial t} + V_x\frac{\partial \mathbf{F}}{\partial x} + V_y\frac{\partial \mathbf{F}}{\partial y} + V_z\frac{\partial \mathbf{F}}{\partial z} \tag{65}$$

for points in the core where $\xi \simeq 10$, $\rho_e \simeq 10$ (4), and $\mathbf{F} = \mathbf{F}_s + \mathbf{F}_e$. If the earth is rotating with angular velocity ω, the velocity of any point in the core is

$$\mathbf{V} = \mathbf{v} + \omega \times \mathbf{r}, \tag{66}$$

where $\mathbf{v}$ is the velocity of the mass center and ω and $\mathbf{r}$ are measured with respect to a coordinate system whose origin moves with the center of the earth and whose coordinate axes are always parallel to the axes of the non-

rotating observer at the center of the sun. An elementary calculation then shows that (see appendix)

$$\frac{\partial \mathbf{F}}{\partial t} + V_x \frac{\partial \mathbf{F}}{\partial x} + V_y \frac{\partial \mathbf{F}}{\partial y} + V_z \frac{\partial \mathbf{F}}{\partial y} =$$

$$- \frac{4\pi\rho_e}{3} G^{\frac{1}{2}} \omega \times \mathbf{r} - \frac{4\pi\rho_s}{3} G^{\frac{1}{2}} (A/R)^3 [\mathbf{v} + \omega \times \mathbf{r}]$$

$$+ 4\pi\rho_s G^{\frac{1}{2}} (A/R)^3 (\mathbf{R}/R) [(\mathbf{R}/R) \cdot \mathbf{v} + (\mathbf{R}/R) \cdot \omega \times \mathbf{r}]. \qquad (67)$$

The first term in Equation (67) leads to the 'rotational' magnetic field. Taking $R \sim 1.5 \times 10^{13}$ cm., $A \sim 7 \times 10^{10}$ cm., $|\mathbf{v}| \sim 30 \times 10^6$ cm./sec., and $|\omega \times \mathbf{r}| \sim 1.2 \times 10^4$ cm./sec. for half the rotational velocity at the core's equator, then $\frac{(A/R)^3 |\mathbf{v}|}{|\omega \times \mathbf{r}|} \sim 2.5 \times 10^{-5}$.

Thus the nonrotational components of the earth's field due to interaction with the sun's gravitational field are negligibly small compared to the rotational component.

IV. Other Effects

A double star with highly elliptic orbits would exhibit a periodic magnetic field. It can be seen from Equation (67) that there would be times when the terms involving $(A/R)^3$ would be small and other times when they would make a significant contribution to the magnetic field. If the rotation of one of the components of the double star were retrograde with respect to its direction of revolution about the other component, it might be possible, in addition, to observe a reversal of magnetic field.

If a star moves without rotation in its own gravitational field, the change of vector and scalar functions following the motion is zero and thus, in Equations (38) and (39),

$$\frac{\partial \mathbf{F}}{\partial t} + V_x \frac{\partial \mathbf{F}}{\partial x} + V_y \frac{\partial \mathbf{F}}{\partial y} + V_z \frac{\partial \mathbf{F}}{\partial z} = 0,$$

and

$$(\text{grad } q) \cdot \mathbf{V} + \frac{\partial q}{\partial t} = 0.$$

Such a star would exhibit no electromagnetic field.

V. Acknowledgment

I should like to thank Dr. E. C. Bullard, F.R.S., for arousing my interest in the subject of geomagnetism.

References

1. BLACKETT, P. M. S. Nature, 159: 658. 1947.
2. BLACKETT, P. M. S. Phil. Mag. Ser. 7, 40: 125. 1949.
3. CORBEN, H. C. Phys. Rev. 69:225. 1946.
4. ELSASSER, W. M. Revs. Modern Phys. 22: 1. 1950.
5. LONDON, F. and LONDON, H. Proc. Roy. Soc. (London), A, 149: 71. 1935.
6. LUCHAK, G. Phil. Mag. Ser. 7, 42: July issue. (In press). 1951.
7. PAPAPETROU, A. Phil. Mag. Ser. 7, 41: 399. 1950.
8. RAMSEY, W. H. Monthly Notices Roy. Astron. Soc. Geophys. Supp. 5 (9): 409. 1949.
9. RUNCORN, S. K. Phil. Mag. Ser. 7, 41: 783. 1950.
10. SWANN, W. F. G. Phil. Mag. 3: 1088. 1927.
11. SWANN, W. F. G. and LONGACRE, A. J. Franklin Inst. 206: 421. 1928.
12. TZU, H. Y. Nature, 160: 746. 1947.
13. WHITTAKER, E. T. Phil. Mag. Ser. 7, 36: 101. 1945.
14. WILSON, H. A. Proc. Roy. Soc. (London), A, 104: 451. 1923.

Appendix

DERIVATION OF EQUATION (67)

Equations (63) and (64) give

$$\mathbf{F} = \mathbf{F}_s + \mathbf{F}_e = -\frac{4\pi}{3} G^{\frac{1}{2}}[\rho_s (A/R)^3 \mathbf{R} + \rho_e \mathbf{r}].$$

If the coordinates of the mass-center of the earth are given by

$$\mathbf{R}_1 = [X_1(t),\ Y_1(t),\ Z_1(t)],$$

then $$\mathbf{r} = \mathbf{R} - \mathbf{R}_1(t);$$

thus $$\mathbf{F} = \frac{-4\pi}{3} G^{\frac{1}{2}} [\rho_s (A/R)^3 \mathbf{R} + \rho_e (\mathbf{R} - \mathbf{R}_1(t))],$$

and
$$\frac{\partial \mathbf{F}}{\partial X} = \frac{-4\pi}{3} G^{\frac{1}{2}} \left[\rho_s (A/R)^3 \mathbf{i} - 3\rho_s (A/R)^3 \frac{X}{R} \frac{\mathbf{R}}{R} + \rho_e \mathbf{i} \right],$$

$$\frac{\partial \mathbf{F}}{\partial Y} = \frac{-4\pi}{3} G^{\frac{1}{2}} \left[\rho_s (A/R)^3 \mathbf{j} - 3\rho_s (A/R)^3 \frac{Y}{R} \frac{\mathbf{R}}{R} + \rho_e \mathbf{j} \right],$$

$$\frac{\partial \mathbf{F}}{\partial Z} = \frac{-4\pi}{3} G^{\frac{1}{2}} \left[\rho_s (A/R)^3 \mathbf{k} - 3\rho_s (A/R)^3 \frac{Z}{R} \frac{\mathbf{R}}{R} + \rho_e \mathbf{k} \right],$$

$$\frac{\partial \mathbf{F}}{\partial t} = \frac{-4\pi}{3} G^{\frac{1}{2}} \left[-\rho_e \frac{\partial \mathbf{R}_1(t)}{\partial t} \right],$$

where $\mathbf{R} = (X\mathbf{i} + Y\mathbf{j} + Z\mathbf{k})$, and $\dfrac{\partial \mathbf{R}_1(t)}{\partial t} = \mathbf{v}$.

Thus Equation (67) readily follows.

THE HALF-LIFE OF IRIDIUM 192[1]

By J. Kastner

Abstract

A Lauritsen electroscope was used to compare the intensity of an Ir^{192} source with a radium standard. The result of a least squares fitting of the decay curve was a half-life of Ir^{192} of 74.37 ± 0.07 days.

Introduction

In an investigation of the use of Ir^{192} as a source of gamma radiation for radiography (6), wide deviations were noticed in the various values of the half-life quoted in the literature (Table I).

TABLE I

Various values of the half-life of Ir^{192}

Value, days	Author	Date
60	Fermi and Amaldi (2)	1936
68	Jaeckel (5)	1938
70 ± 1	Friedlander *et al.* (3)	1944
75 ± 3	Goodman and Pool (4)	1947

It was felt that a more precise knowledge of the half-life would be worthwhile in view of the potential industrial and medical importance of this isotope. Since the commencement of this work two more values not quite in agreement were reported: 74.5 ± 0.7 days by Sinclair and Holloway (7) and 78 days by Cork *et al.* (1).

TABLE II

Analysis of data—Ir^{192}

Relative activity	Logarithm (relative activity)	Time, days	Residuals
1.834	0.2634	0	+ 0.0008
1.412	0.1498	28.01	+ 0.0006
1.125	0.0512	51.13	− 0.0045
1.025	0.0107	62.19	− 0.0001
0.942	− 0.0262	72.01	+ 0.0027
0.812	− 0.0904	86.02	− 0.0048
0.718	− 0.1442	100.16	− 0.0013
0.636	− 0.1965	114.18	+ 0.0031
0.558	− 0.2532	128.14	+ 0.0029
0.486	− 0.3131	142.14	− 0.0003
0.431	− 0.3658	156.00	+ 0.0030
0.381	− 0.4190	170.18	+ 0.0069
0.327	− 0.4849	184.06	− 0.0025

[1] *Manuscript received May 22, 1951.*
Contribution from the Division of Physics, National Research Laboratories, Ottawa. Issued as N.R.C. No. 2540.

A Lauritsen electroscope was used to compare the intensity of the Ir^{192} source used in the radiographic experiments with that of a 100 mgm. radium standard. A careful comparison was made at about two-week intervals for an observation period extending over more than six months (two and one-half half-lives).

The linearity of the decay curve, and thus the radioactive purity of the source, were established by the method of least squares (8) from the data obtained. These data are shown in Table II. The least squares fitting supplied the decay equation, log (relative activity) = 0.2626 − 0.004048 days, from which was calculated the half-life and its probable error. The result was a half-life of Ir^{192} of 74.37 ± 0.07 days, which agrees with and is rather more precise than the value of 74.5 ± 0.7 days published during the course of the present work (7).

Acknowledgments

I wish to thank Dr. Adair Morrison, Radiology Laboratory, for suggesting the need of a precise determination of the iridium half-life, and for his helpful criticism. I also wish to acknowledge the assistance of Miss Helen Kulas in the measurements and calculations.

References

1. CORK, J. M., LEBLANC, J. M., STODDARD, A. E., CHILDS, W. J., BRANYAN, C. E., and MARTIN, D. W. Bull. Am. Phys. Soc. 26 (3): 31. 1951
2. FERMI, E. and AMALDI, E. Ricerca sci. Ser. II, 7 (1): 56. 1936.
3. FRIEDLANDER, H. N., SEREN, L., and TURKEL, S. H. Plutonium Project Report. CP1827 (June, 1944). Reference F103 from Seaborg and Perlman, Revs. Modern Phys. 20: 647. 1948.
4. GOODMAN, L. J. and POOL, M. L. Phys. Rev. 71: 288. 1947.
5. JAECKEL, R. Z. Physik, 110: 330. 1938.
6. MORRISON, A. Non-destructive Testing. In press. 1951.
7. SINCLAIR, W. K. and HOLLOWAY, A. F. Nature, 167: 365. 1951.
8. WORTHING, A. G. and GEFFNER, J. Treatment of experimental data. John Wiley & Sons, New York. 1943. p. 249.

SOME QUANTITATIVE MEASUREMENTS OF THREE-CENTIMETER RADAR ECHOES FROM FALLING SNOW[1]

By R. C. Langille[2] and R. S. Thain[2]

Abstract

In the winter of 1948-49 a series of measurements was made at Ottawa in an attempt to verify, by experiment, the theoretical computations of J. W. Ryde for the intensity of backscattering of 3 cm. radio waves by snowflakes. The radiation backscattered from falling snow was measured, together with the actual mass of snow per cubic meter of atmosphere. Whenever possible the size distribution of the snowflakes was determined. Owing to the small number of snowstorms studied, firm conclusions cannot be drawn. However, the results obtained are in agreement with those predicted by Ryde, and provide useful practical information.

1. Introduction

Rainstorms cause echoes to appear on radar sets, operating at centimeter wave lengths, owing to radiation being backscattered from the raindrops. Similarly, radiation backscattered from snowflakes will cause radar echoes.

From theoretical considerations Ryde (5) has given quantitative measures of the above mentioned phenomena in terms of the radio frequency power backscattered from the respective particles. A theoretical expression for the case of rain, and the modifications of this expression for the case of snow are discussed in Section 2.

In Section 3 a description is given of an experiment which was performed to measure the power of radar signals of wave length 3.3 cm. returned from falling snow. The comparison of the experimental results with those obtained theoretically is given in Section 4.

2. Theoretical Considerations

J. W. Ryde's theoretical expression for the power of the backscattered radiation from rain has been modified by Marshall, Langille, and Palmer (4). Assuming that the cross-sectional area of the radar beam is uniformly filled with falling rain and that the size of the raindrops is small compared with the wave length, the appropriate expression is

$$P_r = \frac{P_0 \pi^4 A h (\eta^2 - 1)^2}{8 r^2 \lambda^4 (\eta^2 + 2)^2} Z,$$

where

P_r = backscattered power received at the radar set,
P_0 = peak output power of the radar,

[1] *Manuscript received June 13, 1951.*
Contribution from Defence Research Telecommunications Establishment (Radio Physics Laboratory), Ottawa, Ont.
[2] *Defence Research Telecommunications Establishment (Radio Physics Laboratory).*

A = effective area of the antenna,
h = pulse length,
η = refractive index of water,
r = range of the rain from the radar set,
λ = wave length,
$Z = \Sigma(D^6)$ = sum of the sixth powers of the diameters of the raindrops in unit volume of atmosphere.

According to Ryde the expression for rain should also hold in the case of snow provided:

(*a*) $\Sigma(m^2)$ be considered rather than $\Sigma(D^6)$, where $\Sigma(m^2)$ is the sum of the squares of the masses in unit volume of atmosphere. Thus D^6 is replaced by $\left[\frac{6m}{\pi\rho}\right]^2$ where ρ is the density of ice.

(*b*) the refractive index for ice is substituted for η.

(*c*) A dimensionless factor ϵ is introduced to account for the nonspherical shape of the snowflakes. According to Ryde ϵ is equal to unity for spheres, and to approximately two for plates and needles. (In this paper ϵ has been assumed to be equal to unity).

After collecting constants and substituting for η the value 1.75 (3), and for ρ the value 0.916 gm./cc., the expression in the case of power reflected from snow becomes

$$P_r = 8.78 \frac{P_0 hA}{\lambda^4 r^2} \Sigma(m^2).$$

For the calculation of $\Sigma(m^2)$ the following two methods may be used:

(*a*) by assuming the snowflakes to be of equal mass, then

$$\Sigma(m^2) = Nm_0^2 = Mm_0,$$

where

N = total number of snowflakes per unit volume of atmosphere,
m_0 = mass of a single snowflake,
M = total mass of snow per unit volume of atmosphere.

(*b*) by assuming that the masses of the snowflakes are nonuniform and by obtaining the snowflake mass distribution from collected samples of snowflakes.

Both methods require measurements of the rate of snowfall, R, and a knowledge of the velocity of fall of the snowflakes.

3. Experimental

The measurements described in this report were made at Ottawa, Canada, in the winter of 1948-49. A modified naval radar equipment (type SU) was used.

Power measurements were made by comparing, on an A-scope presentation, the signal received from falling snow with a signal from a 3.3 cm. signal generator,

fed into the radar by means of a wave guide directional coupler. The attenuator of the signal generator was adjusted at two-minute intervals to match the amplitude of the reference signal with that of the signal reflected from the snow. The range was limited to 1000 yd. in order to study the physical properties of the snow.

The physical properties of the snow producing the echoes were measured from a mobile shelter mounted on a truck. In order to clear local obstructions it was necessary to elevate the radar beam 15° above the horizontal. In this way the radar echoes were received from snow located approximately 800 ft. above the ground surface at a range of 1000 yd. The mobile shelter was placed in a position such that it would intercept the snow that produced the snow signal on the radar. In the calculations an allowance was made for the time necessary for the snow to reach the ground.

The rate of snowfall was determined by weighing the snow that accumulated on a rubber ground sheet. The ground sheet measured 48 × 70 in. and was placed flat on the ground well removed from obstructions. Every five minutes the sheet was lifted and the snow was placed in an aluminum bowl. The bowl and the snow were weighed on a beam balance inside the mobile shelter. This measurement of the rate of snowfall appeared to be quite satisfactory for low wind speeds. At wind speeds greater than 10 miles per hour it is doubtful whether this method gave a reliable measure of the rate of snowfall. Attempts were made to develop a type of snow measuring device which would draw in air and snowflakes and separate out the snow. Four models were tried and, although the last model was quite promising, insufficient measurements were made to trust the results.

The size distribution of the snowflakes was measured by means of the dyed filter paper technique used for determining the size of raindrops (4).

Samples of snowflakes were caught on filter papers which had been lightly dusted with gentian violet dye. The papers were then held over an electric heater for a moment to allow the snowflakes to melt, producing stains the areas of which were proportional to the masses of the original snowflakes.

For each of the measurements of P_r, the value of $\Sigma(m^2)$ was determined from a measurement of the rate of snowfall, R, over the corresponding time interval and from the data obtained by a filter paper exposed during a portion of this time interval. The snowflake stains on the filter paper were divided up into class intervals having $m_1^2, m_2^2, \ldots, m_i^2$ as the means of the squares of the masses of the respective intervals. Thus

$$\Sigma(m^2)_f = \Sigma n_1 m_1^2 + n_2 m_2^2 \ldots\ldots + n_i m_i^2 \text{ where } n_1, n_2, \ldots\ldots, n_i$$

are the numbers of snowflakes in each respective class. The subscript "f" refers to the filter paper measurement.

Assuming that the filter paper represents the true snowflake distribution over the time interval of the corresponding P_r measurement, then $\Sigma(m^2) = k\,\Sigma(m^2)_f$ where k is a numerical constant which is, in fact, the ratio that the

sample bears to a unit volume of atmosphere. This numerical constant could be obtained by considering the size of the filter paper and the length of time of exposure. However, it was considered that the measurement of the latter would constitute a possible large source of error in the results. Hence, it was decided to obtain the value of the numerical constant k by assuming that the velocity of fall, v, of the snowflakes was constant(2), and by using the corresponding measurement of the rate of snowfall, R, to obtain Σm, the total mass of snow per cubic meter of atmosphere.

$$\Sigma m = \frac{R}{3.6v},$$

where Σm is given in gm./cu.m. (atmosphere)
R is given in mm./hr. (water)
v is given in m./sec.

But $\Sigma m = k\,\Sigma m_f$

where $\Sigma m_f = \Sigma n_1 m_1 + n_2 m_2 + \ldots\ldots + n_i m_i.$

Thus $\Sigma m = k\,\Sigma m_f = \dfrac{R}{3.6v}.$

$$k = \frac{\Sigma m}{\Sigma m_f} = \frac{R}{3.6v\,\Sigma m_f},$$

thus
$$\Sigma(m^2) = \frac{R}{3.6v}\,\frac{\Sigma(m^2)_f}{\Sigma m_f}$$
$$= \frac{R}{3.6v}\,\frac{\Sigma n_1 m_1^2 + n_2 m_2^2 + \ldots n_i m_i^2}{\Sigma n_1 m_1 + n_2 m_2 + \ldots n_i m_i},$$

and the equation in the case of snow becomes

$$P_r = 2.44\,\frac{P_0 h A}{\lambda^4 r^2}\,\frac{R\Sigma(m^2)_f}{v\,\Sigma m_f}.$$

Correcting for units and substituting the values for the radar set parameters, $\lambda = 3.31$ cm., $P_0 = 20$ kw., $h = 0.5$ μsec., $A = 1555$ cm.^{2}, $r = 1000$ yd. and taking v as 1 m./sec. the equation becomes

$$P_r = 1.13 \times 10^{-6}\,\frac{R\,\Sigma(m^2)}{\Sigma m},$$

where P_r is in milliwatts,
R is in mm./hr. (water),
m is in mgm.

4. Results

During the winter of 1948-49 measurements were made on 13 snowstorms but sufficient data for analysis was obtained on only four storms. Of these four storms, trustworthy size distribution data were obtained on only one, the 22nd of February.

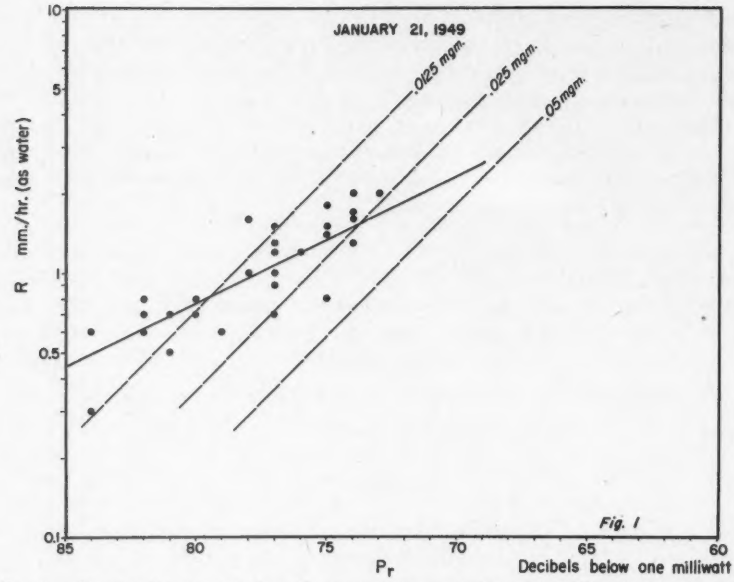

FIG. 1. *The data for Jan. 21 show the power of the snow echo received, P_r, plotted against the rate of snowfall, R. The solid line is the least squares line through the experimental points. If all the snowflakes were of equal mass, the P_r predicted by theory is shown by the broken lines. Broken lines for three possible flake masses are shown. On this day the approximate temperature at 800 ft. altitude was* $-1\frac{1}{2}°C$.

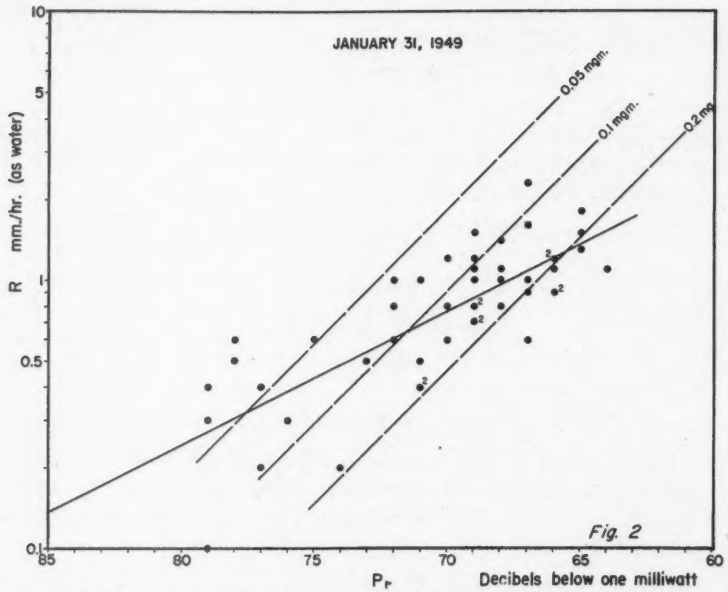

FIG. 2. *The data for Jan. 31 are similar to those of Fig. 1. The number beside some experimental points indicates more than one point at this position. The temperature at 800 ft. altitude was about* $-10°C$.

Fig. 1 shows the results for Jan. 21. On this day insufficient information regarding size distribution was obtained for the purposes of comparison with theory and it was assumed that all the snowflakes were of equal mass. Mass sizes were chosen to agree with the experimental results. The masses required are of a reasonable order of magnitude but the experimental results require that the mass of the flakes should increase as the rate of snowfall increases.

Fig. 2 displays the results for Jan. 31. The situation was similar to that on Jan. 21 except that it was necessary to assume flakes of greater mass to fit the experimental results. On this day also, the experimental results require that the mass of the flakes should increase as the rate of snowfall increases.

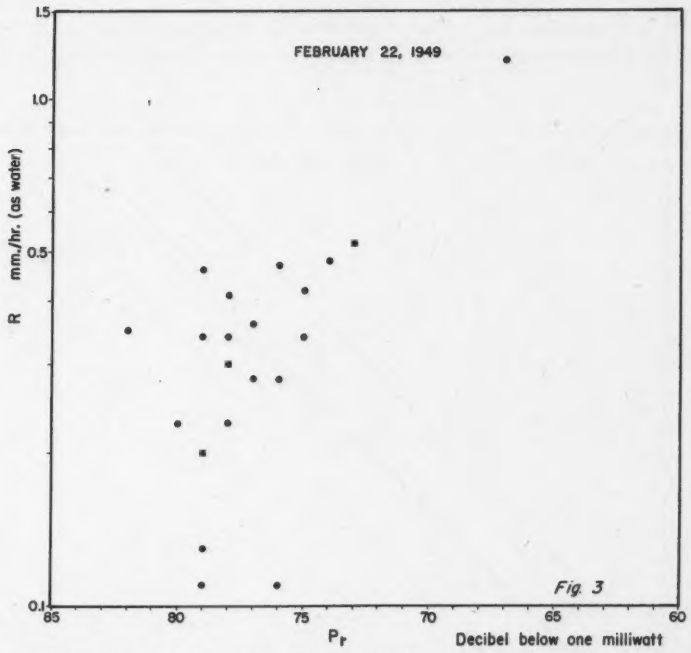

FIG. 3. *This shows all experimental points for Feb. 22. The points for which size distributions were obtained are shown in Fig. 5. The temperature at 800 ft. was approximately + 10°C.*

Fig. 3 shows all the results for Feb. 22. The correlation between P_r and R is poor on this day and no least squares line has been drawn.

Fig. 4 shows the results for Mar. 9 and 10. The slope of the least squares line is different from that of Jan. 21 and 31 and indicates that the masses of the snowflakes were more uniform than on the other days, and according to theory should be about .05 mgm.

Size distribution data were available for only a portion of the power measurements for Feb. 22. These measurements have been plotted in Fig. 5 without applying the correction for the size distribution data. It was found that P_r and R gave a correlation coefficient of 0.67. In Fig. 6 the points in Fig. 5 have been corrected for the size distribution of the snowflakes, and P_r and $\frac{R\Sigma(m^2)}{v\,\Sigma m}$ gave a correlation coefficient of 0.79. The result predicted by theory is shown by the broken line in Fig. 6. There is a difference of approximately four decibels between the experimental and theoretical results and it is possible that this may have been due in part to the method of measurement in which

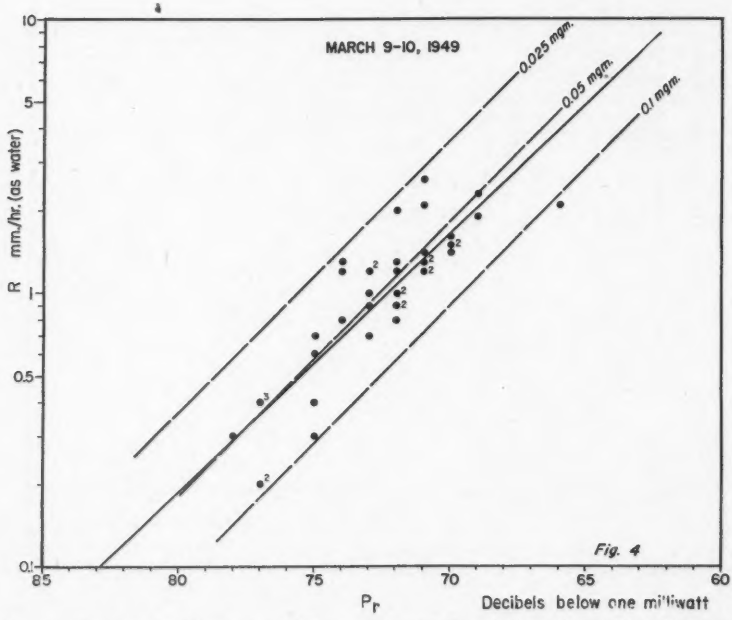

FIG. 4. *The data for March 9 and 10 are similar to those of Jan. 21 and 31. The number beside some points indicates more than one point at this position. The temperature at 800 ft. was approximately* $-3°C$.

a pulsed reference signal was compared with a noise-type snow signal. It is interesting to note that Hood (1) in measurements of the radar echo intensities of rain on 10 and 3 cm. found the experimental results to be low by 4.5 db.

A comparison of rain and snow signals was attempted using both horizontally and circularly polarized radiation at 3 cm. wave length. Unfortunately the quarter-wave plate was not constructed until very late in the winter season and only a few results were obtained. The table below is characteristic of the results obtained.

	Horizontal polarization	Circular polarization
Snow echo	21 db. (above noise)	12 db.
Rain echo	20 db.	11 db.

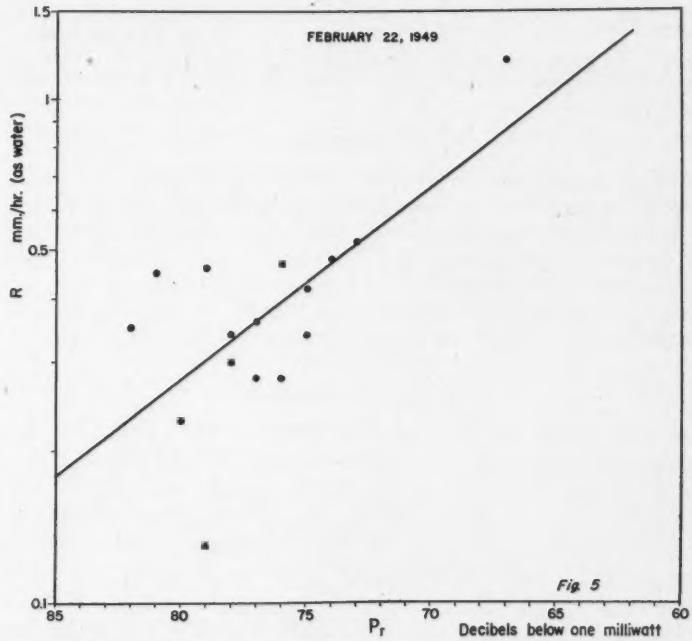

FIG. 5. *The above points have not been corrected for size distribution data. The line is the least squares line for the experimental points. The correlation coefficient for P_r and R is 0.67.*

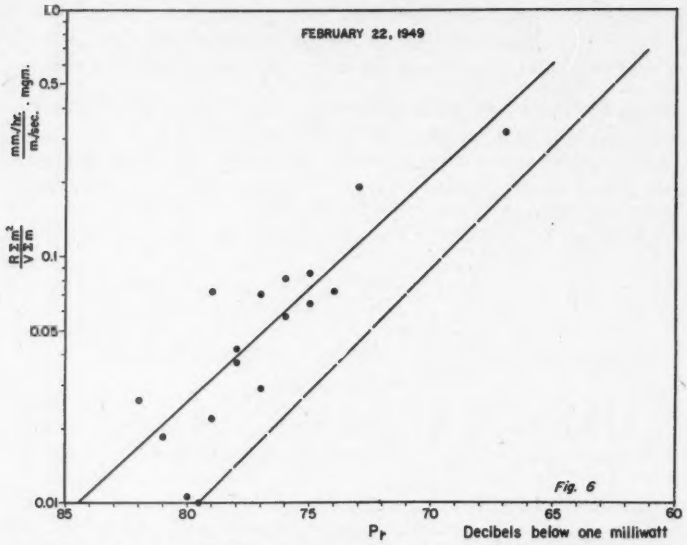

FIG. 6. *This graph shows the effect of applying the size distribution correction to the points in Fig. 5. The broken line is the theoretical result predicted by Ryde. The correlation coefficient for* P_r *and* $\frac{R\Sigma m^2}{v\Sigma m}$ *is 0.79.*

5. Conclusions

Although insufficient snowstorms were studied for firm conclusions, the results are in agreement in magnitude with those predicted by Ryde. The size distribution of snowflakes appears to be important in calculating the radar echo to be expected from a particular snowstorm. However, reasonable estimates may be made from rates of snowfall alone. It would seem that the snow echo for any rate of snowfall for any particular radar set could be calculated with fair accuracy by employing Ryde's theoretical expression.

6. Acknowledgment

The work described in this paper was carried out as a part of the research program of the Radio Physics Laboratory of the Defence Research Telecommunications Establishment. The authors wish to acknowledge the able assistance of Mr. L. A. Mairs and Mr. M. Psutka in the experimental work. The assistance of the National Research Council and, in particular, that of Dr. G. A. Miller, is also gratefully acknowledged.

References

1. HOOD, A. D. National Research Council of Canada Report ERA–180 (NRC No. 2155). June, 1950.
2. HOOPER, N. E. N. and KIPPAX, A. A. Quart. J. Roy. Met. Soc. 76: 125. 1950.
3. LAMB, J. Trans. Faraday Soc. 42: 238. 1946.
4. MARSHALL, J. S., LANGILLE, R. C., and PALMER, W. M. J. Met. 4: 186. 1947.
5. RYDE, J. W. Report of Conference on Meteorological Factors in Radar-Wave Propagation, p. 169. The Physical Society, London, 1946.

SHADOW-CASTING WITH HALIDES IN THE ELECTRON MICROSCOPE[1]

By William H. Barnes and Margaret S. Lambe[2]

Abstract

Experiments on the behavior of halides as shadow-casting agents in electron microscopy are described. The use of calcium fluoride, placed directly on the specimen screen, is suggested as a convenient method for routine qualitative shadowing of preparations in the preliminary stages of an electron microscopic study. No vacuum coating equipment is required.

Introduction

The observation that certain substances in the electron microscope show autoshadowing is not new (2). The effect is most noticeable under intense electron bombardment from a biased gun. The present investigation arose from a routine examination of cryptocrystalline aggregates, interspersed with long slender needles, of lithium fluoride obtained from aqueous solution by Dr. D. F. Stedman in the Applied Physical Chemistry Laboratory, National Research Council. Heavy shadowing of all samples was observed in the electron microscope. It was traced immediately to relatively large masses of the lithium fluoride by selecting several areas of the specimen screens and following the shadows back to their origins by appropriate movement of the specimen stage.

The exceptionally strong autoshadowing of lithium fluoride, of which an example is shown in Fig. 1 (top left), suggested that this salt might be employed as a shadowing agent for other objects. It was realized, of course, that the effect would only be qualitative since there could be no control over the angle of shadowing. Owing to the simplicity of adding one or two particles of a salt directly to a specimen screen, however, as compared with the usual vacuum coating equipment and shadowing procedure, it seemed worthwhile to investigate this possibility in more detail and to examine the shadowing possibilities of other halides.

Experimental

Dow polystyrene latex particles (580G, Lot 3584) (1), were selected as objects for the tests. The following halides were chosen as potential shadowing agents largely on the basis of ready availability in reagent, or reasonably pure, grades: fluorides of aluminum, barium, cadmium, calcium, chromium, lithium, potassium, sodium, zinc; chlorides of calcium, cadmium, chromium, cobalt, copper, potassium, silver, sodium; bromides of cadmium, copper, lead, mercury, potassium, sodium; iodides of barium, cadmium, calcium, sodium.

[1] *Manuscript received July 3, 1951.*
Contribution from the Division of Physics, National Research Council, Ottawa. Issued as N.R.C. No. 2554.

[2] *Present address: Electronic Computer Project, The Institute for Advanced Study, Princeton, N.J.*

The individual salts were added dry to the specimen screens in the form of fine powders or very small crystals. Best results were obtained by the use of very small quantities (0.05 mgm. or less) in the form of an individual crystal or an aggregate. In the latter case, shadowing was not successful unless the size of the constituent particles was larger than about two microns. The salt was placed on the Formvar supporting film covering the specimen screen after a drop of the latex suspension had been added and allowed to dry. Upon insertion of the specimen in the microscope the intensity of the electron beam was kept as low as possible during initial focusing. Some of the salts shadowed even under these conditions; with others, shadowing did not occur until the beam intensity was increased.

Although shadowing was observed on individual screens of most of the salts examined, only a very few of the halides gave consistently good results.

In general, the fluorides shadowed most easily. They usually gave reasonably even and fine grained backgrounds except when too large a particle was employed with a resultant excessive deposit on the objects and supporting film. Sodium and calcium fluorides were consistently the best.

It was difficult to obtain appreciable shadowing with the chlorides even under intense electron bombardment. When shadowing did occur the background frequently was very grainy and sometimes coarsely crystalline. Very fine powders usually gave no shadowing while those having a larger particle size tended to cause the electron beam to behave erratically with consequent rapid variations in intensity and focus. Both sodium and calcium chlorides appeared to have a direct effect on the latex particles causing them to become fluid, to spread out in smears over the screen, and to coalesce.

The bromides and iodides shadowed more easily than the chlorides although rather intense electron beams were required in most cases. The quality of the shadowed images, however, generally was very poor owing to heavy, granular, and uneven backgrounds.

For a particular anion, best results were obtained with salts of the alkali and alkaline earth metals. For a particular cation, the fluoride was the most effective salt.

A few examples of the shadowing effect are presented in Fig. 1 (fluorides) and Fig. 2 (chlorides, bromides, iodides). The magnification factor for each photograph is indicated by a line, representing a length of approximately one micron, below each picture. The reproductions are in the form of negative prints. The shadowed objects are Dow latex particles in each case except Fig. 1, top left, which illustrates the autoshadowing of lithium fluoride, and Fig. 1, second from bottom right, for which a bacterium (*E. coli*, four hour culture) was employed.

The photographs have been selected from a very large number of micrographs as representing a typical cross section of the more satisfactory obser-

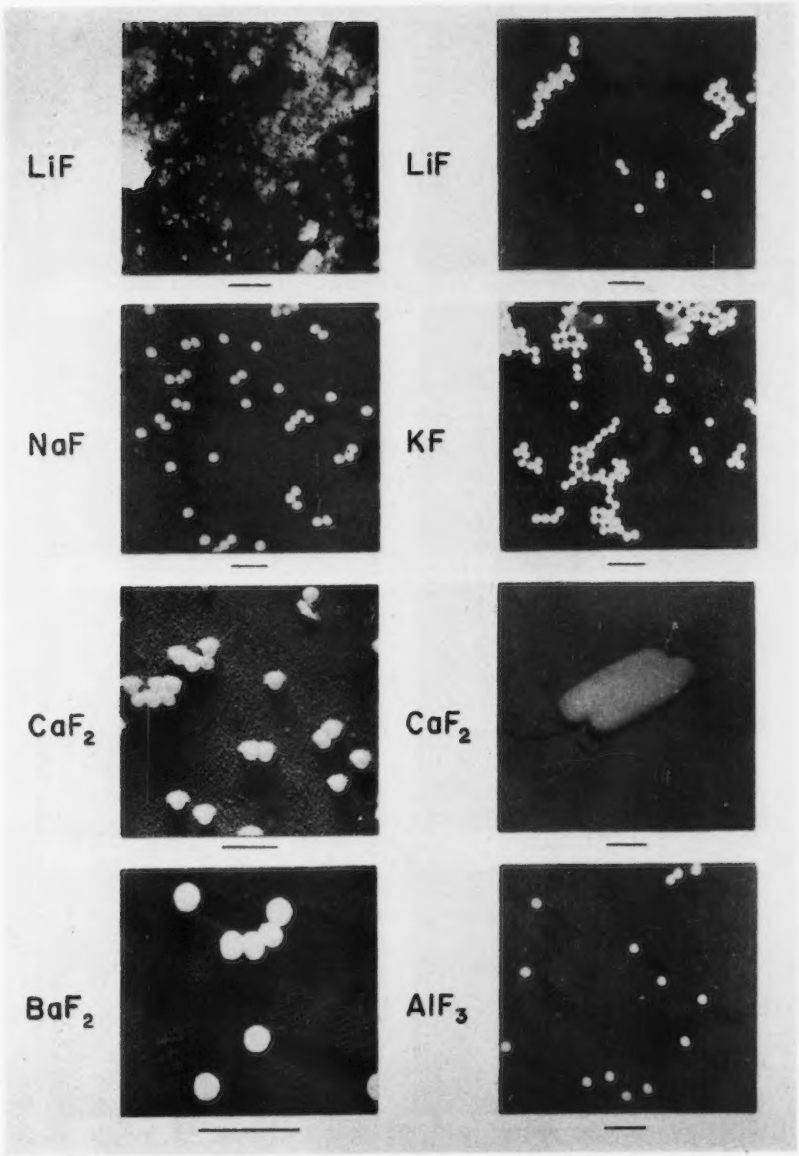

FIG. 1. *Shadow-casting with fluorides.*

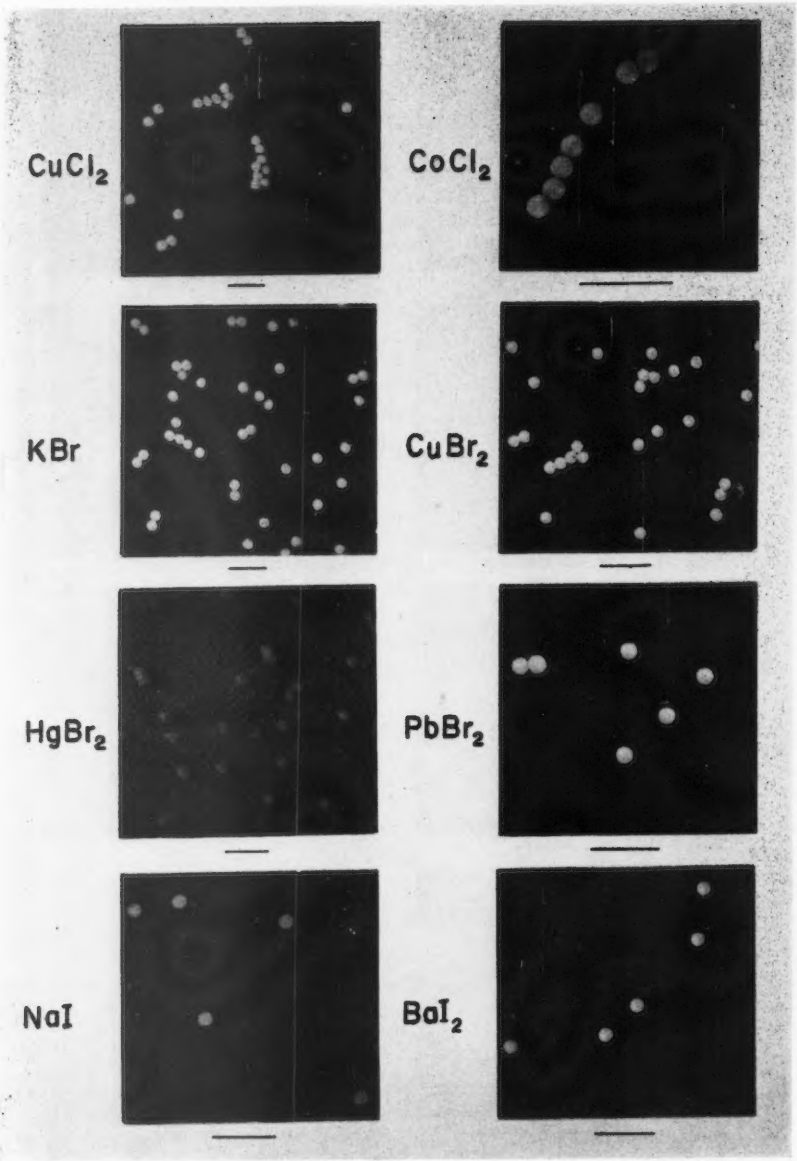

FIG. 2. *Shadow-casting with chlorides, bromides, and iodides.*

vations. Thus, in Fig. 1, the occasional appearance of shadowing from two directions is illustrated with sodium fluoride and barium fluoride. Excessive coating of the latex particles and background when too large a quantity of the shadow-casting agent is used is shown with calcium fluoride. A markedly flat field with doubled shadows (possibly an artifact) appears in Fig. 2, sodium iodide. A similar effect was observed in one or two photographs (not shown) with other iodides. On other occasions, however, the same salts gave better results (e.g., Fig. 2, barium iodide).

Conclusion

The shadow-casting operation is most successful in the case of the fluorides probably because of their relatively high thermal stability which ensures simple sublimation of the salts without decomposition. That shadowing does not occur in more than one or two directions on a given screen indicates that only relatively high peaks of the shadow-casting agent are involved. Scattering and absorption of electrons by the comparatively large mass of the salt gives molecules at the surface sufficient kinetic energy to escape at a faster rate than they return. If the point of departure is relatively high and sharp many of these molecules, travelling in straight lines, reach the surface of the screen at an oblique angle, transfer kinetic energy to the surface, and are trapped by surface forces at a faster rate than they can escape.

The poor quality of the shadowing by bromides and iodides probably is due to the lower stability of these salts. In fact, observations in the electron microscope indicate that sublimation is accompanied (probably preceded) by decomposition so that the shadowing is due in large measure to the metal which in some cases (e.g., mercury, lead) appeared to be molten on the screens.

The behavior of the chlorides is somewhat surprising in view of the relative ease with which they can be sublimed, without decomposition, by heating in air. It is possible that better results might be obtained with specimens other than the Dow latex.

From a practical point of view the only salts examined that are worth consideration as shadow-casting agents are lithium fluoride, sodium fluoride, and calcium fluoride. Calcium fluoride probably is the most readily available in the average laboratory and generally gives a higher proportion of satisfactory micrographs than does the lithium salt. For routine use it has the great advantage over both lithium and sodium fluorides of much lower solubility, and hence toxicity. Calcium fluoride has been adopted for use in this laboratory as a convenient means of enhancing contrast in the preliminary stages of an investigation. It would be useful in laboratories having no facilities for orthodox shadow-casting procedures. No vacuum coating unit is required and virtually no time is consumed in the shadow-casting process. No contamination of the microscope attributable to the use of these salts has been observed to date.

Acknowledgments

We are indebted to Dr. R. C. Backus who supplied this laboratory with a sample of Dow latex 580G in 1948. Mrs. H. M. Sheppard processed many of the plates and films and made the intermediate negatives and negative prints.

References

1 BACKUS, R. C. and WILLIAMS, R. C. J. Applied Phys. 20: 224. 1949.
2. WATSON, J. H L. J. Applied Phys. 19: 713, 714. 1948.

IONIZING POWER OF COSMIC RAY PARTICLES AT SEA LEVEL[1]

By S. D. Chatterjee[2]

Abstract

Using a proportional counter telescope arrangement, experiments have been carried out at sea level to explore the nature and ionizing power of particles in the soft component of cosmic radiation and those produced under 1.8 cm. and 20 cm. of lead. The results indicate a preponderance of relativistic electrons in the soft component and under 20 cm. of lead. Under 1.8 cm. of lead there is some disagreement with the calculated pulse height distribution curve but this can be attributed to the production of showers in the lead. These showers would obscure the presence of a small number of particles of unusually high ionizing power, if such exist.

Introduction

In recent years the measuring of the ionizing power of single cosmic ray particles has attracted careful attention. In explaining some unpublished results of Weisz and Ramsay, Swann (11) has pointed out the importance of statistical variations due to the fact that an appreciable portion of the energy loss due to ionization is carried away in secondaries which are in the energy range of thousands of electron volts. In a chamber of reasonable size the probability of occurrence of these secondaries is such that very poor statistics should be expected in the size of ionization pulses due to single particles. Alichanian, Alichanow, and Nikitin (1) and Nikitin (6) interpret results of measurements on the ionizing power of particles as indicating the existence of positive and negative particles in the soft component which are heavier than the meson, in fact the latter suggests particles which can be classified in three mass groups $(300\text{-}500)m_e$, $(700\text{-}1000)m_e$, and $(2000\text{-}3000)m_e$. In view of these results it was considered worthwhile to remeasure the ionizing power of cosmic ray particles at sea level to ascertain whether these distinctions could be confirmed or whether ionization measurements would reveal anomalies which might indicate the existence of an appreciable number of heavy mesons (3) or the so-called V-particles reported recently by different observers (7, 9).

General Principles and Method of Measurement

The specific ionization of strongly ionizing particles such as α-particles or slow protons is usually measured in an ionization chamber filled with argon at about an atmosphere pressure. Owing to the absence of gas amplification in such chambers, it is essential that the energy spent by the particles within the vessel should be sufficiently high. Otherwise, the resultant small ionization pulses would be masked by amplifier noise due to Shot and Johnson effects and tube fluctuations. Ordinarily the collection of about 5000 electrons at the col-

[1] *Manuscript received April 18, 1951.*
Contribution from National Research Laboratories, Ottawa, Canada.
[2] *Holder of a Postdoctorate Fellowship under the National Research Council, Ottawa, Canada.*

lecting electrode of an ionization chamber of low capacity and connected to a suitable linear amplifier gives a pulse from which the energy dissipated by the particle in producing ion pairs may be determined with reasonable accuracy. This involves an expenditure of energy of 150 kev., since it requires about 30 ev. to produce an ion pair in the gaseous volume. The relativistic particles in cosmic radiation having a specific ionization of the order of about 50 ion pairs per cm. in argon at N.T.P. can therefore hardly be detected in a non-multiplying chamber, unless the mean path length is made inordinately long or the gas pressure extremely high. The latter again leads to other complications as revealed in Swann's experiment (10).

The intrinsic merit of a proportional counter becomes evident in its ability to measure very low ionization. Filled with a suitable mixture of gases, mostly argon and methane, a proportional counter can be operated at a voltage which gives a charge multiplication up to 10^4. It is, however, generally maintained in the multiplication range between 10^2 and 10^3, which is characterized by strict proportionality between the primary ionization and the collected charge. Thus, the formation of 50 electrons or even less within the proportional counter is responsible for a collection of approximately 5000 electrons at the input grid of a linear amplifier, resulting in an output pulse whose amplitude is measurable with reasonable accuracy.

In the realm of cosmic rays the proportional counter was first utilized by Korff (4) when he attempted to measure the number of highly ionizing particles in the upper layers of the atmosphere. In Korff's investigations, however, the cosmic ray particles crossed the proportional counter in all directions, traversing different path lengths in it and producing a pulse height distribution which did not characterize the ionization power of individual particles. It is therefore necessary to use the proportional counter in a telescope system, by means of which a narrow beam of cosmic rays selected by Geiger counters is passed through a proportional counter, the passage of the particle and the number of ion pairs formed by an individual particle being recorded simultaneously. This method of a proportional counter telescope arrangement was adopted both by Weisz and Ramsay and by Alichanian *et al.* for the study of the relative specific ionization of the cosmic ray particles. It is only in the method of recording the ionization pulses from the proportional counter that their experimental arrangements differ in essential details. In the former experiment, the pulse produced by each discharge was recorded photographically giving a differential curve of pulse distribution. In the latter experiment the selection of the pulses was performed by means of a so-called biased multivibrator or a single amplitude discriminator enabling one to measure the number of pulses with the height exceeding a certain value and thus giving an integral curve of the pulse distribution.

Having obtained the size frequency distribution of the ionization pulses due to cosmic ray particles, the next step consists in the calibration of the system. Since the region of strict proportionality in a proportional counter is a function

of initial ionization, α-particles can hardly be used for standardizing the ionizing power of cosmic ray particles. It is more appropriate to use for comparison cosmic ray mesons filtered through a few centimeters of lead which have an ionization about the minimum and to assign to them unit ionization power.

The number of ion pairs created by a fast particle in the counter is determined by its specific ionization power and the path length traversed by the particle within the gas of the counter. When a fast particle loses energy in ionizing a gas a multiple process takes place:

(*a*) primary or parent ion pairs, usually consisting of electron and positive ions, are formed;

(*b*) secondary ion pairs are created by the electrons or positive ions of the primary pairs when such primaries have sufficient energy. In turn these secondaries may create additional secondary pairs. Williams (12) has given an expression for N, the number of ion pairs per cm. viz.,

$$N = \frac{A}{\beta^2}\left[\log_{10} K + \log_{10}\left(\frac{\beta}{1-\beta^2}\right) - \beta^2\right] \tag{1}$$

where N is known as the probable ionization, A and K are constants for a given kind of particle, and $\beta = v/c$, v being the velocity of the particle and c the velocity of light.

The value of N, the most probable ionization, lies between the values of the primary ionization and the total ionization, which includes the secondary ionization produced by electrons ejected from the parent ions. Generally the total number of ion pairs created by a fast particle will fluctuate appreciably about the value of N. This is mainly due to the statistical fluctuation in the number of these secondary electrons, which have appreciable ionizing power themselves.

Landau (5) has calculated the size distribution of fluctuations of ionization produced by fast particles traversing through a thin layer of matter. His curves show a maximum corresponding to the most probable ionization but indicate that considerable fluctuation in the ionization produced by any particular particle is to be expected.

In the present experiment the calibration was carried out according to the method of Alichanian *et al.* viz., by obtaining the fluctuation curve and determining from it the size of the pulse representing the most probable ionization.

Each experiment consists essentially of four steps:

(1) Plotting of the fluctuation or the "bias curve" for mesons in a particular arrangement of the counter telescope after inserting a 5 cm. lead plate between the proportional counter and the bottom tray of Geiger counters.

(2) Plotting of the total ionization "bias curve" without the lead filter.

(3) Decomposition of the ionization spectrum of the soft component by subtracting the first curve from the second.

(4) Adjustment of Landau's fluctuation curve with the ionization spectrum at the point of downward slope of the latter.

An analysis of (4) is expected to furnish an approximate value of the ionization power I of a new particle, if any.

Experimental Arrangement

The counter telescope system, schematically depicted in Fig. 1, consisted of one proportional counter mounted vertically between two trays of Geiger counters. Each tray contained three self-quenching Geiger counters of the

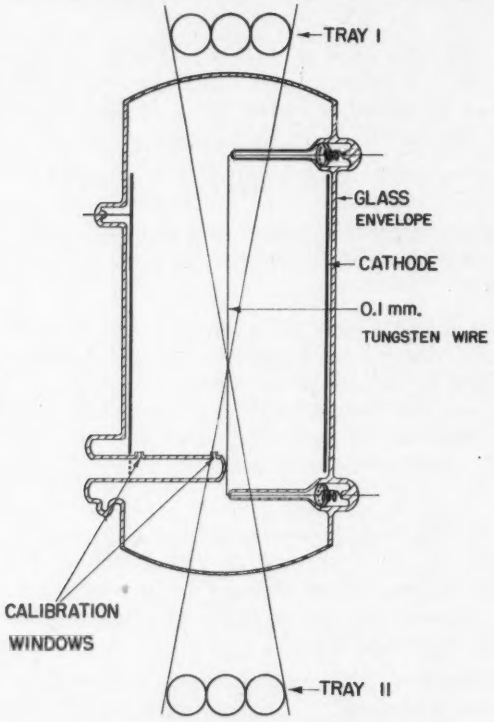

FIG. 1. *The arrangement of the proportional counter telescope.*

metal type, 15 cm. long and 2.5 cm. in diameter connected in parallel to one coincidence channel. The particles could enter the system within an angular aperture of about 20°, traversing nearly equal lengths within the proportional counter. The maximum difference in path length was approximately 10%. Suitable provisions were made for inserting a 5 cm. lead plate between the proportional counter and the bottom tray and also for placing lead plates of appropriate thickness above the top tray.

The arrangement of the proportional counter was somewhat similar to that adopted by Alichanian *et al.* The central wire was supported by side tubes. This design is more convenient to use in a telescope system than the traditional type with the central wire sticking out at both ends. The cathode was a copper cylinder 15 cm. long and 8.5 cm. in diameter. A tungsten wire, 0.1 mm. in diameter, served as the anode and was held in tension by a spiral spring at each end. The cylindrical envelope was made of pyrex glass, the tungsten leads being taken out through nonex glass sleeves. The re-entrant glass barrel was provided with two capillary side tubes which were closed by means of thin glass windows having a stopping power equivalent to about one centimeter of air. It allowed a narrow pencil of α-particles from a polonium source to pass into the counter either in the vicinity of the anode wire or near the cathode cylinder. The inside of the counter was treated with concentrated acetic acid for a few hours, rinsed several times with distilled water, and finally washed with absolute alcohol. The counter was next connected to a vacuum manifold and degassed for a few hours at a temperature of 350°C. under continuous pumping. Finally, the counter was filled with a pure mixture containing 25% argon and 75% methane at a pressure of 20 cm. of mercury. The outer surface of the glass envelope, excepting the lead-carrying sleeves, was coated with a thick conducting layer of colloidal graphite and grounded. Before assembling the apparatus, the pulse-formation characteristics of the proportional counter were tested by firing α-particles through the calibration windows and examining the shape and duration of the pulses by means of a cathode ray oscillograph.

The main requirement of the electronic equipment is to determine coincidences between Geiger counters and the proportional counter as a function of the height of the pulses from the latter. Since the pulses due to the proportional counter are usually about a few thousandths of the amplitude of those due to Geiger counters, it is necessary to have additional stages of amplification preceding the mixer stage. The anode wire of the proportional counter was directly connected to the grid of the first tube of the linear amplifier, which consisted of two stages with an amplification factor of about 2000. The amplifier was of the resistance capacity coupled type, having a frequency characteristic such that it accepted and preferentially amplified the pulses of the desired type.

The selection of the pulses according to their amplitude was performed by means of a biased multivibrator, which accepts only pulses larger than a particular size. The negative pulse from this selector stage was fed to a Rossi tube which was connected in twofold coincidence with a second Rossi tube, the latter being operated by the coincidence pulse from the Geiger counter trays after the usual phase inversion.

The Geiger counters of each tray were connected in parallel, since the total capacity of the wire system and counting rate were small. The anode wires of the counters were directly joined to the grids of the corresponding Rossi tubes, while an appropriate negative potential was applied to the cathode. This made

the resolving time very small, ensuring short duration of the pulses and avoidance of accidentals. However, since the reaction time of a mechanical recorder requires that the recorded pulse be prolonged to a time of the order of about one hundredth of a second, a neon tube coupled multivibrator delay circuit was used between the Rossi and output stages for directly recording the coincident counter pulses. The chief advantages of such a circuit are that every pulse reaching the grid of the output tube is of equal amplitude and duration and it operates on extremely small power without having any extinguishing troubles associated with a thyratron. The double and triple coincidence pulses were recorded separately by an Esterline–Angus pen recorder.

Separate power packs were used for the linear amplifier and coincidence units. The negative bias of the multivibrator was obtained from a calibrated potentiometer across a 45-volt Burgess super service "B" battery. The Geiger and proportional counters were supplied from independent high voltage sources; the high voltage power source for Geiger counters was obtained from a neon stabilivolt, while that of the proportional counter was obtained from a separate battery of 45-volt units in series and contained in a completely shielded box.

By feeding artificial pulses from a signal generator, it was possible to determine whether the linear amplifier and pulse analyzer had drifted during a certain course of measurements. This calibration unit consisted of a completely shielded battery circuit, operated with a microswitch and producing pulses of various sizes which could be selected at will. Together with the calibration corresponding to a proportional counter pulse, an artificial pulse equal in amplitude to the Geiger counter pulses could be taken off from a suitable point in the circuit and coupled through a condenser to the grids of the respective Rossi tubes so as to produce exactly the same effect as an actual threefold coincidence through the Geiger counters and the proportional counter. A careful check was made by means of a cathode ray oscillograph to be sure that the calibration pulses were identical in shape and duration to those of the proportional counter and the Geiger counters. The calibration unit was also instrumental in providing accurate information about the multiplication factor of the proportional counter and the sensitivity of the multivibrator during a particular series of measurements.

Experimental Results

The experiments were carried out in the National Research Laboratories at Ottawa, which has an altitude of approximately 170 ft. above sea level. The counter telescope was installed in a small cabin with a thin roof of wood and asphalt.

The main investigation can be subdivided into three sets of experiments. In the first set an attempt was made to detect highly ionizing particles in the soft component of the cosmic radiation. The results are represented in Fig. 2.

Curve B, the fluctuation curve of the relativistic mesons, was first obtained. For this set of measurements the soft component was absorbed by a 5 cm. lead filter placed between the proportional counter and the bottom tray of Geiger counters, as shown in sketch B in the inset. When the dial reading of the calibrated potentiometer across the bias battery is below 2.5 divisions, i.e. with the bias at the multivibrator less than -11.25 volts, the curve goes parallel to the abcissa. With a further increase of negative bias (greater pulse-height discrimination) the ordinates show a rapid decrease followed by a more gradual slope. The most probable ionization lies at the dial reading at 2.7 divisions of the potentiometer. Since only relativistic mesons were being recorded in this

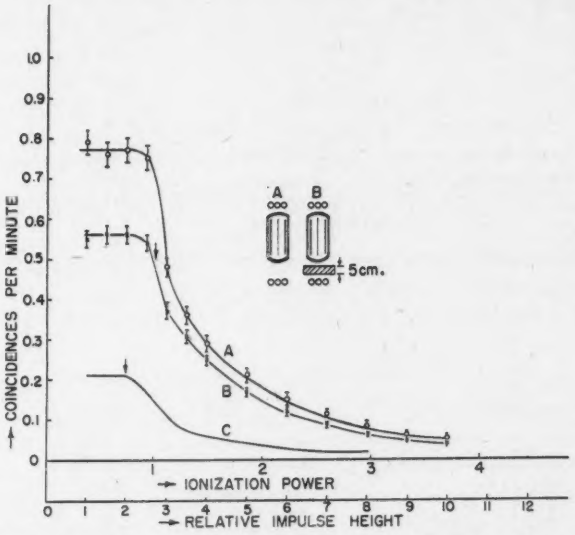

FIG. 2. *Ionization spectra of the hard and soft components of cosmic radiation at sea level.*

arrangement, the dial reading of 2.7 divisions may be equalled to unit ionization power along the abcissa scale. Next the arrangement A was adopted which gave the ionization spectra A constituting the total intensity of cosmic radiation. The ionization spectrum of the soft component was obtained by subtracting curve B from curve A and is represented by curve C. A comparison with the fluctuation curve calculated according to Landau's theory and fitted with C at the point of its downward slope shows that the experimental and theoretical curves coincide with each other.

In the second set of experiments a 1.8 cm. lead plate was placed above the top tray of Geiger counters. This is about the optimum thickness for the formation of cascade showers and would represent Rossi's first maximum in the number of particles observed. The results are shown in Fig. 3. As explained

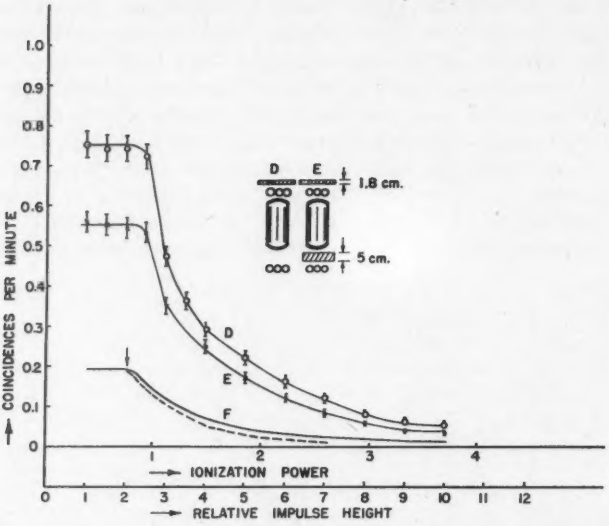

FIG. 3. *Ionization spectra under conditions characterized by Rossi's first maximum.*

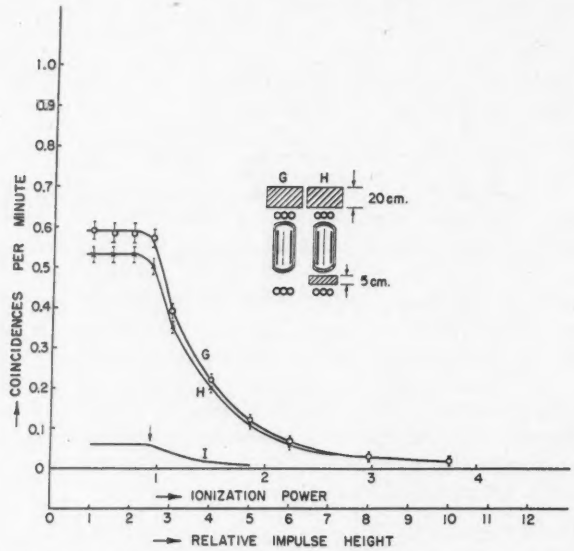

FIG. 4. *Ionization spectra under conditions characterized by Rossi's second maximum.*

above, E and D represent the fluctuation curves for relativistic mesons and the total intensity under these experimental conditions. The difference curve F, however, in this case does not coincide with the calculated Landau fluctuation curve, the latter being represented by the broken line. The difference between F and the Landau curve is small but it extends to large values on the abscissa scale. In contrast to the agreement found in Fig. 2 and Fig. 4, the disagreement in the results with this experimental arrangement seems to have a high probability of being real even though individual points on the curves do not show a high statistical accuracy compared to the difference between F and the Landau curve.

The third set of experiments was carried out with a 20 cm. lead plate above the top tray of Geiger counters. This arrangement was chosen as being most favorable for the study of the ionization power of penetrating particles which are emitted under conditions characterized by Rossi's second maximum. Incidentally such an experiment might also clarify the question of whether many mesons are generated simultaneously in a penetrating shower in such a narrow cone that they cannot be detected by the usual shower-detecting arrangement of Geiger counters. The results are represented in Fig. 4. As in the previous cases, curves G and H represent the fluctuation curve of relativistic mesons and the ionization spectrum of the total intensity under these experimental conditions. Curve I is the ionization spectrum of the soft component obtained by subtracting curve H from curve G. The differential curve I also coincides with Landau's fluctuation curve fitted with I at the point of its downward slope.

Discussion of Results

The results of the first set of experiments show that the soft component of cosmic radiation at sea level consists mostly of relativistic electrons. There is no indication of the presence of highly ionizing particles of the type discovered by Alichanian *et al.* at an altitude of 3250 meters. Rossi and Greisen (8) attempted to explain the total intensity of the soft component under the assumption that all electrons originate from meson decay and knock-on processes. It must be emphasized, however, that, on account of the finite thickness of the walls of the counters, the particles at the low energy end of the spectrum and those with high specific ionizations (small ranges) are automatically excluded from detection in our apparatus. It would be interesting to repeat the experiment with thin-walled counters.

The results of the second set of measurements are interesting. Accepting as real the difference between curve F of Fig. 3 and the Landau curve (broken curve in Fig. 3), these results indicate the presence of either an appreciable number of showers, or of particles of high ionizing power. The former seems most likely since the experimental conditions are appropriate and Dobrotin (2) has attempted to explain a similar deviation in his distribution curve at high altitudes as being due to a large number of air showers. A few particles with ionizing power corresponding to a charge greater than e would cause disagree-

ment with the Landau curve at large values of the ionizing power, but showers of several particles and particles near the end of their range would have the same effect. These results, therefore, are inadequate to show the existence of particles of unusual ionizing power in the cosmic ray flux at ground level. However, they do demonstrate the way in which the statistical variation in ionizing power and the presence of showers make identification by ionization measurements very difficult.

The result of the third set of experiments shows that even under 20 cm. of lead there is an appreciable number of electrons, probably created by the knock-on process by mesons. The differential curve I shows that these electrons are predominantly relativistic. In this set of measurements there is hardly any evidence of the production of pairs of mesons with such small angle of separation that they would escape detection by Geiger counter systems.

Acknowledgments

The author wishes to express his gratitude to Dr. D. C. Rose for helpful advice and encouragement in this work. His sincere thanks are due to Mr. George Ensell for his valuable help in the construction of the proportional counters and also to Miss E. Ford for her help in the preparation of the manuscript.

References

1. ALICHANIAN, A., ALICHANOW, A., and NIKITIN, S. J. Phys. U.S.S.R. 9: 167. 1945.
2. DOBROTIN, N. J. Phys. U.S.S.R. 10: 207. 1946.
3. FORSTER, H. H. Phys. Rev. 77: 733. 1950.
4. KORFF, S. A. Phys. Rev. 59: 949. 1941.
5. LANDAU, L. J. Phys. U.S.S.R. 8: 201. 1944.
6. NIKITIN, S. J. Phys. U.S.S.R. 11: 196. 1947.
7. ROCHESTER, G. D. and BUTLER, C. C. Nature, 160: 855. 1947.
8. ROSSI, B. and GREISEN, K. Phys. Rev. 61: 121. 1942.
9. SERIFF, A. J., LEIGHTON, R. B., HSIAO, C., COWAN, E. W., and ANDERSON, C. D. Phys. Rev. 78: 290. 1950.
10. SWANN, W. F. G. Phys. Rev. 44: 961. 1933.
11. SWANN, W. F. G. J. Franklin Inst. 249: 133. 1950.
12. WILLIAMS, E. J. Proc. Roy. Soc. (London), 135: 108. 1932.

DISTRIBUTION ZENITHALE DU RAYONNEMENT COSMIQUE[1]

PAR ANDRÉ G. VOISIN[2]

Sommaire

Les mesures ont porté sur la *composante pénétrante* qui est surtout composée de mésons μ au niveau du sol. Deux bandes contigues ont été sélectionnées dans le spectre différentiel; les impulsions des particules enregistrées s'étendent de 300 à 410 Mev./c et de 410 à 510 Mev./c pour des mésons. La distribution de leur intensité a été étudiée pour les angles au zénith compris entre 0° et 180°. Les résultats indiquent que la loi qui régit la distribution zénithale des particules étudiées est différente de celle qui exprime la distribution zénithale du spectre intégral.

Introduction

La distribution de l'intensité du rayonnement cosmique en fonction de l'angle au zénith a été étudiée dès 1932 (1). Il est bien connu que, au niveau de la mer, l'intensité maximum du rayonnement provient de la direction verticale et que, par suite de l'absorption atmosphèrique et de la radioactivité des mésons, cette intensité decroît pour des directions éloignées du zénith. La loi empirique qui exprime la distribution du spectre intégral, c'est-à-dire de toutes les particules qui subsistent après avoir été filtrées par un écran absorbant, peut-être représentée par l'équation: $I_\theta = I_0 \cos^\lambda \theta$, dans laquelle I_θ représente l'intensité du rayonnement observé dans une direction faisant un angle θ avec le zénith et I_0 l'intensité verticale. L'exposant λ est égal à 2 environ, pour la totalité du rayonnement et prend une valeur un peu supérieure (environ 2.2) dans le cas des particules pénétrantes (4, 5, 6, 12) filtrées par une dizaine de cm. de plomb. Par contre, nous avons pu montrer, dans une expérience précédente (10) que cette loi ne s'applique pas dans le cas du spectre différentiel des mésons.

L'objet des expériences qui vont être décrites est de préciser la loi qui gouverne la distribution zénithale des mésons dont l'énergie est comprise entre des limites déterminées. En effet, il est important de connaître la *distribution zénithale* ainsi que le *spectre différentiel des mésons* dans les problèmes qui se rapportent au spectre primaire du rayonnement cosmique, à la production des mésons et à l'évolution du rayonnement à travers l'atmosphère. Le début du spectre différentiel des mésons qui est encore assez mal connu a été étudié expérimentalement en collaboration avec Monsieur D. C. Rose, les résultats de ce dernier travail seront publiés séparément. Enfin, nous avons essayé d'étendre les mesures zénithales aux angles suivants: 90°, 120° et 180° avec le zénith, afin d'obtenir la distribution complète des particules pénétrantes. En effet, Powell et ses collaborateurs (3) ont observé une composante rétrograde dans des émulsions photographiques exposées au Jungfrau; par ailleurs Ritson

[1] *Manuscrit reçu le 31 juillet, 1951.*
Contribution de la Division de Physique, Conseil National des Recherches. Issue par le C.N.R. No. 2556.

[2] *Attaché de recherches au Centre National de la Recherche Scientifique, Paris. Bénéficiaire d'une bourse post-doctorat attribuée par le Conseil National de Recherche du Canada.*

(8) a montré à l'aide de compteurs l'existence de mésons rétrogrades au niveau du sol. Il serait intéressant d'étudier la distribution angulaire de ces particules afin d'aider sans doute à en déterminer l'origine. L'expérience que nous avons effectuée ne permet pas de confirmer l'existence de cette composante rétrograde dont l'intensité est extrêmement faible au niveau du sol.

Dispositif Expérimental

Principe de la Méthode

Nous avons utilisé une méthode d'absorption différentielle qui consiste à enregistrer les particules qui peuvent traverser une certaine épaisseur de plomb mais qui sont arrêtées dans un écran absorbant additionel. De cette manière on sélectionne les particules dont le parcours R est ainsi déterminé: $P < R < P + Q$, P et Q étant l'épaisseur des écrans absorbants. La largeur de la bande étudiée est déterminée par l'épaisseur de l'écran différentiel Q et son emplacement dans le spectre par l'épaisseur de l'écran P. Les particules qui sont accompagnées d'une gerbe sont éliminées de façon à n'enregistrer que les particules pénétrantes qui sont, pour la plus grande part, des mésons μ parmi lesquels se trouve probablement mélangé un faible pourcentage de protons dans les conditions de l'expérience. La fréquence des particules ainsi sélectionées est mesurée pour différents angles au zénith et la loi expérimentale qui en exprime la distribution peut-être établie.

Description de l'Appareil

Un télescope de double compteurs $A.B.C$ en triple coincidences (Fig. 1) définit un faisceau de particules qui ont traversé les écrans $P_1 + P_2 + P_3 = P = 15$ cm. de plomb. Deux groupes de compteurs D et E indiquent respectivement les particules qui ont traversé les écrans Q_1 et Q_2 chacun d'une épaisseur de 7.5 cm. de plomb.

Les groupes de compteurs G enregistrent les gerbes. Les compteurs et les écrans de plomb sont montés sur un solide bâti en fer qui permet l'orientation de l'axe du télescope selon un angle quelconque avec le zénith.

La triple coincidence $A.B.C$ constitue l'impulsion principale d'un circuit à groupe maître. L'impulsion maîtresse, provenant du télescope, est elle-même en coincidence avec chacun des groupes de compteurs D, E et G. Les coincidences suivantes sont alors enregistrées: $A.B.C$, $A.B.C.D$, $A.B.C.E$ et $A.B.C.G$ desquelles il peut-être déduit les anti-coincidences $A.B.C$–$(D.E.G)$ qui correspondent aux particules qui ne sont pas accompagnées d'une gerbe et qui s'arrêtent dans l'écran Q_1, ainsi que les anti-coincidences $A.B.C.D$–$(E.G)$ qui correspondent également aux particules solitaires mais qui, cette fois, s'arrêtent dans l'écran Q_2. Deux bandes d'énergie contigues sont ainsi découpées dans le spectre différentiel et enregistrées simultanément en fonction de l'angle au zenith.

La geométrie des compteurs a été étudiée de façon à répondre, autant que possible, aux conditions suivantes:

(*a*) L'ouverture de l'angle solide soutenu par le télescope doit être aussi faible que possible, bien que compatible avec une fréquence de comptage raisonnable. Une finesse relative de l'angle solide défini par le télescope réduit notablement l'effet angulaire dû à la géométrie du télescope et permet de mesurer la distribution zénithale jusqu'à des directions voisines de l'hori-

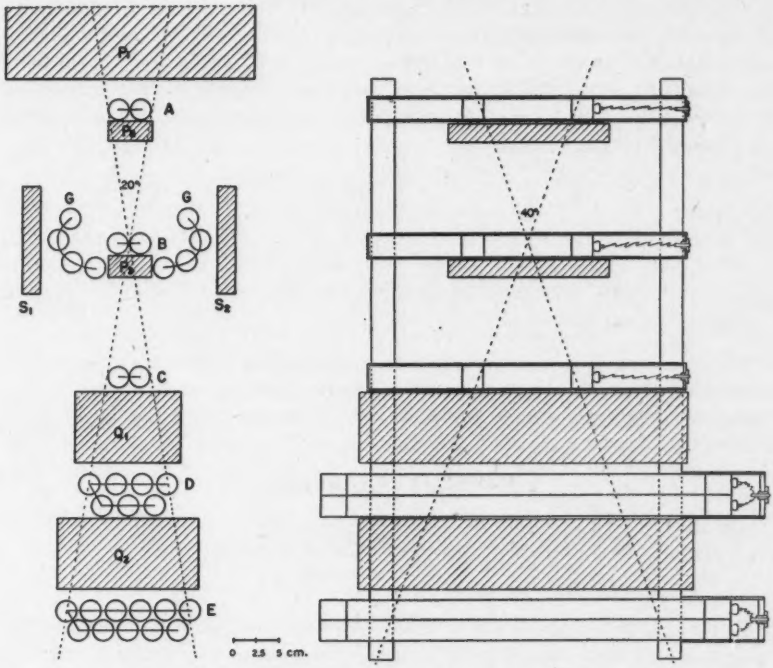

FIG. 1. *Disposition des compteurs et des écrans absorbants.*

zontale. L'angle d'ouverture minimum du télescope mesure 20° et l'angle latéral 40° ce qui a autorisé des mesures pour les angles au zénith jusqu'à 80° sans que le télescope soit traversé à la fois par les particules venant de deux directions azimuthales opposées.

(*b*) Les compteurs anti-gerbes ont été disposés en vue d'une bonne efficacité tant pour les gerbes produites dans les écrans supérieures que pour les gerbes latérales. Les deux groupes de compteurs G sont adjacents au faisceau du rayonnement déterminé par le télescope, ce qui les rend sensibles même aux gerbes dont les particles sont peu divergentes. L'ecran P_2 d'une épaisseur de 2.5 cm. de plomb accroît la probabilité de production de gerbes par les particules gerbigènes et l'écran P_3 arrête les gerbes les plus molles. Nous espérons obtenir ainsi une discrimination suffisamment bonne entre les composantes

molles et pénétrantes du rayonnement cosmique (9) dans le domaine des énergies étudiées.

Afin d'avoir une protection suffisante contre les gerbes latérales, pour lesquelles la fréquence relative est importante aux grands angles, les compteurs G sont placées de manière à couvrir complètement les compteurs B. Les écrans S et S' augmentent la probabilité d'enregistrer les électrons et les photons en accroissant la densité des gerbes au dessus des compteurs G. Des circuits supplémentaires d'amplification réduisent à une valeur négligeable l'inefficacité des compteurs G qui sont en parallèle. Le même dispositif d'amplification est d'ailleurs utilisé pour chacun des groupes D et E dans lesquels les compteurs sont aussi connectés en parallèle.

(*c*) Il y a plusieurs avantages à enregistrer simultanément deux bandes spectrales contingues. En particulier, une estimation expérimentale de la diffusion dans l'écran différentiel Q_2 peut être effectuée. Mais l'utilisation de deux bandes contigues est surtout intéressante dans la détermination du spectre différentiel pour lequel nous obtenons ainsi un recouvrement des deux bandes contigues mesurées.

D'autre part, il peut être exercé un contrôle permanent sur l'efficacité des compteurs D car le nombre des particules manquées par ces compteurs, mais qui sont enregistrées par les compteurs E, doit rester très faible dans les conditions normales.

Résultats et Discussion

Les différentes causes qui peuvent entâcher d'erreurs les résultats et dont il doit être tenu compte seront discutées dans les lignes qui suivent:

(*a*) *Fond continu de l'appareil*

Si l'on retire les écrans différentiels Q_1 et Q_2 il subsiste une certaine fréquence d'anti-coincidences qui constitue le fond continu de l'appareil. A l'origine de ce fond continu il y a plusieurs causes parmi lesquelles les plus importantes sont probablement les suivantes:

(1) *Inefficacité des groupes de compteurs D et E.*—Si une particule traverse un compteur dans une région de faible efficacité, ou pendant l'intervalle du temps mort, c'est à dire moins de quelques 10^{-4} sec. après le passage d'une particule précédente, l'impulsion donnée par le compteur est de faible amplitude. De façon à remédier à cet inconvénient, une amplification convenable des impulsions est appliquée de la même manière que pour les compteurs anti-gerbes. Toutefois, cette cause d'inefficacité des compteurs n'est pas la seule, il peut aussi se produire des impulsions en retard etc. et il subsiste toujours un fond continu dû aux compteurs.

(2) *Absorption dans les parois des compteurs.*—Cette absorption est calculable et représente environ 10% du fond continu total. D'ailleurs, elle n'est pas un effet parasite et provoque de véritables anti-coincidences.

(3) *Coincidences fortuites triples A.B.C.*—Le pouvoir de résolution de l'appareil est: $\gamma = 1.10^{-5}$ sec. Si nous écrivons que la fréquence des triples coincidences fortuites est en première approximation: $C_{1.2.3} = 3(N_1N_2N_3)\gamma^2$, N étant la fréquence d'un double compteur du télescope, nous trouvons qu'il se produit 3.10^{-5} coincidences fortuites par heure. Cette valeur est négligeable en comparaison avec la fréquence du fond continu qui est de l'ordre de 0.5 anti-coincidences par heure.

(4) *Inefficacité des compteurs anti-gerbes.*—Une gerbe latérale de faible extension peut déclencher les compteurs A, B et C sans atteindre les groupes D ou E. Une gerbe de ce type si elle était manquée par les compteurs G serait enregistrée comme anti-coincidence et par conséquent serait indiscernable des particules pénétrantes arrêtées dans les écrans différentiels. Toutefois, nous avons vu que l'efficacité du dispositif anti-gerbes est certainement convenable. Une estimation expérimentale de la limite inférieure de l'efficacité de ce dispositif peut être faite. Dans les conditions les moins favorables, c'est-à-dire quand le télescope est incliné d'un angle de 80° avec le zénith, la fréquence des gerbes latérales est maximum et le taux de comptage du télescope est à son minimum. Dans ces conditions, le télescope est déclenché à la fréquence de 7.1 coincidences par heure dont 2.0 coincidences sont accompagnées de gerbes. Le taux enregistré pour le fond continu est 0.13 coincidence par heure. *Si nous supposons que tout le fond continu* est dû *aux gerbes latérales* nous trouvons que sur deux gerbes par heure il en est manqué seulement 0.13, c'est à dire que l'efficacité du groupe anti-gerbes est bien supérieure à 94%.

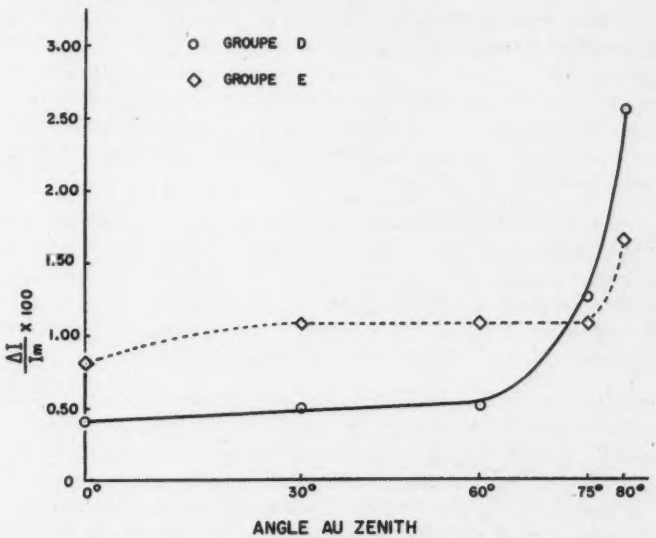

FIG. 2. *Fond continu de l'appareil rapporté à l'intensité des mésons, en fonction de l'angle au zénith.*

Généralement, dans les mesures analogues à celles que nous avons effectuées, le fond continu est mesuré pour la direction verticale et le pourcentage par rapport à l'intensité totale est supposé d'une valeur constante pour tous les angles. Ce pourcentage est utilisé pour corriger du fond continu les anti-coincidences enregistrées quand les écrans différentiels sont en place. Toutefois, une étude systématique du fond continu pour differents angles au zénith indique que le rapport $\frac{\Delta I}{I_m}$, ΔI étant la fréquence des anti-coincidences et I_m celle de l'intensité des mésons traversant le télescope, s'accroît (voir Fig. 2) quand on s'éloigne de la verticale. Cet accroissement *relatif* du fond continu pour les grands angles, en particulier pour 75° et 80°, pourrait être produit non seulement par la plus faible intensité I_m mais aussi par la *présence près de l'horizontale, d'une composante très molle* absorbée dans les parois des compteurs. Cette dernière supposition est d'ailleurs appuyée par le fait que le nombre des anti-coincidences enregistré par le groupe E est plus faible que celui indiqué par le groupe D pour les angles 75° et 80° avec le zénith.

Dans les résultats des mesures qui sont donnés plus bas, le fond continu, mesuré pour chaque angle, a été soustrait de la fréquence par heure ΔI des particules pénétrantes arrêtées par les écrans différentiels Q_1 et Q_2.

(*b*) *Diffusion*

Dans l'écran supérieur P_1 l'effet de la diffusion est négligeable car le nombre des particules qui sont écartées du faisceau défini par le télescope est, au moins partiellement, compensé par le nombre des particules qui originellement étaient en dehors de l'angle solide défini par le télescope et qui, par suite de la diffusion, sont orientées à l'intérieur de l'angle solide. Dans les écrans P_2 et P_3 le même effet peut se produire, de plus, ces écrans étant de faible épaisseur, la diffusion des protons et des mésons rapides n'y est pas considérable. Enfin, les mesures qui sont décrites ici n'ayant pas pour objet la détermination d'une intensité absolue, l'effet de la diffusion a été négligé, sans inconvénient croyons-nous, pour les absorbants $P_1 + P_2 + P_3$.

Dans les écrans Q_1 et Q_2, des particules peuvent aussi être diffusées en dehors du faisceau mais, cette fois, l'effet est préjudiciable car, si de telles particules sont fortement déviées, elles peuvent passer en dehors des compteurs D ou E et être aussi confondues avec les particules absorbées dans les écrans différentiels. Afin de parer autant que possible à ceci, les groupes de compteurs D et E couvrent largement l'angle solide défini par le télescope.

L'étude de la géométrie de l'écran Q_1 et des compteurs D montre que, dans un cas typiquement défavorable, les particules diffusées devraient avoir un angle de 30° au moins avec leur direction primitive à la sortie de l'écran, pour être manquées par les compteurs D. Il est improbable qu'un événement de ce genre se produise avec une fréquence suffisante pour altérer le résultat des mesures. Mais il n'en n'est pas de même en ce qui concerne la diffusion dans le second écran différentiel. Dans ce cas, même une faible déviation des parti-

cules dans l'écran Q_1 peut les écarter de la surface utile des compteurs E. De plus, une particule déjà déviée par le premier écran peut encore être diffusée dans le second. L'estimation de la proportion des particules diffusées qui manque le groupe E peut être fait en comparant les indications des groupes D et E. Afin d'éviter une hypothèse sur la courbe du spectre différentiel, la même bande spectrale est utilisée pour les deux groupes de compteurs, ceci est obtenu en changeant l'épaisseur de P_1. Les valeurs enregistrées pour les fréquences ΔI_D et ΔI_E sont respectivement corrigées du fond continu, correction qui inclus celles attribuables aux inefficacités des groupes de compteurs D et E. La différence qui subsiste entre ΔI_D et ΔI_E qui mesurent la même bande spectrale, peut être attribuée à l'effet de diffusion. Nous trouvons ainsi que la valeur de ΔI_D est environ 5% plus faible que celle trouvée pour ΔI_E. Dans nos résultats la valeur de ΔI_E a été corrigée pour cet effet.

(*c*) *Gerbes*

Les gerbes sont enregistrées par les compteurs G qui sont en coincidence avec le télescope. Le pouvoir de pénétration des gerbes peut être estimé par le nombre de celles qui traversent les écrans Q_1 et Q_2. Quand l'axe du télescope est horizontal, la fréquence des gerbes enregistrées indique la limite supérieure de la fréquence des gerbes latérales, car c'est dans ces conditions que l'appareil enregistre le maximum des gerbes de l'air qui sont principalement de direction verticale. Les courbes représentées sur la figure 3 montrent la fréquence des gerbes en fonction de l'angle au zénith. On peut remarquer que le rapport des

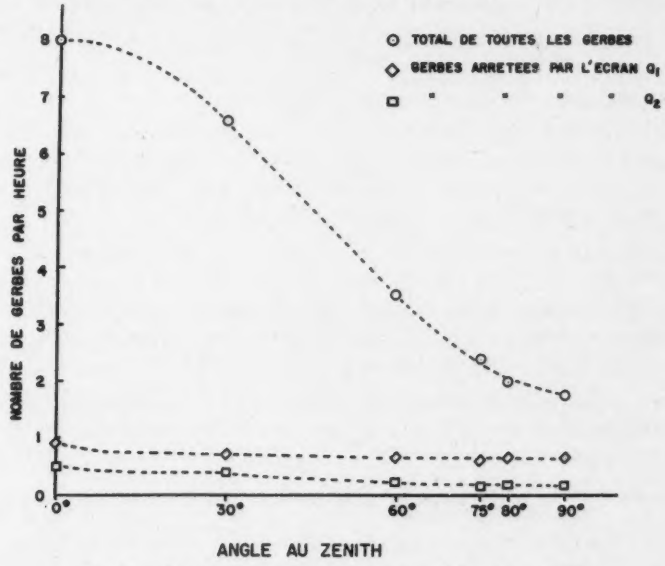

FIG. 3. *Distribution des gerbes en fonction de l'angle au zénith.*

gerbes pénétrantes sur le nombre total des gerbes est élevé. Par exemple, pour la direction verticale on trouve qu'il y a environ 55% de gerbes pénétrantes, si l'on déduit les gerbes latérales. La plupart de ces gerbes pénétrantes sont probablement provoquées par les électrons de collision des mésons. Elles représentent 4.3% de l'intensité de la composante verticale des mésons, valeur qui est du même ordre que celle trouvée à l'aide d'autres méthodes (2-13). Pour les grands angles avec le zénith la fréquence relative des gerbes pénétrantes décroît et le nombre des gerbes latérales devient prépondérant.

(*d*) *Correction barométrique*

Si la valeur de la correction barométrique à effectuer sur les mesures est assez bien connue en ce qui concerne le spectre intégral, il n'en n'est pas de même pour le spectre différentiel. Un travail récent (11) a même montré que parfois la correction pourrait être tantôt positive, tantôt négative suivant le domaine d'énergie considéré. Les mesures qui sont décrites ici ont été effectuées durant une période de plusieurs mois pendant laquelle la pression atmosphérique est demeurée relativement stable. La moyenne de la pression atmosphérique pour chacune des mesures s'établit comme suit:

θ	0°	30°	60°	75°	80°
millibars :	1007.7	1008.5	1007	1006	1009

La pression atmosphérique moyenne pendant la durée des expériences a été de 1007.6 millibars. Par suite de la faible déviation de la pression durant chacune des mesures autour de la pression moyenne (au maximum + 1.4; − 1.6 millibars) et par suite de l'incertitude sur la valeur du coefficient barométrique en ce qui concerne les mesures différentielles, il n'a pas été effectué de correction barométrique sur les résultats.

Distribution zénithales pour les angles $\theta < 90°$

Les mesures ont été effectuées à Ottawa dans un bâtiment de construction légère pour les angles au zénith suivant: 0°, 30°, 60°, 75°, 80°, 90°, 120° et 180° dans la direction de l'Ouest. Les résultats obtenus pour les angles 90°, 120° et 180° seront exposés dans le paragraphe suivant.

Durant ces mesures l'épaisseur des écrans a été maintenu constante et égale à: $P_1 + P_2 + P_3 = 15$ cm. de plomb et $Q_1 = Q_2 = 7.5$ cm. de plomb. Si nous supposons que toutes les particules sélectionnées sont des mésons, leurs impulsions s'etendent, d'aprés les courbes de parcours en fonction de l'impulsion (7) de 300 à 410 Mev./c et de 410 à 510 Mev./c.

Les résultats sont résumés sur les tableaux I et II, qui indiquent le nombre de particules absorbées ΔI_D et ΔI_E dans chacun des écrans différentiels Q_1 et Q_2 respectivement, pour les différents angles au zénith. Dans le tableau III le rapport $r = \dfrac{\Delta I_\theta}{\Delta I_0}$ et $\lambda = \dfrac{\log r}{\log \cos \theta}$. Ce tableau indique comment l'exposant λ varierait si la distribution était représentée par $I_\theta = I_0 \cos^\lambda \theta$ en prenant comme référence la verticale et seulement un angle avec le énith. La figure 4 montre

comment les points expérimentaux se placent par rapport à la courbe théorique en $\cos^2\theta$. Nous pouvons voir que près de la verticale la radiation décroît très rapidement en fonction de l'angle au zénith et que cette décroissance est plus lente quand on s'écarte de la direction verticale. Cet effet est particulièrement visible pour les particles absorbées dans le premier écran différentiel, c'est à dire pour la bande d'énergie la moins élevée. Ainsi que nous venons de le voir,

TABLEAU I

PARTICULES QUI SONT ARRÊTÉES PAR L'ÉCRAN DIFFÉRENTIEL Q_1

	0°	30°	60°	75°	80°
$\Delta I_{D\theta}$	3.59 ± 0.10	2.33 ± 0.18	0.75 ± 0.03	0.19 ± 0.02	0.18 ± 0.02
$r = \frac{\Delta I_\theta}{\Delta I_0}$	1	0.649	0.209	0.053	0.050

TABLEAU II

PARTICULES QUI SONT ARRÊTÉES PAR L'ÉCRAN DIFFÉRENTIEL Q_2

	0°	30°	60°	75°	80°
$\Delta I_{E\theta}$	3.62 ± 0.10	2.36 ± 0.11	0.60 ± 0.03	0.13 ± 0.01	0.09 ± 0.01
$r = \frac{\Delta I_\theta}{\Delta I_0}$	1	0.652	0.166	0.086	0.025

TABLEAU III

VARIATION AVEC L'ANGLE AU ZÉNITH DU RAPPORT $\frac{\log r}{\log \cos \theta} = \lambda$

	θ			
	30°	60°	75°	80°
D (mésons de 300 à 400 Mev./c)	3.00 ± 0.53	2.26 ± 0.07	2.17 ± 0.08	1.71 ± 0.06
E (mésons de 410 à 510 Mev./c)	2.97 ± 0.34	2.59 ± 0.08	2.46 ± 0.06	2.11 ± 0.06

il est impossible de tracer une droite par les points de la courbe de log r en fonction de log cos θ parce que λ n'est pas constant. Par contre, les points qui représentent log $(1 - r_\theta)$ en fonction de log sin θ se placent sur une ligne droite. Ainsi, nous obtenons la loi empirique:

$$r_\theta = \frac{\Delta I_\theta}{\Delta I_0} = 1 - a \sin^b\theta$$

où a et b sont des constantes ayant les valeurs suivantes:

bande spectrale de 300 à 410 Mev./c : $a = 0.98 \pm 0.02$, $b = 1.47 \pm 0.12$,
bande spectrale de 410 à 510 Mev./c : $a = 1.03 \pm 0.03$, $b = 1.61 \pm 0.15$.

En conclusion, les résultats montrent une forte décroissance près du zénith et une tendance à plus d'isotropie pour les directions éloignées de la verticale, en particulier, dans le cas des mésons de 300 à 410 Mev./c. Les phénomènes qui pourraient produire cet effet d'isotropie sont : la diffusion des particules le long de leur trajectoire dans l'atmosphère, la désintégration en vol de mésons

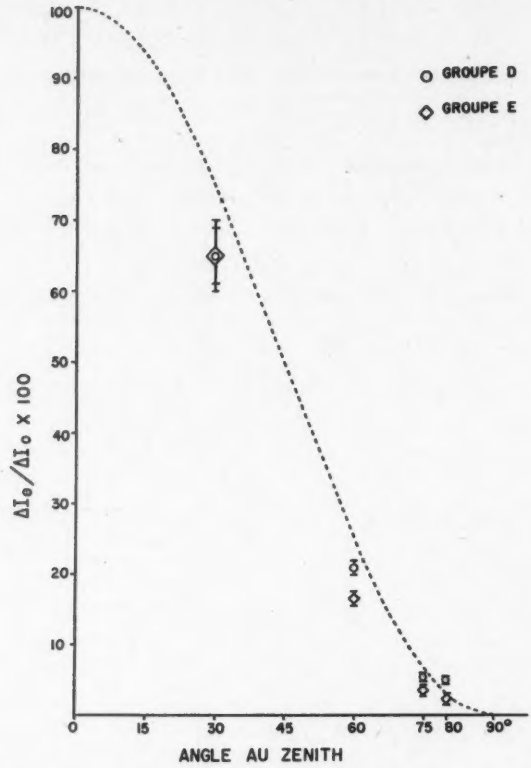

FIG. 4. *Courbe théorique* $Y = \cos^2\theta$ *et les points expérimentaux correspondant aux mesures différentielles.*

lourds donnant lieu à des mésons plus légers et les désintégrations nucléaires dans lesquelles des mésons sont créés. D'autre part, ces deux derniers phénomènes pourraient produire une composante rétrograde c'est-à-dire provenant de direction $\theta > 90°$ avec le zénith.

Distribution pour les angles $\theta \geq 90°$

Les mesures par la méthode des anti-coincidences sont délicates dans le cas des angles $\theta \geq 90°$ car, dans ces dernières mesures, la télescope est aussi déclenché par les particules ayant des directions opposées à celles des particules

à étudier. Néanmoins, des mesures préliminaires ayant donné des résultats encourageants au Pic du Midi, en France, un essai a été tenté au niveau du sol. Comme la pénétration de la radiation rétrograde n'est pas connue, l'épaisseur de l'écran absorbant P_1 a été variée entre 0 et 10 cm. de plomb. Mais, afin de conserver une certaine discrimination entre les particules penétrantes et les particules gerbigènes, les écrans intermédiaires P_2 et P_3, chacun de 2.5 cm. d'épaisseur, ont été maintenus à leur place. Par des mesures croisées, dans lesquelles l'un ou les deux écrans différentiels étaient retirés, nous avons essayé d'estimer l'intensité du flux ascendant.

(1) *Mesures à 90°.*—Le tableau IV donne les résultats des mesures effectuées sous cet angle au zénith. I_m représente la fréquence des particules qui déclenche le télescope sans être accompagnées par une gerbe. Nous pouvons voir, d'après le tableau, que l'intensité des particules de direction horizontale est peu affectée

TABLEAU IV

EFFET DES ÉCRANS ABSORBANTS SUR LA COMPOSANTE HORIZONTALE ($\theta = 90°$)

P	Q_1	Q_2	I_m	I_D	I_E
5	7.5	7.5	0.99 ± 0.12	0.11 ± 0.04	0.02 ± 0.03
10	7.5	7.5	1.02 ± 0.11	0.12 ± 0.04	0.04 ± 0.02
15	7.5	7.5	0.94 ± 0.12	0.17 ± 0.05	0.06 ± 0.02
10	0	0	0.78 ± 0.11	0.04 ± 0.03	0.03 ± 0.02
10	7.5	0	0.77 ± 0.10	0.08 ± 0.02	0.03 ± 0.02
10	7.5	7.5	1.02 ± 0.11	0.12 ± 0.04	0.04 ± 0.02

Les épaisseurs des écrans P_1, Q_1 et Q_2 sont exprimés en centimètres de plomb et I_m, ΔI_D, ΔI_E en nombre d'événements par heure.

par les variations de l'épaisseur de l'écran P_1 comme l'avait déjà remarqué Rogozinski dans une étude de la composante horizontale. En ce qui concerne ΔI_E il n'y a pas d'effet notable d'absorption dans l'écran Q_2. Mais la présence de l'absorbant Q_1 montre une augmentation de la fréquence ΔI_D. Toutefois, il n'est pas possible de dire si cette augmentation est due à l'absorption du rayonnement provenant de l'ouest, ou à la transformation d'une particle neutre, venant de l'est, en une particle chargée.

(2) *Mesures à 120° et 180°.*—Ces deux séries de mesure ne présentent pas d'effet réellement significatif avec ou sans les divers absorbants. Aussi, nous avons effectué une autre série de mesures à l'aide d'une méthode plus sensible basée sur la détection des mésons μ qui se desintègrent dans un absorbant en donnant naissance à un électron. Cette méthode a d'ailleurs été utilisée par Ritson (8) dans des mesures analogues. La figure 5 montre le schéma de l'appareil. Un télescope A.B est en coincidence retardée de 1.2 μsec. à 7.2 μsec., avec les compteurs $C.D$ eux-mêmes en double coincidence. Les coincidences fortuites et le fond continu de l'appareil sont abaissés à une valeur raisonnable par des circuits d'anti-coincidence. Ainsi sont enregistrés les mésons μ qui après avoir traversé le télescope se désintègrent dans la brique de carbone. Cette

méthode présente l'avantage d'éliminer toutes les particules qui ne sont pas des mésons μ, ou bien des mésons π donnant naissance à des mésons μ, provenant de la direction zénithale choisie. Le fond continu de l'appareil est déterminé en retirant la brique de carbone. Il est, dans nos mesures, égal à : 0.42 ± 0.10

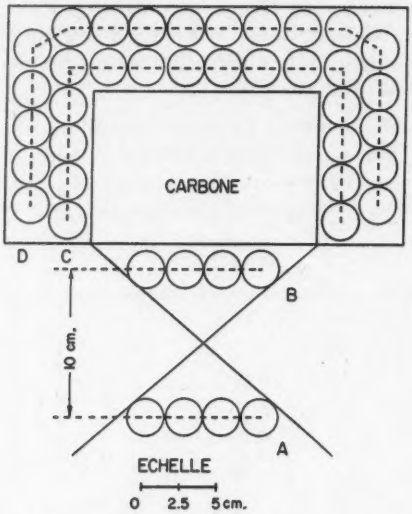

FIG. 5. *Disposition des compteurs et de l'absorbant de carbone dans l'appareil à coincidence différée.*

coincidences par heure. On trouve pour $\theta = 180°$ une fréquence de 0.45 ± 0.06 coincidences par heure quand la brique de carbone est en place. Ainsi cette mesure n'est pas plus concluante que la précédente. En résumé, ces expériences montrent que l'intensité du flux ascendant, s'il existe, est extrêmement faible au niveau du sol.

Conclusions

Les mesures que nous avons effectuées à Ottawa sur la distribution zénithale des particules pénétrantes de parcours compris entre 15 cm. et 22.5 cm. et entre 22.5 et 30 cm. de plomb indiquent que ces particules ne suivent pas la loi habituelle en $\cos^2\theta$, mais que la distribution de leur intensité peut être représentée par la loi empirique:

$$\frac{\Delta I_\theta}{\Delta I_0} = 1 - a \sin^b\theta$$

dans laquelle a est environ égal à l'unité et b prend les valeurs suivantes: $b = 1.47$ pour les particules les moins énergiques et $b = 1.61$ pour la seconde bande étudiée. Le fait le plus intéressant, mis en évidence par les mesures, est l'observation d'une décroissance rapide de l'intensité près du zénith et une tendance à plus d'isotropie près de l'horizontale. La bande spectrale de plus

faible énergie présente ces caractéristiques d'une manière beaucoup plus marquée que la seconde bande, notamment pour les angles au zénith de 75° et 80°. On peut d'ailleurs s'attendre à un tel résultat s'il y a une production locale de particules pénétrantes, ou bien des désintégrations en vol de mésons de masse supérieure au méson μ, ou bien encore des particles très déviées de leurs trajectoires primitives par la diffusion à travers l'atmosphère.

En ce qui concerne la radiation rétrograde, son intensité est très faible au niveau de la mer et des expériences complémentaires en altitude seraient désirables afin d'en déterminer l'intensité et l'origine.

Remerciements

L'auteur désire remercier Monsieur W. Kraushaar pour d'intéressantes discussions sur les résultats expérimentaux et tout particulièrement Monsieur D. C. Rose qui a bien voulu constamment conseiller et aider généreusement à la réalisation des expériences.

Bibliographie

1. Bernardini, G. Nature 129: 578. 1932.
2. Brown, W. W., MacKay, A. S., et Palmatier, E. D. Phys. Rev. 76: 506. 1949.
3. Camerini, U., Muirhead, H., Powell, C. F., et Ritson, D. M. Nature, 162: 433. 1948.
4. Freon, A. et Tsai-Chu. Compt. rend. 229: 753. 1949.
5. Jenkins, J. F. Phys. Rev. 76: 992. 1949.
6. Kraushaar, W. Thesis M.I.T. 1949, et Phys. Rev. 76: 1045. 1949.
7. Montgomery, D. J. X. Cosmic-ray physics. Princeton Univ. Press, Princeton, N.J. 1949. p. 349.
8. Ritson, D. M. Proc. Phys. Soc., A, 370: 1098. 1950.
9. Rogozinski, A. et Lesage, M. Cosmic radiation. Colston Papers. Butterworth Scientific Publication. London. 1949. p. 63.
10. Rogozinski, A. et Voisin, A. G. Compt. rend. 230: 2092. 1950.
11. Rose, D. C. Can. J. Phys. 29: 97. 1951.
12. Voisin, A. G. Compt. rend. 230: 1936. 1950.
13. Voisin, A. G. Can. J. Phys. 29: 205. 1951.

THE SOLUTION OF X-RAY ACTIVATION CURVES FOR PHOTONUCLEAR CROSS SECTIONS[1]

By L. Katz and A. G. W. Cameron

Abstract

A method is presented for the computation of photonuclear cross sections from their X-ray activation or yield curves. It is based on the photon differences between successive Schiff representations of bremsstrahlung spectra and assumes that the activation curves have smooth first and second derivatives. Artificially prepared activation curves have been satisfactorily solved by this method, and the published photonuclear activation curves determined in this laboratory have been reanalyzed. The resulting cross section curves are in essential agreement with those originally determined; however the new values are believed to be more reliable. New constants for two proposed relationships between (γ, n) "resonance" peak energies and atomic mass number have been determined. Appended to the paper are tables of the Schiff bremsstrahlung spectra for maximum photon energies between 8 and 28 Mev. and also of special functions for cross section computations between the same energies.

I. Introduction

In 1948, Baldwin and Klaiber (2) published an analysis of their activation curves for the reactions $C^{12}(\gamma, n)C^{11}$ and $Cu^{63}(\gamma, n)Cu^{62}$. The cross section curves so computed exhibited peaks with half-widths of a few Mev. Goldhaber and Teller (7) and Levinger and Bethe (19) then proposed theories to account for certain characteristics of such peaks as the result of a resonance dipole absorption of photons by a nucleus, followed by de-excitation through various competing modes of decay. The predominant mode should be neutron emission. Interest in the shapes of the cross section curves for photonuclear reactions was greatly stimulated by these theories.

For such investigations the ideal instrument would be a generator of monochromatic γ-rays of variable energy. Many (γ, n) and (γ, p) reactions have been studied with γ-rays from the $Li^7(p, \gamma)Be^8$ reaction (12, 33). Little can be concluded about the cross section shapes from such studies, since these γ-rays are a mixture of 14.5 and 17.5 Mev. photons and are produced from narrow resonances in the proton bombarding energy. Monochromatic γ-rays of energy greater than 19 Mev. are produced from the reaction $H^3(p, \gamma)He^4$. The proton energy resonance for this reaction is much broader, so that one could hope to use it for construction of such a generator. However, this has not yet been done for the study of photonuclear reactions.

The only other source of high energy γ-rays is bremsstrahlung produced when electrons strike a target after being accelerated in a betatron or synchrotron. This process gives a continuous spectrum of photon energies. It is difficult to sort out the photonuclear effects produced by photons of different energies

[1] *Manuscript received June 18, 1951.*
Contribution from the Betatron Group, Department of Physics, University of Saskatchewan, Saskatoon, Sask.

from a given irradiation in such an X-ray beam. In principle, if the energies of all the disintegration products for each of a large number of photonuclear events could be observed, then a frequency distribution of these events as a function of photon energy could be plotted. An approximate knowledge of the shape of the bremsstrahlung spectrum would then suffice for the determination of the cross section curve. So far it has been possible to apply this procedure only to such reactions as $O^{16}(\gamma, 4\alpha)$, where all the reaction products are α-particles which can be observed in a nuclear emulsion (25).

Usually, however, it is possible to measure only the yield of one of the disintegration products of a reaction (such as neutrons, protons, or residual radioactive nuclei) as a function of the dose and maximum energy of the bremsstrahlung spectrum which produced them. The cross section curve for the reaction can be determined in this case only if both the photonuclear yield and the shape of the bremsstrahlung spectrum are known as functions of the maximum energy.

Johns, Katz, Douglas, and Haslam (13) have published curves based on the Schiff bremsstrahlung spectra (1, 30) and outlined a method for the computation of cross section curves from the corresponding X-ray activation curves. This method will be referred to hereafter as the "total spectrum" method. It is open to the objection that a progressive smoothing of the cross section curve must be carried out in the course of computation, and this is to some extent a subjective and hence an arbitrary process. The present authors have developed a method of treatment, suggested by A. S. Penfold, which is computationally simpler and less arbitrary than the total spectrum method. This will be designated as the "photon difference" method.

II. Computational Functions

The intensity of the bremsstrahlung spectrum in the forward direction according to Schiff (1, 30) is proportional to

$$\Gamma = 2(1 - z)(\ln a - 1) + z^2(\ln a - 1/2), \tag{1}$$

where $a^2 = a_1^2 a_2^2/(a_1^2 + a_2^2)$,

$a_1 = 2W(1 - z)/\mu z$,

and $a_2 = C/Z^{1/3}$.

In these expressions μ is the rest energy of the electron, k is the photon energy, $z = k/W$, W is the total energy of the electron, and Z is the atomic number of the target material.

Schiff originally proposed (1, 30) that the constant C should have the value 191. However, from a recent reanalysis of bremsstrahlung theory (31), he has obtained the value $C = 111$. Equation (1) represents the shape of the bremsstrahlung spectrum in the forward direction only for infinitely thin targets, and the relationship thus cannot be used as it stands to give the bremsstrahlung spectra obtained from betatrons and synchrotrons, which have thick targets.

When Schiff's equation, in its angular dependent form (31), is integrated over all angles, the resulting total bremsstrahlung curve is practically indistinguishable in shape from that of Rossi and Greisen (29) and of Heitler (11). Equation (1), with $C = 191$, is actually a compromise in shape between the total bremsstrahlung spectrum and that in the forward direction calculated with $C = 111$. Such a compromise represents better the actual bremsstrahlung spectrum in the forward direction from thick targets, where multiple traversals and scattering of electrons give an additional contribution to the lower energy portion of the bremsstrahlung curve.

Koch and Carter (16) have measured the distribution of bremsstrahlung photon energies by determining the energies of electron pairs produced from 19.5 Mev. X rays in a cloud chamber. Their resulting intensity spectrum is reproduced in Fig. 1. The old and new Schiff curves computed from Equation (1) have been fitted to the experimental points so as to have the same number of photons between 13 and 19.5 Mev., where the results of Koch and Carter are most reliable. It may be seen that the experimental data lie considerably above the curve $C = 111$ at lower photon energies and that the curve $C = 191$ gives a somewhat better fit to the data. In a similar experiment using 322 Mev. X rays, Powell, Hartsough, and Hill (28) obtained excellent agreement with a bremsstrahlung shape calculated by Christian and modified to account for the effects of their target thickness. The modified Christian bremsstrahlung shape is nearly identical with that calculated from Equation (1) using $C = 191$.

Johns *et al.* (13) have investigated the changes introduced into the determination of the $Cu^{63}(\gamma, n)Cu^{62}$ cross section curve by the total spectrum

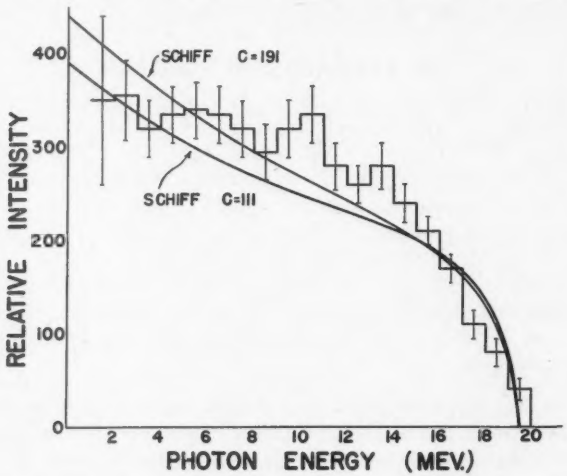

FIG. 1. *The experimental results of Koch and Carter for the shape of the bremsstrahlung intensity curve. Schiff's old and new theoretical curves ($C = 191$ and $C = 111$) have been normalized to include the same number of photons between 13 and 19.5 Mev. as the experiment.*

method when radically different types of bremsstrahlung curve were used, including extreme cases far outside the experimental uncertainties involved in the use of Equation (1) with $C = 191$. The relative shapes of the cross section curves are quite different, but the "resonant" peak positions are nearly the same and the integrated cross sections are practically unchanged.

We have therefore assumed that Equation (1), with $C = 191$, gives an adequate representation of the shape of the bremsstrahlung spectrum obtained from betatrons and synchrotrons. Experimental results check this shape sufficiently well that photonuclear cross section curves, as computed by the photon difference method, should be changed only slightly when accurate experimental shapes become available. In the following calculations the value $Z = 78$ (for a platinum target) was used. It is evident from Equation (1) that large changes in atomic number correspond to small changes in C, so that the tables prepared for this paper should be applicable to any heavy target.

The "standard" irradiation conditions adopted in this laboratory require that a sample be placed in the X-ray beam behind 4 cm. of Lucite and that X-ray dosages be measured by a Victoreen ionization chamber placed in the same position. This thickness of plastic material is necessary in order to bring the bremsstrahlung photons into equilibrium with their secondary electrons. It should be noted that this amounts to an arbitrary definition of the "roentgen" as a unit of X-ray dose. It is different from the "roentgen" defined through the use of lead as a converting material (24), since many more electron pairs are produced in the lead than by the light elements in Lucite. Mayneord (21) has defined the "roentgen" as the extrapolation to zero thickness of the linear portion of the depth dose curve in Lucite. Such a "roentgen" is about 19% smaller than the 4 cm. roentgen for 23 Mev. X rays.

This method of monitoring X-ray dosages has been compared to the Lax chamber method and others by McElhinney and Siewers (23), using bremsstrahlung energies up to 50 Mev. Very good relative agreement was obtained for X-ray energies up to 25 Mev., the region in which the secondary electrons are brought into full equilibrium with the primary beam.

It is thus necessary to modify the Schiff curves to take account of the photon absorption in the donut walls and monitor of the betatron and for the 4 cm. of Lucite. They must then be multiplied by the response curve of the Victoreen r-meter. This was done by Johns *et al.* (13), and the resulting spectrum curves were normalized so that each corresponded to 100 roentgens. These curves will be designated as $P(E, E_0)$, where E is the photon energy (Mev.), and E_0 is the betatron operating energy corresponding to the upper limit of the spectrum.

The saturated activity that would be induced in a sample after an infinitely long irradiation in the X-ray beam is

$$a(E_0) = 0.6023 \int_0^{E_0} \sigma(E) P(E, E_0) dE \qquad (2)$$

where a is the saturated activity per mole of parent isotope; σ is the cross section for the reaction in barns; and $P(E, E_0)$ is the number of photons per cm.^{2} per Mev. interval per unit time. The numerical factor is Avogadro's number divided by 10^{24} to convert the cross section units from cm.^{2} to barns. The unit time may be cancelled out of the above expression, in which case a becomes the number of reactions taking place per 100 r. per mole of parent isotope. A "mole" is here defined as 1 gm-atom of the isotope.

Replacing the integral in Equation (2) by a summation over a series of energy intervals and average cross sections of width ϵ Mev., one obtains

$$a(E_0) = 0.6023 \sum_{n = E_0/\epsilon}^{n = 0} \bar{\sigma}[E_0 - (n + \tfrac{1}{2})\epsilon]\, P[E_0 - (n + \tfrac{1}{2})\epsilon, E_0], \qquad (3)$$

where $P(E, E_0)$ must now be expressed in units of photons per cm.^{2} per ϵ Mev. interval per 100 r., and E_0 must be a multiple of ϵ. The differences between such activities at intervals of ϵ Mev. are

$$\Delta a(E_0) = 0.6023\, \Sigma\, \bar{\sigma}(E)\Delta P(E, E_0), \qquad (4)$$

where
$$\Delta a(E_0) = a(E_0) - a(E_0 - \epsilon),$$
$$\Delta P(E, E_0) = P(E, E_0) - P(E, E_0 - \epsilon),$$

and E takes the values $1/2\epsilon, 3/2\epsilon, \ldots\ldots, E_0 - 1/2\,\epsilon$.
To solve for the cross sections this is rewritten as

$$\bar{\sigma}(E_0 - 1/2\epsilon) = \Delta A(E_0) - \sum \bar{\sigma}(E)\Delta\phi(E, E_0), \qquad (5)$$

where
$$\Delta A(E_0) = B\Delta a(E_0), \qquad (6)$$
$$\Delta\phi(E, E_0) = \Delta P(E, E_0)/\Delta P(E_0 - 1/2\epsilon, E_0), \qquad (7)$$
$$B = [0.6023\, \Delta P(E_0 - 1/2\epsilon, E_0)]^{-1} \qquad (8)$$

and E now runs from $1/2\epsilon$ to $E_0 - 3/2\epsilon$.

Equation (5) is suited for the rapid computation of photonuclear cross sections from their activation curves. Activation differences are taken and multiplied by the factors B of Equation (8) to obtain the quantities $\Delta A(E_0)$. The cross sections may then be computed in tabular form as illustrated in Table I.

TABLE I

ILLUSTRATION OF THE COMPUTATIONAL PROCEDURE FOR THE CALCULATION OF A PHOTONUCLEAR CROSS SECTION FROM AN ACTIVATION CURVE

E_1	E_2	E_3	E_4
$\Delta A\left(E_1 + \frac{1}{2}\epsilon\right)$	$\Delta A\left(E_2 + \frac{1}{2}\epsilon\right)$	$\Delta A\left(E_3 + \frac{1}{2}\epsilon\right)$	$\Delta A\left(E_4 + \frac{1}{2}\epsilon\right)$
$= \bar{\sigma}(E_1)$	$-\bar{\sigma}(E_1)\Delta\phi\left(E_1, E_2 + \frac{1}{2}\epsilon\right)$	$-\bar{\sigma}(E_1)\Delta\phi\left(E_1, E_3 + \frac{1}{2}\epsilon\right)$	$-\bar{\sigma}(E_1)\Delta\phi\left(E_1, E_4 + \frac{1}{2}\epsilon\right)$
	$= \bar{\sigma}(E_2)$	$-\bar{\sigma}(E_2)\Delta\phi\left(E_2, E_3 + \frac{1}{2}\epsilon\right)$	$-\bar{\sigma}(E_2)\Delta\phi\left(E_2, E_4 + \frac{1}{2}\epsilon\right)$
		$= \bar{\sigma}(E_3)$	$-\bar{\sigma}(E_3)\Delta\phi\left(E_3, E_4 + \frac{1}{2}\epsilon\right)$
			$= \bar{\sigma}(E_4)$

Under the series of energies $E_1, E_2, \ldots\ldots$ the quantities $\Delta A(E_0)$ are entered. When the cross section at an energy E_x is determined, it is multiplied by the values $\Delta\phi(E_x, E_0)$ which are subtracted in the appropriate columns of the table. $\bar{\sigma}(E_y)$ is then the sum of all such products under E_y. For accurate computations, account should be taken of the fact that the first activation difference above the threshold of the reaction does not correspond to a width ϵ Mev., and appropriate adjustments should be made.

In order to implement this procedure it was necessary to obtain tables of the functions B and $\Delta\phi(E, E_0)$. It was decided to choose $\epsilon = 0.5$ Mev. The basic curves $P(E, E_0)$ obtained by Johns *et al.* were cross-plotted to give lines of constant photon intensity versus E_0, which were smoothed. By interpolation of this cross-plot a new set of curves $P(E, E_0)$, expressed in units photons per cm.^{2} per 0.5 Mev. interval per 100 r., were obtained for 0.5 Mev. intervals in E_0. The quantities $\Delta P(E, E_0)$ were then obtained by subtraction. Because the bremsstrahlung spectral shape changes slowly as a function of E_0, it was then insisted that $\Delta P(E, E_0)$ should be smooth functions of photon and betatron energies. This smoothness was achieved by a series of cross-plots against the relevant variables. The new $\Delta P(E, E_0)$ were then corrected by small smoothed factors so that they could be summed into good agreement with the original curves $P(E, E_0)$.

The resulting summation is given as Appendix I to this paper. The quantities B, defined by Equation (8), and $\Delta\phi(E, E_0)$, defined by Equation (7), were computed from the smoothed $\Delta P(E, E_0)$ and are given as Appendices II and III, respectively. Only the second decimal place is significant in these tables, but the third has been retained for reasons of smoothness.

III. Derivatives of the Activation Curves

Individual activation points are usually determined only to an accuracy of 2 to 5%, owing to errors in the determination of the initial activity of the sample, in the X-ray dose delivered to the sample, and in many cases the effective betatron operating energy.* It is therefore necessary to smooth the activation curve. This can produce considerable distortion in the computed cross-section curve if the smoothing is not done in a satisfactory manner. To remove the arbitrary features of this step it is necessary to obtain criteria to govern the smoothing procedure.

The various methods of analysis which have been applied to experimental activation curves have all yielded peaked cross section curves (see for example 2, 6, 13, 14, 15, 22, 26). "Resonance" peaks thus seem to be a characteristic feature of photonuclear cross section curves. It would be instructive to examine the characteristics of the derivatives of the activation curve corresponding to such a peaked cross section.

**The energy control circuit used in the University of Saskatchewan betatron is effective to 24 Mev. In this region the energy is believed to be constant at a given setting to ±0.1 Mev. and calibrated to ±0.2 Mev. Above 24 Mev. self-expansion of the electron beam is used which at best holds constant to ±0.3 Mev. with an equal error in calibration.*

The following analysis indicates the general nature of these derivatives. For mathematical simplicity a cross section curve is assumed in the form

$$\sigma(E) = E^2 \exp(-aE). \tag{9}$$

This curve is plotted in Fig. 2(*a*) with $a = 0.4$ Mev.$^{-1}$ It is sufficient to assume a "constant intensity" photon spectrum, which when normalized to constant dose (assuming the r-meter response to be linear), gives

$$P(E, E_0) = (E, E_0)^{-1}. \tag{10}$$

Then

$$\alpha(E_0) = \int_0^{E_0} \sigma(E)P(E, E_0)dE$$

$$= \frac{1}{a^2}[1 - e^{-aE_0}(aE_0 + 1)]. \tag{11}$$

Equation (11), the activation curve, is plotted in Fig. 2(*b*). Note that although the cross section is still quite large for energies above 10 Mev., the activation curve has leveled off in this region and is insensitive to the tail of the cross section curve.

The first and second derivatives of the activation curve are then

$$\partial\alpha(E_0)/\partial E_0 = E_0 \exp(-aE_0), \tag{12}$$

and

$$\partial^2\alpha(E_0)/\partial E_0^2 = (1 - aE_0) \exp(-aE_0). \tag{13}$$

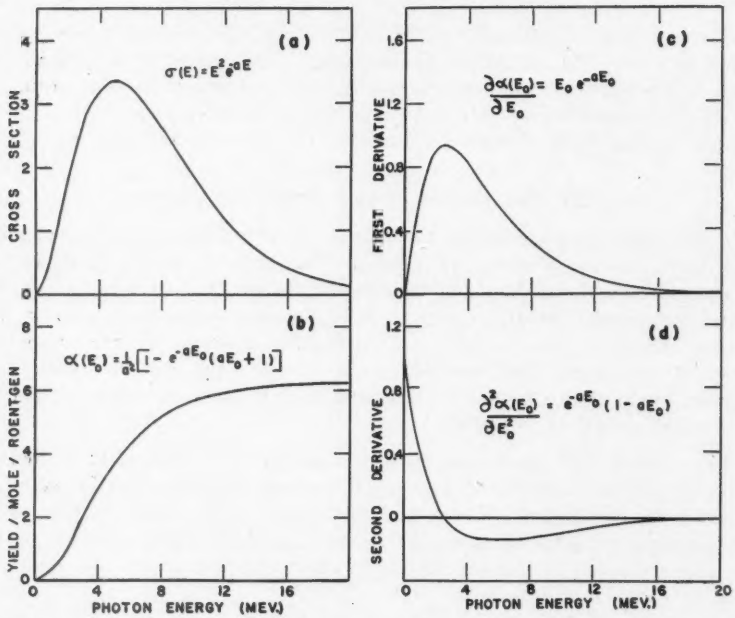

FIG. 2. *An activation curve and its derivatives as calculated for an assumed peaked cross section curve and a "constant intensity" photon spectrum. (a). The assumed cross section curve. (b). The activation curve. (c) The first derivative. (d). The second derivative.*

These are plotted in Figs. 2(*c*) and 2(*d*). They are smooth functions, and the derivatives of an experimental activation curve should resemble them in general shape.

It is felt that the best criterion is to fit experimental activation points by a curve having smooth first and second derivatives of the general shape of those in Figs. 2(*c*) and 2(*d*). With the exception of the reactions $S^{32}(\gamma, d \text{ or } np)P^{30}$, which will be discussed later, it has been possible by this procedure to fit an activation curve to the experimental points, determined in this laboratory for several photonuclear reactions, within the experimental errors. In practice a good smooth curve was drawn through the activation points. The activation differences $\Delta\alpha(E_0)$ (which are proportional to the first derivative) were read off this curve. These were then smoothed in such a way that their derivative was itself smooth and also such that the area under this smoothed curve was the same as the area defined by the activation difference points.

The above procedure has the following pragmatic advantage. When experimental activation points were smoothed in this manner, the progressive computation of the cross section curve according to Equation (5) yielded a smooth succession of cross section points. Any small oscillations in these points were found to damp out rapidly. The introduction during the smoothing procedure of discontinuities or extra inflections into the activation difference curve *in general* caused much larger oscillations which took longer to damp out. As will be shown later, a small bulge in this curve did not cause oscillations in the calculation of the cross section curve for the reactions $S^{32}(\gamma, d \text{ or } np)P^{30}$.

The smoothing procedure has also been tested through the solution of artificial activation curves. A number of geometrical cross section curves were assumed by one of us (L.K.) and the corresponding activation curves were computed by the inverse of the total spectrum method, using the curves published by Johns *et al.* (13). If allowance is made only for errors in reading these curves, then the resulting activation points are subject to uncertainties of about two per cent. The other of us (A.G.W.C.) was unable to predict by inspection any distinctive features of these cross section curves from their activation curves, apart from the obvious fact that they were peaked.

Activation differences were taken from the artificial curves, and these were smoothed according to the above procedure. The original cross section curves, together with the points then computed for these curves, are shown in Figs. 3, 4, and 5. It may be noted that the sharp bends of the original curves were quite well reproduced, although the very sharp bend in the curve of Fig. 5 was somewhat smoothed over. In each case the initial rise of the cross section curve was very well reproduced. Owing to the insensitivity of the activation curves to the "tails" of the cross section curves, these tails were not as well duplicated.

The authors are thus convinced of the validity of the smoothing procedure outlined above.

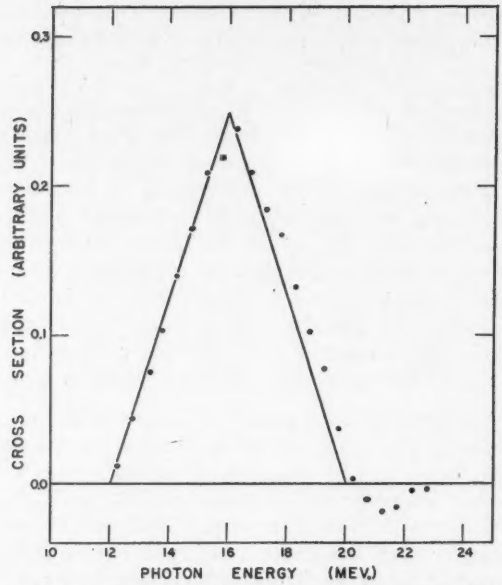

FIG. 3. *The solid line is an assumed triangular cross section curve, which was used in the computation of an activation curve from the spectra of Johns et al. The points were recomputed for the cross section curve by the photon difference method.*

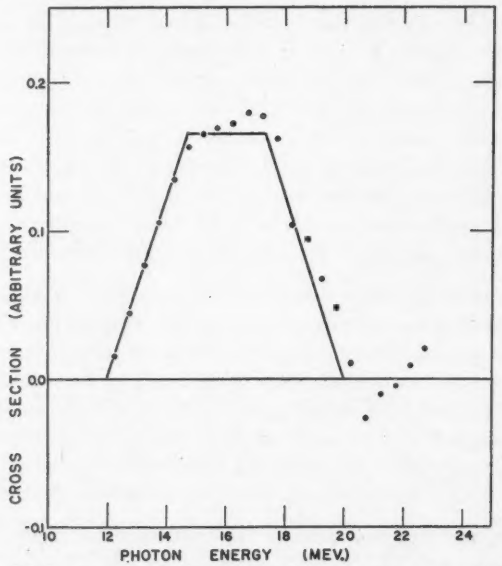

FIG. 4. *The solid line is an assumed quadrilateral cross section curve, which was used in the computation of an activation curve from the spectra of Johns et al. The points were recomputed for the cross section curve by the photon difference method.*

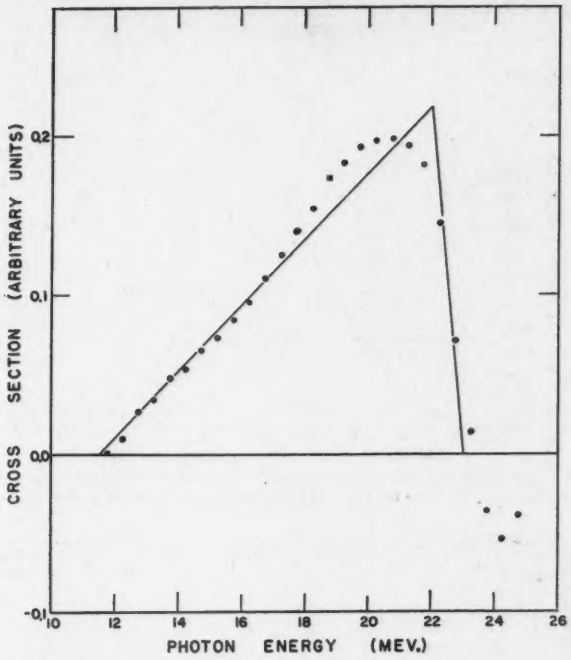

FIG. 5. *The solid line is an assumed triangular cross section curve, which was used in the computation of an activation curve from the spectra of Johns et al. The points were recomputed for the cross section curve by the photon difference method.*

IV. Recomputation of Experimental Activation Curves

The activation curves determined in this laboratory for a number of photonuclear reactions and originally solved for the corresponding cross sections by the total spectrum method have been recomputed by the photon difference method. The activation curve for the reaction $Cu^{63}(\gamma, n)Cu^{62}$ is plotted in Fig. 6. This curve was originally measured by Johns *et al.* (13), but some additional high energy points measured by Mr. R. G. Baker have been included. The activation differences read from the above curve and the smooth curve fitted to them are shown in Fig. 7. The calculated cross section curve is plotted in Fig. 8. This and other computed cross section curves are believed to be reliable only up to the point where the cross section falls to one-third of the maximum value on the high energy side of the peak. If the higher energy values were to be trusted, an accuracy of 1% or better would be required for the entire activation curve.

Because of its widespread interest (see for example 2, 8, 17, 18, 27) the recomputed cross section curve for the reaction $C^{12}(\gamma, n)C^{11}$ is shown in Fig. 9. Haslam, Johns, and Horsley (8), using the total spectrum method, obtained a very skewed cross section curve for this reaction. We believe this to be due

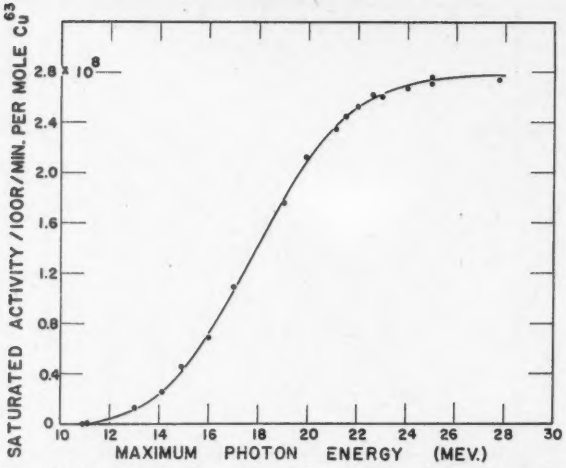

FIG. 6. *The activation curve for the reaction* $Cu^{63}(\gamma, n)Cu^{62}$. *A smooth curve has been drawn through the original points of Johns et al. plus some new higher energy points measured by R. G. Baker.*

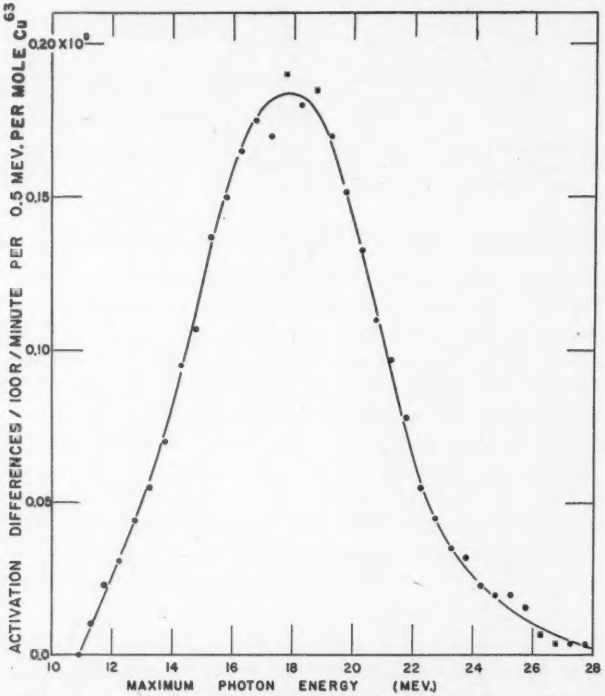

FIG. 7. *The activation difference curve for the reaction* $Cu^{63}(\gamma, n)Cu^{62}$. *The points are the differences at 0.5 Mev. intervals of the smooth curve in Fig. 6.*

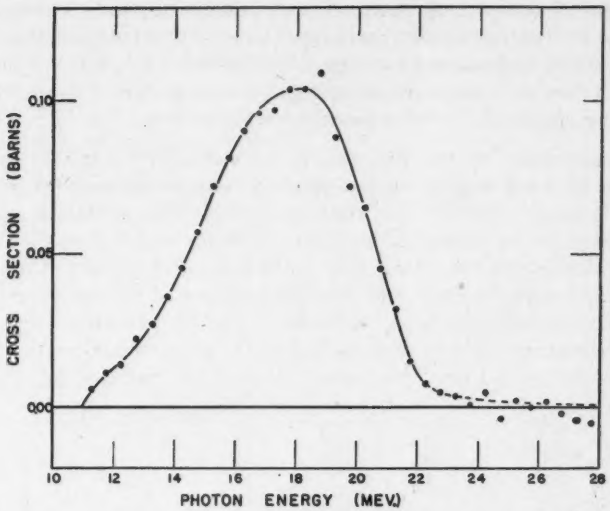

FIG. 8. *The cross section curve for the reaction $Cu^{63}(\gamma, n)Cu^{62}$ as computed by the photon difference method, using the smoothed activation differences of Fig. 7. The tail of this curve is very inaccurately determined.*

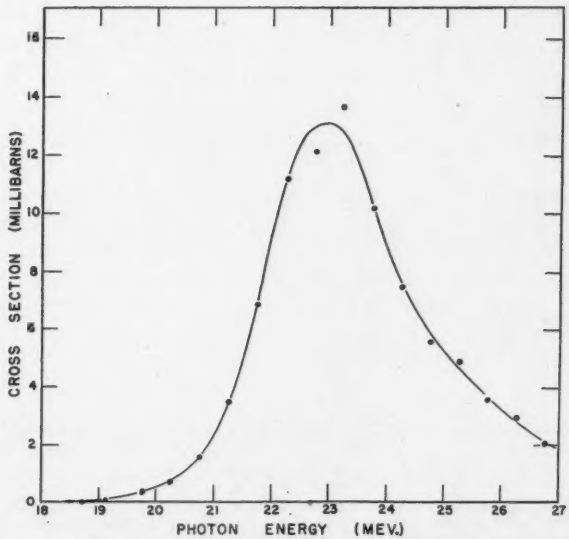

FIG. 9. *The cross section curve for the reaction $C^{12}(\gamma, n)C^{11}$ as recomputed by the photon difference method from the activation points of Haslam, Johns, and Horsley.*

to the progressive smoothing characteristic of the total spectrum method. The present calculation has yielded a more symmetrical curve. Owing to the narrowness of the peak and the small energy difference between peak and threshold for the reaction, the computed tail for this curve is probably somewhat more reliable than those for the other reactions reported here.

The measurement of the 2.55 minute activity of P^{30} resulting from the irradiation of sulphur is of special interest because both of the reactions $S^{32}(\gamma, d)P^{30}$ and $S^{32}(\gamma, np)P^{30}$ can contribute to it. This activation curve has been measured more accurately by Katz and Penfold (15) than that for any other reaction in this laboratory. Any broad structural features of the corresponding cross section curve would therefore be expected to show up in its solution. The activation differences, as shown in Fig. 10, indicated a slight bulge on the lower energy side of their peak, but the experimental points were so accurately determined that this bulge could not be smoothed out according

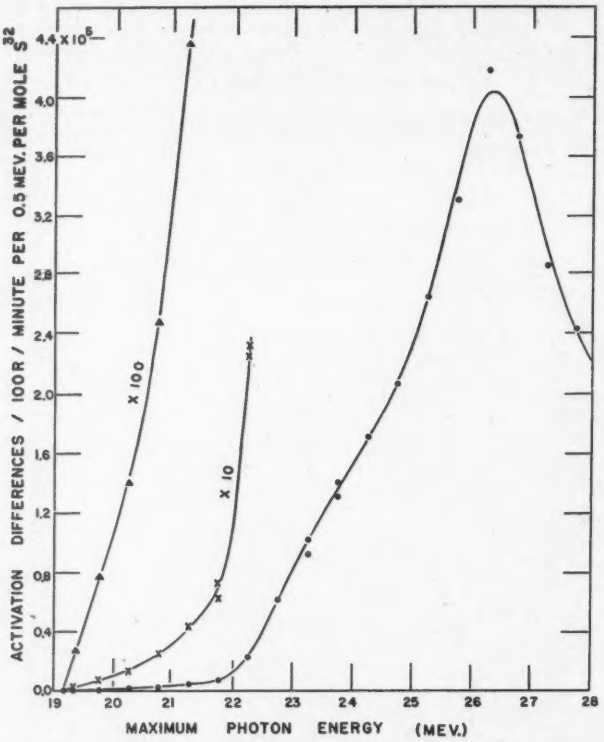

FIG. 10. *The activation difference curve for the reactions $S^{32}(\gamma, d \text{ or } np)P^{30}$. The points were taken from the original activation curve of Katz and Penfold. The experimental accuracy establishes the bulge on the rising portion of this curve.*

to the procedure recommended above. Therefore the first but not the second derivative of the activation curve was smoothed in this case. The resulting cross section curve is plotted in Fig. 11, with the low energy end magnified by factors of 10 and 100. During this computation it was discovered that the published cross section values (15) were too low by about a factor 4, owing to an error in the original computation.

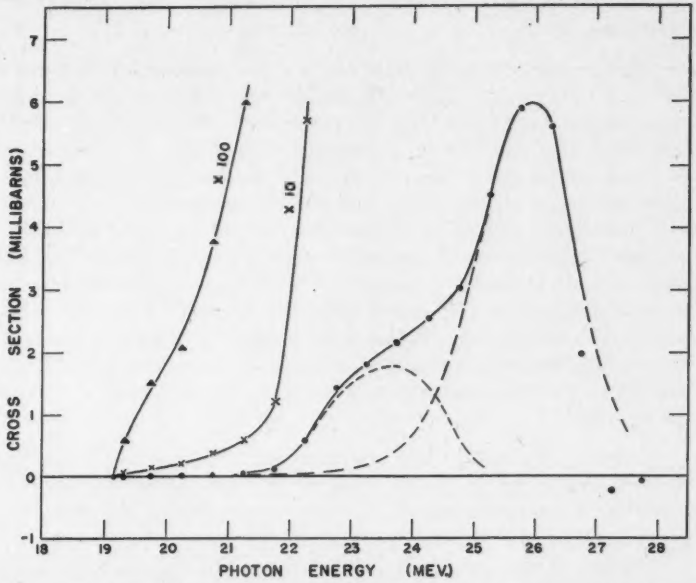

FIG. 11. *The cross section curve for the reactions $S^{32}(\gamma, d \text{ or } np)P^{30}$ as computed by the photon difference method from the activation differences of Fig. 10. The curve might represent a superposition of (γ, d) and (γ, np) peaked curves as shown dotted in the figure.*

The cross section curve of Fig. 11 might be interpreted as a superposition of two "resonance" peaks, probably about as indicated by the dotted lines in the figure. The lower of these could be identified with the reaction $S^{32}(\gamma, d)P^{30}$, and the higher with the reaction $S^{32}(\gamma, np)P^{30}$. The revised integrated cross section for the second of these two reactions is 0.013 Mev.-barns, or about 10 per cent of (γ, n) integrated cross sections in this region of the periodic table. This is of the order of magnitude predicted for this type of reaction from neutron yields (5).

It is also possible to explain the two apparent peaks as entirely due to the (γ, np) reaction in S^{32}. Following photon absorption, a neutron evaporates from S^{32} leaving S^{31} in various states of excitation. The threshold for the emission of a proton from S^{31} is about 2 Mev. lower than that for emission of a second neutron. Thus, as the photon energy is raised, the $S^{32}(\gamma, np)P^{30}$ reaction sets in.

At slightly higher photon energies the (γ, np) cross section is lowered owing to competition with the $(\gamma, 2n)$ reaction, and it rises again at still higher photon energies where the protons can penetrate the S^{31} barrier more efficiently. It is then not possible to evaluate the (γ, d) contribution to the cross section curve in Fig. 11.

It should be noted that the bulge in the activation difference curve did not cause oscillations in the successively computed cross section values for the above reactions.

Values of the cross sections for the above four reactions are listed at intervals of 1 Mev. in γ-ray energy in Tables II and III. Also listed are the recomputed cross sections for (γ, n) reactions in Cu^{65}, Sb^{121}, Sb^{123}, Ta^{181} (13); P^{31} (15); Fe^{54}, Ni^{58}, Zn^{64} (14); and the (γ, α) reaction in Rb^{87} (9). In each case the original experimental activation points served as the starting point for the recomputations. The characteristic features of the cross section curves as originally determined by the total spectrum method are listed in Table IV. The redetermined quantities corresponding to these as computed by the photon difference method are listed in Table V. No major changes were introduced by the recomputation, but the newer values are believed to be more reliable. The new energies for the cross section maxima tend to be slightly higher than the old, but their differences near $Z = 28$ have been much reduced. The new cross section curves also appear somewhat smoother and more symmetrical than the old ones.

The reaction $Cu^{65}(\gamma, n)Cu^{64}$ was originally measured relative to $Cu^{63}(\gamma, n)Cu^{62}$. Unfortunately the reaction $Cu^{63}(n, \gamma)Cu^{64}$ contributes appreciable activity near the photonuclear threshold, and the lower half of the cross section

TABLE II

PHOTONUCLEAR CROSS SECTIONS IN MILLIBARNS FOR VARIOUS REACTIONS AT 1 MEV. INTERVALS AS REDETERMINED BY THE PHOTON DIFFERENCE METHOD

Photon energy	$C^{12}(\gamma, n)C^{11}$	$P^{31}(\gamma, n)P^{30}$	$Fe^{54}(\gamma, n)Fe^{53}$	$Ni^{58}(\gamma, n)Ni^{57}$	$Cu^{63}(\gamma, n)Cu^{62}$	$Cu^{65}(\gamma, n)Cu^{64}$
11 Mev.					2	18
12				0	13	32
13		1.4		11	23	51
14		3.2	1.4	15	40	73
15		5.1	11.1	23	64	96
16		7.6	25	33	86	119
17		10.7	42	46	99	138
18		14.4	62	53	104	150
19	0.05	16.6	67	54	97	149
20	0.50	16.4	60	45	72	130
21	2.30	13.8	49	28	39	81
22	9.4	10.6	40	16		34
23	13.1	8.0	32			
24	8.8	6.0	25			
25	5.2	4.3				
26	3.3					
27	1.9					

TABLE III

PHOTONUCLEAR CROSS SECTIONS IN MILLIBARNS FOR VARIOUS REACTIONS AT 1 MEV. INTERVALS AS REDETERMINED BY THE PHOTON DIFFERENCE METHOD

Photon energy	$Zn^{64}(\gamma, n)Zn^{63}$	$Sb^{121}(\gamma, n)Sb^{120}$	$Sb^{123}(\gamma, n)Sb^{122}$	$Ta^{181}(\gamma, n)Ta^{180}$ minimum	$S^{32}(\gamma, np)^{d}P^{30}$	$Rb^{87}(\gamma, \alpha)Br^{83}$
9 Mev.				6		
10		57	30	15		
11	4	130	69	30		
12	18	264	140	51		
13	39	470	249	73		
14	63	658	348	80		
15	88	665	362	72		0.002
16	108	591	313	42		0.005
17	121	386	204	23		0.015
18	123	189	100	15		0.027
19	116					0.040
20	100				0.0185	0.052
21	79				0.048	0.062
22	56				0.29	0.071
23	34				1.62	0.075
24					2.35	0.075
25					3.63	0.068
26					6.0	(0.050)
27					(2.0)	(0.030)

TABLE IV

PREVIOUSLY PUBLISHED VALUES FOR THE CHARACTERISTICS OF VARIOUS PHOTONUCLEAR CROSS SECTION CURVES. THE SYMBOLS ARE AS USED IN THE TEXT

Reaction	E_m(Mev.)	Maximum σ (barns)	Half-width of σ(Mev.)	Integrated σ (Mev.-barns)	$E_m - Q$ (Mev.)***
$C^{12}(\gamma, n)C^{11}$	22.4	0.0116	4.2	0.047	3.7
$P^{31}(\gamma, n)P^{30}$	19.0	0.0166	7.6	0.13	6.6
$Fe^{54}(\gamma, n)Fe^{53}$	18.3	0.067	5.7	0.42	4.5
$Ni^{58}(\gamma, n)Ni^{57}$	18.5	0.060	4.6	0.33	6.5
$Cu^{63}(\gamma, n)Cu^{62}$	17.5	0.10	6.0	0.63	6.6
$Cu^{65}(\gamma, n)Cu^{64}$	19.0	0.16	6.0	1.26	8.8
$Zn^{64}(\gamma, n)Zn^{63}$	18.5	0.12	7.1	0.83	6.9
$Sb^{121}(\gamma, n)Sb^{120}$	14.5	>0.21	5.5	>1.2	5.2
$Sb^{123}(\gamma, n)Sb^{122}$	14.5	0.34	5.5	2.0	5.2
$Ta^{181}(\gamma, n)Ta^{180}$	13.5	>0.078	4.5	>0.39	5.5
$S^{32}(\gamma, np)^{d}P^{30}$*	24.0	(0.0004)	1.7	(0.0012)	(4.9)
$S^{32}(\gamma, np)P^{30}$**	25.8	(0.0015)	≥1.7	(0.0029)	4.4
$Rb^{87}(\gamma, \alpha)Br^{83}$	22.5	0.00007	6.6	0.00041	~17

*Assuming an approximate lower peak in the original cross section curve.
**The principal cross section peak.
***Energy difference between peak cross section and threshold.

TABLE V

THE CHARACTERISTICS OF VARIOUS PHOTONUCLEAR CROSS SECTION CURVES AS REDETERMINED BY THE PHOTON DIFFERENCE METHOD. THE SYMBOLS ARE AS USED IN THE TEXT

Reaction	E_m(Mev.)	Maximum σ (barns)	Half-width of σ (Mev.)	Integrated σ (Mev.-barns)	$E_m - Q$ (Mev.)***
$C^{12}(\gamma, n)C^{11}$	22.9	0.0131	2.8	0.046	4.2
$P^{31}(\gamma, n)P^{30}$	19.5	0.0167	6.5	0.129	7.1
$Fe^{54}(\gamma, n)Fe^{53}$	18.7	0.067	6.3	0.48	4.9
$Ni^{58}(\gamma, n)Ni^{57}$	18.5	0.054	5.6	0.34	6.5
$Cu^{63}(\gamma, n)Cu^{62}$	18.1	0.104	6.1	0.66	7.2
$Cu^{65}(\gamma, n)Cu^{64}$	18.6	0.151	7.0	1.11	8.4
$Zn^{64}(\gamma, n)Zn^{63}$	18.7	0.124	7.9	0.99	7.1
$Sb^{121}(\gamma, n)Sb^{120}$	14.8	0.685	4.8	3.53	5.5
$Sb^{123}(\gamma, n)Sb^{122}$	14.8	0.362	4.8	1.92	5.5
$Ta^{181}(\gamma, n)Ta^{180}$	13.9	>0.080	4.6	>0.47	5.9
^{d}					4.5†
$S^{32}(\gamma, np)P^{30}$*	23.6	0.0018	2.1	0.0039	
$S^{32}(\gamma, np)P^{30}$**	25.9	0.0060	$\geqslant 1.9$	$\geqslant 0.0127$	4.5
$Rb^{87}(\gamma, \alpha)Br^{83}$	23.4	0.000075	$\leqslant 7.9$	0.00060	~ 18

*Assuming the lower dotted curve of Fig. 11.
**Assuming the higher dotted curve of Fig. 11.
***Energy difference between peak cross section and threshold.
†Assuming the peak to be composed of deuterons.

curve is undoubtedly distorted by this effect. The correction of the observed Cu^{64} activities for self-absorption in the samples was large, so that the large absolute values of the cross section are subject to considerable error. Similar large values were obtained at the University of Pennsylvania (4).

Some questions also arise in connection with the (γ, n) reactions in the antimony isotopes. A single cross section curve was computed for the reactions in both isotopes, since the ratios of the activation points at various X-ray energies were constant within experimental errors. Sb^{122} consists of two isomers with half lives of 3.5 minutes and 2.8 days. The shorter activity decays by γ-ray emission to the longer, so that a measurement of the 2.8 day activity gives the total yield of Sb^{122} formed in an irradiation. Its integrated cross section of 1.92 Mev.-barns agrees nicely with that predicted for antimony on the basis of photoneutron yields (5). Two isomers, of 17 min. and 6.0 day half lives, are reported for Sb^{120}. However, only the 17 min. activity was measured. It decays by positron emission to Sn^{120}, the end point of the beta-spectrum being 1.70 Mev. (3). When the yield of this activity is corrected for the recently published decay scheme (3), the integrated cross section for $Sb^{121}(\gamma, n)Sb^{120}$* becomes 3.5 Mev.-barns. This is 80% higher than that predicted for antimony from photoneutron yields (5). The decay scheme does not take into account a small additional positron component with an end point of 2.4 Mev., and the percentage of K-capture competing with the 1.7 Mev. positrons is assigned on a theoretical basis. The absolute yield is therefore subject to considerable error.

One might expect, however, that the 6.0 day isomer of Sb^{120} should be produced in yield comparable to that of the 17 min. isomer. In that case the integrated cross section for $Sb^{121}(\gamma, n)Sb^{120}$ would be very much more in excess of

that predicted for antimony from photoneutron yields. The 6.0 day activity was observed by Lindner and Perlman (20), who assigned it to Sb^{120} from consideration of a complex of such activities produced in their irradiations of Sn, Sb, and Te with high energy deuterons. It decays by K-capture and emits 1.1 Mev. γ-rays but no beta-particles. It is therefore probable that the 17 min. metastable state of this isotope would be about 1.7 Mev. above ground. It is very surprising that there should be no intervening states to which the metastable level could decay by γ-ray emission.

A 0.57 Mev. γ-ray is reported in the literature to accompany the decay of the 2.8 day level in Sb^{122}. During the course of the antimony irradiations at this laboratory a lead absorption curve of this activity was taken which indicated a γ-ray energy of 0.58 Mev., in good agreement with the above value. This experiment indicates that if the 1.1 Mev. γ-ray accompanied every disintegration of the 6.0 day Sb^{120}, then the yield of this isomer is less than 10 per cent of the yield of Sb^{122}. The authors therefore question the assignment of the 6.0 day activity to Sb^{120} and believe that the yield of the 17 min. activity represents the major portion if not all of the reaction $Sb^{121}(\gamma, n)Sb^{120}$.*

When the cross section curve for Ta^{181} $(\gamma, n)Ta^{180}$ was recomputed from the original activation curve, large negative cross sections were obtained for photon energies above 19 Mev. It was therefore suspected that the activation curve was in error. This curve has recently been remeasured by Haslam, Smith, and Taylor (10), who found appreciably higher activities for betatron energies above 19 Mev. The cross sections reported for this reaction in Table III were therefore calculated from their new activation curve. The decay scheme for Ta^{180} is not known, and the values are therefore the "apparent" cross sections, obtained by correcting the activity observed in the samples for geometry and self-absorption. They are undoubtedly much too low.

Since the $Rb^{87}(\gamma, \alpha)Br^{83}$ reaction was measured relative to $Ta^{181}(\gamma, n)Ta^{180}$ as a monitor, the (γ, α) activation curve needed correction. This accounts for most of the differences between the new and old cross section curves for this reaction.

With the redetermined cross section characteristics listed in Table V it is possible to re-examine the relation between the "resonance" peak energy E_m (Mev.) and mass number A. Steinwedel, Jensen, and Jensen (32) have predicted a variation as $A^{-1/3}$, whereas Goldhaber and Teller (7) prefer $A^{-1/6}$. Fig. 12(a) shows a log-log plot of the 10 recomputed values of E_m for (γ, n) reactions versus A. The best fit for the above type of relationship is given by

$$E_m = 38.3A^{-0.186}. \qquad (14)$$

This favors the prediction of Goldhaber and Teller. However, the five middle points all lie above the straight line, whereas the five extreme points lie below

* *Note added in proof: Blaser, Boehm, Marmier, and Wäffler (Helv. Phys. Acta, 24: 245. 1951.) report that they have been unable to find the 6.0 day Sb^{120} activity from X irradiation of antimony and proton bombardment of tin.*

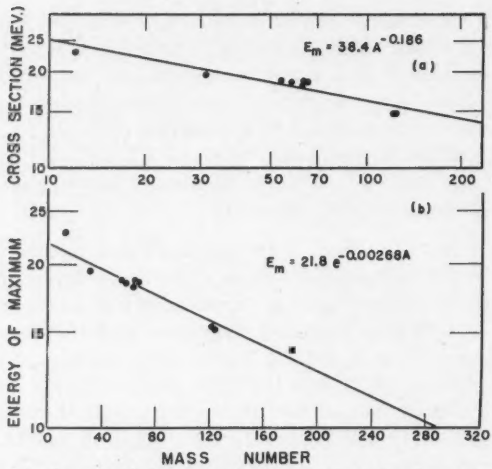

FIG. 12. *(a). A log-log plot of the energy for the maximum* (γ, n) *cross section* (E_m) *versus mass number. (b). A semilog plot of the same quantities. The equations of the best straight lines are as indicated in the figure.*

it. This relationship is therefore not too satisfactory. A semilog plot of the same quantities is shown in Fig. 12(*b*). The best straight line is given by

$$E_m = 21.8 \exp(-0.00268\,A). \tag{15}$$

The constants in this empirical equation are nearly the same as those originally proposed (5) from computations by the total spectrum method; the peak positions have been raised by about 0.3 Mev. This type of relationship appears more satisfactory in that the existing points distribute themselves about the straight line in a random manner.

V. Summary

A new method has been proposed for the computation of photonuclear cross section curves from their X-ray activation or yield curves. It is based on the photon differences between normalized Schiff bremsstrahlung curves. A basic assumption is made that measured activation points can be fitted with a curve having smooth first and second derivatives. An empirical justification has been obtained for this smoothing procedure. The computational procedure is simpler than that of the total spectrum method of Johns *et al.*, and most of the arbitrariness of the solution is removed.

The method requires that samples be irradiated behind 4 cm. of Lucite and that X-ray dosages be measured by a Victoreen ionization chamber under the same conditions. However, little error is introduced if the irradiations are carried out under other conditions relative to a standard reaction whose activation curve under the standard conditions is known. It is also satisfactory to obtain a relative activation curve under other conditions, as long as doses are monitored by a Victoreen chamber in Lucite, and to normalize the curve by a standard irradiation.

Tables of the Schiff curves $P(E, E_0)$ and of the special functions $B(E_0)$ and $\Delta\phi(E, E_0)$ as defined in Equations (7) and (8) are appended to this paper.

Twelve activation curves measured in this laboratory have been solved for the cross section curves by the photon difference method. The results are contained in Tables II, III, and V. The values differ little from those computed by the total spectrum method, but the authors believe them to be more reliable.

New constants have been determined for two suggested relationships between (γ, n) "resonance" peak energies and mass number, as indicated in Equations (14) and (15).

VI. Acknowledgments

The authors would like to thank Mr. J. A. Ash and Mr. R. Montalbetti for their help in the preparation of the graphs of the functions $P(E, E_0)$ and $\Delta P(E, E_0)$. We are indebted to Mr. A. S. Penfold for suggesting the possibility of using photon differences for the solution of activation curves, and to Mr. R. G. Baker for measuring additional activation points for the reaction $Cu^{63}(\gamma, n)Cu^{62}$. We wish to thank Dr. R. N. H. Haslam, Mr. L. A. Smith, and Mr. J. G. V. Taylor for permission to use their new activation points for the reaction $Ta^{181}(\gamma, n)Ta^{180}$.

References

1. Adams, G. D. Phys. Rev. 74: 1707. 1948.
2. Baldwin, G. C. and Klaiber, G. S. Phys. Rev. 73: 1156. 1948.
3. Blaser, J. P., Boehm, F., and Marmier, P. Helv. Phys. Acta, 23: 623. 1950.
4. Byerly, P. R., Jr. and Stephens, W. E. Phys. Rev. 83: 54. 1951.
5. Cameron, A. G. W. Phys. Rev. 82: 272. 1951.
6. Diven, B. C. and Almy, G. M. Phys. Rev. 80: 407. 1950.
7. Goldhaber, M. and Teller, E. Phys. Rev. 74: 1046. 1948.
8. Haslam, R. N. H., Johns, H. E., and Horsley, R. J. Phys. Rev. 82: 270. 1951.
9. Haslam, R. N. H. and Skarsgard, H. M. Phys. Rev. 81: 479. 1951.
10. Haslam, R. N. H., Smith, L. A., and Taylor, J. G. V. To be published.
11. Heitler, W. The quantum theory of radiation. The Clarendon Press, Oxford. 1936.
12. Hirzel, O. and Waffler, H. Helv. Phys. Acta, 20: 373. 1947.
13. Johns, H. E., Katz, L., Douglas, R. A., and Haslam, R. N. H. Phys. Rev. 80: 1062. 1950.
14. Katz, L., Johns, H. E., Baker, R. G., Haslam, R. N. H., and Douglas, R. A. Phys. Rev. 82: 271. 1951.
15. Katz, L. and Penfold, A. S. Phys. Rev. 81: 815. 1951.
16. Koch, H. W. and Carter, R. E. Phys. Rev. 77: 165. 1950.
17. Koch, H. W., McElhinney, J., and Cunningham, J. A. Phys. Rev. 81: 318. 1951.
18. Lawson, J. L. and Perlman, M. L. Phys. Rev. 74: 1190. 1948.
19. Levinger, J. S. and Bethe, H. A. Phys. Rev. 78: 115. 1950.
20. Lindner, M. and Perlman, I. Phys. Rev. 73: 1124. 1948.
21. Mayneord, W. V. Some applications of nuclear physics to medicine. Supplement No. 2, British Institute of Radiology, London. 1950.
22. McElhinney, J., Hanson, A. O., Becker, R. A., Duffield, R. B., and Diven, B. C. Phys. Rev. 75: 542. 1949.
23. McElhinney, J. and Siewers, D. C. Nat. Bur. Standards Rept. 1000. 1951.
24. McMillan, E. M., Blocker, W., and Kenney, R. W. Phys. Rev. 81: 455. 1951.
25. Millar, C. H. and Cameron, A. G. W. To be published.
26. Ogle, W. E. and McElhinney, J. Phys. Rev. 81: 344. 1951.
27. Perlman, M. L. and Friedlander, G. Phys. Rev. 74: 442. 1948.
28. Powell, W. M., Hartsough, W., and Hill, M. Phys. Rev. 81: 213. 1951.
29. Rossi, B. and Greisen, K. Revs. Modern Phys. 13: 240. 1941.
30. Schiff, L. I. Phys. Rev. 70: 87. 1946.
31. Schiff, L. I. Phys. Rev. 83: 252. 1951.
32. Steinwedel, H., Jensen, J. H. D., and Jensen, P. Phys. Rev. 79: 1019. 1950.
33. Waffler, H. and Hirzel, O. Helv. Phys. Acta, 21: 200. 1948.

APPENDIX I

TABLE OF SCHIFF BREMSSTRAHLUNG SPECTRA AS MODIFIED BY 4 CM. LUCITE ABSORBER AND NORMALIZED TO TOTAL INTEGRATED INTENSITY OF 100 ROENTGENS AS MEASURED BY A VICTOREEN CHAMBER. VALUES GIVE PHOTONS PER CM.^{2} PER 100 R. PER 1/2 MEV. INTERVAL. MULTIPLY FIGURES IN TABLE BY 10^8

Photon energy, E	E_0 − 0.25 Mev.									
	8.25	8.75	9.25	9.75	10.25	10.75	11.25	11.75	12.25	12.75
8.25	3.140	6.070	8.560	10.200	11.192	11.814	12.188	12.463	12.636	12.718
8.75		2.965	5.685	7.805	9.183	10.028	10.562	10.909	11.159	11.298
9.25			2.810	5.314	7.091	8.109	8.820	9.273	9.594	9.812
9.75				2.640	4.970	6.442	7.403	8.006	8.415	8.707
10.25					2.490	4.655	5.885	6.737	7.288	7.664
10.75						2.335	4.340	5.331	6.087	6.602
11.25							2.185	4.025	4.917	5.610
11.75								2.040	3.730	4.547
12.25									1.918	3.486
12.75										1.797

APPENDIX I—*Continued*

Photon energy, E	E_0 − 0.25 Mev.									
	13.25	13.75	14.25	14.75	15.25	15.75	16.25	16.75	17.25	17.75
8.25	12.715	12.656	12.570	12.473	12.364	12.248	12.127	12.000	11.869	11.734
8.75	11.355	11.355	11.311	11.248	11.178	11.099	11.016	10.929	10.837	10.742
9.25	9.934	9.977	9.983	9.958	9.921	9.873	9.822	9.763	9.700	9.631
9.75	8.903	9.013	9.056	9.068	9.053	9.026	8.988	8.947	8.900	8.849
10.25	7.932	8.106	8.202	8.245	8.263	8.256	8.238	8.212	8.181	8.148
10.75	6.961	7.205	7.361	7.454	7.498	7.520	7.529	7.523	7.510	7.492
11.25	6.086	6.416	6.640	6.774	6.856	6.902	6.927	6.938	6.938	6.931
11.75	5.179	5.621	5.927	6.132	6.259	6.336	6.382	6.409	6.422	6.426
12.25	4.247	4.825	5.538	5.223	5.713	5.832	5.905	5.952	5.981	5.998
12.75	3.257	3.963	4.494	4.879	5.144	5.320	5.432	5.503	5.550	5.581
13.25	1.681	3.040	3.711	4.213	4.573	4.815	4.978	5.084	5.153	5.201
13.75		1.573	2.834	3.472	3.947	4.285	4.512	4.665	4.766	4.834
14.25			1.475	2.656	3.268	3.715	4.035	4.249	4.392	4.488
14.75				1.380	2.485	3.079	3.502	3.802	4.003	4.137
15.25					1.290	2.323	2.900	3.299	3.581	3.769
15.75						1.203	2.173	2.736	3.110	3.373
16.25							1.119	2.033	2.576	2.925
16.75								1.041	1.897	2.421
17.25									0.970	1.776
17.75										0.897

APPENDIX I—*Continued*

Photon energy, E	E_0 − 0.25 Mev.									
	18.25	18.75	19.25	19.75	20.25	20.75	21.25	21.75	22.25	22.75
8.25	11.595	11.455	11.314	11.171	11.026	10.880	10.733	10.584	10.432	10.276
8.75	10.645	10.546	10.445	10.343	10.239	10.132	10.024	9.914	9.801	9.685
9.25	9.560	9.487	9.411	9.330	9.247	9.162	9.075	8.986	8.895	8.802
9.75	8.793	8.733	8.671	8.607	8.541	8.473	8.401	8.326	8.249	8.170
10.25	8.108	8.063	8.016	7.967	7.915	7.861	7.805	7.746	7.685	7.622
10.75	7.470	7.445	7.416	7.385	7.350	7.310	7.268	7.223	7.177	7.129
11.25	6.919	6.905	6.887	6.865	6.840	6.811	6.780	6.748	6.715	6.680
11.75	6.424	6.417	6.406	6.392	6.375	6.356	6.334	6.310	6.284	6.256
12.25	6.006	6.007	6.003	5.996	5.986	5.973	5.957	5.940	5.920	5.898
12.75	5.601	5.612	5.615	5.614	5.609	5.601	5.591	5.579	5.565	5.549
13.25	5.234	5.255	5.268	5.274	5.274	5.271	5.266	5.259	5.250	5.239
13.75	4.880	4.913	4.933	4.947	4.952	4.953	4.952	4.949	4.944	4.937
14.25	4.553	4.598	4.630	4.650	4.664	4.672	4.674	4.675	4.673	4.669
14.75	4.229	4.291	4.334	4.365	4.386	4.400	4.409	4.414	4.416	4.417
15.25	3.896	3.984	4.047	4.092	4.123	4.146	4.161	4.173	4.179	4.184
15.75	3.550	3.672	3.757	3.821	3.867	3.900	3.925	3.943	3.956	3.965
16.25	3.173	3.340	3.457	3.543	3.607	3.654	3.688	3.714	3.734	3.750
16.75	2.751	2.984	3.146	3.262	3.347	3.412	3.460	3.497	3.526	3.548
17.25	2.282	2.593	2.816	2.971	3.084	3.170	3.235	3.285	3.325	3.357
17.75	1.659	2.139	2.437	2.651	2.802	2.915	3.000	3.067	3.120	3.163
18.25	0.840	1.555	2.012	2.296	2.504	2.650	2.760	2.846	2.915	2.970
18.75		0.780	1.456	1.891	2.162	2.357	2.501	2.613	2.701	2.771
19.25			0.726	1.367	1.778	2.038	2.227	2.369	2.480	2.570
19.75				0.681	1.286	1.675	1.925	2.107	2.246	2.358
20.25					0.636	1.209	1.579	1.816	1.994	2.133
20.75						0.600	1.145	1.493	1.721	1.896
21.25							0.566	1.081	1.414	1.633
21.75								0.530	1.021	1.341
22.25									0.501	0.967
22.75										0.471

APPENDIX I—*Concluded*

Photon energy, E	$E_0 - 0.25$ Mev.									
	23.25	23.75	24.25	24.75	25.25	25.75	26.25	26.75	27.25	27.75
8.25	10.116	9.952	9.784	9.606	9.423	9.233	9.036	8.824	8.607	8.380
8.75	9.567	9.445	9.317	9.183	9.046	8.903	8.755	8.601	8.443	8.278
9.25	8.707	8.610	8.508	8.400	8.289	8.176	8.059	7.939	7.815	7.688
9.75	8.090	8.008	7.925	7.839	7.751	7.661	7.567	7.471	7.373	7.273
10.25	7.558	7.493	7.427	7.360	7.291	7.221	7.150	7.078	7.003	6.927
10.75	7.079	7.027	6.974	6.920	6.864	6.807	6.749	6.689	6.627	6.563
11.25	6.643	6.605	6.566	6.526	6.485	6.443	6.400	6.356	6.311	6.265
11.75	6.227	6.197	6.166	6.134	6.101	6.068	6.034	5.999	5.963	5.925
12.25	5.874	5.849	5.824	5.798	5.771	5.743	5.715	5.686	5.655	5.624
12.75	5.531	5.512	5.491	5.470	5.448	5.425	5.401	5.375	5.348	5.320
13.25	5.226	5.211	5.194	5.176	5.158	5.139	5.119	5.099	5.076	5.052
13.75	4.928	4.917	4.904	4.889	4.872	4.856	4.839	4.820	4.802	4.781
14.25	4.663	4.656	4.647	4.635	4.621	4.606	4.591	4.575	4.558	4.541
14.75	4.415	4.410	4.404	4.396	4.386	4.373	4.359	4.345	4.330	4.315
15.25	4.187	4.187	4.183	4.178	4.171	4.162	4.151	4.138	4.135	4.111
15.75	3.973	3.977	3.978	3.974	3.970	3.964	3.956	3.946	3.935	3.923
16.25	3.761	3.768	3.773	3.775	3.772	3.769	3.764	3.757	3.748	3.738
16.75	3.567	3.579	3.588	3.594	3.596	3.594	3.592	3.588	3.582	3.574
17.25	3.382	3.400	3.414	3.425	3.433	3.436	3.436	3.435	3.433	3.430
17.75	3.198	3.223	3.244	3.261	3.275	3.286	3.293	3.299	3.303	3.306
18.25	3.013	3.050	3.082	3.108	3.129	3.147	3.160	3.172	3.183	3.193
18.75	2.828	2.877	2.919	2.955	2.986	3.010	3.032	3.053	3.073	3.090
19.25	2.642	2.703	2.756	2.802	2.841	2.875	2.905	2.932	2.958	2.983
19.75	2.454	2.530	2.595	2.651	2.699	2.741	2.779	2.813	2.845	2.875
20.25	2.247	2.342	2.422	2.490	2.550	2.601	2.647	2.689	2.728	2.766
20.75	2.035	2.151	2.248	2.329	2.400	2.461	2.516	2.565	2.611	2.653
21.25	1.803	1.943	2.059	2.157	2.240	2.313	2.378	2.435	2.487	2.536
21.75	1.553	1.720	1.858	1.973	2.072	2.157	2.232	2.298	2.359	2.413
22.25	1.275	1.481	1.645	1.782	1.898	1.997	2.083	2.160	2.229	2.291
22.75	0.915	1.213	1.413	1.574	1.709	1.825	1.926	2.013	2.092	2.161
23.25	0.441	0.865	1.152	1.347	1.505	1.640	1.755	1.858	1.947	2.027
23.75		0.417	0.822	1.100	1.291	1.448	1.581	1.697	1.801	1.891
24.25			0.396	0.784	1.053	1.241	1.398	1.532	1.648	1.752
24.75				0.378	0.749	1.009	1.194	1.348	1.483	1.600
25.25					0.360	0.716	0.968	1.149	1.304	1.439
25.75						0.344	0.684	0.930	1.109	1.264
26.25							0.329	0.656	0.896	1.073
26.75								0.315	0.629	0.864
27.25									0.302	0.604
27.75										0.290

APPENDIX II

TABLE OF THE FACTOR $B = [0.6023\Delta P(E_0 - 0.25, E_0)]^{-1}$.
HERE $E = E_0 - 0.25$ AND B HAS A COMMON FACTOR 10^{-8}.
THIS TABLE MUST BE USED TO COMPUTE THE MODIFIED ACTIVATION DIFFERENCES $\Delta A = B\Delta a$

E	B	E	B	E	B	E	B
8.25	0.529	13.25	0.986	18.25	1.973	23.25	3.756
8.75	0.551	13.75	1.052	18.75	2.125	23.75	3.975
9.25	0.590	14.25	1.123	19.25	2.281	24.25	4.190
9.75	0.628	14.75	1.201	19.75	2.435	24.75	4.390
10.25	0.665	15.25	1.287	20.25	2.605	25.25	4.604
10.75	0.710	15.75	1.379	20.75	2.762	25.75	4.820
11.25	0.758	16.25	1.482	21.25	2.927	26.25	5.045
11.75	0.813	16.75	1.591	21.75	3.127	26.75	5.260
12.25	0.865	17.25	1.710	22.25	3.307	27.25	5.495
12.75	0.923	17.75	1.849	22.75	3.516	27.75	5.720

APPENDIX III

TABLE OF THE FUNCTION $\Delta\phi(E, E_0)$. THE SUCCESSIVELY DETERMINED CROSS SECTIONS $\sigma(E)$ MUST BE MULTIPLIED ALONG THE HORIZONTAL ROWS OF THIS TABLE TO DETERMINE THE QUANTITIES TO BE SUBTRACTED FROM THE MODIFIED ACTIVATION DIFFERENCES ΔA

Photon energy, E	E_0 − 0.25 Mev.								
	8.75	9.25	9.75	10.25	10.75	11.25	11.75	12.25	12.75
8.25	0.988	0.885	0.621	0.398	0.268	0.172	0.135	0.090	0.046
8.75		0.967	0.802	0.553	0.362	0.244	0.170	0.130	0.077
9.25			0.949	0.713	0.485	0.325	0.222	0.167	0.122
9.75				0.935	0.630	0.440	0.294	0.213	0.162
10.25					0.929	0.562	0.419	0.288	0.210
10.75						0.916	0.486	0.394	0.286
11.25							0.903	0.465	0.386
11.75								0.882	0.455
12.25									0.872

APPENDIX III—*Continued*

Photon energy, E	E_0 − 0.25 Mev.									
	13.25	13.75	14.25	14.75	15.25	15.75	16.25	16.75	17.25	17.75
8.25	−0.002	−0.037	−0.058	−0.070	−0.085	−0.096	−0.108	−0.122	−0.135	−0.151
8.75	0.034	0.000	−0.030	−0.046	−0.054	−0.066	−0.074	−0.083	−0.095	−0.106
9.25	0.073	0.027	0.003	−0.018	−0.029	−0.040	−0.046	−0.057	−0.065	−0.077
9.75	0.117	0.070	0.029	0.009	−0.012	−0.022	−0.034	−0.039	−0.048	−0.057
10.25	0.159	0.111	0.065	0.031	0.014	−0.006	−0.016	−0.025	−0.032	−0.037
10.75	0.213	0.155	0.106	0.067	0.034	0.018	0.008	−0.006	−0.013	−0.020
11.25	0.283	0.210	0.152	0.097	0.064	0.038	0.022	0.011	0.000	−0.008
11.75	0.376	0.281	0.208	0.149	0.098	0.064	0.041	0.026	0.013	0.004
12.25	0.452	0.367	0.280	0.206	0.147	0.099	0.065	0.045	0.030	0.019
12.75	0.868	0.449	0.360	0.279	0.205	0.146	0.100	0.068	0.048	0.035
13.25		0.862	0.455	0.364	0.279	0.201	0.146	0.102	0.071	0.052
13.75			0.856	0.462	0.368	0.281	0.203	0.147	0.104	0.076
14.25				0.856	0.475	0.372	0.286	0.205	0.147	0.107
14.75					0.856	0.493	0.379	0.288	0.207	0.149
15.25						0.858	0.517	0.383	0.291	0.209
15.75							0.868	0.540	0.386	0.293
16.25								0.876	0.560	0.389
16.75									0.894	0.584
17.25										0.900

APPENDIX III—*Continued*

Photon energy, E	E_0 − 0.25 Mev.									
	18.25	18.75	19.25	19.75	20.25	20.75	21.25	21.75	22.25	22.75
8.25	−0.166	−0.180	−0.194	−0.210	−0.228	−0.243	−0.260	−0.281	−0.303	−0.331
8.75	−0.115	−0.127	−0.139	−0.150	−0.164	−0.179	−0.191	−0.208	−0.226	−0.246
9.25	−0.085	−0.094	−0.105	−0.119	−0.130	−0.142	−0.154	−0.168	−0.181	−0.197
9.75	−0.067	−0.077	−0.085	−0.094	−0.104	−0.113	−0.127	−0.142	−0.154	−0.168
10.25	−0.048	−0.058	−0.065	−0.072	−0.082	−0.090	−0.099	−0.111	−0.122	−0.134
10.75	−0.026	−0.032	−0.040	−0.046	−0.055	−0.067	−0.074	−0.085	−0.092	−0.102
11.25	−0.014	−0.018	−0.025	−0.032	−0.039	−0.048	−0.055	−0.060	−0.066	−0.074
11.75	−0.002	−0.009	−0.015	−0.020	−0.027	−0.032	−0.039	−0.045	−0.052	−0.059
12.25	0.010	0.001	−0.006	−0.011	−0.016	−0.022	−0.028	−0.032	−0.040	−0.047
12.75	0.023	0.014	0.004	−0.001	−0.008	−0.013	−0.018	−0.023	−0.028	−0.034
13.25	0.039	0.026	0.018	0.007	0.000	−0.005	−0.009	−0.013	−0.018	−0.023
13.75	0.055	0.042	0.028	0.020	0.010	0.002	−0.002	−0.006	−0.010	−0.015
14.25	0.077	0.058	0.044	0.030	0.022	0.013	0.004	0.001	−0.004	−0.008
14.75	0.110	0.080	0.059	0.046	0.033	0.024	0.016	0.009	0.004	0.002
15.25	0.151	0.113	0.087	0.064	0.049	0.038	0.026	0.020	0.015	0.011
15.75	0.211	0.156	0.117	0.094	0.072	0.055	0.044	0.034	0.026	0.019
16.25	0.295	0.214	0.161	0.126	0.101	0.078	0.060	0.049	0.040	0.034
16.75	0.393	0.299	0.223	0.170	0.134	0.108	0.085	0.070	0.058	0.047
17.25	0.603	0.399	0.307	0.228	0.178	0.143	0.115	0.094	0.080	0.068
17.75	0.907	0.615	0.410	0.315	0.238	0.188	0.150	0.127	0.106	0.091
18.25		0.916	0.630	0.417	0.327	0.243	0.194	0.162	0.138	0.117
18.75			0.930	0.638	0.426	0.325	0.255	0.212	0.176	0.149
19.25				0.941	0.646	0.433	0.334	0.268	0.222	0.191
19.75					0.950	0.649	0.441	0.344	0.278	0.238
20.25						0.955	0.653	0.448	0.355	0.295
20.75							0.962	0.657	0.455	0.371
21.25								0.971	0.665	0.465
21.75									0.980	0.678
22.25										0.990

APPENDIX III—*Concluded*

Photon energy, E	E_0 − 0.25 Mev.									
	23.25	23.75	24.25	24.75	25.25	25.75	26.25	26.75	27.25	27.75
8.25	−0.363	−0.393	−0.425	−0.461	−0.509	−0.553	−0.600	−0.673	−0.719	−0.783
8.75	−0.268	−0.292	−0.323	−0.355	−0.381	−0.416	−0.450	−0.457	−0.425	−0.569
9.25	−0.215	−0.233	−0.258	−0.286	−0.308	−0.329	−0.356	−0.381	−0.411	−0.438
9.75	−0.181	−0.197	−0.210	−0.228	−0.244	−0.262	−0.286	−0.304	−0.324	−0.345
10.25	−0.145	−0.156	−0.167	−0.177	−0.192	−0.204	−0.216	−0.228	−0.248	−0.262
10.75	−0.113	−0.125	−0.134	−0.143	−0.156	−0.166	−0.176	−0.191	−0.206	−0.221
11.25	−0.084	−0.091	−0.098	−0.106	−0.114	−0.122	−0.131	−0.140	−0.149	−0.159
11.75	−0.066	−0.072	−0.078	−0.085	−0.092	−0.096	−0.103	−0.111	−0.119	−0.131
12.25	−0.054	−0.060	−0.063	−0.069	−0.075	−0.081	−0.085	−0.092	−0.104	−0.107
12.75	−0.041	−0.046	−0.052	−0.056	−0.061	−0.067	−0.073	−0.081	−0.089	−0.096
13.25	−0.029	−0.036	−0.043	−0.048	−0.050	−0.055	−0.062	−0.065	−0.077	−0.083
13.75	−0.020	−0.026	−0.033	−0.041	−0.046	−0.048	−0.053	−0.059	−0.060	−0.072
14.25	−0.013	−0.017	−0.024	−0.031	−0.039	−0.044	−0.046	−0.051	−0.056	−0.058
14.75	−0.005	−0.012	−0.015	−0.022	−0.029	−0.037	−0.042	−0.044	−0.049	−0.053
15.25	0.007	−0.001	−0.011	−0.013	−0.020	−0.027	−0.035	−0.040	−0.042	−0.047
15.75	0.016	0.010	0.002	−0.010	−0.011	−0.018	−0.025	−0.033	−0.038	−0.040
16.25	0.024	0.020	0.013	0.004	−0.008	−0.009	−0.016	−0.023	−0.031	−0.036
16.75	0.041	0.029	0.024	0.017	0.006	−0.005	−0.007	−0.012	−0.019	−0.028
17.25	0.057	0.046	0.035	0.029	0.022	0.009	0.000	−0.003	−0.007	−0.010
17.75	0.079	0.060	0.053	0.045	0.039	0.031	0.021	0.019	0.013	0.010
18.25	0.097	0.089	0.081	0.069	0.057	0.052	0.040	0.038	0.036	0.035
18.75	0.129	0.117	0.106	0.095	0.086	0.070	0.067	0.067	0.066	0.059
19.25	0.163	0.146	0.134	0.121	0.108	0.099	0.091	0.086	0.086	0.086
19.75	0.218	0.181	0.164	0.148	0.133	0.122	0.116	0.108	0.106	0.103
20.25	0.258	0.228	0.202	0.180	0.167	0.148	0.140	0.133	0.129	0.126
20.75	0.315	0.278	0.245	0.214	0.197	0.177	0.167	0.156	0.152	0.145
21.25	0.385	0.336	0.293	0.259	0.233	0.212	0.198	0.181	0.172	0.169
21.75	0.480	0.400	0.348	0.304	0.275	0.247	0.228	0.210	0.202	0.186
22.25	0.698	0.494	0.415	0.363	0.322	0.288	0.262	0.244	0.228	0.214
22.75	1.005	0.715	0.505	0.426	0.375	0.335	0.307	0.276	0.262	0.238
23.25		1.016	0.725	0.515	0.439	0.392	0.350	0.327	0.295	0.276
23.75			1.021	0.735	0.531	0.456	0.405	0.368	0.344	0.310
24.25				1.025	0.748	0.546	0.478	0.425	0.384	0.358
24.75					1.030	0.756	0.562	0.489	0.447	0.404
25.25						1.033	0.766	0.575	0.514	0.465
25.75							1.037	0.781	0.593	0.535
26.25								1.039	0.795	0.610
26.75									1.041	0.810
27.25										1.043

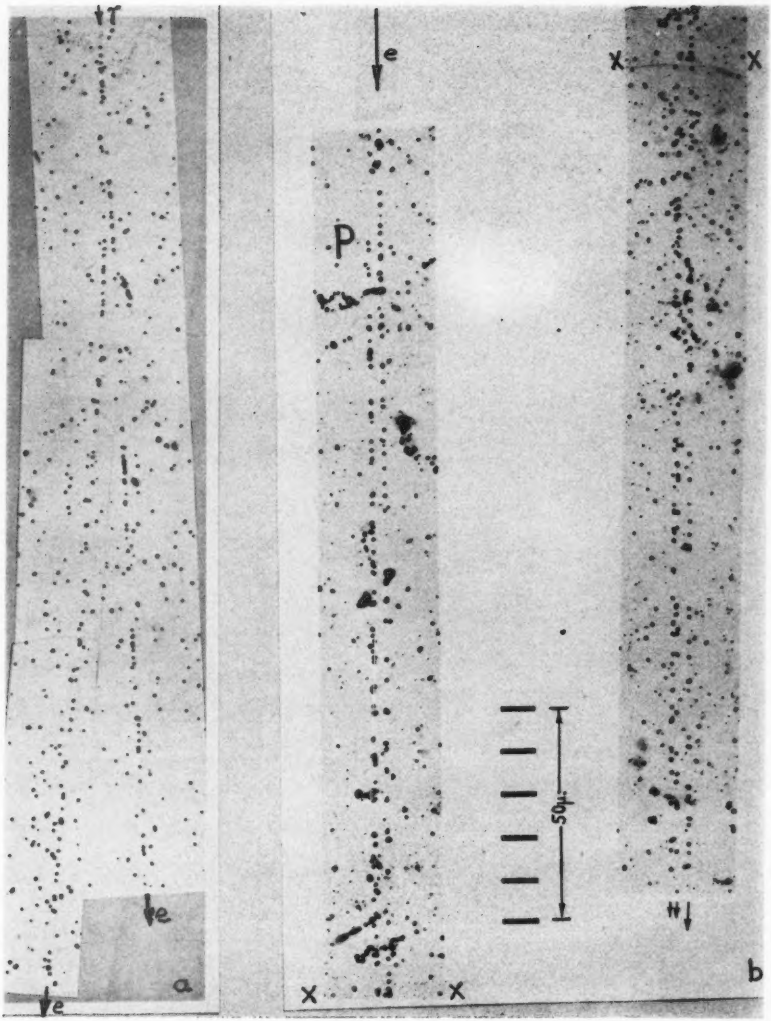

FIG. 1. *Examples of electron events.*
(a) Electron pair of low quantum energy.
(b) The materialization of an energetic photon at P, close to and parallel with the track of a fast particle. It is reasonable to suppose that the photon represents Bremsstrahlung from the parent electron.

ELECTROMAGNETIC CASCADES IN PHOTOGRAPHIC EMULSIONS[1]

By J. E. Hooper, D. T. King, and A. H. Morrish

Abstract

Photographic emulsion techniques are described for observation and identification of electromagnetic processes which occur in the soft component of the cosmic radiation. Several cascade showers are illustrated and measurements on these are discussed in the light of theoretical predictions.

Introduction

The introduction of photographic emulsions sensitive to the passage of relativistic particles of charge $/e/$ has led to new results in the study of electromagnetic processes initiated by the cosmic radiation. A number of experiments designed to investigate the properties of the fluxes of energetic electrons and photons at great altitudes have been carried out in this laboratory during the past two years. Ilford G5 emulsions 400 μ thick and capable of recording the tracks of electrons ionizing at the minimum rate were carried to great altitudes by free balloons filled with hydrogen. After recovery and suitable photographic processing, the emulsions were examined systematically through microscopes fitted with oil immersion objectives.

In the course of this search, sets of nearly parallel tracks of low and constant grain density have been observed. When the points of origin of these tracks can be found in the emulsion, it is usually possible to interpret them as electromagnetic events of one of the following types:

(i) Electron* pair production by a γ-ray. (Fig. 1*a*).

(ii) Direct pair production by a fast electron ('trident').

(iii) The apparent conversion of a *Bremsstrahlung* γ-ray to an electron pair beside the track of a fast electron (Fig. 1*b*).

(iv) Energetic electron recoil from a fast particle.

(v) Multiple electron pair production in which four electrons are apparently created by the conversion of a single γ-ray (12).

(vi) Cascade generation which may involve any or all of the above processes.

Because the emulsion is thin, cascade events complete enough to provide material for analysis are rare. The observation and measurement of these phenomena in the emulsion permits an insight into cascade development hitherto unattainable.

[1] *Manuscript received May 30, 1951.*
Contribution from the H. H. Wills Physical Laboratory, University of Bristol, Bristol, England.

* *The term 'electron' is used here to designate both positrons and negatrons.*

Techniques of Observation

Experience has shown that the ×45 objective is suitable for the arduous and prolonged search which is involved in the accumulation of large numbers of these events. It has been necessary to limit the observations to those events of path length in the emulsion sufficient to permit an energy determination by multiple scattering (9).

The following methods of search have therefore been adopted. Parallel strips, across the plate, 250 μ wide, are examined closely. These are spaced at a distance that will ensure the discovery of the majority of events, of path length in the emulsion exceeding the required value. This procedure greatly increases the rate at which significant events are detected.

The majority of such events found are single electron pairs produced by γ-radiation. A pair is most readily detected as two apparently related and nearly parallel tracks of minimum grain density, and is rarely found through the direct perception of its point of origin. In a systematic search a marked discrimination may be noted against finding those pairs for which the paths of the two particles are not appreciably parallel for any distance in the emulsion. This reduction in search efficiency applies to those pairs of low quantum energy, to those of marked disparity in the energies of the two electrons, and to those energetic pairs of which the two electron tracks never become noticeably separated in the emulsion.

Further difficulties of discrimination arise with regard to the selection of material for measurement. It has been found convenient to apply a criterion of minimum path length in the emulsion for each track of an event, but this is not necessarily the most desirable for an analysis of data obtained by multiple scattering. Thus, few pairs of low quantum energy satisfy a length requirement of more than 1 mm. per track, whereas the errors of measurement on the tracks of very energetic pair particles may be disproportionately high for path lengths limited to only 2 mm. in the emulsion. The length criterion may also cause the rejection of a pair of marked disparity by the loss of the more scattered track through one of the emulsion boundaries. The same effect applies to those pairs of wide angle which separate in a plane nearly perpendicular to that of the plate.

Another source of experimental error arises in these observations from variations in the efficiency of individual observers. Such factors as the conditions of physical and mental comfort prevailing in the laboratory may noticeably influence the data. Visual faults may also exercise some effect, such as possible discrimination by an astigmatic observer against pairs orientated at a particular angle in the field of view. These factors vary from day to day and from observer to observer and are always difficult to assess.

Identification of Electron Tracts

The track of an electron with total energy exceeding 1.5 Mev. exhibits a specific ionization within 10% of the minimum value. Since the minimum

specific ionization of relativistic particles of charge /e/ is independent of mass, a further identification of the tracks of energetic electrons must be made by one or more of the following characteristics.

(i) *Multiple Scattering*

A mean angle of scattering greater than 0.25° per 100 μ path length indicates a momentum of less than 100 Mev./c for the particle. This identifies the particle as an electron since the μ-mesons produce tracks of minimum ionization only when the mean angle of scattering is less than 0.25° per 100 μ. It is assumed that no charged particles exist intermediate in mass between electrons and μ-mesons.

(ii) *Radiative Energy Loss*

The theory of Heitler shows that the cross section for the energy loss in radiative collisions is proportional to the reciprocal of the square of the mass of the incident particle. Therefore the probability is very small that the process will be found to occur on the tracks of particles other than electrons. A sudden increase in the mean angle of scattering of a track is thus an indication of the electronic nature of the particle. Apparent energy loss by radiation has frequently been detected on the tracks of particles originating in pair events but has never been found to occur in the tracks of particles emerging from nuclear explosions. The work of Camerini *et al.* (7) has established that electrons are rarely, if ever, emitted in the course of nuclear disintegrations.

(iii) *Phenomenological Evidence*

The foregoing criteria provide evidence that the majority of particles originating in such events as tridents, multiple pair production, and cascade processes, are of electronic mass. In addition it is reasonable to assume that particles more massive than electrons are not created by the materialization of γ-rays. When identification is based on these phenomenological grounds (Fig. 1*b*), it must be remembered that cascade showers may possibly form close to, and in a direction nearly parallel with, the track of a relativistic meson or proton. This situation arises through the simultaneous generation of charged and neutral π-mesons in energetic nuclear explosions. The majority of cascade showers at great altitudes originate from the conversion of the photons which result from the spontaneous decay of the short-lived neutral π-mesons.

Characteristics of Electron Tracks

(i) *Ionization Loss*

Bloch (5) first derived the relation between the rate of energy loss by ionization, and the velocity, for charged particles. A calculation, assuming perfect screening of the nucleus by the atomic electrons and a mean value of the ionization potential of 13.5 Z ev. per atom, yields 0.57 Mev. as the minimum ionization loss per mm. of a charged particle in the G5 or NT4 emulsions. The order of magnitude of this result has been confirmed by the experiments of Brown *et al.* (6).

(ii) *Radiation Length*

The *radiation length*, X_0, is defined as the path length in which the initial energy of a fast electron is reduced through radiative collisions, on the average by a factor e (3). For great energies, at which this rate of energy loss is nearly constant, X_0 is given by the equation:—

$$X_0 = \left(\frac{4Z^2N_0}{137} r_0^2 \log \frac{183}{Z^{1/3}}\right)^{-1} \tag{1}$$

where N_0 is the number of atoms per cc. of the medium and r_0 is the classical radius $\frac{e^2}{m_0c^2}$ of the electron. Evaluation of X_0 for the nuclear emulsion yields a value of 2.9 cm. Measurements have been made of the mean angle of scattering, $\bar{\alpha}$, over 5 mm. intervals on electron tracks exceeding 1.5 cm. in the emulsion. Preliminary results shown in Fig. 2 verify the order of magnitude of the theoretical result. The ordinates indicate the mean value of the ratio $(\bar{\alpha}_{X=0}/\alpha_X)$ in each interval at distance X along the tracks. It is of interest to note that the method is independent of the scattering constant and the initial energy of the particles.

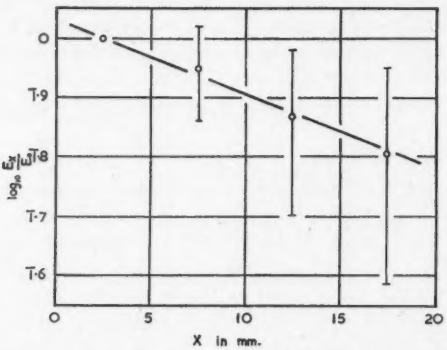

FIG. 2. *Measurements of radiative energy loss on 18 tracks of fast electrons. The slope of the curve yields the value 3.4 cm. for the radiation length in the emulsion. The limits of error indicated are the standard deviations.*

(iii) *Critical Energy*

When fast electrons traverse matter, energy is lost both by ionization and by radiative collisions. The rate of loss by the latter process varies with energy, and the particular energy at which the radiative loss is equal to the ionization loss is called the *critical energy*. It may be noted that in a radiation length, an electron loses, through ionization, energy nearly equal to the critical energy. This quantity is characteristic of the absorbing material, and for nuclear emulsions is in the neighborhood of 20 Mev.

(iv) *Conversion Length*

The *conversion length* is that in which a beam of photons is reduced by pair production to e^{-1} of the initial intensity. This length decreases with increasing

quantum energy to a nearly constant value above 300 Mev. From theory it may be seen that the conversion length in the emulsion at great energies is 3.8 cm. or 9/7 of the radiation length.

Cascade Showers

In the course of the examination of about 3 cc. of electron-sensitive photographic emulsion exposed to the cosmic radiation at 68,000 ft., eight striking examples of electron cascade phenomena have been found. Facsimile drawings representing the tracks of three of these multiplicative events are shown in Figs. 3, 4, and 5. A similar example has been published previously (13). In these drawings the lateral scale has been expanded by a factor of 20 or greater relative to the axial scale, since otherwise the high collimation of the electron tracks would obscure the details of the cascade development.

The cascade process was first investigated theoretically by Bhabha and Heitler (4) and by Carlson and Oppenheimer (8). Experimental measurements in Wilson cloud chambers have been made by many workers. Typical of these investigations are those of Hazen (10) who studied the development of showers in absorbers of various thicknesses. Others, such as Lovati *et al.* (15) have applied cascade theory to the determination of great quantum energies in the course of investigations of the π^0-mesons.

The photographic method offers peculiar advantages in the study of these 'soft' showers. The points of origin and the spatial distribution of the individual events are readily determined relative to the cascade axis. This enables a reasonable discrimination between tridents and electron pairs arising from the conversion of *Bremsstrahlung*. In Wilson cloud chambers, the details of the multiplicative processes are of necessity obscured within the thickness of metal absorbers, whereas in these studies the sensitive material is itself the absorber. The degeneration of the initial energy among the daughter particles may be analyzed at all stages by the methods of multiple scattering.

These events are rare because the primary must be of high energy and closely parallel with the plane of a thin emulsion, so that the secondary tracks have a reasonable probability of remaining within the sensitive layer. A correction has to be made in the observations to take into account a continuous escape of low energy particles through the emulsion boundaries even in the initial stages of the cascade. It is anticipated that it will prove possible within the next few years to manufacture, process, and examine considerably thicker emulsions. Such improvements will greatly minimize these difficulties.

In our study of cascade showers we have compared our observations with deductions from the one-dimensional theory as tabulated by Janossy (14). Following this author we have employed the quantity X_0 defined in Equation 1 as the unit cascade length. It should be noted that this is not the same definition of cascade length as that used by some other workers, for example Arley (1). Since the efficiency of detecting those electrons of less than 20 Mev. in a cascade is poor, we have restricted our computations to the numbers of

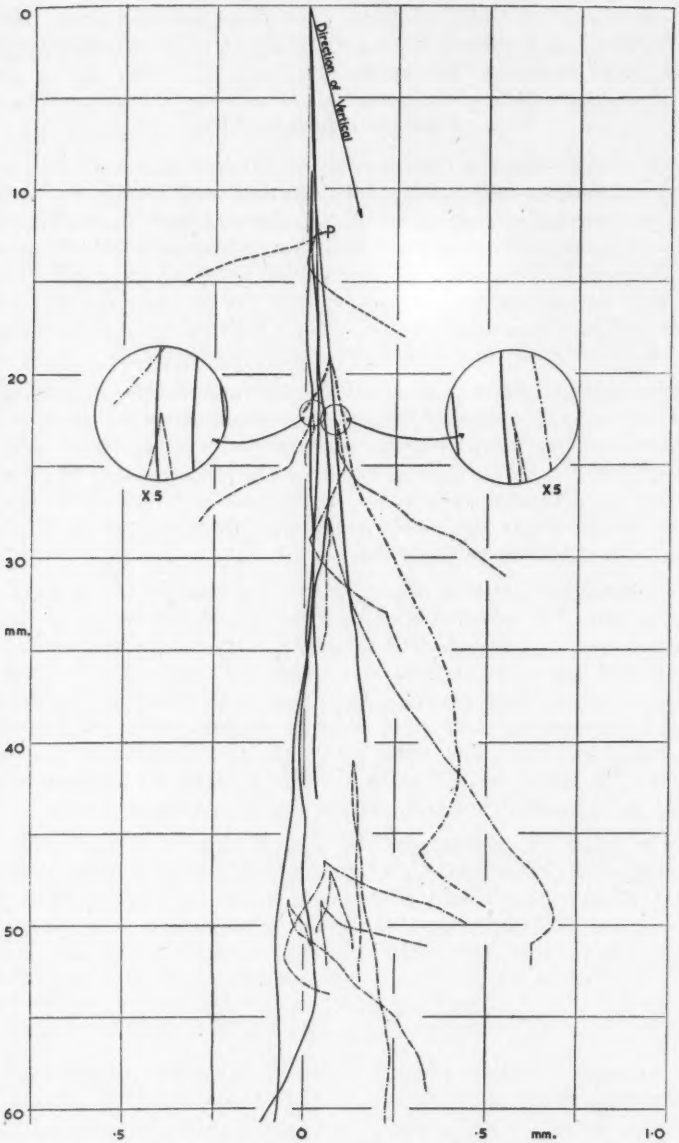

FIG. 3. *A facsimile drawing representing the tracks of a cascade shower observed in the emulsion. The shower originates by the conversion of an energetic photon. The plain and dot-dash lines indicate electrons of pairs produced by γ-rays. The dashed lines indicate the tracks of two secondary electrons of low energy from the trident. Lateral scale × 20.*

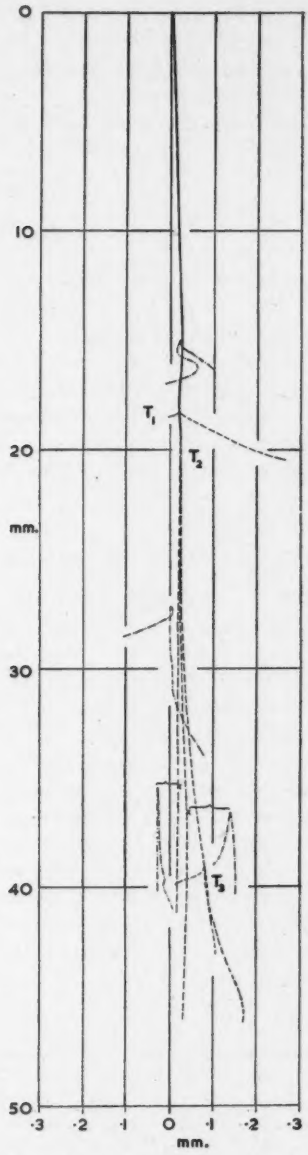

FIG. 4. *A reproduction of the tracks of a soft shower originated by a fast electron (plain line). The dashed lines indicate trident secondaries and the dot-dash lines the tracks of electrons of pairs which are produced by Bremsstrahlung. Lateral scale* × *20.*

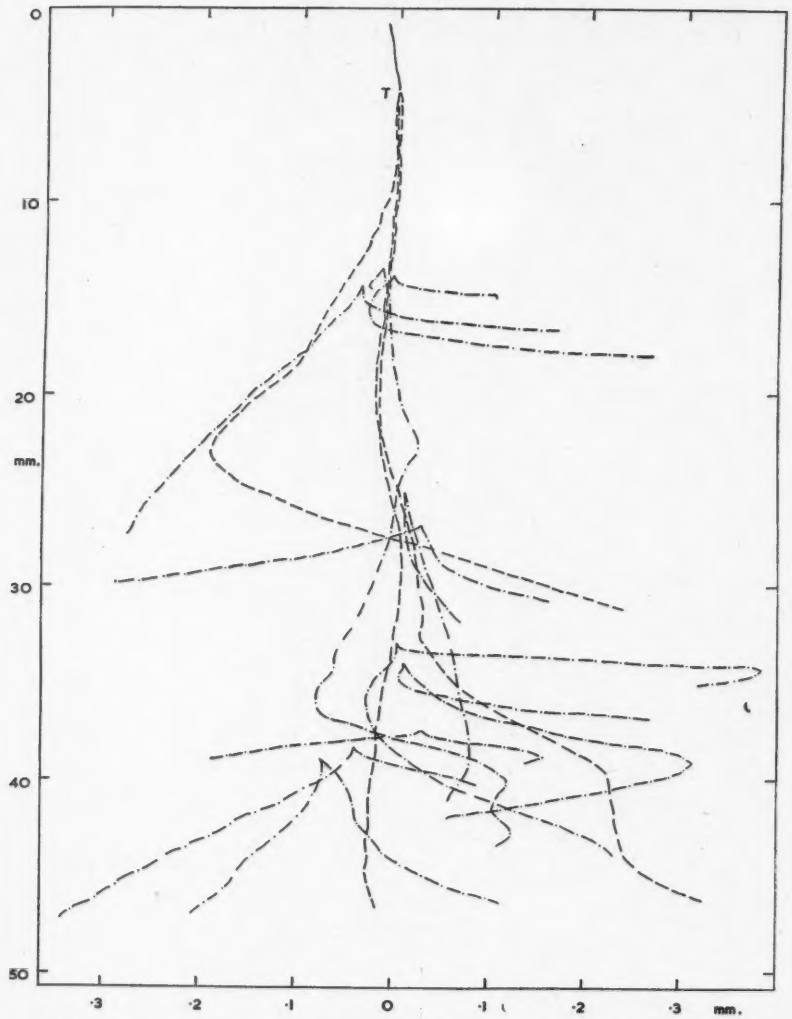

FIG. 5. *An electron (full line track) initiates a cascade of one trident (dashed lines) and ten associated electron pairs (dot-dash lines). Lateral scale × 50.*

electrons expected above this energy. Also, because the loss of energy above 20 Mev., the critical energy, is predominantly by radiation, we have neglected the ionization term in the cascade diffusion equations. It can then be shown that the number Q_0 of electrons or photons, with energies exceeding w, produced by a primary of energy w_0 after a length L cascade units is given by the integral:

$$Q_0(w, w_0, L) = \frac{1}{2\pi i}\int_{\eta_0-i\infty}^{\eta_0+i\infty}\left(\frac{w_0}{w}\right)^{\eta-1}\cdot\frac{1}{\eta-1}\left\{M(\eta)\exp\left[-a_1(\eta)L\right]+N(\eta)\exp\left[-a_2(\eta)L\right]\right\}d\eta, \quad (2)$$

where the particular functions of M and N depend on whether the cascade was initiated by a photon or electron. Further details may be found in Janossy's book (14). This author also gives tables of Q_0 derived by the use of the saddle-point method of approximating the integral. Since the showers which we have found in the photographic emulsions are confined to observable lengths of the order of only one or two cascade units, it is necessary to retain the second exponential in Equation 2.

Observations on the Illustrated Cascades

As an example of the application of Equation 2 to the observed showers, Fig. 3 is discussed in some detail. This drawing represents a cascade initiated by a photon of energy about 1.8×10^4 Mev. A trident appears at P, and, in addition, 10 associated electron pairs are formed by the conversion of *Bremsstrahlung* photons. All the tracks ultimately disappear as a result of the electrons passing through the air or glass interfaces of the emulsion. The origin of the first pair is taken as the beginning of the shower, because the exact distance travelled by the primary photon before conversion is not known. The shower is now considered as the sum of two individual cascades, the primaries of which are the two electrons of the first pair. The energies of these are 10,000 and 8000 Mev. On this basis, the average number of electrons of energy above 20 Mev. expected for $L = 1$ is 4.7 and 4.4 respectively, or a total of 9.1. For $L = 2$ the corresponding numbers are 13.9 and 12.4, which give about 26. The initial energies of all electrons observed in the shower are set out in Table I. The experimental number at any value of L is taken to be made up of two parts:

(*a*) those tracks actually seen; and

(*b*) those electrons which were created earlier, left the emulsion before L, and which probably would have had an energy exceeding 20 Mev. at L.

Taking account of these considerations, we find for the shower under consideration that for values of L of 1 and 2, the observed numbers are 12 and 15 respectively.

TABLE I

ENERGIES OF ELECTRONS OBSERVED IN FIG. 3

Event	Energy$_1$, Mev.	Energy$_2$, Mev.
Pair 1	10,000	8000
Pair 2	2700	1400
Trident 1 (7900 Mev.)*	34	23
Pair 3	475	50
Pair 4	70	50
Pair 5	75	60
Pair 6	425	300
Pair 7	180	30
Pair 8	130	60
Pair 9	135	20
Pair 10	260	80
Pair 11	22	13

* *A trident has three secondary particles.*

It should be pointed out that cascade theory predicts expected numbers only, and that fluctuations of the observed values from the mean may be very large (16). Another factor which influences the observations is the failure to observe cascade development which would occur if the emulsion were not of limited thickness. This effect is difficult to estimate but depends upon the initial energy and the value of L considered. The relatively small number of tracks at $L = 2$ in Fig. 3 may be attributed to either one or both of these factors.

The majority of the cascade showers found so far arise, however, from the degradation in energy of one or more fast electrons which enter the emulsion. It is conceivable that under these circumstances one or more photons may accompany the electrons. In at least one shower it is clear that this has in fact occurred since a secondary pair has been formed prior to the entry from the glass of the parent electron.

Another factor which appears to be of importance in the development of cascades is the trident process (13). This modifies the rate of production of secondary electrons at great energies and is an effect which has, up to the present, been neglected in the diffusion equations. We have found that five out of seven of the showers incorporate one or more tridents. It should be noted, however, that on account of unequal energy division among the secondary particles, this process is relatively less important than it would be if equipartition of energy invariably occurred. From our earlier studies we have observed that, in more than 90% of the tridents, more than half the available energy is given to one of the secondary electrons. Indeed, in rather more than 50% of the examples, one of the outgoing electrons carries more than two-thirds of the primary energy.

The cascade reproduced in Fig. 4 is an interesting example of a soft shower. In this event three tridents occur, together with four associated pairs, in a

path length of 1.5 cascade units. The energy of the primary electron is about 1.3×10^4 Mev.; at this energy, the cross section for trident production is approximately 1/10th of that for radiative collisions (17).

Fig. 5 represents a soft shower initiated by an electron of 4×10^3 Mev. In this cascade, the development begins with a trident, and this is followed by the creation of 10 pairs in a path length of 4.5 cm. The number of electrons with $E > 20$ Mev. at $L = 1.5$ is calculated to be 6.3: the corresponding experimental number is estimated at 12. In this event the geometrical loss is probably small, because the event remains close to the median plane between surface and glass. The large discrepancy observed may be explicable in terms of any of the other effects mentioned above.

Origins of Cascade Primaries

Considerations of the decay processes of charged and neutral π-mesons indicate that at altitudes exceeding 20 km. the great majority of electron cascades originate from the γ-rays which occur through the decay of the short lived π° particles. Some of these γ-rays may materialize in the emulsion, resulting in an energetic cascade (Fig. 3), while others may materialize in the atmosphere at a considerable distance from the plate assembly, so that the observations of a pair of associated electrons entering the plates would be rare. The single electrons arising in such circumstances are considered to form the majority of our shower primaries. (Figs. 4 and 5, and others not illustrated.) Rossi (18, 19) has shown that only a very small proportion of fast electrons entering the emulsion at these altitudes can be due to the spontaneous decay of energetic μ-mesons, or to recoil processes. In the emulsion, however, the probability of energetic electron recoils from relativistic mesons is much greater. Two cascades arising in this way have been identified in this laboratory; one of these has been previously published (13).

Conclusions

The observations which have been described lead us to the conclusion that the photographic method provides a new and powerful approach to the detailed study of electromagnetic shower phenomena. It is expected that present limitations will be largely removed when it becomes possible to process thicker emulsions without distortion and to examine these with reflecting microscopes (2).

It is predicted by the mathematical theory that there are very large statistical fluctuations (16) in the numbers of particles expected at any given stage in the development of a cascade. In the light of this result, the present observations are not inconsistent with the cascade theory. We have also been able to examine in detail the individual processes of cascade formation. In particular, the importance of the trident process in the initial stages of energetic cascades has been demonstrated.

Acknowledgments

We are indebted to Prof. C. F. Powell, F.R.S., for extending to us the hospitality and facilities of this laboratory, and for his continued interest and encouragement during the course of the work. We wish to acknowledge many helpful discussions with Mr. A. G. Ekspong*, and his assistance with some of the earlier measurements. We also wish to thank Mrs. J. Cowie, Mrs. D. M. Ford, Miss J. Jones, Miss M. Jones, and Miss J. Witchell for their assistance in collecting data. Two of the authors (J.E.H. and D.T.K.) were supported by grants from the Department of Scientific and Industrial Research and the Medical Research Council respectively; the other (A.H.M.) held a Post-doctorate Overseas Fellowship under the National Research Council of Canada. This work has been carried out as part of a research program supported by the Department of Scientific and Industrial Research.

References

1. ARLEY, N. Proc. Roy. Soc. (London), A, 168: 519. 1938.
2. BATES, J. W. and OCCHIALINI, G. P. S. Nature, 161: 473. 1948.
3. BETHE, H. A. and HEITLER, W. Proc. Roy. Soc.(London), A, 146: 83. 1934.
4. BHABHA, H. J. and HEITLER, W. Proc. Roy. Soc. (London), A, 159: 432. 1937.
5. BLOCH, F. Ann. Physik, 16: 285; Z. Physik, 81: 363. 1933.
6. BROWN, R. H., CAMERINI, U., FOWLER, P. H., MUIRHEAD, H., POWELL, C. F., and RITSON, D. M. Nature, 163: 47, 82. 1949.
7. CAMERINI, U., FOWLER, P. H., LOCK, W. O., and MUIRHEAD, H. Phil. Mag. 41: 413. 1950.
8. CARLSON, J. F. and OPPENHEIMER, J. R. Phys. Rev. 51:220. 1937.
9. GOTTSTEIN, K. L. F., MENON, M. G. K., MULVEY, J. H., O'CEALLAIGH, C., and ROCHAT, O. Phil. Mag. 42: 708. 1951.
10. HAZEN, W. E. Phys. Rev. 69: 298. 1946.
11. HEITLER, W. Quantum theory of radiation. 2nd ed. Oxford University Press. 1944.
12. HOOPER, J. E. and KING, D. T. Phil. Mag. 41: 1194. 1950.
13. HOOPER, J.E., KING, D. T., and MORRISH, A. H. Phil. Mag. 42. 304. 1951.
14. JANOSSY, L. Cosmic rays. 2nd ed. Oxford University Press. 1950.
15. LOVATI, A., MURA, A., SALVINI, G., and TALGIAFERRI, G. Nuovo Cim. 7: 943. 1950.
16. MESSEL, H. Proc. Roy. Irish Acad. In press. 1951.
17. RAVENHALL, D. G. Proc. Phys. Soc. (London), A, 63: 1177. 1950.
18. ROSSI, B. Revs. Modern Phys. 20: 537. 1948.
19. ROSSI, B. Revs. Modern Phys. 21: 104. 1949.

**Formerly known as Mr. A. G. Carlson.*

A 200 kv. HIGH TENSION SET FOR THE ACCELERATION OF H^3 AND He^3[1]

By K. W. Allen,[2] E. Almqvist, J. T. Dewan,[3] and T. P. Pepper

Abstract

A 200 kv. high tension set suitable for the acceleration of H^3 and He^3 is described. Special features incorporated in the accelerator include a radio-frequency type ion source capable of giving large beam currents with low gas consumption, a differential pumping system for recovering the gas used by the ion source, and an electronic stabilizer which reduces voltage fluctuations to a negligible value.

Introduction

The advantages of using H^3 and He^3 as bombarding particles in the study of nuclear reactions have long been recognized. Both nuclei have low binding energies per nucleon and consequently should induce reactions that are in general exothermic and that, for light elements, might be expected to have adequate yields at low energies. In addition compound nuclei are formed which have many possible modes of disintegration; in some cases these lead to product nuclei that cannot easily be studied by any other means.

Until recently neither H^3 nor He^3 has been available in sufficient quantities to allow a systematic study of their interactions with other nuclei. Tritium is a β^- emitter, decaying with a half-life of 12.5 yr. into He^3, which, although stable, comprises only $10^{-4}\%$ of atmospheric helium. However, the advent of high power nuclear reactors has made possible, through the neutron bombardment of lithium, the production of sufficient quantities of tritium and hence He^3 to begin such a systematic study. The purpose of this paper is to describe a 200 kv. accelerator which has been built at Chalk River for the bombardment of light elements with tritons and He^3 ions. Three special features are incorporated in the accelerator, the first two being dictated by the scarcity of gas available and the radioactivity of H^3. These are:

(1) a radio-frequency type ion source capable of producing beam currents of the order of 200 μa. with a hydrogen gas consumption of 9 cc. per hr. at N.T.P.;

(2) a differential pumping system with mercury diffusion pumps which allows recovery of more than 95% of the gas admitted to the ion source;

(3) an electronic stabilizer which reduces voltage fluctuations to less than 0.05%.

General Description

The main features of the high tension set are shown in Fig. 1. The accelerating potential is provided by two transformer-rectifier units, *A* and *B*, in

[1] *Manuscript received July 3, 1951.*
Contribution from the Nuclear Physics Branch, Atomic Energy Project, National Research Council of Canada, Chalk River, Ont., Canada. Issued as N.R.C. No. 2555.
[2] *Physicist, United Kingdom Staff; now at the University of Liverpool, England.*
[3] *Now with Schlomberger Well Surveying Corp., Houston, Texas.*

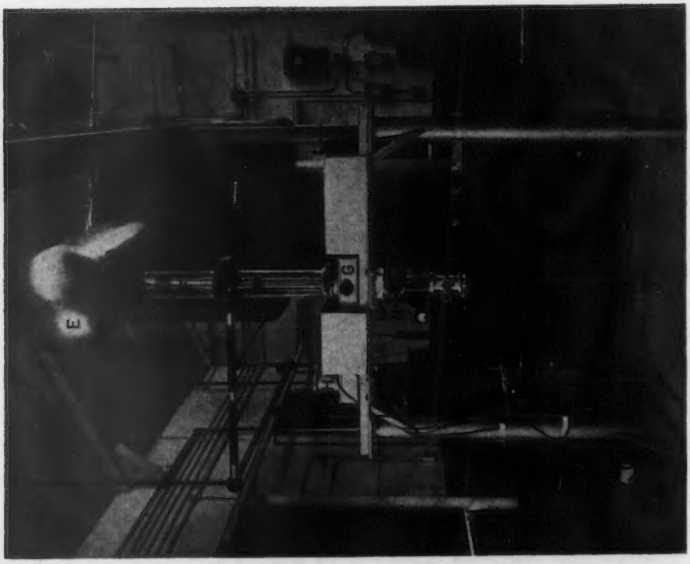

FIG. 2. *General view of the front of the accelerator.*

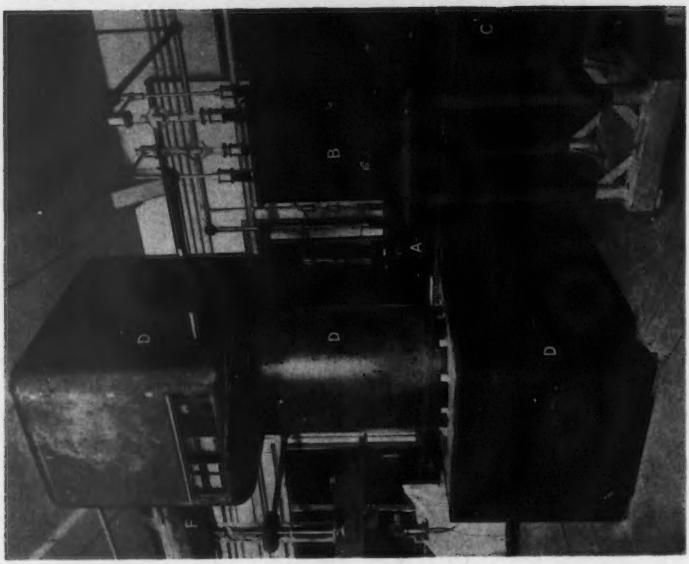

FIG. 1. *General view of the accelerator from the side.*

cascade. Power is fed to these through the isolating transformer *C*. The large structure *D* is the power stack. A metal base covered with plywood supports an insulating column, 5 ft. long and 3 ft. in diameter made of Grade XX Rolled Dilecto Tubing chosen for its combined strength and high resistivity. On top of this is the high tension enclosure, a wood and masonite box having a smooth exterior painted with conducting paint* to provide an equipotential surface. This houses a 4 kva., 500 cycle generator providing power for diffusion pumps and all electronic equipment at high potential. The generator is driven by long V belts from a 10 h.p. repulsion induction motor in the base and is carbon-pile regulated. Extending horizontally from one wall of the high tension box is a cylindrical aluminum tunnel *E*, 5 ft. long and 2 ft. in diameter, capped at the far end by a 2 ft. diameter hemispherical spinning (Fig. 2). This tunnel contains the ion source, differential pumping system, and gas recovery reservoirs. The upper half of the tunnel is made of removable wire mesh to allow observation of and access to the ion source. Directly below the ion source may be seen the accelerating tube *F* of conventional design with two accelerating gaps. Two 6 in. diameter Pyrex cylinders each 2 ft. long form the vacuum housing. At the bottom of the tube is the pumping manifold *G*, liquid air trap *H*, water baffle and diffusion pumps *K*, and backing pump *L*. An O-ring vacuum valve (3) at *M* may be used to isolate the target assembly below. In many experiments the beam, after passing through the Sylphon bellows *N*, is bent through 90° by a resolving magnet into the target chamber. The H.T. voltage is measured by a potentiometer method at the grounded end of the 250 megohm precision resistor chain *P*, a part of which is shown in Fig. 2.

Detailed Description

(*a*) *200 kv. Power Supply*

A circuit diagram of the unit which produces the main accelerating potential is shown in Fig. 3. It consists of two cascaded half-wave voltage doublers (*A* and *B* of Fig. 1), each capable of producing 20 ma. at 100 kv. The chassis of the two units are respectively 50 kv. and 150 kv. above ground so that it is necessary to feed power to them through an isolating transformer *C*. The voltage is varied by means of a Variac in the primary of the isolating transformer. In series with the primary are various time delays and safety switches to protect the high voltage supply. The ripple is approximately 0.3% per ma. and is reduced considerably by the stabilizing circuit described below. Connections to the accelerator are made at the 100 kv. and 200 kv. levels through 4-megohm 400 w. protective resistors.

(*b*) *Voltage Measurements and Stabilization*

The accelerating voltage is measured with a 250 megohm resistor chain (Fig. 2) consisting of 50 XR-5 wirewound units† of 5 megohms each with a tolerance of 0.1%. A 30 μa. meter, accurate to 0.5%, is arranged in a dividing

* *Rubalt #538-L supplied by Alfred Hague and Co. Inc., 227-34th St., Brooklyn, N.Y., U.S.A.*
† *Supplied by Shallcross Mfg. Co., Collingdale, Pa.*

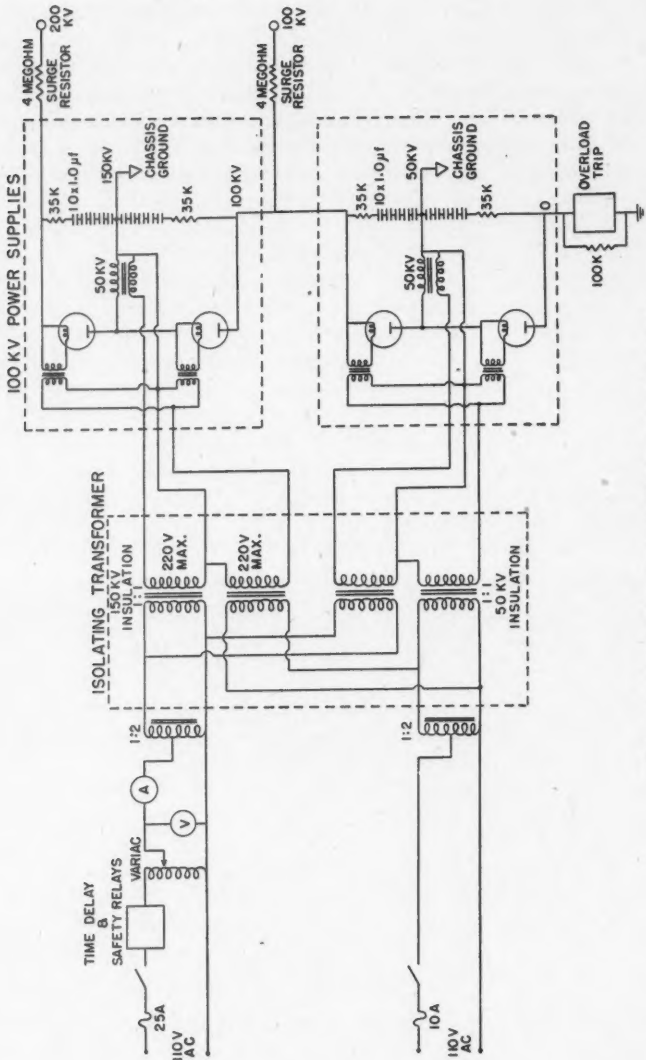

FIG. 3. *Circuit diagram of the 200 kv. potential supply.*

circuit at the bottom of the chain to read full scale at 300 kv. Provision is made for inserting a potentiometer in place of the meter for more accurate readings.

A schematic diagram of the method of stabilization is shown in Fig. 4. It has been fully described elsewhere (2). Briefly, a type 4E27 stabilizing tube, capable of handling variations of several thousand volts, is placed in series with the high tension supply and its plate-to-cathode voltage is controlled by an amplified error signal taken from the upper end of the resistance chain. A stabilization factor of about 40 is achieved, which suffices to reduce output voltage variations to less than 0.05%. This, in conjunction with a constant current supply for the beam deflecting magnet, permits attainment of very steady resolved beams.

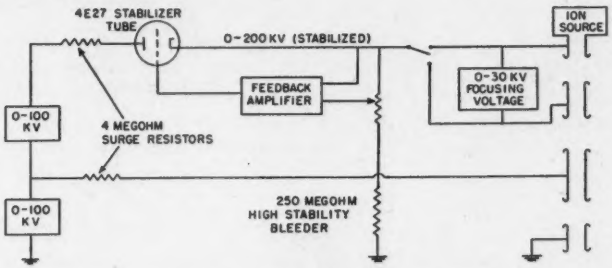

FIG. 4. *Schematic method of stabilization of the H.T. voltage.*

It is evident from Fig. 4 that the resistor chain may be connected to either the "top" or "bottom" end of the focusing supply. The former connection has the advantages that the resistor chain measures the over-all voltage (with the exception of 2–3 kv. extracting potential) and that this voltage is stabilized. An additional 30 kv. may be obtained by using the second connection at the expense of some voltage stability. This is done in the study of reactions with low yield in order to obtain maximum intensity of emitted particles.

(*c*) *Ion Source*

Details of the ion source are shown in Fig. 5. It is of the radio-frequency type described by Thonemann *et al.* (5) and was chosen for its ability to produce large beam currents of high atomic percentage with low gas consumption and with small energy spread in the emerging ions.

In this source a 25 Mc. per second r-f. discharge is maintained in an air cooled pyrex envelope, gas being allowed to enter at the top. The flow of hydrogen or tritium is regulated by a palladium leak; when helium is accelerated this leak is replaced by a fine control needle valve.* In order to maintain a high percentage of atomic ions the glass envelope must be cleaned occasionally and hence it is made easily removable. Hydrochloric acid is very effective in removing metal sputtered on the inside walls.

* *Obtained from W. Edwards and Co., Worsley Bridge Road, Lower Sydenham, London, S.E. 26, England.*

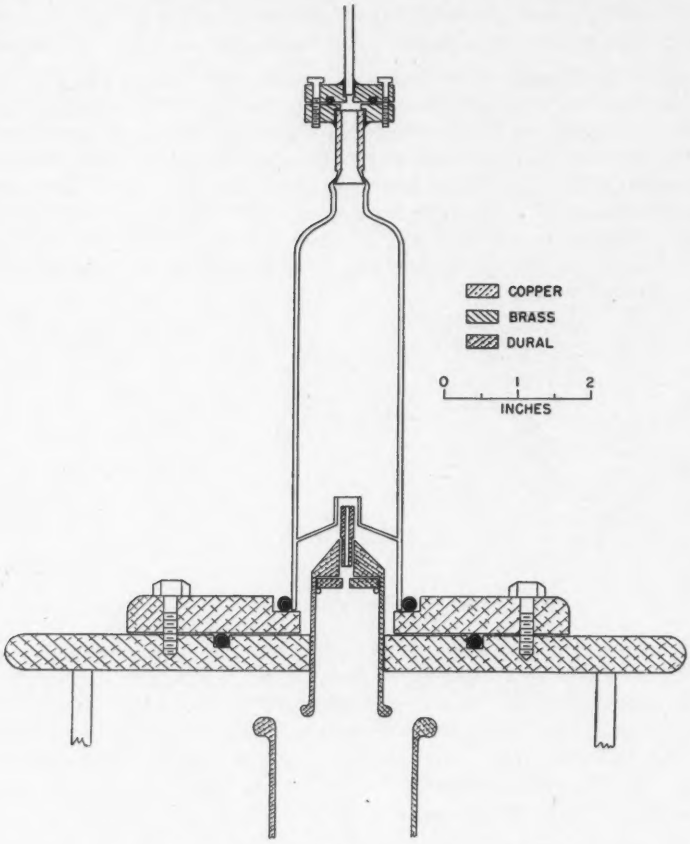

FIG. 5. *Details of the r-f. ion source assembly.*

Ions are drawn from the discharge by a small dural probe containing a canal 0.070 in. in diameter and 3/4 in. long. This probe is also made easily replaceable as it becomes charred and pitted after several weeks of operation. It was found necessary to provide a baffle plate below the probe to prevent return electrons welding it to the support.

The geometry of the probe and the glass chimney surrounding it is fairly critical. Poor ion extraction results if the height of the glass chimney above the probe is too great. If the chimney is too small in diameter it will suffer severe overheating from ion bombardment, while if it is too large excessive probe current will be drawn. The dimensions shown in Fig. 5 represent a satisfactory compromise.

A potential of 0–5 kv. applied between the probe and top of the ion source extracts ions through the probe, and a further potential of 0–40 kv. focuses the ions through a second small canal, 1/4 in. in diameter and 1 in. long, into the accelerating tube. The lower electrode of the focusing lens rests on three cams attached to shafts which protrude through the walls; these permit tilting the electrode to secure maximum beam current through the second hole. In the assembly of the electrodes the two canals are aligned along the axis of the accelerating tube. Design of the r-f. oscillator and voltage supplies (Fig. 6) is quite conventional. However, the r-f. coil wound about the glass envelope must be at the same potential as the extracting probe or sparking through the glass will occur. The position of the coil should be adjusted to give maximum beam current. It is not very critical.

Typical operation of the ion source is as follows. With 3.5 kv. extracting voltage, 10 ma. extracting current, and 30 kv. focusing voltage, a target current of 200 μa. is obtained with a hydrogen gas consumption of 9 cc. per hr. at N.T.P. This current is in the form of an unresolved beam collimated to 1/8 in. in diameter. The beam contains about 70% monatomic, 10% diatomic, and 20% triatomic hydrogen.

(d) Differential Pumping and Gas Recovery System

More than 95% of the gas admitted to the ion source is recovered by a differential pumping system (Fig. 7) which maintains the pressure in the focusing region at about 2×10^{-5} mm. of mercury. This all metal system consists of three mercury diffusion pumps, a D.P.I. MHG-50 backed by an Edwards Type 6 followed by another pump of the same type which has been modified to operate with a backing pressure up to 15 mm. of mercury. In addition to operating against higher pressures, mercury pumps are preferred to oil pumps because of greater cleanliness and because hot oil may cause loss of tritium by exchange. The pumps are cooled by transformer oil circulated via gear pumps and long Saran tubes through a water cooled heat exchanger at ground potential.

Gas passing through the pumps accumulates in a cylindrical steel tank having a large piston fitted with an O-ring to make a vacuum seal with the wall of the tank. Thence the gas is forced into a storage reservoir containing spongy uranium which absorbs tritium. At the end of a run all the tritium is absorbed in the spongy uranium and the recovery system isolated from the main accelerating tube by means of a vacuum valve (3) to prevent mercury contamination of the ion source. At the beginning of a new run the whole recovery system is first pumped out with the mechanical backing pump. Heating the uranium then forces the hydrogen–tritium mixture into the 200 cc. bottle beside the ion source. This flask holds sufficient gas for many hours of operation.

Spongy uranium is an excellent purifier as well as storage reservoir for tritium as it absorbs hydrogen isotopes and impurities at low temperatures and

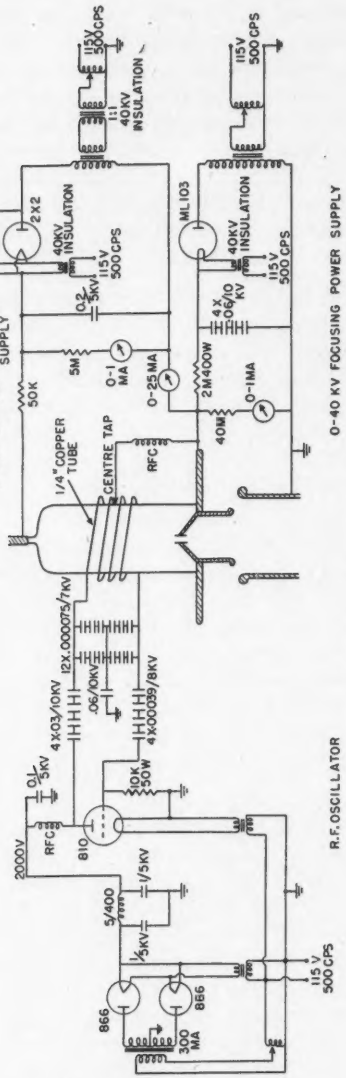

FIG. 6. *Circuit diagram of electronic apparatus for the ion source.*

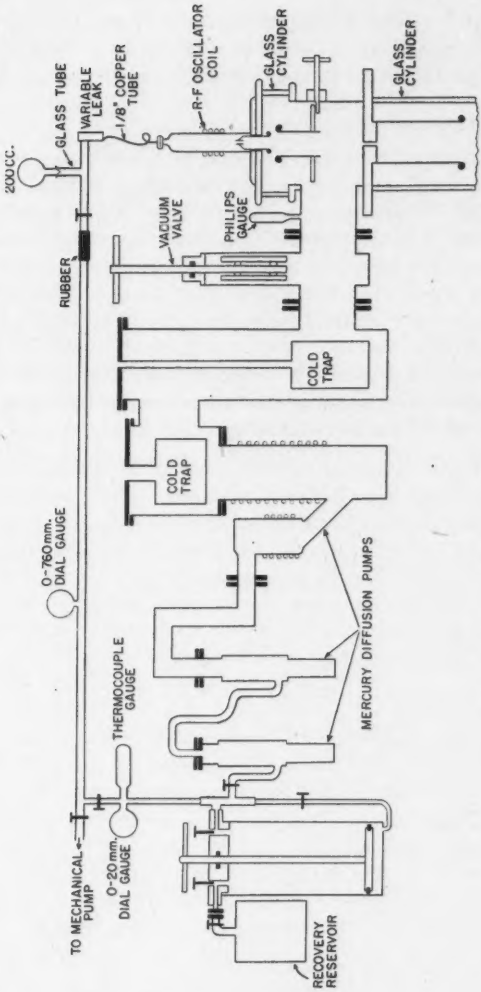

FIG. 7. *Differential pumping and gas recovery system.*

gives up only the hydrogen isotopes when heated to 450° C. A comprehensive account of the purification and manipulation of tritium in this system is to be published elsewhere.

In the acceleration of He^3 the recovery reservoir is merely an empty 1500 cc. container into which the gas is forced by the piston arrangement. The dead space in the connection to the piston assembly is about one cubic centimeter.

(*e*) *Accelerating Tube and Main Pumping System*

The main accelerating electrodes are three inches in diameter and are made of highly polished mild steel, the two accelerating gaps being approximately 1-1/2 in. in length. These electrodes are centered by external screw adjustments using O-ring seals. Experience has shown a disadvantage of this type of accelerating gap to be collection of charge on the glass and resultant shifting of the ion beam. Re-entrant electrodes would be preferable. Normally this shifting is not serious and is compensated by applying a variable voltage across a pair of parallel plates installed inside the vacuum manifold. This provides adequate compensation in one plane while adjustment of the magnetic field of the resolving magnet provides compensation in the plane at right angles. Thus complete control of the ion beam is attainable.

The main pumping system consists of a D.P.I. MC-275 oil diffusion pump using Octoil, equipped with both water baffle and liquid air trap. This is backed by a D.P.I. MB-100 vertical booster using butyl sebecate. The fore pump is a Kinney Type 556. Pressure in the pumping manifold is measured with an ionization gauge, operating pressures of the order of 5×10^{-6} mm. of mercury being normally obtained with a beam on. An arrangement of a Pirani gauge with a Sensitrol meter automatically switches off the diffusion pumps if the pressure in the accelerating tube rises above 10μ.

(*f*) *Controls and Metering*

Control of the accelerator conforms to standard practice and requires little elaboration. As the power supplies and variable gas leak for the ion source and the high tension voltage stabilizer are at high potential they must be remotely controlled. Inside the Dilecto column are long bakelite shafts rotated by selsyns at the bottom, which in turn are activated by mate selsyns at the control panel. On–off switching is effected by means of solenoid relays at the base of the power stack connected via nonconducting cord to microswitches at the top.

A panel in the high tension stack with a Lucite face (Fig. 1) houses meters displaying the generator output voltage, r-f. oscillator current, extracting current and voltage, focusing potential, voltage across the stabilizing tube, and pressure in the differential pumping manifold. A Philips gauge is used to indicate this pressure. Two dial gauges and a thermocouple gauge meter, which monitor various pressures in the recovery system, are mounted in the "tunnel" so as to be visible from the floor.

(g) *Tritium Monitoring**

To safeguard personnel it has been necessary to provide means of detecting accidental escape of tritium into the laboratory. To this purpose a large exhaust fan and a monitoring system with an alarm bell have been installed in the roof above the accelerator. This system consists of two identical air ion chambers, one sealed off and one open at the ends to receive the air which proceeds from the laboratory via an ion collector. The outputs of the two ion chambers are connected to a d-c. amplifier so that zero signal results if the ion current is equal in the two chambers thus cancelling background due to penetrating radiations. Ionization produced by tritium decay in the chamber through which laboratory air is passing will produce a signal which is amplified to ring an alarm bell and open louvres thus increasing by a factor of 10 the rate of exhaust of air from the laboratory.

Operation

The high tension set described in this paper has been operating for approximately one year and has given very little trouble. This may be attributed to the effectiveness of O-rings as vacuum seals and to the robustness of the electrical supplies both for the main accelerating potential and the ion source.

So far the accelerator has been used chiefly for the study of nuclear reactions induced by tritons bombarding tritium and lithium targets (1, 4). At the present time acceleration of pure He^3 is being undertaken and, as He^3 is so scarce, provision has been made for recovering the small amount of gas passing down the accelerating tube. A Swedish General Electric Type JHF33 mercury diffusion pump with a rated backing pressure of 20 mm. of mercury has been connected between the main diffusion pump and the Kinney backing pump. The set can be operated for many hours with the Kinney pump isolated and all gas from the main tube being pumped through the oil and mercury diffusion pumps into a 6 liter reservoir. At the end of the run, the gas accumulated in the reservoir is pumped back up the accelerating tube to the recovery system.

Whenever tritium is accelerated α-particles from the very prolific reaction

$$T + D \rightarrow He^4 + n + 17.6 \text{ Mev.}$$

appear, even though deuterium gas has never been allowed in the system. The natural isotopic content of deuterium present in hydrogenous oil vapor deposited on the target is sufficient to give large yields of α-particles if precautions are not taken. These α-particles are somewhat useful for calibration purposes but in other cases constitute a very annoying background. In the acceleration of He^3 it was necessary to change the ion source completely to eliminate tritium contamination.

* *Designed by H. Carmichael and J. C. Hilchcock of this laboratory.*

Acknowledgments

The authors wish to express their thanks to Mr. N. H. Neilson, Mr. J. C. Reynaud, and Mr. D. W. Medd for aid in the design and engineering of the accelerator, and to Mr. G. J. Leighton and Mr. J. Rothfels for technical assistance in its construction and operation.

References

1. ALLEN, K. W., ALMQVIST, E., DEWAN, J. T., PEPPER, T. P., and SANDERS, J. H. Phys. Rev. 82: 262. 1951.
2. DEWAN, J. T. Rev. Sci. Instruments, 21: 771. 1950.
3. KING, L. D. P. Rev. Sci. Instruments, 19: 83. 1948.
4. PEPPER, T. P., ALLEN, K. W., ALMQVIST, E., and DEWAN, J. T. Phys. Rev. 81: 315. 1951.
5. THONEMANN, P. C., ROAF, D., MOFFATT, J., and SANDERS, J. H. Proc. Phys. Soc. (London), 61: 483. 1948.

SOME STUDIES IN ANGULAR CORRELATION[1]

By E. K. Darby

Abstract

The beta-gamma-angular correlation in Sb^{124} has been measured as a function of beta energy using a 12 channel kicksorter and a thick crystal counter as beta-detector. The differential correlation coefficient $a(E)$ has been found to change from -0.17 at 1 Mev. to -0.44 at the end of the beta spectrum. When integrated numerically over all beta energies greater than 1 Mev. the integrated angular correlation coefficient so obtained agrees with the value measured directly. Experiments on the gamma-gamma-angular correlation in Co^{60} and Sc^{46} performed with the same apparatus are in agreement with previous results of other workers.

Introduction

The main purpose of the present paper is to describe some experiments on the angular correlation between the beta particles and gamma photons emitted in cascade by the Sb^{124} nucleus. In particular the dependence of the angular correlation on the energy of the beta particles was the object of this detailed investigation, the results of which have already been discussed briefly in a preliminary report (3).*

The present experiments on beta-gamma-angular correlation in Sb^{124} were undertaken because the results on the subject available in the literature were contradictory. Ridgway (10) reported the correlation coefficient as $a = -0.17$, while the results of Beyster and Wiedenbeck (1) gave $a = -0.26$. It was rightly hoped that if the integrated angular correlation was as strong as reported by Beyster and Wiedenbeck (1), a measurement of the dependence upon beta energy could be attempted, such an energy dependence being theoretically predicted by Falkoff and Uhlenbeck (4), but so far in no case being observed experimentally in a quantitative way.

Prior to the experiments on beta-gamma-angular correlation some experiments on the gamma-gamma-angular correlation in Co^{60} and Sc^{46} were done. Although the results of these latter experiments are not new, Brady and Deutsch (2) having observed this previously, it seems worthwhile to discuss them briefly as well. This is done because the same apparatus was employed as in the beta-gamma experiments, so the consistency of the gamma-gamma correlation results lends support to the subsequent beta-gamma-correlation results. Moreover, the accuracy obtained in the present gamma-gamma correlation experiments is perhaps slightly better than in the previously reported work.

[1] *Manuscript received July 20, 1951.*
Contribution from the Department of Physics, the University of British Columbia, Vancouver, B.C.

* *Although many nuclei have been investigated for beta-gamma-angular correlation, only in four cases, namely Sb^{124}, Tm^{170}, Rb^{86}, and K^{42} has any correlation been observed. The results of different observers for Rb^{86} are contradictory, while no confirmation of the results for Tm^{170} on K^{42} has been reported. The only report of an attempted measurement of the beta-gamma-angular correlation as a function of the beta energy is a very brief one on Sb^{124} by Stevenson (11), in which he made use of a lens spectrometer.*

Consequently, Part I and Part II of the present paper will be devoted to the gamma-gamma- and the beta-gamma-angular correlation experiments respectively.

I. Gamma-Gamma-Angular Correlation in Co^{60} and Sc^{46}

The apparatus employed in measuring the gamma-gamma coincidence rates as a function of θ employed RCA-5819 photomultipliers in conjunction with $1 \times 1 \times \frac{1}{2}$ in. anthracene crystals as gamma counters. The source was mounted at the center of a spectrometer table with the counters placed about $3\frac{1}{2}$ in. from it. The Co^{60} source was in the form of metallic cobalt, while the Sc^{46} source was in the form of scandium oxide. Pulses from the photomultiplier were amplified by a single stage head amplifier and transmitted by cathode follower to a "ring of three" linear pulse amplifier with a rise time of 0.15 μsec. and a gain of 100. Following the linear amplifier was a pulse height discriminator and a coincidence mixer with resolving time 0.17 μsec. The discriminator had a dead time of 2 μsec., so counting rates of 5000 per sec. could be handled with a counting loss of about 1%. With a source strength selected to give this counting rate, the accidental coincidence rate was about one half of the true coincidence rate.

The main difficulty experienced in the coincidence measurements is due to radiation being scattered from one counter to the other. The Co^{60} gamma rays interact with the counter crystal mainly by Compton scattering. The scattered photon may enter the second counter and be counted, thus producing a false coincidence count. If the counters have about the same efficiency for detection of the scattered radiation as for the emitted gammas, then these scattered coincidence counts may amount to as much as 50% of the true coincidence counting rate, with the counters and source in a straight line. The scattered coincidence rate will increase as one counter is moved around to the 90° position which will lead to errors in the observed angular correlation. The photons scattered in the backward direction in the case of the Co^{60} gamma rays have energies of about 200 kev. In this case it is possible to discriminate effectively against the pulses from the scattered radiation and still allow most of the pulses due to the gamma rays (1.17 and 1.33 Mev.) to be counted. Accordingly, the discriminators were set to eliminate pulses corresponding to particles with energies less than 200 kev. The absence of scattered coincidence counts was demonstrated by placing the counters in the 90° position and comparing the rates with and without a lead shield between them.

Readings were taken at 10° intervals ranging from 90° to 180°. The efficiencies of the counters may vary slightly, owing to a variation in the photomultiplier high tension supply. Since in the first approximation the coincidence rate is proportional to the product of the two gamma counting rates, the slight variations in efficiency may be corrected for by dividing the coincidence counting rate by this product. For counters subtending a very small solid angle at the source, the coincidence rate as a function of θ is proportional to the angular correlation function $W(\theta)$. $W(\theta)$ is the relative probability of emission of the second photon at an angle θ with respect to the direction of

emission of the first photon. However, the counters must subtend a finite solid angle, so it is necessary to apply a correction to the coincidence rate in order to obtain $W(\theta)$. The correction was calculated from the geometry of the counters on the assumption that $W(\theta)$ is of the form $W(\theta) = 1 + a \cos^2 \theta$ which is suggested by the uncorrected curve and is consistent with the theory. The angle subtended by the gamma counters was measured, using annihilation radiation from a Cu^{64} source. An included angle of 20° was selected in order to give sufficiently high counting rates without too great a loss in resolution. In the case of Co^{60} the correction to the measured correlation coefficient of $+0.147$ was $+0.006$ giving $a = +0.153$.

The disintegration of Sc^{46} follows a scheme similar to that of Co^{60}, the cascade gammas being only slightly lower in energy. The techniques as discussed for Co^{60}, therefore, apply as well to Sc^{46}. The results of the measurements on Co^{60} and Sc^{46} are plotted in Fig. 1. The curve shown was calculated from Hamilton's theory (5) for two successive quadrupole transitions involving nuclear states with angular momenta: $4 \rightarrow 2 \rightarrow 0$. These results are in good agreement with those obtained by Brady and Deutsch (2).

II. Beta-Gamma-Angular Correlation in Sb^{124}

Since the beta particles from a disintegrating nucleus have a continuous energy spectrum, it might be expected that the beta-gamma-angular correlation (if any) would be a function of beta particle energy. The theory de-

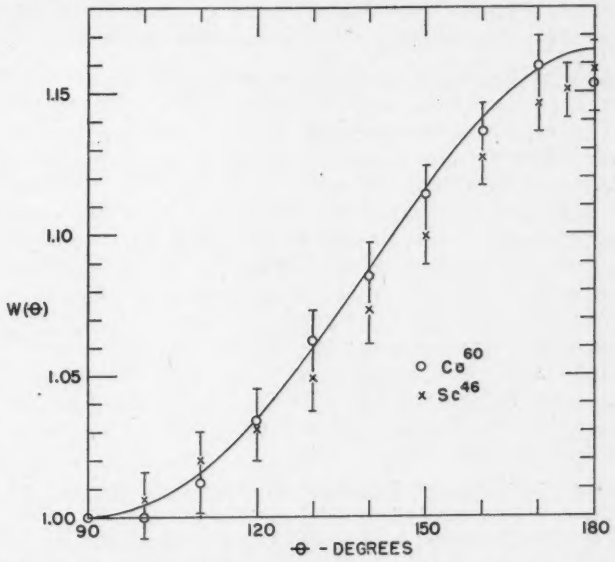

FIG. 1. *The gamma-gamma-angular correlation functions $W(\theta)$ for Co^{60} and Sc^{46}. The solid curve is calculated from the theory mentioned in the text.*

veloped by Falkoff and Uhlenbeck (4) indicates that, in general, this is the case. Consequently, we have to distinguish between the differential angular correlation function $w(\theta, E)$ and the integrated angular correlation function $W(\theta, E)$. The function $w(\theta, E)$ represents the relative probability of emission of a gamma photon in direction with respect to the direction of emission of the preceding beta particle, in a small range of beta energy ΔE at energy E. If the beta detector is sensitive to all beta particles of energy greater than E then the quantity measured will be proportional to $W(\theta, E) = \int_E^{E_0} w(\theta, E)N(E)dE$ where $N(E)$ is the number of beta particles in the energy interval $(E, E + dE)$ and E_0 is the maximum energy of the beta spectrum.

The *integrated* angular correlation was measured using a beta counter consisting of a layer of anthracene flakes approximately 20 mgm. per cm.^{2} in thickness on an RCA-5819 photomultiplier. The counter was practically 100% efficient as a beta counter but had low sensitivity to gamma photons. The gamma counter was the same as used previously in the gamma-gamma correlation experiments. The source in the form of sodium antimonate was deposited from solution on a zapon film, using insuline to obtain a uniform thickness, and was about 0.5 mgm. per cm.^{2} in thickness. It was enclosed in a 5 in. diameter vacuum chamber with the beta counter placed immediately outside an aluminum window 10 mgm. per cm.^{2} in thickness.

First a beta-gamma angular correlation experiment was performed with Sc^{46} to test for the presence of scattering. The distribution was isotropic within the statistical accuracy (which was 1%) in agreement with Novey (8).

Next the integrated beta-gamma-angular correlation function for Sb^{124} was measured. The decay scheme of Sb^{124} is complex, involving five beta groups (9). However, if the beta particles below 1 Mev. are absorbed, the beta-gamma coincidence rate will involve mainly the 2.37 Mev. group with an admixture of coincidences due to the 1.6 Mev. group; 270 mgm. per cm.^{2} of aluminum was used as absorber in front of the beta counter, with which arrangement beta particles having an energy greater than about 0.9 Mev. were counted. Readings were taken at intervals of 10° from 90° to 180°. The gamma-gamma coincidence rate, which appeared as a background amounting to 11% of the beta-gamma coincidence rate, is isotropic and has been subtracted. The correction for the finite angular resolution of 20° has been applied and the results plotted in Fig. 2. The vertical lines indicate the statistical deviation. The solid curve represents: $W(\theta) = 1 - 0.23 \cos^2 \theta$ which is in essential agreement with Beyster and Wiedenbeck (1) but is somewhat different from the results obtained by Ridgway (10).

The *differential* beta-gamma angular correlation coefficient

$$a(E) = \left[w(\pi, E) - w\left(\frac{\pi}{2}, E\right)\right] \Big/ w\left(\frac{\pi}{2}, E\right)$$

was measured in Sb^{124} by the following method. An anthracene crystal $\frac{1}{2}$ in. thick with an RCA-5819 photomultiplier was employed as a beta counter

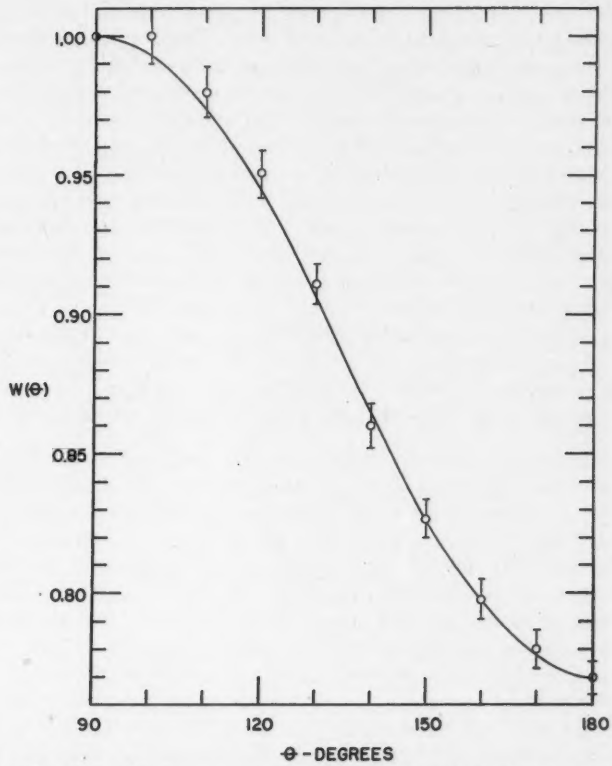

FIG. 2. *The integrated beta-gamma-angular correlation function for Sb^{124} for the beta energy larger than 1 Mev. The solid curve represents the function: $1-0.23\cos^2\theta$.*

to give pulses proportional to the energy of the beta particles. The work of Hopkins (6) indicates that, in an experimental setup similar to this one, the pulses are proportional to beta energy at least up to 3.2 Mev. The counter bias was set to discriminate against pulses corresponding to beta energies less than about 1 Mev. This bias also discriminates effectively against most of the gamma pulses; however, gamma-gamma coincidences amounted in this case to 15-20% of the beta-gamma coincidences. The beta pulses were transmitted through a gating circuit to a 12 channel kicksorter of Chalk River design (7). The gating circuit was controlled by the output of the coincidence mixer, so that it was opened whenever a coincidence occurred. The beta pulse which was delayed 0.25 μsec. to allow the gate to open, was then transmitted to the kicksorter. The 12 kicksorter channels were evenly spaced over the upper part of the beta spectrum from 1.0 Mev. to 2.37 Mev. The accidental coincidence counts in each kicksorter channel were obtained by measuring the shape of the beta pulse spectrum with the kicksorter and calculating from the total beta count which was obtained during each run.

The photomultiplier high tension (1000 v.) was stabilized with a battery reference and was maintained to within ± 0.2 v. This was sufficient variation, however, to cause a slight change in the beta pulse distribution, so coincidence readings were taken alternately for 12 hr. periods in the 90° and 180° positions, so the effects of any drift present would be minimized. The results of the four individual runs agreed in the worst cases to within two standard deviations. (See our previous communication in this connection (3).) The coincidence rates were divided by the product of the single channel rates to compensate for any change in counter efficiencies due to changing the position of the gamma counter. A correction was also applied for decay of the source. The gamma-gamma coincidence rate in this case was not quite isotropic, being about 10% greater in the position at 90° than at 180°. This effect was due to scattering from one counter to the other, the gamma counter necessarily being sensitive to low energy gamma photons. The background gamma-gamma coincidence rate was subtracted to give the true beta-gamma correlation coefficient and the correction was applied for the angular resolution of 20°.

The energy scale in terms of beta pulse size was fixed by determining the end point of the beta pulse spectrum as obtained on the kicksorter and constructing a trial Kurie plot for each of the four runs separately, the maximum beta energy being taken as 2.37 Mev. According to the results of Langer, quoted by Wu (12), the Sb^{124} beta spectrum (presumably the most energetic group of it) is of the "a-type". Consequently, when constructing the Kurie plots, a corresponding forbidden shape correction factor was introduced, although within the accuracy of the kicksorter measurements this is hardly necessary. The Kurie plots so obtained, one of which is shown in Fig. 3, could be resolved into two approximately straight lines, the lower energy beta group being in agreement with the accepted value of 1.6 Mev. The accuracy of the end point (2.37 Mev.) of the high energy beta group was about ± 0.05 Mev.

The results of the four separate series of measurements, each involving four to five days' counting, have been averaged, and the curve for $a(E)$ so obtained plotted in Fig. 4. (The points corresponding to the separate measurements are also indicated in the figure.) As a check on the consistency of the measurements, the curve for $a(E)$ and the beta spectrum as determined on the kicksorter were used to calculate (by numerical integration) the integrated angular correlation coefficient a, for $E > 0.96$ Mev. The value of a so obtained, -0.26, is in satisfactory agreement with the value -0.23, measured directly, as reported above. It may also be mentioned that the values of $a(E)$ reported by Stevenson (11) for two values of E are consistent with the curve for $a(E)$ shown in Fig. 4.

In view of the Sb^{124} decay scheme, lack of accurate experimental data concerning the shape of the beta spectra involved and the low accuracy of the $a(E)$ curve, an unambiguous comparison of this curve with theory seems hardly possible, at this stage. If we are to believe that the most energetic beta spec-

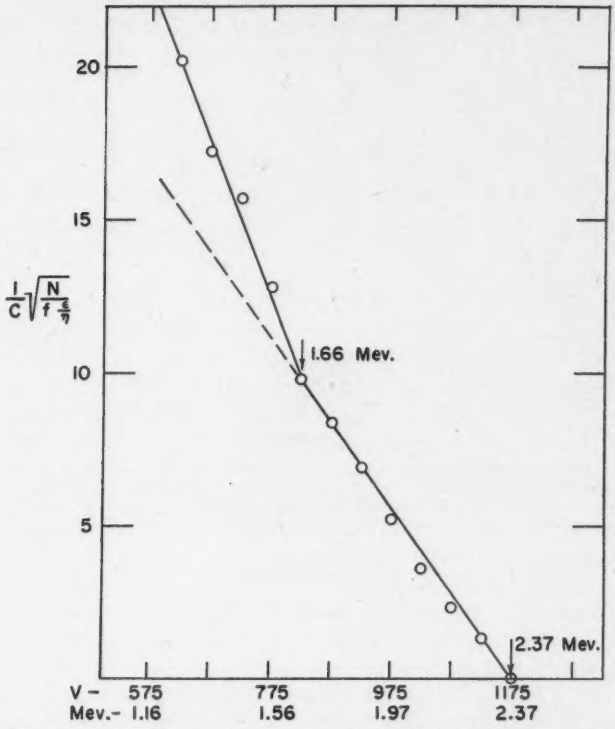

FIG. 3. *The Kurie plot of the beta spectrum as obtained with the kicksorter. The scale labelled V represents the kicksorter bias in arbitrary units. The energy scale in Mev. is proportional to V being adjusted so 2.37 Mev. is at the end point of the beta spectrum. N is the number of counts in a given channel, f is the Fermi function for Z = 52, and C = $[(\epsilon_0 - \epsilon)^2 + \eta^2]^{1/2}$ is the shape correction factor. ϵ is the total energy in units of mc^2, ϵ_0 the maximum energy in the same units, and η is the momentum in units of mc.*

trum is of an α-type (see a remark above), than it is not unreasonable to assume that the theoretical $a(E)$ curve above 1.6 Mev. (end point of the less energetic beta spectrum) would be mainly determined by the B_{ij} matrix element of the Fermi theory. On this assumption, and taking the angular momentum quantum number of the ground state of Te^{124} (even-even nucleus) to be zero, one still has a variety of possibilities regarding the angular momenta of the other two levels involved. In Fig. 4 the two dotted curves represent the theoretical $a(E)$ curves reported previously (3), which correspond to two tentative assignments of angular momenta: $1 \rightarrow 1 \rightarrow 0$ and $3 \rightarrow 2 \rightarrow 0$. Of course the curves may have significance (if any) only for energies above 1.6 Mev. All other assignments of angular momenta consistent with the above assumptions seem to be definitely contradicted by our experimental results; at least, if the gamma radiation involved is of multipolarity not higher than two.

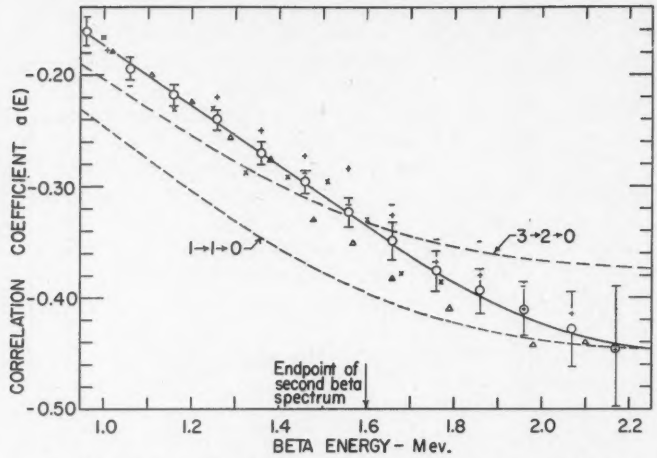

FIG. 4. *The beta-gamma angular correlation coefficient $a(E)$ as a function of the beta energy E. Experimental points corresponding to different series of measurements are indicated by symbols (+, −, ×, Δ). The average value of $a(E)$ with the standard deviation is indicated by the symbol ⊕ and the solid curve. The dashed curves are calculated from the theory mentioned in the text.*

Acknowledgments

I am indebted to Prof. W. Opechowski for valuable discussions in the course of these experiments and to Dr. A. H. Morrish for his suggestions in the early stage of the gamma-gamma correlation experiments. I am also indebted to Mr. G. W. Williams for his assistance in design and construction of the apparatus. This research was made possible by a grant from the National Research Council of Canada, and the author was aided by a Fellowship from the National Research Council of Canada.

References

1. BEYSTER, J. R. and WIEDENBECK, M. L. Phys. Rev. 79: 169. 1950.
2. BRADY, E. L. and DEUTSCH, M. Phys. Rev. 78: 558. 1950.
3. DARBY, E. K. and OPECHOWSKI, W. Phys. Rev. 83: 676. 1951.
4. FALKOFF, D. L. and UHLENBECK, G. E. Phys. Rev. 79: 323. 1950.
5. HAMILTON, D. R. Phys. Rev. 58: 122. 1940.
6. HOPKINS, J. I. Rev. Sci. Instruments, 22: 29. 1951.
7. MOODY, N. F., BATTELL, W. J., HOWELL, W. D., and TAPLIN, R. H. N.R.C. of Canada Report, CREL 464.
8. NOVEY, T. B. Phys. Rev. 78: 66. 1950.
9. Nuclear Data Circular 499, U.S. National Bureau of Standards.
10. RIDGWAY, S. L. Phys. Rev. 78: 821. 1950.
11. STEVENSON, D. T. Phys. Rev. 82: 333. 1951.
12. WU, CHIEN-SHIUNG. Revs. Modern Phys. 22: 386. 1950.

THE MAGNETIC DIPOLE OVER THE HORIZONTALLY STRATIFIED EARTH[1]

By James R. Wait

Abstract

The behavior of a small current-carrying wire loop over a horizontally stratified earth is investigated. The layers are considered to have a contrast in conductivity and dielectric constant only. Both harmonic steady-state and step-function current sources are considered.

Introduction

The earth's crust is an example of an electrically dissipative medium since it possesses a finite conductivity. The conductivity exists by virtue of the resulting total effect of the electronic and the electrolytic current conduction on the application of an electric field to the medium (7, p. 632). For many purposes this effective conductivity is a constant with respect to frequency over wide limits.

Depending on the nature of the soil or rock the conductivity may vary from a rather extreme high value of one mho per meter to a rather extreme low value of 10^{-4} mhos per meter. The conductivity may sometimes be estimated from geological maps based on the previous results of tests for similar geologic formations. A study of these maps may indicate what type of variation in resistivity with depth is to be expected. For example, if there is a top layer of sand with shales at greater depth, the conductivity is likely to increase from a very low value near the surface to a high value for greater depths. On the other hand if the surface layer is clay while the underlying rock is granite the opposite type of variation can be expected. The connection between earth conductivity and geological age and formation has been investigated by Card (1) who examines the results of a large number of measurements.

The relative dielectric constant varies from a low value of two for dry rock or clay to a high value of 50 for moist soil or clay. The results of measurements made at radio frequencies for various rocks and soils are given by Heiland (7, p. 667). The displacement currents are usually very small for all significant frequencies compared to the conduction currents. For this reason the conductivity changes will far overshadow permittivity changes at least for power and geophysical frequencies (i.e. frequencies less than one megacycle).

The relative permiability of rock formations and soil is generally within 1% of unity for nearly all cases (7, p. 312). Except for static magnetic fields (i.e. the earth's)the permeability μ always appears as a product with the conductivity σ (i.e. $\sigma\mu$) and hence again the conductivity variations greatly overweigh permeability changes (10).

[1] *Manuscript received May 9, 1951.*
Contribution from the Department of Electrical Engineering, University of Toronto, Toronto, Ont.

For many cases the earth can be represented as a horizontally stratified medium with homogeneous and isotropic properties in each layer. The analysis of direct current flow in such a medium requires the solution of Laplace's equation. The conditions at the boundary and at the current source or sink are sufficient to determine the potential everywhere. The classical solution of this problem for a two layer earth has been solved by Maxwell (11) who used an infinite series of image sources with modified moments. Ollendorf (12) and Stefanescu and Schlumberger (19) have given solutions in the form of integrals involving Bessel functions. Formulas in terms of images have been given by Hummel (8) for three layers. He also gives approximate curves for this case. A similar analysis is given by Ehrenburg and Watson (3) for any number of layers.

A maximum of information is obtained concerning the subsurface conductivity variation when a spectrum of frequencies is used for the source current. The behavior of the observed field at low frequencies is characteristic of potential theory. On the other hand, the behavior at high frequencies is due partly to propagation effects and is characteristic of wave theory.

When a source of time varying current is situated in the vicinity of a layered earth the field components U(t) must satisfy the wave equation

$$\left(\nabla^2 - \sigma\mu \frac{\partial}{\partial t} - \epsilon\mu \frac{\partial^2}{\partial t^2}\right) U(t) = 0$$

in the media, the boundary conditions at the interfaces, and behave in the proper manner near the current source and at infinity.

Sommerfeld (18) has derived general expressions for infinitesimal electric and magnetic dipoles energized by a harmonic current on the surface of a semi-infinite flat homogeneous earth. The case of the electric dipole has been extended to the two layer case by Riordan and Sunde (16) . Foster (4) has developed mutual impedance formulas for finite wires on the surface of a homogeneous earth by a double integration of Sommerfeld's horizontal electric dipole. Formulas for the field due to a transient current in an infinite wire on the surface of a flat homogeneous earth have been published by Ollendorf (12) and Peterson (14). Riordan (15) has investigated the corresponding case for parallel finite wires. West (23), using a numeral method, has evaluated the steady state impedance for a certain special case of two collinear grounded wires on the flat homogeneous earth.

In this paper the formal solutions for harmonic time dependence will be carried out for the vertical magnetic dipole over the two layer earth. Interesting cases will then be treated by suitable specializations and approximations of the above. The transient solutions will also be given for several cases.

Magnetic Dipole on Two Layer Earth

A magnetic dipole or small loop is oriented with its axis in the z direction and is located at the origin of the cylindrical coordinate system (ρ, ϕ, z).

The medium above the upper plane interface will be characterized by constants $\sigma_0, \epsilon_0, \mu$. The layer of thickness d has constants $\sigma_1, \epsilon_1, \mu$. Meter-kilogram-second units will be used throughout.

The vector fields $\boldsymbol{E}$ and $\boldsymbol{H}$ everywhere can be written in terms of a single magnetic vector potential $\boldsymbol{F}$ as defined by Schelkunoff (17, p. 128)* and are given by

$$\boldsymbol{E} = -\operatorname{curl} \boldsymbol{F}, \tag{1}$$

$$\boldsymbol{H} = -(\sigma + i\omega\epsilon)\boldsymbol{F} + \frac{1}{i\mu\omega}\operatorname{grad}\operatorname{div}\boldsymbol{F}. \tag{2}$$

The time factor $\exp(i\omega t)$ will be omitted.

The primary field is the same as that due to a magnetic dipole of strength IdA where I is the loop circulating current and dA is the area of the loop. Since the primary exciting current has only a ϕ component then correspondingly the magnetic vector potential has only a z component. The primary vector potential F_p is then given by Schelkunoff (17, p. 338), and has only a component in the z direction.

$$\mathrm{F}_p = i\mu\omega dAI \exp(-\gamma_0 r)/4\pi r \qquad \text{for } z \geqslant 0, \tag{3}$$

or

$$\mathrm{F}_p = i\mu\omega dAI \exp(-\gamma_1 r)/4\pi r \qquad \text{for } -d \leqslant z \leqslant 0, \tag{4}$$

where $\gamma_0 = [i\mu\sigma_0\omega - \epsilon_0\mu\omega^2]^{\frac{1}{2}}$

and $\gamma_1 = [i\mu\sigma_1\omega - \epsilon_1\mu\omega^2]^{\frac{1}{2}}$

and $r = (\rho^2 + z^2)^{\frac{1}{2}}$.

Now the resulting magnetic vectors F_i $(i = 0, 1, 2)$ in the three media must be a solution of the wave equation;

$$\frac{1}{\rho}\frac{\partial}{\partial\rho}\left(\rho\frac{\partial F_i}{\partial\rho}\right) + \frac{1}{\rho^2}\frac{\partial^2 F_i}{\partial\phi^2} + \frac{\partial^2 F_i}{\partial z^2} - \gamma_i^2 F_i = 0, \tag{5}$$

where $\gamma_i = [i\sigma_i\mu\omega - \epsilon_i\mu\omega^2]^{\frac{1}{2}}, \qquad (i = 0, 1, 2).$

Solutions for these equations follow from the theory of cylindrical harmonics. They are made up of solutions of the following type:

$$\begin{matrix}\cos \\ \sin\end{matrix} n\phi \exp(\pm(\lambda^2 + \gamma_i^2)^{\frac{1}{2}}z)\begin{matrix}J_n \\ Y_n\end{matrix}(\lambda\rho), \tag{6}$$

$$n = 0, 1, 2, 3, \ldots.$$

The fields are to be finite when $\rho = 0$, $z \neq 0$ so evidently solutions containing the Bessel functions of the second type $Y_n(\lambda\rho)$ are not permissible. There is obvious axial symmetry to the problem so that the plus or minus sign in the exponential must be chosen so as to reject the solutions that are not finite as z tends to plus or minus infinity.

The general expressions for the magnetic vector potentials are then obtained by integration over all values of λ. These vectors have only a component in the z direction.

* *The function* $\boldsymbol{F}$ *occurring here is related simply to the often used magnetic Hertz potential* Π^*. *They are connected as follows:*

$$\boldsymbol{F} = i\mu\omega\Pi^*.$$

$$F_0 = k \exp(-\gamma_0 r)/r + k\int_0^\infty \psi_1(\lambda) \exp(-(\lambda^2 + \gamma_0^2)z) J_0(\lambda\rho) d\lambda, \tag{7}$$

$$F_1 = k \exp(-\gamma_1 r)/r + k\int_0^\infty [\psi_2(\lambda) \exp(+(\lambda^2 + \gamma_1^2)^{\frac{1}{2}}z) + \psi_3(\lambda) \exp(-\lambda^2 + \gamma_1^2)^{\frac{1}{2}}z)] J_0(\lambda\rho) d\lambda, \tag{8}$$

$$F_2 = k\int_0^\infty \psi_4(\lambda) \exp(+(\lambda^2 + \gamma_2^2)z) J_0(\lambda\rho) d\lambda, \tag{9}$$

where $$k = i\mu\omega dAI/4\pi.$$

The characteristic functions (i.e. eigenfunctions) will now be determined from the boundary conditions which require that the tangential electric and magnetic fields are continuous across the plane interfaces. By using Equations (1) and (2) the tangential fields are given as:

$$E_{\phi i} = \frac{\partial F_i}{\partial \rho}, \quad H\rho_i = \frac{1}{i\mu\omega} \frac{\partial^2 F_i}{\partial \rho \partial z}. \tag{10}$$

The equations imposed by the boundary conditions are then:

$$\frac{\partial F_0}{\partial \rho} = \frac{\partial F_1}{\partial \rho}, \quad \frac{\partial^2 F_0}{\partial \rho \partial z} = \frac{\partial^2 F_1}{\partial \rho \partial z}, \text{ at } z = 0 \tag{11}$$

and

$$\frac{\partial F_1}{\partial \rho} = \frac{\partial F_2}{\partial \rho}, \quad \frac{\partial^2 F_1}{\partial \rho \partial z} = \frac{\partial^2 F_2}{\partial \rho \partial z}, \text{ at } z = -d. \tag{12}$$

These conditions hold for all values of ρ hence they can be integrated with respect to ρ. The function and their derivatives vanish as ρ tends to infinity so that the constant of integration must be zero. The conditions then reduce to the following four equations;

$$F_0 = F_1, \quad \frac{\partial F_0}{\partial z} = \frac{\partial F_1}{\partial z}, \text{ at } z = 0 \tag{13}$$

and

$$F_1 = F_2, \quad \frac{\partial F_1}{\partial z} = \frac{\partial F_2}{\partial z}, \text{ at } z = -d. \tag{14}$$

To apply these conditions the primary excitation must be expanded in terms of an infinite integral involving cylindrical wave functions. This representation makes use of the Sommerfeld integral (18)

$$\exp(-\gamma_0 r)/r = \int_0^\infty \lambda(\lambda^2 + \gamma_0^2)^{-\frac{1}{2}} \exp(-(\lambda^2 + \gamma_0^2)^{\frac{1}{2}}z) J_0(\lambda\rho) d\lambda, \quad \text{for } z \geqslant 0.$$

$$\exp(-\gamma_1 r)/r = \int_0^\infty \lambda(\lambda^2 + \gamma_1^2)^{-\frac{1}{2}} \exp(+(\lambda^2 + \gamma_1^2)^{\frac{1}{2}}z) J_0(\lambda\rho) d\lambda, \quad \text{for } -d \leqslant z \leqslant 0. \tag{15}$$

Sommerfeld used this representation but did not prove it for γ_i complex. It can be checked however as shown in Appendix A.

The four equations (11) and (12) then can be solved for $\psi_1(\lambda), \psi_2(\lambda)\ \psi_3(\lambda)$, and $\psi_4(\lambda)$. The result of this algebraic process is:

$$\psi_1(\lambda) = \frac{u_1}{u_0}\left[\left(1+\frac{u_0}{u_1}\right)\left(\frac{\lambda}{u_2}-\frac{\lambda}{u_1}\right)-\left(1-\frac{u_1}{u_2}\right)\left(\frac{\lambda}{u_1}-\frac{u_0\lambda}{u_1^2}\right)\right.$$
$$\left.-\left(\frac{\lambda}{u_1}-\frac{u_0\lambda}{u_1^2}\right)\left(1+\frac{u_1}{u_2}\right)e^{2u_1d}+\left(\frac{\lambda}{u_2}-\frac{\lambda}{u_1}\right)\left(\frac{u_0}{u_1}-1\right)\right]\frac{1}{\Delta}, \tag{16}$$

$$\psi_2(\lambda) = \left[\left(\frac{\lambda}{u_1}-\frac{u_0\lambda}{u_1^2}\right)\left(1+\frac{u_1}{u_2}\right)e^{2u_1d}-\left(\frac{\lambda}{u_2}-\frac{\lambda}{u_1}\right)\left(\frac{u_0}{u_1}-1\right)\right]\frac{1}{\Delta}, \tag{17}$$

and $$\psi_3(\lambda) = \left[\left(1+\frac{u_0}{u_1}\right)\left(\frac{\lambda}{u_2}-\frac{\lambda}{u_1}\right)-\left(1-\frac{u_1}{u_2}\right)\left(\frac{\lambda}{u_1}-\frac{u_0\lambda}{u_1^2}\right)\right]\frac{1}{\Delta}, \tag{18}$$

where $$\Delta = \left(1+\frac{u_0}{u_1}\right)\left(1+\frac{u_1}{u_2}\right)e^{2u_1d}-\left(1-\frac{u_1}{u_2}\right)\left(\frac{u_0}{u_1}-1\right)$$

and
$$u_0 = (\lambda^2+\gamma_0^2)^{\frac{1}{2}},$$
$$u_1 = (\lambda^2+\gamma_1^2)^{\frac{1}{2}},$$
$$u_2 = (\lambda^2+\gamma_2^2)^{\frac{1}{2}}.$$

On the surface of the earth (i.e. $z = 0$) the magnetic vector potential is then written:

$$F_1 = \frac{i\mu\omega IdA}{2\pi}\int_0^\infty R(\lambda)J_0(\lambda\rho)d\lambda, \tag{19}$$

where I is the circulating current in the loop and dA its area and

$$R(\lambda) = \frac{\lambda[\mu_1+\mu_2+(\mu_1-\mu_2)e^{-2du_1}]}{(\mu_0+\mu_1)(\mu_1+\mu_2)+(\mu_0-\mu_1)(\mu_1-\mu_2)e^{-2du_1}}. \tag{20}$$

The electric field E_y at P also on the surface of the earth as shown in Fig. 1 is given by:

$$E_y = -\frac{\partial F_1}{\partial x} = \frac{i\mu\omega IdA}{2\pi}\frac{x}{\rho}\int_0^\infty R(\lambda)J_1(\lambda\rho)\lambda d\lambda. \tag{21}$$

The voltage induced in the element ds is then equal to $E_y ds$.

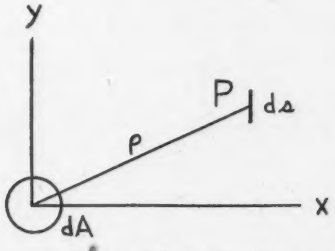

FIG. 1. *Plan view of the magnetic dipole and the receiving linear wire element on the surface of the earth.*

By the principle of reciprocity as given by Schelkunoff (17, p. 478) the voltage dv induced in a loop of area dA by an electric current element of length ds as shown in Fig. 2 is given by:

$$dv = \frac{i\mu\omega IdAds}{2\pi} \frac{x}{\rho} \int_0^\infty R(\lambda) J_1(\lambda\rho) \lambda d\lambda. \tag{22}$$

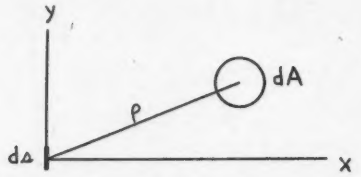

FIG. 2. *Plan view of the electric current element and the receiving loop.*

By Stokes' theorem this induced voltage is also given by

$$dv = \left[\frac{\partial E_y}{\partial x} - \frac{\partial E_x}{\partial y} \right] dA.$$

Therefore
$$E_y = \frac{i\mu\omega Ids}{2\pi} \int_0^\infty R(\lambda) J_0(\lambda\rho) d\lambda + E_y' \tag{23}$$

and
$$E_x = E_x'.$$

The E_x' and E_y' terms are the components of an undetermined solenoidal field.

The mutual impedance dZ then between the current element ds and a finite circuit between the points A and B along a contour C as shown in Fig. 3 is given by

$$dZ = \frac{i\mu\omega ds}{2\pi} \int_A^B \int_0^\infty R(\lambda) J_0(\lambda\rho) \cos\epsilon \, d\lambda dS + \int_A^B \mathbf{E}' \cdot \mathbf{n} \, dS,$$

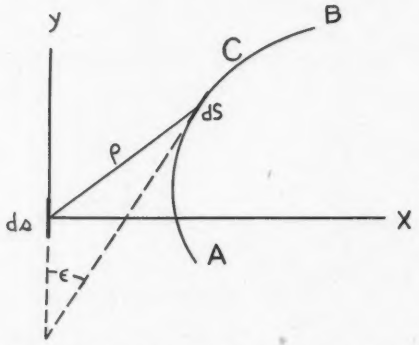

FIG. 3. *The scheme for formulating mutual inductance of wires on the surface of the earth.*

where $\mathbf{E}'$ is a two dimensional vector whose components are E_x' and E_y', $\mathbf{n}$ is a unit vector in the direction of the wire element dS on the wire contour C.

When A and B are the same point so that the contour C is a closed loop the latter integral is zero since $\mathbf{E}'$ is a solenoidal field. The mutual impedance is then given by

$$dZ = \oint_C \frac{i\mu\omega ds}{2\pi} \int_0^\infty R(\lambda) J_0(\lambda\rho) d\lambda \cos\epsilon \, dS = i\omega dM.$$

The above equation defines the mutual inductance dM between the two circuits.

The mutual inductance d^2M between two coplanar circuits of length ds and dS with an angle ϵ between their directions on the surface of the earth is then given by:

$$\frac{d^2M}{dSds} = \frac{\mu}{2\pi} \int_0^\infty R(\lambda) \cos\epsilon \, J_0(\lambda\rho) d\lambda. \tag{24}$$

The elements ds and dS are considered to be both or one part of a closed loop.

The mutual inductance between two coplanar circuits of contour C_1 and C_2 on the surface of a horizontally stratified earth is then written

$$M = \int_{C_1} \int_{C_2} \frac{d^2M}{dsdS} dsdS.$$

The general formulation will now be specialized in various ways to facilitate evaluation.

Homogeneous Flat Earth

The upper and lower layer are to become identical so that $u_1 = u_2 = u$ and $\gamma_1 = \gamma_2 = \gamma$. The upper medium is considered to have a negligible propagation constant $\gamma_0 \simeq 0$ so that $u_0 = \lambda$. The expression for the magnetic vector potential F_1 anywhere within the earth then reduces to:

$$F_1 = \frac{i\mu\omega IdA}{2\pi} \int_0^\infty \frac{\lambda}{\lambda + u} \exp(uz) J_0(\lambda\rho) d\lambda, \quad (z \leqslant 0) \tag{25}$$

where $$u = (\gamma^2 + \lambda^2)^{\frac{1}{2}}, \gamma^2 = i\sigma\mu\omega.$$

That is, all displacement currents are neglected.

This can be written in the following form:

$$F_1 = \frac{i\mu\omega}{2\pi\gamma^2} \left[\frac{\partial^2 P}{\partial z^2} + \frac{\partial}{\partial z} \left(\gamma^2 N - \frac{\partial^2 N}{\partial z^2} \right) \right] IdA, \tag{26}$$

where $$P_1 = \int_0^\infty J_0(\lambda\rho) u^{-1} \exp(zu) \lambda d\lambda = \exp(-\gamma r)/r \tag{27}$$

and $$N = \int_0^\infty J_0(\lambda\rho) \exp(zu) u^{-1} d\lambda = I_0[(\gamma/2)(r + z)] K_0[(\gamma/2)(r - z)]. \tag{28}$$

The integral involving P has been already encountered and the integral involving N has been derived by Foster (4) who carried out a similar analysis for the electric dipole on the homogeneous earth. Wolf (24) has also derived this latter integral.

When $z = 0$ the vector potential becomes

$$F_1 = \frac{iu\omega IdA}{2\pi} \int_0^\infty \frac{\lambda}{\lambda + u} J_0(\lambda\rho)d\lambda. \tag{29}$$

The following relations are used for the above derivations.

$$\frac{dI_0(z)}{dz} K_0(z) - I_0(z) \frac{dK_0(z)}{dz} = 1/z$$

and (30)

$$\left| \frac{df(r+z)}{d(r+z)} \right|_{z=a} = \frac{d}{dr} |f(r+z)|_{z=a} .$$

The required differentiations of P and N then yield the relatively simple expression for F_1:

$$F_1 = \frac{i\mu\omega IdA}{2\pi} \quad \frac{1 - (1 + \gamma\rho) \exp(-\gamma\rho)}{\gamma^2\rho^3} . \tag{31}$$

The electric field on the surface of the earth has only a ϕ component and is given by

$$E_\phi = -\frac{\partial F_1}{\partial \rho} = \frac{IdA}{2\pi\sigma\rho^4}[3 - (3 + 3\gamma\rho + \gamma^2\rho^2) \exp(-\gamma\rho)]. \tag{32}$$

The mutual impedance between wire element of length ds and a wire loop of area dA on the surface of a homogeneous earth is then given by:

$$Z(i\omega) = \frac{dAds}{2\pi\sigma\rho^4} [3 - (3 + 3\gamma\rho + \gamma^2\rho^2) \exp(-\gamma\rho)] \sin\epsilon, \tag{33}$$

where ϵ is the angle between the direction of the wire element and the line joining the wire element and the wire loop.

Proceeding in a similar manner to that used in the case of the electric dipole in the infinite medium as carried out by the author in a previous paper (21), the step function mutual impedance (i.e. voltage response in one circuit to a unit step function current in the other) is then given by:

$$A(t) = \frac{1}{2\pi i} \int_{c-i\infty}^{c+i\infty} \frac{Z(i\omega)}{i\omega} \exp(i\omega t)d(i\omega), \tag{34}$$

where c is some small positive real constant.

Integrations are carried out and the results combined. The step function impedance is given by:

$$A(t) = \frac{dsdA}{2\pi\sigma\rho^4} H(t) \sin\epsilon\, u(t), \tag{35}$$

where $u(t) = 1$ for $t > 0$, $= 0$ for $t < 0$.

$$H(t) = 3 \operatorname{erf}(a/2t^{\frac{1}{2}}) - [3a/2t^{\frac{1}{2}} + 2(a/2t^{\frac{1}{2}})^3] \operatorname{erf}'(a/2t^{\frac{1}{2}}) \tag{36}$$

and $a = (\sigma\mu)^{\frac{1}{2}}\rho$. The integrals are evaluated in Appendix B. The characteristic function $H(t)$ is plotted in Fig. 4.

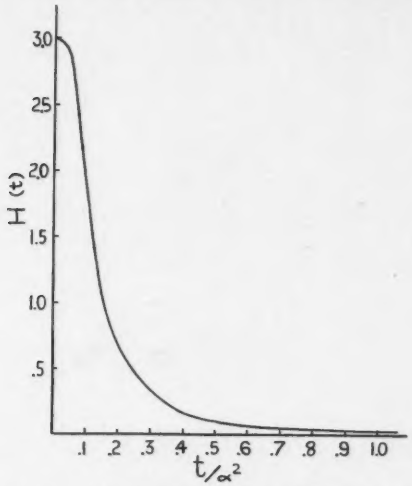

FIG. 4. *The step function mutual impedance between a small linear wire element and a small wire loop on the surface of a homogeneous conducting earth.*

The vertical magnetic field on the surface of the earth can also be found

$$H_z = -\gamma^2 F_1 + \frac{\partial^2 F_1}{\partial z^2}.$$

Now F_1 satisfies the wave equation so this can be written:

$$H_z = -\left[\frac{\partial^2 F_1}{\partial x^2} + \frac{\partial^2 F_1}{\partial y^2}\right]. \tag{37}$$

The voltage $e(\omega)$ induced in another small loop of area dA_1 at distance from the source loop of area dA is then given by:

$$e(\omega) = i\mu\omega\left[\frac{\partial^2 F_1}{\partial x^2} + \frac{\partial^2 F_1}{\partial y^2}\right] dA_1.$$

Then the steady state mutual impedance between two horizontal loops of area dA and dA_1 on the surface of the homogeneous earth is given by:

$$Z(i\omega) = \frac{dA_1 dA}{2\pi\sigma\rho^4}[(9 + 9\gamma\rho + 4\gamma^2\rho^2 + \gamma^3\rho^3)\exp(-\gamma\rho) - 9]. \tag{38}$$

The step function impedance $A(t)$ again is given by the contour integral, Equation (34). The integrations are then carried out by using the integrals listed in Appendix B.

$$A(t) = -\frac{dA dA_1}{2\pi\sigma\rho^4} P(t)u(t),$$

where
$$P(t) = 9\,\mathrm{erf}\,(a/2t^{\frac{1}{2}}) + 2(a/2t^{\frac{1}{2}})^4\,\mathrm{erf}''\,(a/2t^{\frac{1}{2}}) - [9\,(a/2t^{\frac{1}{2}}) - 6\,(a/2t^{\frac{1}{2}})^3]\,\mathrm{erf}'\,(a/2t^{\frac{1}{2}})$$

and
$$a = (\sigma\mu)^{\frac{1}{2}}\rho.$$

The characteristic function $P(t)$ is plotted in Fig. 5.

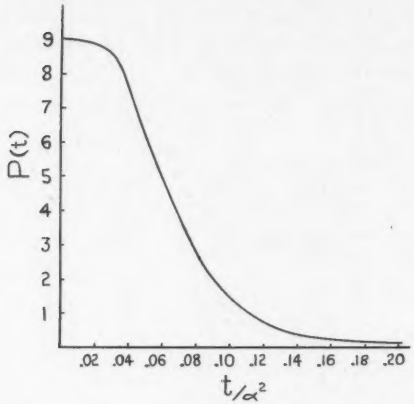

FIG. 5. *The step function mutual impedance between two small wire loops on the surface of a homogeneous conducting earth.*

Poorly Conducting Upper Layer

In many cases the conductivity of the lower layer will be much higher than the conductivity of the upper layer (i.e. $\sigma_2 >> \sigma_1$). There will then be a range of frequencies where propagation effects in the upper medium are negligible (i.e. $|\gamma_1 d|, |\gamma_1 \rho| << 1$). This assumption will then also be valid for the air (i.e. $|\gamma_0 \rho| << 1$). In other words it is assumed that Laplace's equation is valid in regions above the lower conducting layer. To effect this simplification Equation (8) is rewritten with the following substitutions:

$$u_1 = (\lambda^2 + \gamma_1^2)^{\frac{1}{2}} = \lambda, \quad u_0 = (\lambda^2 + \gamma_0^2)^{\frac{1}{2}} = \lambda$$

and

$$u_2 = \sqrt{\lambda^2 + \gamma_2^2} = \sqrt{\lambda^2 + \gamma^2} = u.$$

Then the magnetic vector potential between the surface of the earth and the surface of the conducting layer is given by

$$F_1 = k \int_0^\infty \left[e^{\lambda z} + \left(\frac{\lambda - u}{\lambda + u} \right) e^{-\lambda(z+2d)} \right] J_0(\lambda\rho) d\lambda, \quad (0 \geqslant z \geqslant -d). \tag{42}$$

The field components anywhere in the range $-d \geqslant z \geqslant 0$ can then be found:

$$E_\rho = 0, \quad E_\phi = \frac{\partial F_1}{\partial z}, \quad E_z = 0,$$

$$H_\rho = \frac{\partial^2 F_1}{\partial \rho \partial z}, \quad H_\phi = 0, \quad H_z = -\gamma^2 F_1 + \frac{\partial^2 F_1}{\partial z^2}. \tag{43}$$

It is possible to represent F_1 in terms of tabulated functions valid for a fairly wide range of frequency and conductivity values of the lower layer. The expression (41) for the magnetic vector potential F_1 for this case can be written in the following way:

$$F_1/k = \underbrace{\int_0^\infty \exp(\lambda z) J_0(\lambda\rho) d\lambda}_{\text{(I)}} + \underbrace{\int_0^\infty \left(\frac{\lambda - u}{\lambda + u}\right) J_0(\lambda\rho) d\lambda}_{\text{(II)}} + \underbrace{\int_0^\infty \{1 - \exp[-\lambda(z + d)]\} \frac{u - \lambda}{u + \lambda} J_0(\lambda\rho) d\lambda}_{\text{(III)}}. \tag{44}$$

These three integrals (I), (II), and (III) are then respectively given by

$$\text{(I)} = (\rho^2 + z^2)^{-\frac{1}{2}}, \tag{45}$$

$$\text{(II)} = -\int_0^\infty J_0(\lambda\rho) d\lambda + \int_0^\infty \frac{2\lambda}{\lambda + u} J_0(\lambda\rho) d\lambda,$$

$$= -\frac{1}{\rho} + 2\left[\frac{1 - (1 + \gamma\rho)\exp(-\gamma\rho)}{\gamma^2\rho^3}\right], \tag{46}$$

where the second integral of (II) is given by Equations (29) and (31),

$$\text{(III)} = \frac{1}{\delta}\int_0^\infty \{1 - \exp[-g(2d + z)/\delta]\}\left[\frac{(g^2 + 2i)^{\frac{1}{2}} - g}{(g^2 + 2i)^{\frac{1}{2}} + g}\right] J_0(g\rho/\delta) dg$$

$$= -\frac{iN_1}{\delta}[\rho/\delta, (2d + z)/\delta] \tag{47}$$

where the substitution $\lambda = g/\delta$, $\delta = \left(\frac{2}{\sigma\mu\omega}\right)^{\frac{1}{2}}$, is made. The function $N_1(r', s')$ has been tabulated by Foster (4) in connection with mutual impedance of finite grounded wires over a homogeneous earth.

On the surface of the earth $z = 0$, then the magnetic vector potential is given by:

$$\frac{F_1}{IdA} = \frac{i\mu\omega}{2\pi}\left[\frac{1 - (1 + \gamma\rho)\exp(-\gamma\rho)}{\gamma^2\rho^3}\right] + \frac{i\mu\omega}{4\pi\delta} N_1(\rho/\delta, 2d/\delta), \tag{48}$$

where the second term is a correction due to the fact that magnetic dipole is a height d above the conducting plane. This expression should be compared to Equation (31). From Equation (24) it is seen that mutual inductance d^2M between two coplanar circuits of length ds and dS for this case is

$$\frac{d^2M}{ds dS} = \frac{\mu}{2\pi}\left[\frac{1 - (1 + \gamma\rho)\exp(-\gamma\rho)}{\gamma^2\rho^3}\right] + \frac{\mu}{4\pi\delta} N_1(\rho/\delta, 2d/\delta).$$

Magnetic Dipole over a Thin Conducting Sheet of Infinite Extent

In a similar manner to that used in the problem of the magnetic dipole over a two layer earth the fields of a dipole over a three layer earth can be calculated. A cylindrical coordinate system is used with the z axis again perpendicular to the layers.

The conductivity of all regions outside the finite layer of thickness d at depth $z = -h$ will be considered negligible. The vector magnetic potential F in the region $0 \geqslant z \geqslant -h$ is given by:

$$F = k\int_0^\infty \exp(\lambda z) J_0(\lambda\rho)d\lambda - k\int_0^\infty \exp(-\lambda z - 2\lambda h) J_0(\lambda\rho)d\lambda \qquad (49)$$

$$+ 2k\int_0^\infty \left[\frac{(u+\lambda)\lambda + (u-\lambda)\lambda\exp(-2ud)}{(\lambda+u)^2 - (\lambda-u)^2\exp(-2ud)}\right] \exp(-\lambda z - 2\lambda h) J_0(\lambda\rho)d\lambda,$$

where $$u = (\lambda^2 + \gamma^2)^{\frac{1}{2}},\ \gamma^2 = i\sigma\mu\omega$$

and $$k = i\mu\omega dA\,I/4\pi.$$

The term in square brackets in the latter integral can be written as follows:

$$\left[\quad\right] = \frac{\dfrac{\lambda}{\lambda+u} + \dfrac{(u-\lambda)\lambda}{(\lambda+u)^2}}{1 - \left(\dfrac{u-\lambda}{u+\lambda}\right)^2 \exp(-2ud)}. \qquad (50)$$

Now the case will be considered where the thickness d of the conducting layer becomes very small. Also the conductivity σ becomes very large. The following expansions are then made:

$$\exp(-2ud) = 1 - 2ud + \ldots$$

$$\frac{\lambda}{\lambda+u} = \frac{\lambda}{u}\left(1 - \frac{\lambda}{u} + \ldots\right)$$

$$\frac{u-\lambda}{u+\lambda} = 1 - \frac{2\lambda}{u}\ldots$$

$$\left(\frac{u-\lambda}{u+\lambda}\right)^2 = 1 - \frac{4\lambda}{u}\ldots$$

Now if d is allowed to approach zero and σ approach infinity in such a way that the product σd is finite then the square bracket term becomes simply:

$$\left[\quad\right] = \frac{\lambda}{2(\lambda + iq)} \qquad (51)$$

where $$q = \lim_{\substack{\sigma\to\infty \\ d\to\infty}} \frac{u^2 d}{2i} = \frac{(i\sigma\mu\omega + \lambda^2)d}{2i} = \frac{\sigma\mu\omega d}{2}.$$

In these limit processes λ is considered to be a finite parameter since the total integrand converges very rapidly for large values of λ in any case.

The magnetic vector potential can then be written:

$$F = k\left[(\rho^2 + z^2)^{-\frac{1}{2}} + iq\int_0^\infty (\lambda + iq)^{-1} \exp[-\lambda(z+2h)] J_0(\lambda\rho)d\lambda\right]. \qquad (52)$$

The second term in Equation (52) represents the secondary field. It is convenient to transform the integral by the following substitution:

$$\frac{1}{\lambda + iq} = -i\int_0^\infty e^{-(q-i\lambda)m}\,dm. \tag{53}$$

An integration with respect to λ can be immediately carried out to yield:

$$F = k\left[(\rho^2 + z^2)^{-\frac{1}{2}} - q\int_0^\infty [\rho^2 + (z + 2h - im)^2]^{-\frac{1}{2}} \exp(-qm)dm\right] \tag{54}$$

This is in agreement with a formula given by Anton Graf (6) who used rather a different approach. He gives several expansion formulae for the secondary fields which are useful for computation for this steady state case.

A similar analysis has been carried out by Stefanescu (20) for the case of a horizontal electric dipole over a thin conducting plate. His method is similar to the method used here for the magnetic dipole. He gives his fields to the first order of $1/q$ only and makes the usual assumption that the surrounding medium has negligible propagation characteristics.

The transient fields will now be calculated for the case when the loop is energized by a step function current.

The steady state magnetic vector potential can be written in the following form:

$$\begin{aligned}\frac{F(i\omega)}{I(i\omega)} &= \frac{i\mu\omega dA}{4\pi}\left[\frac{1}{r} - \frac{1}{r_1}\right] \\ &\quad + \frac{i\mu\omega dA}{4\pi}\int_0^\infty \frac{\lambda}{\lambda + i\omega p}\exp[-\lambda(z + 2h)]J_0(\lambda\rho)d\lambda,\end{aligned} \tag{55}$$

where

$$p = \sigma\mu d/2$$

and

$$r = (\rho^2 + z^2)^{\frac{1}{2}}, \quad r_1 = [\rho^2 + (z + 2h)^2]^{\frac{1}{2}}.$$

The transient vector potential response $f(t)$ for a step function current $I_0\,u(t)$ is then given by:

$$\begin{aligned}\frac{f(t)}{I_0} &= \frac{\mu dA}{4\pi}\frac{1}{2\pi i}\int_{c-i\infty}^{c+i\infty}\exp(i\omega t)\int_0^\infty \frac{\lambda}{\lambda + i\omega p}\exp[-\lambda(z + 2h)]J_0(\lambda\rho)d\lambda d(i\omega) \\ &\quad + \frac{\mu dA}{4\pi}\frac{1}{2\pi i}\int_{c-i\infty}^{c+i\infty}\left(\frac{1}{r} - \frac{1}{r_1}\right)\exp(i\omega t)d(i\omega).\end{aligned} \tag{56}$$

The change of the order of integration here is permissible so that integrating first with respect to $(i\omega)$ there results:

$$\begin{aligned}\frac{f(t)}{I_0} &= \frac{\mu dA}{4\pi}\int_0^\infty \exp(-\lambda t/p)\exp[-\lambda(z + 2h)u(t)\lambda J_0(\lambda\rho)d\lambda \\ &\quad + \frac{\mu dA}{4\pi}\left[\frac{1}{r} - \frac{1}{r_1}\right]u_1(t).\end{aligned} \tag{57}$$

The integration with respect to λ can now be easily effected. $U_1(t)$ is the unit impulse function as defined by Gardner and Barnes (5).

$$\frac{f(t)}{I_0} = \frac{\mu dA}{4\pi}\left(\frac{1}{r}-\frac{1}{r_1}\right)u_1(t) + \frac{\mu dA}{4\pi}(t/p+z+2h)[(t/p+z+2h)^2+\rho^2]^{-3/2}. \quad (58)$$

The electric field component is then given by:

$$\frac{e_\phi(t)}{I_0} = -\frac{1}{I_0}\frac{\partial f(t)}{\partial \rho} = -\frac{\mu dA}{4\pi}\frac{\partial}{\partial \rho}\left(\frac{1}{r}-\frac{1}{r_1}\right)u_1(t) + \frac{3\mu dA}{4\pi}(t/p+z+2h)\rho[(t/p+z+2h)^2+\rho^2]^{-5/2}. \quad (59)$$

The step function mutual impedance $A(t)$ between a loop of area dA and a current element of length ds on the surface of the earth where there is a conducting plate at depth h is given by

$$A(t) = \frac{e_\phi(t)ds}{I_0} = \frac{\mu dA ds \sin\epsilon}{4\pi}\left[\frac{\partial}{\partial \rho}\left(\frac{1}{r_1}-\frac{1}{r}\right)u_1(t) + \frac{6}{\sigma\mu d}Z(t/hp, \rho/h)\right] \quad (60)$$

where ϵ is the angle between the direction of ds and the direction of the line joining the center of the loop dA and the center of the wire element. The characteristic function $Z(t/hp, \rho/h)$ is plotted in Fig. 6 and is given by

$$Z(t/hp, \rho/h) = \rho/h\ (t/hp+2)[(t/hp+2)^2 + (\rho/h)^2]^{-5/2}. \quad (61)$$

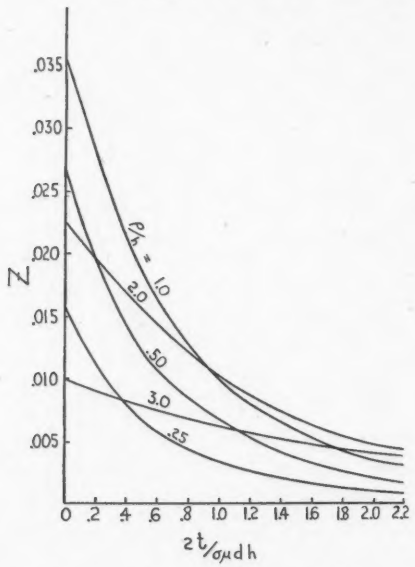

FIG. 6. *The step function mutual impedance between a wire element and a wire loop above a conducting sheet for various values of the ratio* ρ/h.

Here the first term is characterized by a unit impulse function $u_1(t)$ for the case when the medium is of infinite resistivity. Actually, owing to the finite conductivity of the medium surrounding the conducting sheet, the primary impulse will have a finite duration. Its nature can be expected to be similar to the step function mutual impedance between the loop and the wire element on the surface of a homogeneous earth of finite conductivity as given by Equation (35). In any case it appears that if the measuring time t is $>> \sigma_1\mu h^2$ where σ_1 is the conductivity of the surrounding earth or rock material that the predominant contribution to the field is due only to the eddy current term involving $Z(t/h\rho, \rho/h)$.

It is then noted, on observing the curves in Fig. 6, that for a given conducting sheet at depth h the maximum transient response is at the point where the ratio ρ/h is unity. It can also be seen that the decay time of the field is considerably greater for larger values of the ratio ρ/h.

Appendix A

Since $\exp(-\gamma_i r)$ is a solution of the wave equation, is finite at infinity, and has axial symmetry, then it must be of the form

$$\exp(-\gamma_i r)/r = \int_0^\infty \lambda B(\lambda) \exp(\pm(\lambda^2 + \gamma^2)^{\frac{1}{2}} z) J_0(\lambda\rho) d\lambda,$$

$$\begin{bmatrix} + \text{ for } -z \geqslant 0 \\ - \text{ for } -z \leqslant 0 \end{bmatrix}.$$

At $z = 0$ the above equation reduces to

$$\exp(-\gamma_i \rho)/\rho = \int_0^\infty \lambda B(\lambda) J_0(\lambda\rho) d\lambda.$$

By the Fourier Bessel theorem

$$B(\lambda) = \int_0^\infty \exp(-\gamma_i \rho) J_0(\lambda\rho) d\rho = (\lambda^2 + \gamma_i^2)^{-\frac{1}{2}},$$

where $$\text{Re}(\gamma_i) > 0.$$

Therefore

$$\exp(-\gamma_i r)/r = \int_0^\infty \lambda(\lambda^2 + \gamma_i^2)^{-\frac{1}{2}} \exp[\pm(\lambda^2 + \gamma_i^2) z] J_0(\rho) d\lambda$$

$$\begin{bmatrix} + \text{ for } -z \geqslant 0 \\ - \text{ for } -z \leqslant 0 \end{bmatrix}.$$

The free space case when γ_i is purely imaginary is a special case of Sonine's integral which is given by Watson (22, p. 416).

Appendix B

A well known contour integral is given by Churchill (2) in his tables of Laplace transforms:

$$\frac{1}{2\pi i}\int_{c-i\infty}^{c+i\infty} \exp(-as^{\frac{1}{2}}) \exp(st)ds = [1 - \operatorname{erf} x]u(t). \quad (c > 0)$$

where $x = at^{-\frac{1}{2}}/2$ and where erf x is the error function of argument x. Each side of this equation can be differentiated three times, with respect to a, to yield the following three integrals:

$$\frac{1}{2\pi i}\int_{c-i\infty}^{c+i\infty} as^{-\frac{1}{2}} \exp(-as^{\frac{1}{2}}) \exp(st)ds = [x \operatorname{erf}' x]u(t)$$

$$\frac{1}{2\pi i}\int_{c-i\infty}^{c+i\infty} a^2 \exp(-as^{\frac{1}{2}}) \exp(st)ds = [2x^3 \operatorname{erf}' x]u(t)$$

and $$\frac{1}{2\pi i}\int_{c-i\infty}^{c+i\infty} a^2 s^{\frac{1}{2}} \exp(-as^{\frac{1}{2}}) \exp(st)ds = [2x^4 \operatorname{erf}'' x - 4x^3 \operatorname{erf}' x]u(t)$$

where erf′ x and erf″ x are the first and second derivatives, respectively, of the error function. The error function and its derivatives are defined and tabulated by Jahnke and Emde (9).

References*

1. Card, R. H. Am. Inst. Mining Met. Engrs. Tech. Pub. No. 829. 1937.
2. Churchill, R. V. Modern operational mathematics. McGraw-Hill Book Co. Inc., New York. 1944. p. 299.
3. Ehrenburg, D. O. and Watson, R. J. Trans. Am. Inst. Mining Met. Engrs. (Geophysical Prospecting), 423. 1932.
4. Foster, R. M. Bell System Tech. J. 10:528. 1931.
5. Gardner, M. F. and Barnes, J. L. Transients in linear systems. John Wiley and Sons Inc., New York. 1942. p. 255.
6. Graf, A. Beitr. angew. Geophys. 4:165. 1934.
7. Heiland, C. A. Geophysical exploration. Prentice-Hall Inc., New York. 1946.
8. Hummel, J. N. Beitr. angew. Geophys. 5: 165. 1929.
9. Jahnke, E. and Emde, F. Tables of functions. Dover, New York. 1945.
10. Kato, Y. Science Repts. Tohoku Imp. Univ. 29: 629. 1941.
11. Maxwell, J. C. Electricity and magnetism. 1873.
12. Ollendorf, F. Erdestrome. Julius Springer. Berlin. 1928.
13. Ollendorf, F. Elek. Nachr. Tech. 7: 220. 1930.
14. Peterson, L. C. Bell System Tech. J. 9: 400. 1930.
15. Riordan, J. Bell System Tech. J. 10: 420. 1931.
16. Riordan, J. and Sunde, E .D. Bell System Tech. J. 12: 162. 1933.
17. Schelkunoff, S. A. Electromagnetic waves. D. Van Nostrand Co. Inc., New York. 1943.
18. Sommerfeld, A. Ann. Physik, 4: 1135. 1926.
19. Stefanescu, S. S. and Schlumberger, R. M. J. phys. radium, 1: 132. 1930.
20. Stefanescu, S. S. Beitr. angew. Geophys. 4: 165. 1934.
21. Wait, J. R. Geophysics, 16: 220. 1951.
22. Watson, G. N. Theory of Bessel functions. Cambridge University Press, London. 1944.
23. West, S. S. Geophysics, 8: 8. 1943.
24. Wolf, A. Geophysics, 11: 518. 1946.

The work of the following two authors is also of interest:
(*a*) Belluigi, I. Geophysics, 15: 687. 1950.
(*b*) Slichter, L. B. Geophysics, 16: 431. 1951.

THE QUANTIZATION OF THE CLASSICAL THEORY OF SPINNING PARTICLES[1]

By S. Shanmugadhasan[2]

Abstract

The classical theory of particles, possessing charge and dipole moment, and moving in an electromagnetic field, is considered on the assumptions that there is no constraint connection between the rotational variables and the velocity of the particle, and that the two invariant squares of the dipole moment six-vector are constants of the motion. Two different schemes are obtained according as the two invariant scalar products of the dipole moment and total spin angular momentum six-vectors are or are not constants of the motion. The Bhabha–Corben theory fits into the former scheme. The classical schemes are put into canonical form by using for each particle the relativistic connection between the momenta and the rest-mass, modified to include the effect of the kinetic and potential energies due to spin and dipole moment, as the Hamilton–Jacobi equation and the usual Poisson brackets for the translational and total spin variables. The Wentzel field and the λ-limiting process are used mainly in dealing with the field. The variational principle for the Bhabha–Corben equations is given with the field treated according to the limiting process of Dirac or the relativistic cutoff method of Feynman. The quantization is completed by using the analogy rules. The changes required when the interacting field is a vector meson field are discussed.

Introduction

The quantum theory of a dynamical system is obtained by first putting the classical equations of motion of the system into the canonical (Hamiltonian) form, and then quantizing the theory by using the standard rules connecting the canonical form of classical dynamics to quantum dynamics. Since in quantum mechanics the dynamical variables of the system are linear operators satisfying a noncommutative algebra while in classical mechanics they satisfy a commutative algebra, this procedure for quantization may lead to ambiguities in the order in which the factors must appear in the quantum theory. In spite of this difficulty the method can be used to obtain definite results in many problems.

The relativistic quantum mechanics of spinless electrons is obtained by the above method, the elementary Lorentz classical theory of the electron yielding the Gordon-Klein wave equation in the quantum theory. But the spinning electron occurring in nature is described correctly by the Dirac linear wave equation for particles with spin half a quantum, and not by the Gordon-Klein equation. In view of the success of the Dirac equation little interest has been shown in extending the Gordon-Klein equation to include the effect of spin and dipole moment. The first attempts at setting up a relativistic classical theory of spinning particles possessing dipole moment were made by J. Frenkel and L. H. Thomas. But there has been no systematic formulation of the corresponding

[1] *Manuscript received May 22, 1951.*
Contribution from the Division of Physics, National Research Council, Ottawa, Canada. Issued as N.R.C. No. 2577.
[2] *National Research Council of Canada Postdoctorate Fellow.*

quantum theoretical equations. It is therefore worthwhile from the point of view of theoretical completeness to investigate such equations.

Following Dirac in his theory of radiating point electrons, Bhabha and Corben (2) have set up a general classical theory of spinning particles proceeding from the assumptions that the dipole moment is proportional to the spin of the particle, and that the invariant square of the spin tensor is constant during the motion. Without making use of these assumptions the present author (10) has arrived at a general form for the rotational and translational equations of motion when there is no constraint relation between the rotational and translational variables. This scheme is not sufficient to determine the motion of the particles without further assumptions as regards the rotational motion of the particles. Such assumptions can be made by referring to situations in the three dimensional dynamics of tops and gyroscopes. In a pure gyroscope the magnitude of the total spin angular momentum three-vector remains constant. The relativistic analogue of this has been dealt with in (10). The present paper deals with rotational motions more complicated and possessing more rotational degrees of freedom than a pure gyroscopic motion. Then the total spin angular momentum vector is represented as the sum of the so-called spin and an extra vector of angular momentum. This extra vector can be chosen in many ways. But two simple cases are obtained by choosing this vector so that (i) its magnitude is constant and the angle between the two vectors is variable, (ii) its magnitude is variable and the angle between the two vectors is constant (particularly with the two vectors orthogonal). The relativistic analogues of these two cases are considered below. Since the second case corresponds to a symmetric top, it leads to the Bhabha-Corben equations.

The classical theory can be put into canonical form if the equations of motion follow from a variational principle (3, 6). It is then possible to introduce canonical coordinates and momenta, and hence obtain the Hamilton-Jacobi equations and the Poisson brackets (P.B.'s hereafter) of the dynamical variables. However an action principle is not necessary, provided that the suitable Hamilton-Jacobi equations and a consistent scheme of P.B.'s can be postulated from general considerations (4, 5), as in the cases considered below. Yet it is of interest to have the action principle for at least one case, and the Bhabha-Corben scheme is chosen for this purpose. Quasi-coordinates appear in the covariant form of the action principle.

The present-day forms of electrodynamics are not entirely satisfactory, because difficulties arise in dealing with the interaction of the particle with its own field. For the sake of definiteness the discussion in the present paper is confined mainly to the form of electrodynamics using the Wentzel field and the λ-limiting process. There are features in the theory considered below that are unaffected by these questions, and they could be taken over into a satisfactory form of field dynamics. Modifications in the treatment of the field have been suggested recently by several authors. The changes in the action principle necessary to incorporate the limiting procedure of Dirac (6) or the relativistic cutoff procedure of Feynman (7, 8) are briefly indicated.

The extension of the theory when the interacting wave field is a (Proca) vector meson field is quite straightforward in most respects, and has been dealt with in (10). But the P.B. relations for the field variables given there are not correct, because they lead to inconsistencies when dealing with the extra condition involving these variables. This difficulty is resolved here by postulating suitable P.B.'s for the field.

In the quantum theory the Schrödinger equations for the particles are natural extensions of the Gordon-Klein equation. The physical interpretation therefore must be based on the Gordon-Klein probability rule which is not positive definite. In the wave equations the field intensity tensor appears coupled with the spin. This is not so in the linear wave equation for an electron unless it is modified, as Pauli has done, to give the particle an abnormal magnetic moment. In the present theory the same type of wave equation is applicable to particles of any spin and any value of the dipole moment.

It remains to be seen whether the theory is applicable to any of the elementary particles known experimentally. The quantum theory analogous to a pure gyroscopic rotation in the classical theory is not suitable for an electron, as has been seen from the computation of the Compton effect (11). The total cross section for Compton scattering increases indefinitely with the energy of the incident photons, which is also true of the cross section based on the Pauli modified linear wave equation. Since the heavy particles like the nucleons have an explicit spin interaction with the meson field, the theory may be of interest in this connection. The calculation of scattering cross sections, which can be used to check the new quantum schemes with the facts of nature, is yet to be done.

The Classical Equations of Motion

Relativistic notation is used in most of the following work. A departure from the usual convention of tensor analysis is the one (adopted by Dirac in this type of work) of denoting contravariant quantities by subscripts, and covariant quantities by superscripts. The velocity of light is taken to be unity, so that the metric tensor $g^{\mu\nu}$ (Greek indices take on values 0, 1, 2, 3) has all components vanishing except $g^{00} = -g^{11} = -g^{22} = -g^{33} = 1$. Four-vector notation is used whenever convenient. A point in space-time x_μ is then denoted by $\mathbf{x}$. The square $a_\mu a^\mu$ of a_μ is written as $\mathbf{a}^2$. The notation for the scalar product $a_\mu b^\mu$ of a_μ and b_μ is $(\mathbf{a}, \mathbf{b})$. It is convenient at some stages of the work to introduce three-vector notation. A three-vector is denoted by sans-serif bold type. Thus the three-vector with components (a_1, a_2, a_3) is denoted by $\mathbf{a}$. $(\mathbf{a}, \mathbf{b})$ and $[\mathbf{a} \times \mathbf{b}]$ are used for the scalar product and vector product respectively of two three-vectors $\mathbf{a}, \mathbf{b}$.

With tensors of the second rank, $X_{\mu\nu}X^{\mu\nu}$ and $X_{\mu\nu}Y^{\mu\nu}$ are denoted by X^2 and (XY) respectively. The antisymmetric tensor formed by transvection from two antisymmetric tensors $X_{\mu\nu}$, $Y_{\mu\nu}$, namely $X_{\mu\rho}Y^{\rho}_{.\nu} - X_{\nu\rho}Y^{\rho}_{.\mu}$, is denoted by $[X \,.\, Y]_{\mu\nu}$. The antisymmetric tensor $X^*_{\mu\nu}$ dual (some writers call it supplementary) to the antisymmetric tensor $X_{\mu\nu}$ is defined in terms of $X_{\mu\nu}$ by

$X^*_{23} = X_{01}, X^*_{31} = X_{02}, X^*_{12} = X_{03}, X^*_{01} = -X_{23}, X^*_{02} = -X_{31}, X^*_{03} = -X_{12}.$

This connection is just equivalent to $X^{*\mu\nu} = \frac{1}{2}\epsilon^{\mu\nu\sigma\tau}X_{\sigma\tau}$, $X^{\mu\nu} = -\frac{1}{2}\epsilon^{\mu\nu\sigma\tau}X^*_{\sigma\tau}$, where $\epsilon^{\mu\nu\sigma\tau}$ is the permutation symbol antisymmetric in each pair of indices and such that $\epsilon^{0123} = 1$. From the above definition, it follows that $(X^*)^*_{\mu\nu} = -X_{\mu\nu}$. Further, if $X_{\mu\nu}$, $Y_{\mu\nu}$ are two antisymmetric tensors, then

$$(X^*Y^*) = -(XY),\ (XY^*) = (X^*Y),$$
$$[X^* \,.\, Y^*]_{\mu\nu} = -[X \,.\, Y]_{\mu\nu},\ [X \,.\, Y]^*_{\mu\nu} = [X \,.\, Y^*]_{\mu\nu} = [X^* \,.\, Y]_{\mu\nu}.$$

An antisymmetric tensor $X_{\mu\nu}$ is said to be self-dual if $X^*_{\mu\nu} = \pm iX_{\mu\nu}$, where $i^2 = -1$. Any given antisymmetric tensor gives rise to two self-dual tensors (the factor $\frac{1}{2}$ being introduced for convenience)

$$U_{\mu\nu} = \tfrac{1}{2}(X_{\mu\nu} + iX^*_{\mu\nu}),\ V_{\mu\nu} = \tfrac{1}{2}(X_{\mu\nu} - iX^*_{\mu\nu}),$$

since

$$U^*_{\mu\nu} = \tfrac{1}{2}(X^*_{\mu\nu} - iX_{\mu\nu}) = -iU_{\mu\nu},\ V^*_{\mu\nu} = \tfrac{1}{2}(X^*_{\mu\nu} + iX_{\mu\nu}) = iV_{\mu\nu}.$$

A self-dual tensor has three independent components only, since

$$U_{23} = iU_{01},\ U_{31} = iU_{02},\ U_{12} = iU_{03},\ V_{01} = iV_{23},\ V_{02} = iV_{31},\ V_{03} = iV_{12}.$$

The three independent components, the (23), (31), (12), or the (01), (02), (03) components form a three-vector. It is through this step that three-vectors play a role in the theory. Now let $P_{\mu\nu} = \frac{1}{2}(Y_{\mu\nu} + iY^*_{\mu\nu})$, $Q_{\mu\nu} = \frac{1}{2}(Y_{\mu\nu} - iY^*_{\mu\nu})$, where $Y_{\mu\nu}$ is antisymmetric. Then

$$(PU) = i(P^*U) = \tfrac{1}{2}\{(XY) + i(X^*Y)\},\ (UQ) = (VP) = 0.$$

An equation of the type $N_{\mu\nu} = [X \,.\, Y]_{\mu\nu}$, where $X_{\mu\nu}$ and $Y_{\mu\nu}$ are as above, can be written in terms of self-dual tensors in the form

$$\tfrac{1}{2}(N_{\mu\nu} + iN^*_{\mu\nu}) = 2U_{\mu\lambda}P^{\lambda}_{\cdot\nu} = [U \,.\, P]_{\mu\nu},\ \tfrac{1}{2}(N_{\mu\nu} - iN^*_{\mu\nu}) = 2V_{\mu\lambda}Q^{\lambda}_{\cdot\nu} = [V \,.\, Q]_{\mu\nu}.$$

Consider a typical particle having coordinates $\mathbf{z}(s)$ and velocity $\mathbf{v} \equiv \dot{\mathbf{z}}$ (with $\mathbf{v}^2 = 1$). Here s is the proper-time, and the dot denotes differentiation with respect to s. Let the charge of the particle be e, and let its dipole moment (both electric and magnetic dipoles) be described by the antisymmetric tensor $Z_{\mu\nu}$, which may be considered as a function of s. The total spin angular momentum of the particle is described by the antisymmetric tensor $N_{\mu\nu}$. The field quantities $F_{\mu\nu}$ are obtained from the four-potentials A_μ according to $F_{\mu\nu} = \partial_\mu A_\nu - \partial_\nu A_\mu$, where ∂_μ denotes $\partial/\partial x^\mu$. The actual field at any point is expressed in terms of the ingoing and retarded fields, or the outgoing and advanced fields, by the relation

$$\mathbf{A}^{act.} = \mathbf{A}^{in.} + \mathbf{A}^{ret.} = \mathbf{A}^{out.} + \mathbf{A}^{adv.}.$$

When the system consists of several particles, the label i is affixed to the quantities associated with the ith particle.

The starting point of the present work is the general form, given in (10), for the translational and rotational equations of motion of particles of the above type, when no constraint connection between the rotational variables and the

velocity of the particle is assumed. The translational equation of motion has the form

$$\frac{d}{ds}[\{m - \tfrac{1}{2}(Zf)\}v_\mu] = ef_{\mu\sigma}v^\sigma - \tfrac{1}{2}Z^{\rho\sigma}\partial_\mu f_{\rho\sigma}, \tag{1}$$

where m is a scalar representing the total mechanical mass of the particle, and the rotational equation of motion, the form

$$\dot{N}_{\mu\nu} = [Z \,.\, f\,]_{\mu\nu}. \tag{2}$$

The effective field $f_{\mu\nu}$ in the above equations of motion of a single particle is the mean of the ingoing and outgoing fields. When there are several particles, the equations of motion of the ith particle have exactly the same form as above, except that the effective field $f_{\mu\nu i}$ is now

$$\begin{aligned} f_{\mu\nu i} &= \tfrac{1}{2}(F^{in.}_{\mu\nu} + F^{out.}_{\mu\nu}) + \tfrac{1}{2}\sum_{j\neq i}(F^{ret.}_{\mu\nu i} + F^{adv.}_{\mu\nu i}) \\ &= F^{in.}_{\mu\nu} + \sum_{j\neq i}F^{ret.}_{\mu\nu i} + \tfrac{1}{2}(F^{ret.}_{\mu\nu i} - F^{adv.}_{\mu\nu i}). \end{aligned} \tag{3}$$

The invariant equations that can be deduced from (1) and (2) are

$$dm/ds = \tfrac{1}{2}(\dot{Z}f), \tag{4}$$

$$(\dot{N}Z) = 0, \ (\dot{N}f) = 0. \tag{5}$$

Two definite schemes of equations of motion corresponding to the two cases mentioned in the introduction are obtained below.

Case I. Suppose that $Z_{\mu\nu} = CS_{\mu\nu}$, where C is a constant, and that $N_{\mu\nu} = S_{\mu\nu} + R_{\mu\nu}$, where S^2 = constant, (SS^*) = constant, R^2 = constant, (RR^*) = constant.

The variation of $R_{\mu\nu}$ with s, consistent with the constancy of R^2 and (RR^*), is given by

$$\dot{R}_{\mu\nu} = [X \,.\, R]_{\mu\nu}, \tag{6}$$

where $X_{\mu\nu}$ is some antisymmetric tensor yet to be determined (Ref. (1)). Then

$$\dot{S}_{\mu\nu} = C[S \,.\, f\,]_{\mu\nu} - [X \,.\, R]_{\mu\nu}. \tag{7}$$

Since $(S\dot{S}) = 0$, Equation (7) leads to

$$(S[X \,.\, R]) = (R[S \,.\, X]) = 0\,. \tag{8}$$

It is now assumed that $X_{\mu\nu}$ is independent of $R_{\mu\nu}$, and that $R_{\mu\nu}$ is independent of $S_{\mu\nu}$. Then, for (8) to be true for all $R_{\mu\nu}$, the condition

$$[S \,.\, X]_{\mu\nu} \equiv S_{\mu\lambda}X^{\lambda}_{\cdot\nu} - S_{\nu\lambda}X^{\lambda}_{\cdot\mu} = 0 \tag{9}$$

must hold at every point of the world-line of the particle.

The six homogeneous linear equations equivalent to (9) can be written in the matrix form

$$\begin{Vmatrix} 0 & S^{21} & S^{31} & S^{02} & 0 & S^{30} \\ S^{12} & 0 & S^{32} & S^{10} & S^{03} & 0 \\ S^{13} & S^{23} & 0 & 0 & S^{20} & S^{01} \\ S^{20} & S^{01} & 0 & 0 & S^{31} & S^{32} \\ 0 & S^{30} & S^{02} & S^{13} & 0 & S^{12} \\ S^{03} & 0 & S^{10} & S^{23} & S^{21} & 0 \end{Vmatrix} \begin{Vmatrix} X^{01} \\ X^{02} \\ X^{03} \\ X^{12} \\ X^{23} \\ X^{31} \end{Vmatrix} = 0.$$

The 6×6 antisymmetric matrix is singular. Since its rank must be even, it is at most four. The determinant on the lower right, bounded by the third row and third column, and by the last row and last column, has the value $(S^{02}S^{23} - S^{01}S^{21})^2$, which is not zero in general. Thus the rank of the matrix is four. The solution of the system of equations therefore contains two arbitrary parameters. $X_{\mu\nu} = S_{\mu\nu}$ is evidently a solution of the system. Since the antisymmetric tensor on the left side of (9) vanishes, it follows that the tensor dual to this also must vanish. Hence $[S^*. X]_{\mu\nu} = 0$, which gives $X_{\mu\nu} = S^*_{\mu\nu}$ as a solution. The general solution of the system (9) is

$$X_{\mu\nu} = AS_{\mu\nu} + BS^*_{\mu\nu}, \tag{10}$$

where A, B are two arbitrary scalar parameters.

In view of (10), Equation (7) becomes

$$\dot{S}_{\mu\nu} = C[S\,.f\,]_{\mu\nu} + A[R\,.S]_{\mu\nu} + B[R\,.S^*]_{\mu\nu};$$

its invariant equation is $\dot{S}_{\mu\nu}(Cf^{\mu\nu} - AR^{\mu\nu} - BR^{*\mu\nu}) = 0$. With the help of this result, and of $(R\dot{R}) = (R\dot{R}^*) = (\dot{R}S) = (\dot{R}^*S) = 0$, (4) leads to

$$dm/ds = \tfrac{1}{2}C(\dot{S}f) = \tfrac{1}{2}A(\dot{S}R) + \tfrac{1}{2}B(R^*\dot{S})$$

$$= \tfrac{1}{2}\frac{d}{ds}\{A(SR) + B(SR^*)\} - \tfrac{1}{2}(SR)\frac{dA}{ds} - \tfrac{1}{2}(SR^*)\frac{dB}{ds}. \tag{11}$$

If, on grounds of simplicity, the arbitrary parameters are chosen to be constants, integration of (11) gives $m = M + \frac{1}{2}A(RS) + \frac{1}{2}B(R^*S)$, where M is an arbitrary constant. The constants A^{-1} and B^{-1} are of the nature of moments of inertia. The second and third terms in the expression for m represent the kinetic energy due to rotation of the particle, which naturally appears in a relativistic theory as an addition to the constant rest-mass M of the particle. The translational motion is given by

$$\frac{d}{ds}[\{M + \tfrac{1}{2}A(RS) + \tfrac{1}{2}B(R^*S) - \tfrac{1}{2}C(Sf)\}v_\mu] = ef_{\mu\sigma}v^\sigma - \tfrac{1}{2}CS^{\rho\sigma}\partial_\mu f_{\rho\sigma}, \tag{12}$$

while the rotational motion is given by the two equations

$$\dot{S}_{\mu\nu} = C[S\,.f\,]_{\mu\nu} - A[S\,.R]_{\mu\nu} - B[S\,.R^*]_{\mu\nu}, \tag{13}$$

$$\dot{R}_{\mu\nu} = A[S\,.R]_{\mu\nu} + B[S\,.R^*]_{\mu\nu}. \tag{14}$$

Case II. Assume that $N_{\mu\nu}$ and $Z_{\mu\nu}$ satisfy the relations

$$(NZ) = \text{constant}, \quad (NZ^*) = \text{constant}, \tag{15}$$

$$Z^2 = \text{constant}, \quad (ZZ^*) = \text{constant}. \tag{16}$$

Note that (NZ) and (NZ^*) are not constant in Case I.

From (16), $$\dot{Z}_{\mu\nu} = [Y \,.\, Z]_{\mu\nu}, \tag{17}$$

where $Y_{\mu\nu}$ is some antisymmetric tensor, assumed to be independent of $Z_{\mu\nu}$, and which is yet to be determined. Since $(N\dot{Z}) = 0$ from (5) and (15), (17) gives $(N[Y.Z]) = (Z[N.Y]) = 0$. For this to hold everywhere on the world-line for arbitrary $Z_{\mu\nu}$, $[N \,.\, Y]_{\mu\nu} = 0$ must be true at all points of the world-line. Hence $Y_{\mu\nu} = DN_{\mu\nu} + EN^*_{\mu\nu}$, where D and E are arbitrary scalars. For simplicity, D and E are chosen to be constants in the work that follows.

With the above choice of $Y_{\mu\nu}$, Equation (4) becomes

$$\begin{aligned} dm/ds &= \tfrac{1}{2}(\dot{Z}f) = \tfrac{1}{2}([DN + EN^* \,.\, Z]f) \\ &= \tfrac{1}{2}(DN_{\mu\nu} + EN^*_{\mu\nu})\dot{N}^{\mu\nu} = \tfrac{1}{4}d\{DN^2 + E(NN^*)\}/ds. \end{aligned}$$

Hence, by integration, $m = M + \frac{1}{4}DN^2 + \frac{1}{4}E(NN^*)$, where M is an arbitrary constant. The constants D^{-1} and E^{-1} are again analogous to moments of inertia, and the rotational kinetic energy represented by the second and third terms in the expression for m appears as an addition to the rest-mass M. The motion of the particle is thus described by

$$\frac{d}{ds}[\{M + \tfrac{1}{4}DN^2 + \tfrac{1}{4}E(NN^*) - \tfrac{1}{2}(Zf)\}v_\mu] = ef_{\mu\sigma}v^\sigma - \tfrac{1}{2}Z^{\rho\sigma}\partial_\mu f_{\rho\sigma} \tag{18}$$

for the translation, and by

$$\dot{N}_{\mu\nu} = [Z \,.\, f\,]_{\mu\nu}, \tag{19}$$

$$\dot{Z}_{\mu\nu} = D[N \,.\, Z]_{\mu\nu} + E[N^* \,.\, Z]_{\mu\nu} \tag{20}$$

for the rotation. A closer examination of these equations of motion, with the help of self-dual tensors, shows that $N_{\mu\nu}$ can be expressed in terms of $Z_{\mu\nu}$ and $\dot{Z}_{\mu\nu}$, and their duals. Then the scheme of equations reduces to the same form as that of Bhabha and Corben (2).

Introduce now the three-vectors arising from the self-dual tensors. The corresponding sans-serif bold lower case letter denotes the three-vector from a given six-vector; for example, z corresponds to $Z_{\mu\nu}$. The self-dual tensor with the $+\,i$ combination like $U_{\mu\nu}$ is used here, though there is no particular reason for this preference. Then Equation (20) becomes

$$\dot{\mathsf{z}} = 2[\mathsf{y} \times \mathsf{z}] = 2(D - iE)[\mathsf{n} \times \mathsf{z}].$$

Hence

$$[\mathsf{z} \times \dot{\mathsf{z}}] = 2(D - iE)[\mathsf{z} \times [\mathsf{n} \times \mathsf{z}]] = 2(D - iE)\{\mathsf{z}^2\mathsf{n} - (\mathsf{z},\mathsf{n})\mathsf{z}\},$$

that is,

$$\mathsf{z}^2\mathsf{n} = (\mathsf{z},\,\mathsf{n})\mathsf{z} + \tfrac{1}{2}(D - iE)^{-1}[\mathsf{z} \times \dot{\mathsf{z}}]. \tag{21}$$

Also,

$$\mathsf{z}^2 = 4(D - iE)^2([\mathsf{n} \times \mathsf{z}])^2 = 4(D - iE)^2\{\mathsf{n}^2\mathsf{z}^2 - (\mathsf{n},\,\mathsf{z})^2\}. \tag{22}$$

These three-vector equations can be immediately translated into tensor equations. Equation (21) corresponds to

$$\begin{aligned} \{Z^2 + i(ZZ^*)\}(N_{\mu\nu} + iN^*_{\mu\nu}) = \{(ZN) + i(Z^*N)\}(Z_{\mu\nu} + iZ^*_{\mu\nu}) + 2(D - iE)^{-1} \\ \{[Z \,.\, \dot{Z}]_{\mu\nu} + i[Z \,.\, \dot{Z}]^*_{\mu\nu}\}. \end{aligned}$$

Hence $N_{\mu\nu}$ has the form

$$N_{\mu\nu} = D_1 Z_{\mu\nu} + D_2 Z^*_{\mu\nu} + D_3[Z \cdot \dot{Z}]_{\mu\nu} + D_4[Z \cdot \dot{Z}]^*_{\mu\nu} \tag{23}$$

Similarly, from (22),

$$\{Z^2 + i(ZZ^*)\}\{N^2 + i(NN^*)\} = \{(NZ) + i(N^*Z)\}^2 + 2(D - iE)^{-2}\{\dot{Z}^2 + i(\dot{Z}\dot{Z}^*)\},$$

so that N^2 and (NN^*) have the form

$$N^2 = E_1\dot{Z}^2 + E_2(\dot{Z}\dot{Z}^*) + E_3,\ (NN^*) = E_4\dot{Z}^2 + E_5(\dot{Z}\dot{Z}^*) + E_6. \tag{24}$$

$D_1, \ldots, D_4$ in (23), and $E_1, \ldots, E_6$ in (24) are constants, which can be expressed in terms of D, E, and of Z^2, (ZZ^*), (ZN), (ZN^*), and which are related in such a way that the equations of motion are consistent. Bhabha and Corben have used exactly the form (23) for the total spin angular momentum and the m obtained by using (24) as the total mechanical mass of the particle.

The Bhabha-Corben equations can be considered from the following point of view. Put in Equation (2) $Z_{\mu\nu} = CS_{\mu\nu}$, where C is a constant, and $S_{\mu\nu}$ is the spin angular momentum about the axis of spin. The total spin angular momentum of a symmetrical top in ordinary dynamics (for instance Ref. (9)) is $\mathbf{s} + K[\mathbf{s} \times \dot{\mathbf{s}}]$, where $\mathbf{s}$ is the so-called spin along the axis (with $\mathbf{s}^2$ = constant), and $K\mathbf{s}^2$ is the moment of inertia perpendicular to the axis. The relativistic analogue of this is $S_{\mu\nu} + K[S \cdot \dot{S}]_{\mu\nu}$, where $S_{\mu\nu}$ is the spin angular momentum along the axis of spin (with S^2 = constant), and K is a constant. If this value is chosen for $N_{\mu\nu}$ in Equation (2), the rotational equation of motion becomes

$$\dot{N}_{\mu\nu} = \dot{S}_{\mu\nu} + K[S \cdot \ddot{S}]_{\mu\nu} = C[S \cdot f]_{\mu\nu}, \tag{25}$$

with the invariant equation $C(\dot{S}f) = K(\dot{S}\ddot{S})$. Hence

$$dm/ds = \tfrac{1}{2}C(\dot{S}f) = \tfrac{1}{2}K(\dot{S}\ddot{S}).$$

By integration $m = M + \frac{1}{4}K\dot{S}^2$, where M is a constant. With this m, the translational equation becomes

$$\frac{d}{ds}[\{M + \tfrac{1}{4}K\dot{S}^2 - \tfrac{1}{2}C(Sf)\}v_\mu] = ef_{\mu\sigma}v^\sigma - \tfrac{1}{2}CS^{\rho\sigma}\partial_\mu f_{\rho\sigma}. \tag{26}$$

$\dot{S}_{\mu\nu}$ is given in terms of $N_{\mu\nu}$ and $S_{\mu\nu}$ by

$$\dot{S}_{\mu\nu} = 2\{K(S^2)^2 + K(SS^*)^2\}^{-1}\{S^2[N \cdot S]_{\mu\nu} + (SS^*)[N \cdot S^*]_{\mu\nu}\}.$$

In the expression for $N_{\mu\nu}$, one could add constant multiples of the dual tensors $S^*_{\mu\nu}$ and $[S \cdot \dot{S}]^*_{\mu\nu}$ with the subsequent modifications in m to give the general form of the Bhabha-Corben equations. But it is simpler to consider the form (25, 26) of the Bhabha-Corben equations.

The classical equations of motion considered so far apply to one particle only. The generalization to a system of several particles is quite straightforward. The typical ith particle has the equations of motion of exactly the same form as those for a single particle except that the label i is added on to all the constants

and tensors describing the ith particle, and that the effective field is given by Equation (3).

The effective field in all the above equations of motion can be expressed in terms of a new field, called the Wentzel field. The Wentzel potential, $\mathbf{A}_{\mathrm{W}}(\mathbf{x})$, of particles possessing charge e_i and dipole moment $Z_{\mu\nu i}$ has been defined in Ref. (10) as

$$A_{\mu\mathrm{W}}(\mathbf{x}) = A_{\mu}^{in.}(\mathbf{x}) + \sum_i e_i \int_{-\infty}^{s_i} v_{\mu i}(s_i')\Delta(\mathbf{x} - \mathbf{z}_i(s_i'))ds_i' + \sum_i \partial^{\rho} \int_{-\infty}^{s_i} Z_{\rho\mu i}(s_i')\Delta(\mathbf{x} - \mathbf{z}_i(s_i'))ds_i', \tag{27}$$

where $\Delta(\mathbf{x})$ is the Jordan-Pauli relativistic δ-function, defined by

$$|x_o|\Delta(\mathbf{x}) = 2x_o\delta(\mathbf{x}^2).$$

$f_{\mu\nu i}$ is then obtained from the potential

$$\mathbf{A}(\mathbf{x}) = \tfrac{1}{2}\{\mathbf{A}_{\mathrm{W}}(\mathbf{x} + \lambda) + \mathbf{A}_{\mathrm{W}}(\mathbf{x} - \lambda)\}, \tag{28}$$

where λ is a small time-like four-vector made to tend to zero ultimately, provided that

$$(\mathbf{z}_i - \mathbf{z}_j \pm \lambda) < 0, \quad i \neq j. \tag{29}$$

The potential $\mathbf{A}$ defined by (27) and (28) satisfies the equations

$$\Box\mathbf{A} = 0, \quad \Box \equiv \partial_{\mu}\partial^{\mu}, \tag{30}$$

$$R(\mathbf{x}) \equiv \partial^{\mu}A_{\mu}(\mathbf{x}) + \sum_i e_i D(\mathbf{x}, \mathbf{z}_i, \lambda) = 0, \tag{31}$$

$$dA_{\mu}(\mathbf{x})/ds_i = e_i v_{\mu i} D(\mathbf{x}, \mathbf{z}_i, \lambda) + \partial^{\rho}(Z_{\rho\mu i} D(\mathbf{x}, \mathbf{z}_i, \lambda)), \tag{32}$$

where
$$D(\mathbf{x}, \mathbf{z}_i, \lambda) \equiv \tfrac{1}{2}\{\Delta(\mathbf{x} - \mathbf{z}_i + \lambda) + \Delta(\mathbf{x} - \mathbf{z}_i - \lambda)\}. \tag{33}$$

Canonical Form of the Classical Theory

The general (canonical) equation of motion of a dynamical variable ξ of a system is $d\xi/ds = [\xi, F]$, where $[\xi, F]$ denotes the P.B. of ξ and F, and where $F = 0$ is the Hamilton-Jacobi equation of the system. A change from the independent variable s to a new independent variable τ would necessitate the use of $Fds/d\tau = 0$ as the new Hamilton-Jacobi equation. In order to apply this result to a particular problem, one must know the Hamilton-Jacobi equations of the system, and the P.B. relations connecting the various dynamical variables describing the system. According to Dirac (5), it is permissible to postulate the P.B.'s without the explicit introduction of canonical coordinates and momenta, provided that the postulated relations satisfy the following properties of P.B.'s:

$$[\xi, \eta] = -[\eta, \xi], \quad [\Phi(\xi_1, \xi_2, \ldots), \Psi(\eta_1, \eta_2, \ldots)] = \sum_{i,j}^{r} \frac{\partial\Phi}{\partial\xi_i}\frac{\partial\Psi}{\partial\eta_i}[\xi_i, \eta_i],$$

$$[\xi, [\eta, \zeta]] + [\eta, [\zeta, \xi]] + [\zeta, [\xi, \eta]] = 0.$$

Case I. Consider the equations of motion (12)—(14). These equations reduce to those of a spinless electron when $R_{\mu\nu}$ and $S_{\mu\nu}$ are zero for all s. The required Hamilton-Jacobi equation must be such that it reduces to that of a spinless electron, which is known to be of the Gordon-Klein type, when $R_{\mu\nu}$ and $S_{\mu\nu}$ are put equal to zero. But the quantity $M + \frac{1}{2}A(RS) + \frac{1}{2}B(R^*S) - \frac{1}{2}C(Sf)$ instead of a constant M plays the role of total effective mass of the particle in (12), in conformity with relativistic ideas that the kinetic energy of spin and the potential energy due to the dipole moment in the field appear as additions to the rest-mass of the spinless particle. Hence the required Hamilton-Jacobi equation is taken to be that obtained from the Gordon-Klein type by replacing the constant rest-mass by the effective mass of the particle, namely,

$$-2mF \equiv (\mathbf{p}-e\mathbf{A})^2-m^2 = 0, \quad m \equiv M + \tfrac{1}{2}A(RS)+\tfrac{1}{2}B(R^*S)-\tfrac{1}{2}C(Sf), \quad (34)$$

where $\mathbf{p}$ is the momentum four-vector, and $\mathbf{A}(\mathbf{x})$ is the field, Equation (28).

The choice of the P.B.'s is not difficult. The usual P.B. relations for the coordinates and momenta, and those for the spin angular momentum variables are taken over. One notes also that the translational and rotational variables of the particle refer to different degrees of freedom. Thus for the particle variables

$$[p_\mu, z_\nu] = g_{\mu\nu}, \ [z_\mu, z_\nu] = 0, \ [p_\mu, p_\nu] = 0, \quad (35)$$

$$[z_\mu, \text{spin variables}] = 0, \ [p_\mu, \text{spin variables}] = 0, \quad (36)$$

$$\left.\begin{aligned} &[S^{\alpha\beta}, S^{\mu\nu}] = -[S^{*\alpha\beta}, S^{*\mu\nu}] = -g^{\alpha\mu}S^{\beta\nu} + g^{\beta\mu}S^{\alpha\nu} + g^{\alpha\nu}S^{\beta\mu} - g^{\beta\nu}S^{\alpha\mu}, \\ &[S^{\alpha\beta}, S^{*\mu\nu}] = [S^{*\alpha\beta}, S^{\mu\nu}] = -g^{\alpha\mu}S^{*\beta\nu} + g^{\beta\mu}S^{*\alpha\nu} + g^{\alpha\nu}S^{*\beta\mu} - g^{\beta\nu}S^{*\alpha\mu}, \\ &[R^{\alpha\beta}, S^{\mu\nu}] = 0, \ [R^{\alpha\beta}, S^{*\mu\nu}] = 0. \end{aligned}\right\} \quad (37)$$

$R_{\mu\nu}$ has P.B. relations similar to those of $S_{\mu\nu}$. From the P.B.'s for $S_{\mu\nu}$, one gets

$[S^{\alpha\beta},S^{\alpha}] = 2[S^{\alpha\beta},S^{\mu\nu}]S_{\mu\nu} = 2(-g^{\alpha\mu}S^{\beta\nu}+g^{\beta\mu}S^{\alpha\nu}+g^{\alpha\nu}S^{\beta\mu}-g^{\beta\nu}S^{\alpha\mu})S_{\mu\nu} = -4[S.S]^{\alpha\beta}=0,$

$[S^{\alpha\beta},(SS^*)] = [S^{\alpha\beta},S^{\mu\nu}]S^*_{\mu\nu} + S_{\mu\nu}[S^{\alpha\beta},S^{*\mu\nu}] = 2[S^*.S]^{\alpha\beta}+ 2[S.S^*]^{\alpha\beta} = 0.$

Similar relations hold for $S^{*\alpha\beta}$, and for $R^{\alpha\beta}$, $R^{*\alpha\beta}$.

Since the particle variables and the field variables belong to different degrees of freedom, $A_\nu(\mathbf{x})$ has vanishing P.B.'s with z_μ, p_μ, $S_{\alpha\beta}$, $R_{\alpha\beta}$. The P.B. of two field variables is to be taken to be

$$[A_\mu(\mathbf{x}), A_\nu(\mathbf{x}')] = g_{\mu\nu}D(\mathbf{x}, \mathbf{x}', \lambda), \quad (38)$$

where $D(\mathbf{x}, \mathbf{x}', \lambda)$ is defined by (33). Further discussion of the field equations is deferred to the end of this section, since they have the same form in both the cases considered here.

The correct connection between velocity and momentum is given by

$$v_\mu = \dot{z}_\mu = [z_\mu, F] = -\partial F/\partial p^\mu = (p_\mu - eA_\mu(\mathbf{z}))/m. \quad (39)$$

Since $m \neq 0$, and $[\xi, \eta^{-1}] = -[\xi, \eta]\eta^{-2}$ from the definition of a P.B., it follows that

$$\dot{p}_\mu = [p_\mu, F] = -\frac{\partial F}{\partial z^\mu} = \frac{e}{m}(p_\nu - eA_\nu(\mathbf{z}))\frac{\partial A^\nu}{\partial z^\mu}(\mathbf{z}) - \tfrac{1}{2}CS^{\rho\sigma}\partial_\mu f_{\rho\sigma}\left(1+\frac{F}{m}\right)$$
$$= ev^\nu \partial A_\nu(\mathbf{z})/\partial z^\mu - \tfrac{1}{2}CS^{\rho\sigma}\partial_\mu f_{\rho\sigma}. \tag{40}$$

Equations (39) and (40) together give the correct translational equation of motion

$$d(mv_\mu)/ds = [ev^\nu(\partial_\mu A_\nu - \partial_\nu A_\mu) - \tfrac{1}{2}CS^{\rho\sigma}\partial_\mu f_{\rho\sigma}]_{\mathbf{x}=\mathbf{z}}.$$

The equations of motion for $S_{\mu\nu}$ and $R_{\mu\nu}$ are

$$\begin{aligned}
\dot{S}_{\mu\nu} &= [S_{\mu\nu}, F] = \tfrac{1}{2}[S_{\mu\nu}, A(RS) + B(R^*S) - C(Sf)] \\
&= \tfrac{1}{2}A[S_{\mu\nu}, S_{\alpha\beta}]R^{\alpha\beta} + \tfrac{1}{2}B[S_{\mu\nu}, S_{\alpha\beta}]R^{*\alpha\beta} - \tfrac{1}{2}C[S_{\mu\nu}, S_{\alpha\beta}]f^{\alpha\beta} \\
&= -A[S\,.\,R]_{\mu\nu} - B[S\,.\,R^*]_{\mu\nu} + C[S\,.\,f]_{\mu\nu}, \\
\dot{R}_{\mu\nu} &= [R_{\mu\nu}, F] = \tfrac{1}{2}A[R_{\mu\nu}, R_{\alpha\beta}]S^{\alpha\beta} + \tfrac{1}{2}B[R_{\mu\nu}, R_{\alpha\beta}]S^{*\alpha\beta} \\
&= -A[R\,.\,S]_{\mu\nu} - B[R\,.\,S^*]_{\mu\nu},
\end{aligned}$$

which describe correctly the rotational motion of the particle. Also, S^2, (SS^*), R^2, (RR^*) have vanishing P.B.'s with all the dynamical variables of the system, and therefore with F, which should hold for them to be constants of the motion.

Case II. The Hamilton-Jacobi equation suitable for dealing with Equations (18)—(20) is

$$-2mF \equiv (\mathbf{p}-e\mathbf{A})^2 - m^2 = 0,\ m \equiv M + \tfrac{1}{4}DN^2 + \tfrac{1}{4}E(NN^*) - \tfrac{1}{2}(Zf), \tag{41}$$

with the field $\mathbf{A}(\mathbf{x})$ given by (28). z_μ and p_μ have the usual P.B. relations (35) among themselves and have vanishing P.B.'s with $Z_{\alpha\beta}$ and $N_{\alpha\beta}$. The P.B. relations for $N_{\mu\nu}$ are taken to be the usual ones for spin angular momentum. $Z_{\mu\nu}$ is taken to play the role of generalized coordinates in relation to the angular momentum $N_{\mu\nu}$. Thus the P.B.'s for the rotational variables are

$$\left.\begin{aligned}
&[Z^{\alpha\beta}, Z^{\mu\nu}] = 0, \\
&[N^{\alpha\beta}, Z^{\mu\nu}] = -g^{\alpha\mu}Z^{\beta\nu} + g^{\beta\mu}Z^{\alpha\nu} + g^{\alpha\nu}Z^{\beta\mu} - g^{\beta\nu}Z^{\alpha\mu}, \\
&[N^{\alpha\beta}, N^{\mu\nu}] = -g^{\alpha\mu}N^{\beta\nu} + g^{\beta\mu}N^{\alpha\nu} + g^{\alpha\nu}N^{\beta\mu} - g^{\beta\nu}N^{\alpha\mu},
\end{aligned}\right\} \tag{42}$$

and the corresponding relations involving the dual tensors. The field variables again have the same P.B.'s as in Case I. Then, since $N^{\alpha\beta}$, $Z^{\alpha\beta}$ have vanishing P.B.'s with Z^2, (ZZ^*), (NZ), and (NZ^*), and since

$$[N^{\alpha\beta}, N^2] = 0,\ [N^{\alpha\beta}, (NN^*)] = 0,\ [N^{\alpha\beta}, (Zf)] = -2[Z\,.\,f]^{\alpha\beta},$$
$$[Z^{\alpha\beta}, N^2] = 4[N\,.\,Z]^{\alpha\beta},\ [Z^{\alpha\beta}, (NN^*)] = 4[N^*.\,Z]^{\alpha\beta},$$

the equations of the motion check out correctly, and Z^2, (ZZ^*), (NZ), (NZ^*) are constants of the motion.

The equivalence of the equations under consideration to the Bhabha-Corben equations has already been shown. Since the P.B.'s for $\dot{Z}_{\mu\nu}$ can be obtained from

(42) by using (20), the above discussion covers the canonical formulation of the Bhabha-Corben equations. However, a separate discussion of the canonical formulation of Equations (25) and (26) is given below.

Introduce the three-vectors $\mathbf{n}$ and $\mathbf{s}$ connected by the relation $\mathbf{n} = \mathbf{s} + 2K[\mathbf{s} \times \dot{\mathbf{s}}]$. Hence

$$\dot{\mathbf{s}} = (2K\mathbf{s}^2)^{-1}[\mathbf{n} \times \mathbf{s}]. \tag{43}$$

The P.B.'s satisfied by $\mathbf{n}$ and $\mathbf{s}$ are

$$[s_a, s_b] = 0, \; [n_a, s_b] = s_c, \; [n_a, n_b] = n_c, \tag{44}$$

where the suffixes a, b, c take values that are a cyclic permutation of 1, 2, 3. Therefore, from (43) and (44), $\dot{\mathbf{s}}$ has the P.B.'s

$$\begin{aligned} [s_a, \dot{s}_b] &= (2K\mathbf{s}^2)^{-1}(\mathbf{s}^2\delta_{ab} - s_a s_b), \\ [n_a, \dot{s}_b] &= \dot{s}_c, \\ [\dot{s}_a, \dot{s}_b] &= -(4K^2\mathbf{s}^2)^{-1}n_c, \end{aligned} \tag{45}$$

where δ_{ab} is the usual Kronecker symbol. In terms of the original tensors, the P.B.'s for the spin variables are those corresponding to (42), and

$$\left.\begin{aligned} [S^{\alpha\beta}, \dot{S}^{\mu\nu}] &= K^{-1}(-g^{\alpha\mu}S^{\beta\lambda}\tilde{S}_{\lambda}^{\cdot\nu} + g^{\beta\mu}S^{\alpha\lambda}\tilde{S}_{\lambda}^{\cdot\nu} + g^{\alpha\nu}S^{\beta\lambda}\tilde{S}_{\lambda}^{\cdot\mu} - g^{\beta\nu}S^{\alpha\lambda}\tilde{S}_{\lambda}^{\cdot\mu} \\ &\qquad - 2S^{\alpha\mu}\tilde{S}^{\beta\nu} + 2S^{\beta\mu}\tilde{S}^{\alpha\nu}), \\ [N^{\alpha\beta}, \dot{S}^{\mu\nu}] &= -g^{\alpha\mu}\dot{S}^{\beta\nu} + g^{\beta\mu}\dot{S}^{\alpha\nu} + g^{\alpha\nu}\dot{S}^{\beta\mu} - g^{\beta\nu}\dot{S}^{\alpha\mu}, \\ [\dot{S}^{\alpha\beta}, \dot{S}^{\mu\nu}] &= -K^{-2}(-g^{\alpha\mu}\tilde{N}^{\beta\nu} + g^{\beta\mu}\tilde{N}^{\alpha\nu} + g^{\alpha\nu}\tilde{N}^{\beta\mu} - g^{\beta\nu}\tilde{N}^{\alpha\mu}), \end{aligned}\right\} \tag{46}$$

where

$$\begin{aligned} \tilde{S}_{\mu\nu} &= 2\{(S^2)^2 + (SS^*)^2\}^{-1}\{S^2 S_{\mu\nu} + (SS^*)S^*_{\mu\nu}\}, \\ \tilde{N}_{\mu\nu} &= 2\{(S^2)^2 + (SS^*)^2\}^{-1}\{S^2 N_{\mu\nu} + (SS^*)N^*_{\mu\nu}\}. \end{aligned}$$

z_μ, p_μ and $A_\nu(\mathbf{x})$ have the same P.B.'s as before. The above scheme of P.B.'s and the Hamilton-Jacobi equation

$$-2mF \equiv (\mathbf{p} - e\mathbf{A})^2 - m^2 = 0, \; m \equiv M + \tfrac{1}{4}K\dot{S}^2 - \tfrac{1}{2}C(Sf), \tag{47}$$

lead to the canonical formulation of Equations (25) and (26).

The generalization to the case of several particles can be carried out on the same lines as in the work of Dirac, or as in Ref. (10). Any dynamical variable ξ is in general a function of all the proper-times s_i of the particles. The equations of motion are $d\xi/ds_i = [\xi, F_i]$, where $F_i = 0$ is the Hamilton-Jacobi equation of the ith particle. For the consistency of these equations, the condition $[F_i, F_j] = 0$ must be satisfied. The correct equations of motion are obtained, if it is assumed that (i) the P.B. of two variables referring to different particles is zero, (ii) the P.B. of the field variable $A_\mu(\mathbf{x})$ and any particle variable is zero, (iii) the P.B.'s of the variables referring to any particle are of the same form as for a single particle, and (iv) the Hamilton-Jacobi equation $F_i = 0$ for each particle is of the same form as for a single particle. The dynamical variables ξ_i (here they are tensor quantities) of the ith particle depend only on s_i, and are

independent of s_j $(i \neq j)$. Hence $d\xi_i/ds_j = [\xi_i, F_j] = 0$ follows from the above assumptions. The equation $d\xi_i/ds_i = [\xi_i, F_i]$ just gives the equations of motion of the ith particle, since they are exactly of the same form as for a single particle. Also it is easily verified that the consistency condition $[F_i, F_j] = 0$ is satisfied when the inequalities (29) hold.

The equation of motion for the field variables is $dA_\mu(\mathbf{x})/ds_i = [A_\mu(\mathbf{x}), F_i]$. This agrees with Equation (32), provided that $[A_\mu(\mathbf{x}), A_\nu(\mathbf{x}')] = g_{\mu\nu}D(\mathbf{x}, \mathbf{x}', \lambda)$, a result which has been postulated earlier. Hence

$$\left.\begin{aligned}[A_\alpha(\mathbf{x}), f_{\mu\nu}(\mathbf{x}')] &= (-g_{\alpha\nu}\partial_\mu + g_{\alpha\mu}\partial_\nu)D(\mathbf{x}, \mathbf{x}', \lambda),\\ [f_{\alpha\beta}(\mathbf{x}), f_{\mu\nu}(\mathbf{x}')] &= (-g_{\alpha\mu}\partial_\beta\partial_\nu + g_{\beta\mu}\partial_\alpha\partial_\nu + g_{\alpha\nu}\partial_\beta\partial_\mu - g_{\beta\nu}\partial_\alpha\partial_\mu)D(\mathbf{x}, \mathbf{x}', \lambda).\end{aligned}\right\} \quad (48)$$

Equations (30) and (31), which are not consequences of the equations of motion, have to be imposed as extra conditions. They are consistent with the equations of motion, since, as in Ref. (10),

$$[\Box\mathbf{A}, F_i] = 0, \quad [R(\mathbf{x}), F_i] = 0.$$

Equation (31) plays the role of the Hamilton-Jacobi equation for the field. There is one of these equations for each $\mathbf{x}$, and they are consistent with each other since $[R(\mathbf{x}), R(\mathbf{x}')] = 0$.

Formulation of the Action Principle

The action principle for the translational motion of spinless electrons is well known (for instance (3)). In the case of particles with spin and dipole moment, the action principle must give both the translational and rotational equations of motion. Before proceeding to the solution of the general problem, it is simpler to consider first the situation when the particle has only rotational motion without translation. It should then be possible to combine this action function with the action function for the translational motion, the form of which is known from the action function for spinless electrons, to give the complete action principle.

In terms of the three-vectors, the Bhabha-Corben rotational equation of motion (25) takes the form

$$\dot{\mathbf{s}} + 2K[\mathbf{s} \times \ddot{\mathbf{s}}] = 2C[\mathbf{s} \times \mathbf{f}]. \quad (49)$$

Before discussing (49), consider first the action principle for the equation of motion

$$\dot{\mathbf{s}} = 2C[\mathbf{s} \times \mathbf{f}]. \quad (50)$$

Since it is assumed that there is no translational motion, the dot in Equations (49) and (50) denotes differentiation with respect to the time.

Let $Oxyz$ be a fixed orthogonal triad in ordinary three-space. A moving triad having Eulerian angles θ, ϕ, ψ is obtained from position $Oxyz$ by rotating successively through ϕ about Oz, through θ about the new position Oy, and through ψ about the new position of Oz. The formal extension of complex Eulerian angles in a complex three-space (analogous to the one above) is used below in the

further discussion. In the fixed complex three-space $\dot{\mathbf{s}}$ is the velocity of the representation of $\mathbf{s}$. Since $\mathbf{s}^2 =$ constant, $\dot{\mathbf{s}}$ has the form

$$\dot{\mathbf{s}} = [\mathbf{p} \times \mathbf{s}], \tag{51}$$

when $\mathbf{p}$ is the total angular velocity of $\mathbf{s}$ given by

$$\mathbf{p} = \dot{\phi}\mathbf{i} + \dot{\theta}\mathbf{j} + \dot{\psi}\mathbf{k}, \tag{52}$$

$\mathbf{i}, \mathbf{j}, \mathbf{k}$ being unit vectors along the directions about which the rotations θ, ϕ, ψ are respectively performed. Hence $(\mathbf{s}, \mathbf{p}) = (\mathbf{s}^2)^{\frac{1}{2}}(\dot{\psi} + \dot{\phi}\cos\theta)$. Note that $\dot{\psi}$ is arbitrary in (52).

Now treat $\mathbf{p}$ as the quasi-velocity vector corresponding to a quasi-coordinate vector $\mathbf{q}$, the true coordinates of the system being θ, ϕ, ψ, so that

$$d\mathbf{q} = d\phi\mathbf{i} + d\theta\mathbf{j} + d\psi\mathbf{k}, \quad \delta\mathbf{q} = \delta\phi\mathbf{i} + \delta\theta\mathbf{j} + \delta\psi\mathbf{k}. \tag{53}$$

The symbols d and δ do not commute when operating on quasi-coordinates $\mathbf{q}$, that is $\delta d\mathbf{q} \neq d\delta\mathbf{q}$. Now

$$\left.\begin{aligned} d\mathbf{i} &= \delta\mathbf{i} = 0, \\ d\mathbf{j} &= [(d\phi\mathbf{i} + d\theta\mathbf{j}) \times \mathbf{j}], \ \delta\mathbf{j} = [(\delta\phi\mathbf{i} + \delta\theta\mathbf{j}) \times \mathbf{j}], \\ d\mathbf{k} &= [(d\phi\mathbf{i} + d\theta\mathbf{j}) \times \mathbf{k}], \delta\mathbf{k} = [(\delta\phi\mathbf{i} + \delta\theta\mathbf{j}) \times \mathbf{k}]. \end{aligned}\right\} \tag{54}$$

The transitivity equation for the quasi-coordinate vector $\mathbf{q}$ is, with the help of (53) and (54),

$$\delta d\mathbf{q} - d\delta\mathbf{q} = d\theta\delta\mathbf{b} + d\psi\delta\mathbf{c} - \delta\theta d\mathbf{b} - \delta\psi d\mathbf{c} = [\delta\mathbf{q} \times d\mathbf{q}]. \tag{55}$$

Consider the action integral

$$I_1 = \int^t \{(\mathbf{s}, \mathbf{p}) + 2C(\mathbf{s}, \mathbf{f})\}dt \tag{56}$$

previous to a certain time t, and form its variation allowing t to vary. Since from (55),

$$\begin{aligned} (\mathbf{s}, \delta d\mathbf{q}) - (\mathbf{s}, d\delta\mathbf{q}) &= (\mathbf{s}, [\delta\mathbf{q} \times d\mathbf{q}]) = -(\delta\mathbf{s}, d\mathbf{q}), \\ (\mathbf{s}, \delta\mathbf{p}) + (\delta\mathbf{s}, \mathbf{p}) &= (\mathbf{s}, d(\delta\mathbf{q})/dt), \end{aligned}$$

and from (51),

$$(\delta\mathbf{s}, \mathbf{f}) = ([\delta\mathbf{q} \times \mathbf{s}], \mathbf{f}) = ([\mathbf{s} \times \mathbf{f}], \delta\mathbf{q}),$$

one gets, from (56),

$$\begin{aligned} \delta I_1 &= \{(\mathbf{s}, \mathbf{p}) + 2C(\mathbf{s}, \mathbf{f})\}\delta t + \int\{(\delta\mathbf{s}, \mathbf{p}) + (\mathbf{s}, \delta\mathbf{p}) + 2C(\delta\mathbf{s}, \mathbf{f})\}dt \\ &= (\mathbf{s}, \delta\mathbf{q}) + \{(\mathbf{s}, \mathbf{p}) + 2C(\mathbf{s}, \mathbf{f})\}\delta t + \int\{-(\dot{\mathbf{s}}, \delta\mathbf{q}) + 2C(\delta\mathbf{s}, \mathbf{f})\}dt \\ &= (\mathbf{s}, \Delta\mathbf{q}) + 2C(\mathbf{s}, \mathbf{f})\,\delta t + \int(-\dot{\mathbf{s}} + 2C[\mathbf{s} \times \mathbf{f}], \delta\mathbf{q})\,dt \\ &= (\mathbf{s}^2)^{\frac{1}{2}}\Delta\psi + s_z\Delta\phi + 2C(\mathbf{s}, \mathbf{f})\delta t + \int(-\dot{\mathbf{s}} + 2C[\mathbf{s} \times \mathbf{f}], \delta\mathbf{q})dt, \end{aligned} \tag{57}$$

where δt denotes the variation in t, Δq denotes the total variation in the final q, namely $\Delta q = \delta q + \dot{q}\delta t$, and $s_z = (\mathbf{s}^2)^{\frac{1}{2}}\cos\theta$. The coefficient of $\delta\mathbf{q}$ under the integral sign in (57) gives the correct equation of motion (50).

The terms under the integral sign cancel when the equation of motion is used. The first term of the remaining ones on the right hand side of (57) is a perfect

differential, and can therefore be discarded. By the standard procedure for introducing canonical coordinates and momenta, s_3 is the momentum conjugate to the canonical coordinate ϕ, and $-2C(\mathbf{s}, \mathbf{f})$ is the energy of the system. Hence $[\phi, s_3] = 1$, a result that can be used to evaluate the P.B.'s of the variables s_1, s_2, s_3. Thus

$$[s_1, s_2] = [(\mathbf{s}^2 - s_3^2)^{\frac{1}{2}} \cos \phi, (\mathbf{s}^2 - s_3^2)^{\frac{1}{2}} \sin \phi] = s_3,$$
$$[s_2, s_3] = s_1 \quad , \quad [s_3, s_1] = s_2 \quad ,$$

which are just the P.B.'s postulated in Ref. (10) for the discussion of Equation (50).

Consider now Equation (49). Take the action integral to be

$$I_2 = \int^t \{(\mathbf{s}, \mathbf{p}) + K\dot{\mathbf{s}}^2 + 2C(\mathbf{s}, \mathbf{f})\}dt, \tag{58}$$

and perform the usual variation as before. Then

$$\begin{aligned}\delta I_2 &= \{(\mathbf{s}, \mathbf{p}) + K\dot{\mathbf{s}}^2 + 2C(\mathbf{s}, \mathbf{f})\}\delta t + (\mathbf{s}, \delta\mathbf{q}) + 2K(\dot{\mathbf{s}}, \delta\dot{\mathbf{s}}) \\ &\quad + \int\{-(\dot{\mathbf{s}}, \delta\mathbf{q}) - 2K(\ddot{\mathbf{s}}, \delta\mathbf{s}) + 2C(\delta\mathbf{s}, \mathbf{f})\}dt \\ &= (\mathbf{s}, \Delta\mathbf{q}) + 2K(\dot{\mathbf{s}}, \Delta\mathbf{s}) + \{2C(\mathbf{s}, \mathbf{f}) - K\dot{\mathbf{s}}^2\}\delta t \\ &\quad + \int(-\dot{\mathbf{s}} - 2K[\mathbf{s}\times\ddot{\mathbf{s}}] + 2C[\mathbf{s}\times\mathbf{f}], \delta\mathbf{q})dt. \end{aligned} \tag{59}$$

The coefficient of $\delta\mathbf{q}$ under the integral sign in (59) gives the correct equation of motion.

With the help of (51) and (53), (59) becomes

$$\begin{aligned}\delta I_2 &= (\mathbf{s} + 2K[\mathbf{s}\times\dot{\mathbf{s}}], \Delta\mathbf{q}) + \{2C(\mathbf{s}, \mathbf{f}) - K\dot{\mathbf{s}}^2\}\delta t \\ &= (\mathbf{s} + 2K\mathbf{s}^2\mathbf{p} - 2K(\mathbf{s}, \mathbf{p})\mathbf{s}, \Delta\mathbf{q}) + \{2C(\mathbf{s}, \mathbf{f}) - K\dot{\mathbf{s}}^2\}\delta t \\ &= \Delta((\mathbf{s}^2)^{\frac{1}{2}}\psi) + 2K\mathbf{s}^2\dot{\theta}\Delta\theta + \{2K\mathbf{s}^2\dot{\phi}\sin^2\theta + (\mathbf{s}^2)^{\frac{1}{2}}\cos\theta\}\Delta\phi \\ &\quad + \{2C(\mathbf{s}, \mathbf{f}) - K\dot{\mathbf{s}}^2\}\delta t.\end{aligned}$$

The first term on the right is discarded, since it is a perfect differential. The other terms give the canonical coordinates Q_1, Q_2 and their respective momenta P_1, P_2

$$Q_1 = \phi, P_1 = 2K\mathbf{s}^2\dot{\phi}\sin^2\theta + (\mathbf{s}^2)^{\frac{1}{2}}\cos\theta, \quad Q_2 = \theta, P_2 = 2K\mathbf{s}^2\dot{\theta}. \tag{60}$$

Since

$$[Q_r, Q_s] = 0, \ [P_r, P_s] = 0, \ [Q_r, P_s] = \delta_{rs}, \ (r, s = 1, 2), \tag{61}$$

the P.B.'s of the various dynamical variables can be evaluated from (60) and (61). Thus

$$\begin{aligned}[s_1, s_2] &= \mathbf{s}^2[\sin Q_2 \cos Q_1, \sin Q_2 \sin Q_1] = 0, \\ [s_1, \dot{s}_1] &= (2K)^{-1}[\sin Q_2 \cos Q_1, P_2 \cos Q_2 \cos Q_1 \\ &\qquad - \{P_1 - (\mathbf{s}^2)^{\frac{1}{2}}\cos Q_2\}\sin Q_1 \operatorname{cosec} Q_2] \\ &= (2K)^{-1}(\cos^2 Q_1 \cos^2 Q_2 + \sin^2 Q_1) = (2K\mathbf{s}^2)^{-1}(\mathbf{s}^2 - s_1^2),\end{aligned}$$

$$[s_2, \dot{s}_3] = -(2K)^{-1}[\sin Q_2 \sin Q_1, P_2 \sin Q_2]$$
$$= -(2K)^{-1} \sin Q_1 \sin Q_2 \cos Q_2 = -(2K\mathbf{s}^2)^{-1} s_2 s_3,$$
$$[\dot{s}_2, \dot{s}_3] = -(4K^2\mathbf{s}^2)^{-1}[P_2 \cos Q_2 \sin Q_1$$
$$+ \{P_1 - (\mathbf{s}^2)^{\frac{1}{2}} \cos Q_2\} \cos Q_1 \operatorname{cosec} Q_2, P_2 \sin Q_2]$$
$$= -(4K^2\mathbf{s}^2)^{-1}\{ -P_2 \sin Q_1 - (P_1 - (\mathbf{s}^2)^{\frac{1}{2}} \cos Q_2)$$
$$\cos Q_1 \cos Q_2 \operatorname{cosec} Q_2 + (\mathbf{s}^2)^{\frac{1}{2}} \cos Q_1 \sin Q_2\}$$
$$= -(4K^2\mathbf{s}^2)^{-1}\{s_1 + 2K(s_2\dot{s}_3 - s_3\dot{s}_2)\} = -(4K^2\mathbf{s}^2)^{-1} n_1,$$

and similar relations, which together lead to the P.B.'s (44) and (45) considered earlier.

The real action function for the rotational motion is known immediately by combining the three-vector complex form and its complex conjugate. The action function for both the translational and rotational equations of motion is obtained by generalizing the action function for the translational motion of a spinless electron to include the action function for the rotational motion. However, it must be remembered that, in dealing with the action function for rotational motion, the equations have been considered in ordinary Euclidean space whose underlying metric is of the form $dx_1^2 + dx_2^2 + dx_3^2$. With such a metric there is no difference between covariant and contravariant quantities. The translational and rotational equations have been worked out in Lorentz space, where the scalar product of two four-vectors has a negative sign in the terms involving the space components. But if the metric of the three-space used is $-dx_1^2 - dx_2^2 - dx_3^2$, then the value of the rotational action function in this space can be taken over immediately into Lorentz space. The change from the ordinary Euclidean space to the new pseudo-Euclidean space means replacing every typical scalar product $(\mathbf{l}, \mathbf{m})$, say, by $-(\mathbf{l}, \mathbf{m})$. This will then automatically show the difference (in sign) between the contravariant and covariant components of any vector. Thus the action function for the rotational motion has to be taken over as $-I_2$. The form of the P.B.'s, however, remains the same as before.

The field equations can also be obtained from the action principle. The usual infinities associated with a point model of the particle have been avoided in the above work by using the Wentzel field and the λ-limiting process. The action principle for this case can be given in the same manner as by Dirac (3). However, a more general form of limiting process due to Dirac (6) can be used as in the action principle (62).

In parametric problems of the calculus of variations, the integrals to be varied must be independent of the parametric representations used. This condition is satisfied if the integrands are functions which are positively homogeneous of degree one in the derivatives with respect to the parameter. In the discussion of the action principle here, the action integrals for the particles involve the proper-time as parameter. The homogeneity condition can be satisfied for the action integral by introducing suitable powers of $\mathbf{v}^2$ as factors in terms where

this step is called for, as is done below. Then the action integral is in proper parametric form, and a change to any parameter other than the proper-time is possible.

The action integral for the equations of motion of several particles and the field is

$$I = \Sigma \int \{M(\mathbf{v}^2)^{\frac{1}{2}} + e(\mathbf{A}(\mathbf{z}), \mathbf{v}) - \tfrac{1}{4}(SP) - \tfrac{1}{4}K\dot{S}^2(\mathbf{v}^2)^{-\frac{1}{2}} - \tfrac{1}{2}C(Sf)(\mathbf{v}^2)^{\frac{1}{2}}\} ds + (8\pi)^{-1} \int \partial_\mu \tilde{A}_\nu(\mathbf{x}) \partial^\mu A^\nu(\mathbf{x}) d\mathbf{x}, \quad (62)$$

where $d\mathbf{x} \equiv dx_0 dx_1 dx_2 dx_3$, and the Σ denotes summation over the several particles (the label i is omitted for convenience). In (62) $P_{\mu\nu}$ is the quasi-velocity corresponding to the quasi-coordinate $Q_{\mu\nu}$, so that $dQ_{\mu\nu} = P_{\mu\nu} ds$. Further, $P_{\mu\nu}$ is connected with $\dot{S}_{\mu\nu}$ according to $\dot{S}_{\mu\nu} = \frac{1}{2}[P \,.\, S]_{\mu\nu}$. $Q_{\mu\nu}$ satisfies the transitivity equation (generalization of (55)) $\delta dQ_{\mu\nu} - d\delta Q_{\mu\nu} = \frac{1}{2}[\delta Q \,.\, dQ]_{\mu\nu}$. $\tilde{A}_\mu$ in (62) is connected with A_μ by the equation

$$\tilde{A}_\mu(\mathbf{x}) = \int A_\mu(\mathbf{x}') \gamma(\mathbf{x} - \mathbf{x}') d\mathbf{x},$$

where $\gamma(\mathbf{x})$ is a function such that $\gamma(\mathbf{x}) = \gamma(-\mathbf{x})$; $\gamma(\mathbf{x})$ approximates to the function $\delta(\mathbf{x})(\equiv \delta(x_0)\delta(x_1)\delta(x_2)\delta(x_3))$ and is made to tend to $\delta(\mathbf{x})$ in the limit; other properties for $\gamma(\mathbf{x})$ are assumed in further work. The action function for the field, namely, the last integral in (62), has the Fermi form, thus avoiding the difficulty of a zero value for the momentum conjugate to A_0. The details of handling the action principle with the above type of field equations are found in Ref. (6).

The relativistic cutoff procedure of Feynman (7, 8) can be taken over into the present theory by considering the action integral

$$I' = \Sigma \int \{M(\mathbf{v}^2)^{\frac{1}{2}} + e(\bar{A}(\mathbf{z}), \mathbf{v}) - \tfrac{1}{4}(SP) - \tfrac{1}{4}(K\dot{S}^2(\mathbf{v}^2)^{-\frac{1}{2}} - \tfrac{1}{2}C(S\bar{f})(\mathbf{v}^2)^{\frac{1}{2}}\} ds, \quad (63)$$

where $\bar{f}_{\mu\nu}$ is the field tensor derived from the potential four-vector

$$\bar{A}_\mu(\mathbf{x}) = \Sigma e \int v_\mu \epsilon(\mathbf{x} - \mathbf{z})^2 ds + \Sigma \partial^\rho \int CS_{\rho\mu} \epsilon(\mathbf{x} - \mathbf{z})^2 ds.$$

$\epsilon(\mathbf{x}^2)$ behaves like $\delta(\mathbf{x}^2)$ for large dimensions but differs for small, and it is normalized so that

$$\int_{-\infty}^{\infty} \epsilon(\mathbf{x}^2) d(\mathbf{x}^2) = 1.$$

The properties of $\epsilon(\mathbf{x}^2)$, with special examples, and their consequences have been discussed by Feynman.

Quantization

On passing to the quantum theory all the classical dynamical variables are replaced by linear operators, with real classical variables corresponding to self-

adjoint operators. The operators operate on a vector $|>$, called a ket-vector, in a many-dimensional space, which vector specifies the states of the dynamical system in quantum mechanics. The coordinates of $>$ in any representation that can be set up give the Schrödinger wave functions. The linear operators are in general noncommutative, and satisfy commutation relations corresponding to the classical P.B. relations according to the formula $2\pi(\alpha\beta - \beta\alpha) = ih[\alpha, \beta]$. This noncommutative character of the operators gives rise to an ambiguity, whenever there is a product of two factors, which have a nonvanishing P.B. in the classical theory and therefore noncommuting in the quantum theory. In simple examples, considerations of simplicity are invoked to choose the order of the factors leading to a consistent theory, as in the example considered below. The Hamilton-Jacobi equations and supplementary conditions give operator equations on $>$, called the Schrödinger wave equations. All the other equations become relations between the operators of the quantum theory. When there are several wave equations of the type $F_i| > = 0$, they are consistent provided that the P.B.'s $[F_i, F_j] = 0$ for all i, j.

When the dynamical system consists of several particles and the wave field, the above rules lead to wave equations of the form

$$F_i > = 0 \tag{64}$$

for each particle, where F_i has one or other of the forms (34), (41), (47). The supplementary condition (31) gives the wave equation

$$R(\mathbf{x}) > = 0 \tag{65}$$

for the field. The extra condition $\Box \mathbf{A} = 0$ goes over unchanged into the quantum theory as a relation between the corresponding operators. The wave equations are all consistent, since it has been verified that

$$[F_i, F_j] = 0, \ [R(\mathbf{x}), F_i] = 0, \ [R(\mathbf{x}), R(\mathbf{x}')] = 0.$$

In the quantum theory corresponding to the Bhabha-Corben classical equations, (25) and (26), linear operators corresponding to their classical counterparts $z_\mu, p_\mu, S_{\mu\nu}, \dot{S}_{\mu\nu}, A_\mu, f_{\mu\nu}$ are the dynamical variables satisfying commutation relations corresponding to (35), (46), (38), and (48). It is more convenient, however, to use $\mathbf{s}$ and $\dot{\mathbf{s}}$ (or $\mathbf{s}$ and $\mathbf{n}$) and their commutation relations corresponding to (44) and (45) to set up the matrix representation of the spin variables. From $[s_a, \dot{s}_b] + [\dot{s}_a, s_b] = 0$, it follows that $[\mathbf{s} \times \dot{\mathbf{s}}] = -[\dot{\mathbf{s}} \times \mathbf{s}]$ is true in the quantum theory, the order of the factors appearing as shown. From the commutation relations for $\mathbf{s}$ and $\mathbf{n}$, it is seen that $[\mathbf{n} \times \mathbf{s}] \neq -[\mathbf{s} \times \mathbf{n}]$ in the quantum theory. This difficulty is overcome by using the form $\frac{1}{2}\{[\mathbf{n} \times \mathbf{s}] - [\mathbf{s} \times \mathbf{n}]\}$ wherever $[\mathbf{n} \times \mathbf{s}]$ occurs in the classical theory. If, instead of the λ-limiting process, the limiting process corresponding to the action principle (62) is used, then it would be necessary to write the wave equation for the field in terms of the Fourier components of the field variables in exactly the same way as in Ref. (6).

The relativistic cutoff procedure for quantum electrodynamics corresponding to the action principle (63) can be given on the same lines as in Ref. (8).

Extension of the Theory to a Vector Meson Field

The extension of the preceding type of theory to the case when the interacting field is a vector meson field $\mathbf{U}$, satisfying the equation $(\Box + \chi^2)\mathbf{U} = 0$, has been considered in Ref. (10). The classical equations of motion, the Wentzel field, and the Hamilton-Jacobi equations have the same form as in the electromagnetic case except that the vector meson field variables U_μ, $G_{\mu\nu}$ replace the variables A_μ, $f_{\mu\nu}$, respectively, and the generalized Jordan-Pauli function $\Delta^*(\mathbf{x})$, defined by

$$|x_0|\Delta^*(\mathbf{x}) = 2x_0\delta(\mathbf{x}^2) - x_0\chi(\mathbf{x}^2)^{-\frac{1}{2}}J_1(\chi(\mathbf{x}^2)^{\frac{1}{2}}),$$

where J_1 is the Bessel function of order one, replaces the $\Delta(\mathbf{x})$.

In the classical theory, the electromagnetic field equations (with $\chi = 0$) can be obtained from the meson field equations (with $\chi \neq 0$) by letting $\chi \to 0$. This is not true, however, of the quantized field equations. It is known that the P.B. relations for the electromagnetic field cannot be obtained from those for the meson field by letting $\chi \to 0$. Further, the P.B.'s for the meson field can be chosen so that they are consistent with the condition analogous to the Lorentz condition, while this is not the case with the electromagnetic field, where the Lorentz condition has to be introduced as a supplementary condition. In Ref. (10), the P.B.'s postulated for the field variables and the subsequent treatment of the extra condition

$$R^*(\mathbf{x}) \equiv \partial^\mu U_\mu(\mathbf{x}) + \Sigma e D^*(\mathbf{x}, \mathbf{z}, \lambda) = 0, \tag{66}$$

where $D^*(\mathbf{x}, \mathbf{z}, \lambda) \equiv \frac{1}{2}\{\Delta^*(\mathbf{x} - \mathbf{z} + \lambda) + \Delta^*(\mathbf{x} - \mathbf{z} - \lambda)\}$, are not correct. The correct treatment of these questions is as follows.

Split up the potential $U_\mu(\mathbf{x})$ in the form

$$U_\mu = {}^*U_\mu + \partial_\mu g \tag{67}$$

where

$$\partial^\mu {}^*U_\mu = 0, \tag{68}$$

and g is such that $(\Box + \chi^2)g = 0$. Hence $^*\mathbf{U}$ satisfies the equation $(\Box + \chi^2)^*\mathbf{U} = 0$. Since

$$\partial^\mu U_\mu = \partial^\mu {}^*U_\mu + \partial^\mu \partial_\mu g = -\chi^2 g = -\Sigma e D^*(\mathbf{x}, \mathbf{z}, \lambda),$$

one gets $g = -\chi^{-2}\Sigma e D^*(\mathbf{x}, \mathbf{z}, \lambda)$. From the definition of U_μ in terms of the Wentzel potentials,

$$dU_\mu/ds_i = d\{{}^*U_\mu + \partial_\mu g\}/ds_i = e v_{\mu i} D^*(\mathbf{x}, \mathbf{z}_i, \lambda) + \partial^\rho(Z_{\rho\mu i} D^*(\mathbf{x}, \mathbf{z}_i, \lambda)). \tag{69}$$

But

$$d^*U_\mu/ds_i = [{}^*U_\mu, F_i]. \tag{70}$$

Equations (69) and (70) agree provided that the P.B. relations for $^*U_\mu$ are taken to be

$$[{}^*U_\mu(\mathbf{x}), {}^*U_\nu(\mathbf{x}')] = (g_{\mu\nu} + \chi^{-2}\partial_\mu\partial_\nu)D^*(\mathbf{x}, \mathbf{x}', \lambda). \tag{71}$$

Hence

$$[\partial^{\mu}{}^{*}U_{\mu}(\mathbf{x}),{}^{*}U_{\nu}(\mathbf{x}')]=\partial^{\mu}(g_{\mu\nu}+\chi^{-2}\partial_{\mu}\partial_{\nu})D^{*}(\mathbf{x},\mathbf{x}',\lambda)=\partial_{\nu}(1+\chi^{-2}\Box)D^{*}(\mathbf{x},\mathbf{x}',\lambda)=0, \tag{72}$$

and therefore

$$[\partial^{\mu}{}^{*}U_{\mu}(\mathbf{x}),\ \partial'^{\nu}{}^{*}U_{\nu}(\mathbf{x}')]=0,\quad [\partial^{\mu}{}^{*}U_{\mu}(\mathbf{x}),\ F_{i}]=0.$$

Also, from (71), with ${}^{*}G_{\mu\nu}=\partial_{\mu}{}^{*}U_{\nu}-\partial_{\nu}{}^{*}U_{\mu}$,

$$\left.\begin{aligned}[{}^{*}U_{\alpha}(\mathbf{x}),\ {}^{*}G_{\mu\nu}(\mathbf{x}')] &= (g_{\alpha\mu}\partial_{\nu}-g_{\alpha\nu}\partial_{\mu})D^{*}(\mathbf{x},\mathbf{x}',\lambda),\\ [{}^{*}G_{\alpha\beta}(\mathbf{x}),\ {}^{*}G_{\mu\nu}(\mathbf{x}')] &= (-g_{\alpha\mu}\partial_{\beta}\partial_{\nu}+g_{\beta\mu}\partial_{\alpha}\partial_{\nu}+g_{\alpha\nu}\partial_{\beta}\partial_{\mu}-g_{\beta\nu}\partial_{\alpha}\partial_{\mu})D^{*}(\mathbf{x},\mathbf{x}',\lambda).\end{aligned}\right\} \tag{73}$$

Equation (72) shows that the extra condition (66) can be taken over unchanged into the quantum theory. In the Hamilton-Jacobi equations, and therefore in the wave equations, U_{μ} is replaced by ${}^{*}U_{\mu}+\chi^{-2}\partial_{\mu}\Sigma eD^{*}(\mathbf{x},\mathbf{z},\lambda)$, and $G_{\mu\nu}$ by ${}^{*}G_{\mu\nu}$. The P.B.'s for ${}^{*}U_{\mu}$ and ${}^{*}G_{\mu\nu}$ are given by (71) and (73).

The Stueckelberg variation of the above formulation is to split up ${}^{*}U_{\mu}$ in the form

$${}^{*}U_{\mu}=V_{\mu}+\chi^{-1}\partial_{\mu}W, \tag{74}$$

where $(\Box+\chi^{2})W=0$, $(\Box+\chi^{2})V_{\mu}=0$. The extra condition (68) is then equivalent to

$$\partial^{\mu}V_{\mu}-\chi W=0. \tag{75}$$

The P.B. relations for V_{μ} and W are taken to be

$$\left.\begin{aligned}[V_{\mu}(\mathbf{x}),\ V_{\nu}(\mathbf{x}')] &= g_{\mu\nu}D^{*}(\mathbf{x},\mathbf{x}',\lambda),\ [V_{\mu}(\mathbf{x}),\ W(\mathbf{x}')]=0,\\ [W(\mathbf{x}),\ W(\mathbf{x}')] &= -D^{*}(\mathbf{x},\mathbf{x}',\lambda).\end{aligned}\right\} \tag{76}$$

Equation (75) is not consistent with (76). But since

$$\begin{aligned}[\partial^{\mu}V_{\mu}(\mathbf{x})-\chi W(\mathbf{x}),\ \partial'^{\nu}V_{\nu}(\mathbf{x}')-\chi W(\mathbf{x}')]\\ =(\partial^{\mu}\partial'^{\nu}g_{\mu\nu}-\chi^{2})D^{*}(\mathbf{x},\mathbf{x}',\lambda)=-(\Box+\chi^{2})D^{*}(\mathbf{x},\mathbf{x}',\lambda)=0,\end{aligned}$$

Equation (75) is treated as a supplementary condition (analogous to the electromagnetic case).

I am deeply indebted to Prof. P. A. M. Dirac for invaluable advice and kind interest in the above work. I am grateful to Miss Lorraine Ourom for help in the preparation of the paper. My thanks are also due to Dr. G. Herzberg, Director of the Division of Physics, for research facilities, and to the National Research Council of Canada for financial support at Ottawa, while on leave of absence from the Tata Institute of Fundamental Research, Bombay.

References

1. Bhabha, H. J. Proc. Indian Acad. Sci. A, 11: 247. 1940.
2. Bhabha, H. J. and Corben, H. C. Proc. Roy. Soc. (London), A, 178: 273. 1941.
3. Dirac, P. A. M. Proc. Roy. Soc. (London), A, 180: 1. 1942.
4. Dirac, P. A. M. Communs. Dublin Inst. Advanced Studies, A, No. 1. 1943.
5. Dirac, P. A. M. Phil. Mag. 39 (Ser. 7): 31. 1948.
6. Dirac, P. A. M. Phys. Rev. 74 (Ser. 2): 817. 1948.
7. Feynman, R. P. Phys. Rev. 74 (Ser. 2): 939. 1948.
8. Feynman, R. P. Phys. Rev. 74 (Ser. 2): 1430. 1948.
9. Newboult, H. O. Analytic method in dynamics. Oxford at the Clarendon Press. 1946. Section 4.2.
10. Shanmugadhasan, S. Proc. Cambridge Phil. Soc. 43: 106. 1947.
11. Shanmugadhasan, S. Proc. Cambridge Phil. Soc. 45: 411. 1949.

CONTENTS OF VOLUME 29

*See Additions and Corrections, p. 615.

ADDITIONS AND CORRECTIONS

Page 59. Concerning the half life figure for Cu^{66} given in this paper, the author states "The half life figure for Cu^{66} which I gave is in error and should be disregarded."

Page 403. In the first line of the **Abstract**, "system" should be deleted before "systems".

Page 456. In Line 3 of **Acknowledgments**, J. G. Odgers should read G. J. Odgers.

CANADIAN JOURNAL OF PHYSICS

Notice to Contributors

GENERAL: Manuscripts should be typewritten, double spaced, and the **original and one extra copy** submitted. Style, arrangement, spelling, and abbreviations should conform to the usage of this Journal. Names of all simple compounds, rather than their formulas, should be used in the text. Greek letters or unusual signs should be written plainly or explained by marginal notes. Superscripts and subscripts must be legible and carefully placed. Manuscripts should be carefully checked before being submitted, to reduce the need for changes after the type has been set. If authors require changes to be made after the type is set, they will be charged for changes that are considered to be excessive. **All pages, whether text, figures, or tables, should be numbered.**

ABSTRACT: **An abstract of not more than about 200 words, indicating the scope of the work and the principal findings, is required.**

ILLUSTRATIONS:

(i) *Line Drawings:* All lines should be of sufficient thickness to reproduce well. Drawings should be carefully made with India ink on white drawing paper, blue tracing linen, or co-ordinate paper **ruled in blue only**; any co-ordinate lines that are to appear in the reproduction should be ruled in black ink. Paper ruled in **green, yellow, or red should not be used** unless it is desired to have all the co-ordinate lines show. Lettering and numerals should be neatly done in India ink preferably with a stencil (**do not use typewriting**) and be of such size that they will be legible and not less than one millimeter in height when reproduced in a cut three inches wide. All experimental points should be carefully drawn with instruments. Illustrations need not be more than two or three times the size of the desired reproduction, but the ratio of height to width should conform with that of the type page. **The original drawings and one set of small but clear photographic copies are to be submitted.**

(ii) *Photographs:* Prints should be made on glossy paper, with strong contrasts; they should be trimmed to remove all extraneous material so that essential features only are shown. Photographs should be submitted **in duplicate**; if they are to be reproduced in groups, one set should be so arranged and mounted on cardboard with rubber cement; the duplicate set should be unmounted.

(iii) *General:* **The author's name, title of paper, and figure number should be written in the lower left hand corner (outside the illustration proper) of the sheets on which the illustrations appear.** Captions should not be written on the illustrations, but typed on a separate page of the manuscript. All figures (including each figure of the plates) should be numbered consecutively from 1 up (arabic numerals). **Each figure should be referred to in the text.** If authors desire to alter a cut, they will be charged for the new cut.

TABLES: Each table should be typed on a separate sheet. Titles should be given for all tables, which should be numbered in Roman numerals. Column heads should be brief and textual matter in tables confined to a minimum. **Each table should be referred to in the text.**

REFERENCES: **These should be listed alphabetically by authors' names, numbered in that order, and placed at the end of the paper.** The form of literature citation should be that used in this Journal. **Titles of papers should not be given.** The first page only of the references cited should be given. **All citations should be checked with the original articles.** Each citation should be referred to in the text by means of the key number.

REPRINTS: A total of 50 reprints of each paper, without covers, are supplied free to the authors. Additional reprints will be supplied according to a prescribed schedule of charges. On request, covers can be supplied at cost.

Approximate charges for reprints may be calculated from the number of printed pages, obtained by multiplying by 0.6 the number of manuscript pages (double-spaced typewritten sheets, 8½ in. by 11 in.) and making allowance for space occupied by line drawings and half-tones (not inserts). The cost per page is tabulated at the back of the reprint request form sent with the galley.

Manuscripts should be addressed: *Canadian Journal of Physics,*
National Research Council,
Ottawa, Canada.

Contents

Printed in Canada *by* University of Toronto Press